GEORG-AUGUST-UNIVERSITÄT
GÖTTINGEN

Characterization of the stepwise maturation of the telomerase RNA *TLC1* and assembly of the telomerase in *Saccharomyces cerevisiae*

Dissertation

for the award of the degree
"Doctor rerum naturalium"
of the Georg-August-Universität Göttingen

within the doctoral program "Molecular Biology of Cells"
of the Georg-August University School of Science (GAUSS)

submitted by

Anna Greta Hirsch
from Berlin, Germany

Göttingen, July 2021

Thesis Committee:

Prof. Dr. Heike Krebber
Department of Molecular Genetics
Institute for Microbiology and Genetics

Prof. Dr. Ralph Kehlenbach
Department of Molecular Biology
Institute for Molecular Biology

Prof. Dr. Jörg Großhans
Campus Institute for Dynamics of Biological Networks (CIDBN)
Georg-August-University

Members of the Examination Board:

Referee: Prof. Dr. Heike Krebber
Department of Molecular Genetics
Institute for Microbiology and Genetics

2nd Referee: Prof. Dr. Ralph Kehlenbach
Department of Molecular Biology
Institute for Molecular Biology

Further Members of the Examination Board:

Prof. Dr. Jörg Großhans
Campus Institute for Dynamics of Biological Networks (CIDBN)
Georg-August-University

Prof. Dr. Ralf Ficner
Department of Molecular Structural Biology
Institute for Microbiology and Genetics

Prof. Dr. Kai Heimel
Department of Molecular Microbiology and Genetics
Institute for Microbiology and Genetics

PD Dr. Wilfried Kramer
Department of Molecular Genetics
Institute for Microbiology and Genetics

Date of oral examination: 07th October 2021

Affidavit

I hereby declare that I prepared this doctoral thesis titled “Characterization of the stepwise maturation of the telomerase RNA *TLC1* and assembly of the telomerase in *Saccharomyces cerevisiae*” independently and with no other sources and aids than quoted.

Göttingen, July 2021

_____

Anna Greta Hirsch

Table of Contents

TABLE OF FIGURES I

TABLE OF TABLES II

1. ABSTRACT 1

2. INTRODUCTION 2

2.1. Telomeres: essential nucleoprotein structures for viability 3

2.2. Capping of telomere ends 4

2.3. Telomere replication and telomerase mediated telomere elongation 6

2.4. The telomerase in *S. cerevisiae* 7

2.4.1. Telomerase RNA (*TLC1*) 8
2.4.1.1. Structure and conserved regions of the telomerase RNA 8
2.4.1.2. *TLC1* level and localization 10
2.4.1.3. Transcription termination of RNAP II transcripts 11
2.4.1.4. 5´- and 3´-end processing of *TLC1* 12

2.4.2. Accessory proteins 13
2.4.2.1. Est proteins 13
2.4.2.2. Pop proteins 14
2.4.2.3. The Sm-ring in *TLC1* maturation and RNP biogenesis 15

2.5. Assumed lifecycle of *TLC1* and the telomerase 16

2.6. Recombination based telomere elongation 18

2.7. Nucleo-cytoplasmic transport 20

2.7.1. Mex67-Mtr2 mediated transport 20

2.7.2. Karyopherin mediated transport 21

2.7.3. Nucleo-cytoplasmic transport of *TLC1* 23

2.8. Aim of the study 24

3. MATERIAL AND METHODS 25

3.1. Chemicals and Consumables 25

3.2. Equipment, Hardware and Software 28

3.3. Strains 29

3.3.1. *Escherichia coli* 29

3.3.2. *Saccharomyces cerevisiae* 29

3.4. Plasmids 31

3.5. Oligonucleotides 32

3.6. Cell biological methods 33

3.6.1. Cell cultivation 33
3.6.1.1. Cultivation of *E. coli* 34
3.6.1.2. Cultivation of *S. cerevisiae* 34

3.6.2. Transformation of *E. coli* 36
3.6.2.1. Transformation of *E. coli* via heat shock 36
3.6.2.2. Transformation of *E. coli* via electroporation 36

3.6.3. Passaging of yeast cells 37

3.6.4. Measurement of yeast cell density in liquid culture 38

3.6.5. Transformation of *S. cerevisiae* 38

3.6.6. Crossing of *S. cerevisiae* strains 39

3.6.7. Growth analysis of yeast strains 40

3.7. DNA methods 40

3.7.1. Isolation of chromosomal DNA from yeast 40

3.7.2. Isolation of high-quality chromosomal DNA from yeast for Southern blotting 41

3.7.3. Isolation of plasmid DNA from *E. coli* 41

3.7.4. Measurement of DNA and RNA concentration 41

3.7.5. Polymerase chain reaction 42

3.7.6. Cleavage of DNA by restriction digestion 42

3.7.7. Agarose gel electrophoresis 43

3.7.8. DNA extraction from agarose gels 43

3.7.9. Site directed mutagenesis by Quick Change PCR 44

3.7.10. Endogenous mutation of *TLC1* transcription termination sites 44

3.7.11. Sequencing 45

3.8. Molecular biological methods with yeast 46

3.8.1. RNA extraction from yeast 46

3.8.2. Complementary DNA (cDNA) synthesis 46

3.8.3. Quantitative Real time PCR (qPCR) 47

3.8.4. Nucleo-cytoplasmic fractionation experiments 48

3.8.5. Southern blot analysis 49
3.8.5.1. Telomere restriction fragment (TRF) analysis 49

3.9. Microscopic studies 51

3.9.1. Fluorescence *in situ* hybridization experiments (FISH) 51

3.9.2. GFP-Microscopy 53

3.9.3. Immunofluorescence experiments 54

3.10. Biochemical methods 55

3.10.1. Preparation of yeast cell lysate 55

3.10.2. Immunoprecipitation (IP) experiments 55

3.10.3. SDS-Polyacrylamide gel-electrophoresis (SDS-PAGE) 56

3.10.4. Western blot analysis 57

3.10.5. RNA Co-Immunoprecipitation (RIP) experiments 58

3.11. Quantification and statistical analysis 59

4. RESULTS 60

4.1. The *TLC1* amount increases in mutants of the NNS complex 60

4.1.1. The *poly(A)*, NNS** and *poly(A)*NNS** termination site mutants show an altered *TLC1* abundance *in vivo* 62

4.1.2. Cytoplasmic accumulation of *TLC1* in transcription termination mutants 63

4.2. The Cap-binding complex component Cbp20 and *TLC1* physically interact 66

4.3. Loading of the Sm-ring onto immature *TLC1* occurs in the cytoplasm 67

4.4. Cse1 is involved in the nuclear import of *TLC1* 70

4.5. Cse1 and Mtr10 physically interact with *TLC1* 73

4.6. The *cse1-1* mutation does not affect the overall level of total *TLC1 in vivo* 74

4.7. Cse1 stabilizes the interaction of immature *TLC1* and Smb1 prior to the re-import 76

4.8. The import factor Mtr10 contacts the Smb1 protein presumably for re-import 78

4.9. The re-import of *TLC1* is independent of the importin α pathway 79

4.10. Southern blot analysis revealed an altered telomere structure with amplified Y´ elements in the *cse1-1* mutant 81

4.11. Mutation of *CSE1* altered the localization Rap1 84

4.12. Loading of the Est and Pop proteins occurs in the cytoplasm 86

4.13. TMG-cap formation and trimming of immature *TLC1* is facilitated after re-import of *TLC1* into the nucleus 89

4.14. The guard protein Npl3 physically interacts with *TLC1* 92

5. DISCUSSION 93

5.1. Transcription termination of *TLC1* involves the CPF-CFI complex and the NNS complex 93

5.2. *TLC1* interacts with the cap binding complex component Cbp20 and the guard protein Npl3 99

5.3. Telomerase holoenzyme assembly occurs in the cytoplasm 100

5.4. Nuclear import of immature *TLC1* is facilitated by Cse1 and Mtr10 in dependence of the Sm-ring 102

5.5. A novel role of Cse1 in telomere biology 105

5.6. 3´-end processing of *TLC1* occurs after re-import and processing is finalized by TMG-cap formation as prerequisite for telomerase function 108

5.7. Novel model of *TLC1* maturation and Telomerase assembly in *S. cerevisiae* 110

6. REFERENCES 113

7. ACKNOWLEDGEMENT 128

8. CURRICULUM VITAE 129

9. APPENDIX 130

Table of figures

Figure 1: Schematic representation of subtelomeric and telomeric DNA. 4
Figure 2: Schematic illustration of yeast telomeres in a capped status. 5
Figure 3: Secondary structure of ciliate, vertebrate and yeast telomerase RNA. 9
Figure 4: Predicted secondary structure of *TLC1* and the telomerase holoenzyme. 10
Figure 5: Genomic localization and transcription termination sites in *TLC1*. 12
Figure 6: Current model of *TLC1* processing and telomerase assembly in *S. cerevisiae.* 17
Figure 7: Different classes of functional telomeres in *S. cerevisiae*. 19
Figure 8: Karyopherin mediated nucleo-cytoplasmic transport and the Ran cycle. 22
Figure 9: Schematic representation of the *TLC1* RNA with the indicated termination factor binding sites. Used primers and probes are shown. 60
Figure 10: *nrd1-102* and *sen1-1* mutants lead to an increased *TLC1* amount. 61
Figure 11: *TLC1* termination site mutants used in this study. 62
Figure 12: Mutation of the PAS site and the NNS binding site led to a decreased abundance of total *TLC1* but read-through transcripts occur in upon PAS mutation *in vivo*. 63
Figure 13: FISH analysis revealed a mislocalization of *TLC1* to the cytoplasm in the *NNS** and the *poly(A)*NNS** mutants compared to wild type. 64
Figure 14: Nucleo-cytoplasmic fractionation experiment revealed altered localization of *TLC1* in the termination site mutants. 65
Figure 15: Cbp20 and *TLC1* physically interact. 67
Figure 16: Decreased binding of *TLC1* to Smb1-GFP in *mex67-5 xpo1-1* mutants. 68
Figure 17: Increased binding of *TLC1* to Smb1-GFP in *mtr10Δ*. 69
Figure 18: *TLC1* mislocalizes to the cytoplasm in the *cse1-1* and *cse1-1 mtr10Δ* mutants. 71
Figure 19: Immature *TLC1* accumulates in the cytoplasm upon re-import block. 72
Figure 20: Mtr10 and Cse1 physically interact with *TLC1*. 73
Figure 21: Growth analysis revealed a genetic interaction between *MTR10* and *CSE1*. 74
Figure 22: Mutation of *MTR10* but not of *CSE1* affects the total *TLC1* level, but the combination of both leads to an accumulation of immature *TLC1*. 75
Figure 23: The Sm-ring loading onto *TLC1* occurs in the cytoplasm and is stabilized via Cse1. 77
Figure 24: Mtr10 physically interacts with Smb1. 78
Figure 25: Localization of *TLC1* is not affected in the *srp1-31* mutant. 79
Figure 26: Pop1-GFP mislocalizes to the cytoplasm in the *srp1-31* mutant. 80
Figure 27: Schematic representation of yeast wild type Y´ telomere and Type I survivor telomere. Probe targeting the TG-repeats of the telomeres is indicated as Southern probe. 81
Figure 28: Southern blot analysis of XhoI digested chromosomal DNA revealed no telomere shortening defect for *cse1-1* but amplification of an approximately 5.5 kb fragment. 82
Figure 29: The Y´ elements are amplified in the *cse1-1* mutant, which is reversible by complementation with *CSE1*. 83
Figure 30: Cdc13-GFP is not mislocalized in the *cse1-1* mutant. 84
Figure 31: Rap1-GFP mislocalizes in the *cse1-1* mutant. 85
Figure 32: *TLC1* export and import factor mutants affect the localization of Pop1 and Est1. 87
Figure 33: Pop1-GFP loading onto *TLC1* occurs in the cytoplasm. 88
Figure 34: TMG-capping of *TLC1* is reduced in import factor mutants. 90
Figure 35: 3´-end processing of *TLC1* occurs in the nucleus after *TLC1* re-import. 91
Figure 36: Npl3 and immature *TLC1* physically interact. 92
Figure 37: Termination factor binding sites in *TLC1*. 96
Figure 38: Abundance of *TLC1* transcripts according their 3´-end. 98
Figure 39: Model for *TLC1* and telomerase maturation in *S. cerevisiae*. 111
Figure 40: Model for *TLC1* maturation and telomere elongation in *S. cerevisiae* in the *cse1-1* mutant. 112

Table of tables

Table 1: List of consumable materials 25
Table 2: Kits used in this study 26
Table 3: Enzymes used in this study 26
Table 4: Antibodies used in this study 27
Table 5: Marker and standards used in this study 27
Table 6: Equipment and hardware used in this study 28
Table 7: Software used in this study 28
Table 8: *Escherichia coli* strain used in this study 29
Table 9: *Saccharomyces cerevisiae* strains used in this study 29
Table 10: Plasmids used in this study 31
Table 11: Oligonucleotides used in this study 32
Table 12: Oligonucleotides used for cloning and mutation via Mutagenic PCR 33
Table 13: Yeast cultivation and mating media 35
Table 14: PCR reaction mix composition 42
Table 15: PCR protocols 42
Table 16: Gibson Assembly reaction buffers 45
Table 17: qPCR reaction mixture 47
Table 18: qPCR cycler program 47
Table 19: Southern blot detection solutions 51
Table 20: Solutions for microscopic analysis 53
Table 21: Composition of SDS Polyacrylamide gels 56

1. Abstract

Telomere length homeostasis is a prerequisite for cell viability. It is challenged through successive shortening, which is due to the “end-replication-problem”. This limits the cellular life span in multicellular organisms enabling senescence and antagonizing unlimited growth, important for the prevention of cancer. Telomerases, are specialized and conserved enzymes, that evolved to counteract telomere shortening in stem and germ cells as well as in the single cell eukaryote *Saccharomyces cerevisiae,* through their reverse transcriptase activity. By using budding yeast as a model organism, we aimed to define the stepwise order in which the scaffolding telomerase RNA *TLC1* matures and how the telomerase ribonucleoparticle (RNP) is assembled. As shown earlier, first, an immature ~ 1.3 kb long precursor of *TLC1* is synthesized by RNAP II and the transcript is subsequently exported into the cytoplasm. Export occurs via Mex67-Mtr2 and Xpo1. Both transport factors do not contact the RNA directly but rather require adaptor proteins. In this work we have shown that the Mex67-adaptor Npl3 and the Xpo1 interacting m^7G-cap-binding factor Cbp20 contact *TLC1*. Furthermore, we confirm a model in which the Est- and Pop-protein loading as well as the association of the Sm-ring occurs in the cytoplasm. These proteins are important for the functionality of the enzyme as their correct assembly on *TLC1* is crucial for the reverse transcriptase activity, and thus for telomere elongation. Re-import of the pre-RNP into the nucleus is facilitated via the import receptor Mtr10. We identified a second *TLC1* import factor, Cse1, that supports nuclear re-import of pre-*TLC1* in an importin α independent pathway. Both import factors cooperate in the nuclear re-import of pre-*TLC1*, and we discovered additional functions for them in *TLC1* protection. Mutation of *CSE1* leads to the destabilization of the Sm-ring on *TLC1*, while mutation of *MTR10* leads to less mature *TLC1*, although the Sm-ring was bound properly. Both import receptors re-import *TLC1* through contact with the Sm-ring. Therefore, we suggest that this resembles a quality control step in the life cycle of *TLC1*, because only Sm-ring containing pre-*TLC1* RNPs can enter the nucleus. The re-imported pre-*TLC1* is subsequently trimmed by the nuclear exosome up to the Sm-ring to form the 1157 nt long mature *TLC1.* Maturation of *TLC1* is finalized by the trimethylation of the m^7G-cap, which prevents repeated Xpo1 contact and export. Unrevealing this stepwise maturation process helps to explain why and how immature *TLC1* does not disturb telomere maintenance before the mature and functional ribonucleoenzyme is assembled.

2. Introduction

In most eukaryotic organisms the genetic information is encoded on linear chromosomes. The storage, maintenance and the error-free as well as the complete replication of genetic information is a prerequisite for cell viability. However, the linear nature of chromosomes and the semi-conservative replication mechanism of DNA polymerase give rise to the fundamental problem of incomplete replication leading to successive shortening of chromosome ends, known as the "end-replication problem" (Olovnikov, 1973; Watson, 1972; Wynford-Thomas and Kipling, 1997). This limits the proliferation number of most cells to 40 to 60 replications, the Hayflick limit, before cells will either break down through programmed cell death or enter replicative senescence (Greider and Blackburn, 1989; Harley B. et al., 1990; Hayflick, 1965; de Lange et al., 1990; Lindsey et al., 1991). However, stem and germ cells as well as the yeast *Saccharomyces cerevisiae* (*S. cerevisiae*) overcome this limitation by expression of a specialized enzyme, the telomerase, which counteracts the successive shortening via elongation of the very end of the chromosomes, called telomeres (D'mello and Jazwinski, 1991; Harley B. et al., 1990; Hiyama and Hiyama, 2007; Levy et al., 1992). Interestingly, the telomerase is silenced in human somatic cells, which is mainly achieved by preventing expression of the catalytically active subunit hTERT (Meyerson et al., 1997; Yi et al., 2001). The absence of the telomerase should suppress tumor formation by the proliferation barrier of the cells (Maciejowski and De Lange, 2017). However, if tumor suppression fails, the unprotected telomere ends are linked via end-to end fusion resulting in genome instability (Maciejowski and De Lange, 2017). For genome re-stabilization, the telomerase is activated, however this leads to immortal cells which can be observed in over 85 % of cancer types (Armstrong and Tomita, 2017; Maciejowski and De Lange, 2017). In addition to telomerase-associated cancers, 10 - 20 % of cancers involve a recombination-based mechanism, called alternative lengthening of telomeres (ALT), to overcome the replication limit (Bryan et al., 1997; Conomos et al., 2013). Remarkably both elongation pathways might coexist (Perrem et al., 2001). The correct cellular telomerase concentration is crucial for cells. Too little and too much of the telomerase is critical. Thus, defects in its activity, maturation, or recruitment to the telomere ends can lead to cancer and other human diseases (Armanios and Blackburn, 2012; Calado and Young, 2009; Collins and Mitchell, 2002; Lim and Cech, 2021; McNally et al.,

2019; Nagpal and Agarwal, 2020). Overall skin abnormalities, bone marrow failure and brain malformation can be observed with high mortality rates (Armanios and Blackburn, 2012; Calado and Young, 2009; Collins and Mitchell, 2002; Lim and Cech, 2021; McNally et al., 2019; Nagpal and Agarwal, 2020). The telomerase represents an evolutionary conserved ribonucleoprotein (RNP) (Blackburn, 1992; Bosoy et al., 2003). Interestingly, in *S. cerevisiae*, no successive shortening of telomere ends is observed over time, which is achieved by the constitutive presence of the telomerase (D'mello and Jazwinski, 1991; Marcand et al., 2000; Vasianovich and Wellinger, 2017). Thus, *S. cerevisiae* is an excellent model organism to study the maturation of the telomerase.

2.1. Telomeres: essential nucleoprotein structures for viability

The very end of chromosomes consists of species-specific double-stranded repetitive DNA sequences which end in a 3´ single-stranded overhang, the G-overhang. These sequences act together with protein complexes to shelter the telomeric ends of chromosomes. Telomeres are organized as heterochromatin-like structures repressing transcription of adjacent genes, called telomere positioning or telomere silencing effect (Blackburn, 2001). The main function of telomeres is to cap chromosome ends and thus maintain integrity and stability of the genome by preventing the ends from being recognized as double strand breaks. Especially the single-stranded G-overhang resembles the structure of a double strand break that would trigger the DNA Damage Response and would lead to end-to-end fusions or prevention of cell division (Denchi and De Lange, 2007; Dewar and Lydall, 2012; Lowell and Pillus, 1998; Lydall, 2003; Palm and De Lange, 2008). Despite the overall conserved structure and function of telomeres in eukaryotes, sequences differ in structure and length between species (Armstrong and Tomita, 2017; Meyne et al., 1989; Rhodes and Giraldo, 1995). In yeast, two different types of telomeres are present, classified according to their subtelomeric regions into X and Y´ telomeres (Wellinger and Zakian, 2012). The X element (0.3 to 3.75 kb) is naturally present once in each telomere and is followed by 5'- $TG_{1\text{-}3}$ -3' repeats towards the chromosome end (Chan and Tye, 1983b, 1983a; Shampay et al., 1984). The Y' element is present in about half of all telomeres. Here, one to four copies of the Y´ element are present per telomere either in a short (5.2 kb) or a long (6.7 kb) form, followed by TG-repeats (Chan and Tye, 1983b, 1983a; Horowitz et al., 1984; Shampay et al., 1984). In yeast, the telomeric DNA consists of a

200 – 350 nucleotides long repetitive double-stranded DNA sequence represented by 5'- TG_{1-3} - 3' repeats and terminates with a 3' G-rich single-strand of 12 - 14 nucleotides (Figure 1), (Wellinger et al., 1993).

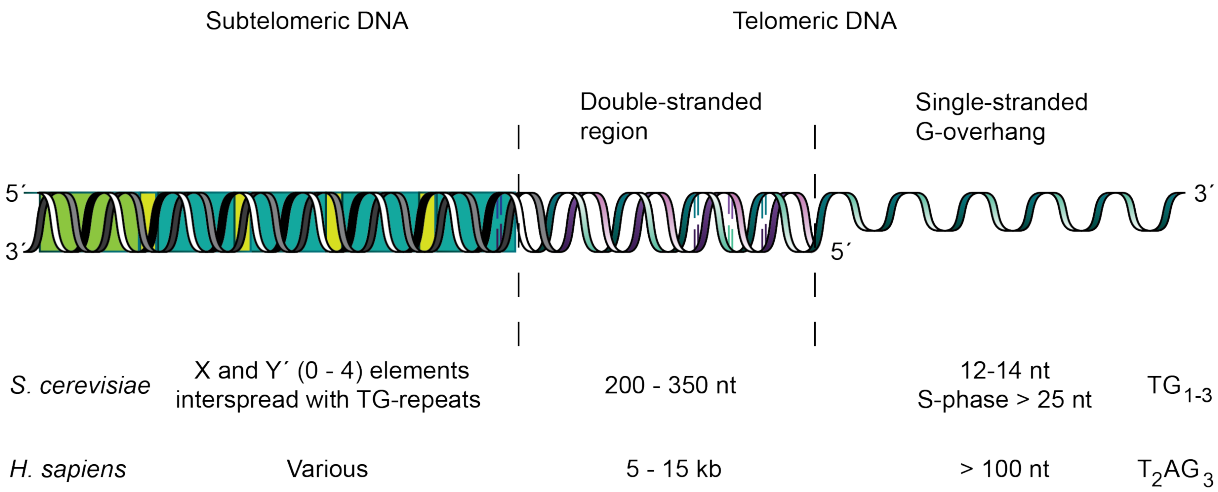

Figure 1: Schematic representation of subtelomeric and telomeric DNA.
The X element (green), the Y´ elements (turquoise) and the TG-repeats (light green) are indicated. (Adapted from Chakhparonian and Wellinger (2003).

2.2. Capping of telomere ends

Telomere ends undergo a regular switch between the capped state in which they are protected from recognition as a double-strand break, important for genome integrity, and an uncapped state allowing telomere elongation (Blackburn, 2001; Kupiec, 2014; Lim and Cech, 2021; Teixeira et al., 2004). The repetitive sequences of telomeres provide protein binding sites generating multimeric complexes. The composition and the amount of associated proteins determines how the cell senses and responds to changes at the ends of telomeres (Kupiec, 2014; Marcand et al., 1997). Three different complexes determine telomere fate, the telosome complex, the Yku complex and the CST complex (Figure 2).

The telosome complex consists of the Repressor/Activator site binding Protein (Rap1) and the Rap1-interacting Factor 1 and 2 (Rif1 and Rif2). The core protein Rap1 binds to telomeric dsDNA every 20 nt and acts as binding platform for accessory proteins (Conrad et al., 1990; Gilson et al., 1993; Gotta et al., 1996; Wotton and Shore, 1997).The telosome complex is found within the double stranded terminal TG-repeat sequence of telomeres (Wright et al., 1992). It protects the ends from resection but also controls overlengthening by limiting the association

of the telomerase via a Rap1/Rif1/Rif2-countening mechanism (Gallardo et al., 2011; Levy and Blackburn, 2004; Marcand et al., 1997; Teixeira et al., 2004; Wotton and Shore, 1997; Wright et al., 1992). In addition, Rap1 interacts with the Sir complex, composed of Sir2, Sir3 and Sir4, on centromere proximal telomeric repeats, which functions in telomeric silencing and telomere tethering to perinuclear regions (Bourns et al., 1998; Gilson and Géli, 2007; Gilson et al., 1993; Gotta et al., 1996; Kyrion et al., 1993; Mekhail and Moazed, 2010; Strahl-Bolsinger et al., 1997; Wotton and Shore, 1997).

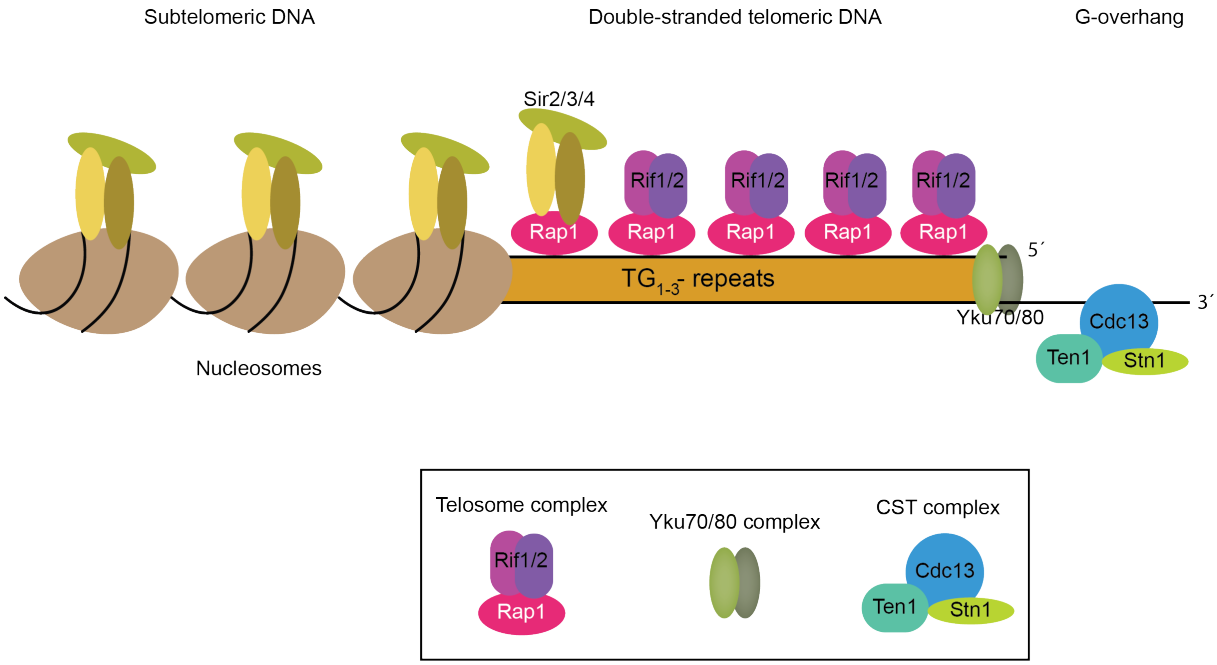

Figure 2: Schematic illustration of yeast telomeres in a capped status.
Schematic illustration of a yeast telomere showing the subtelomeric DNA covered with the Sir complex composed of the proteins Sir2/3/4. Terminal double-stranded TG-repeats are covered centromere proximally with Rap1 and the Sir complex and centromere distally with the telosome complex composed of Rap1, Rif1 and Rif2. The Yku heterodimer binds at the very end to telomeric dsDNA. The CST complex binds via Cdc13 to the terminal single-stranded telomeric G-overhang. Adapted from Gilson and Géli (2007) and Auriche et al. (2008).

The heterodimeric Yku complex, consisting of the proteins Yku70 and Yku80, binds directly to telomeric DNA (Gravel et al., 1998; Wellinger and Zakian, 2012). The complex protects the ends from degradation by exonucleases, inhibits Non Homologous End Joining (NHEJ) at telomeres and is involved in formation of telomeric heterochromatin (Boulton and Jackson, 1998; Gravel et al., 1998; Mishra and Shore, 1999; Polotnianka et al., 1998). However, it has a dual role, as it also functions in DNA repair mechanisms via NHEJ at non telomere regions both

in human and yeast (Boulton and Jackson, 1996b, 1996a; Fell and Schild-Poulter, 2015). Furthermore, the Yku complex is a feature of the active telomerase, important for telomerase tethering at telomeres (Chen et al., 2018; Fisher et al., 2004; Gallardo et al., 2008; Wellinger and Zakian, 2012). Its absence leads to short but stable telomeres (Boulton and Jackson, 1996b; Laroche et al., 1998; Peterson et al., 2001).

The third important complex is the CST complex composed of Cdc13, Stn1 and Ten1. The CST complex is crucial for telomere capping because it shelters the single stranded G-overhang (Churikov et al., 2013; Grandin et al., 2001a). The core component Cdc13 interacts with the single-stranded TG-repeats and acts as binding platform for Stn1 and Ten1 (Lin and Zakian, 1996; Nugent et al., 1996; Pennock et al., 2001). In addition to its capping function, the CST complex is involved in telomere replication and limits the telomerase mediated telomere elongation (Churikov et al., 2013; Gilson and Géli, 2007; Lim and Cech, 2021).

2.3. Telomere replication and telomerase mediated telomere elongation

Due to the semi-conservative replication mechanism of the DNA Polymerase two problems arise: First, the leading strand (C-rich strand) is replicated continuously resulting in a blunt ended strand. This is not accessible for the telomerase and the CST complex which both need a single-stranded G-overhang. For this reason, restoration of a single-stranded overhang is facilitated by C-rich strand resection and fill in synthesis (Dionne and Wellinger, 1998; Frank et al., 2006; Vodenicharov and Wellinger, 2006). Second, the lagging strand (G-rich strand) is replicated discontinuously and shortens about 4 - 8 nucleotides per cell cycle (Levy et al., 1992).

After replication is completed in late S phase, this shortening can be compensated via elongation of the G-rich strand by the telomerase (Lingner et al., 1995; Marcand et al., 2000). Thereby the telomerase is preferentially recruited to short telomeres via a Rap1/Rif1/Rif2-countening mechanism (Levy and Blackburn, 2004; Marcand et al., 1997; Teixeira et al., 2004). The single-strand DNA binding protein Cdc13 is the center for telomere length homeostasis. Cdc13 associates mutually exclusive with either Stn1 and Ten1 to assemble the CST complex, or interacts directly with Est1, which is crucial for telomerase loading onto the telomere (Chakhparonian and Wellinger, 2003; Churikov et al., 2013; Evans and Lundblad, 1999; Grandin et al., 1997, 2001a, 2001b; Nugent et al., 1996; Pennock et al., 2001; Teixeira et al.,

2004). Posttranslational modifications of Cdc13 regulate the interaction with Est1 and Stn1 (Li et al., 2009; Liu et al., 2014). The phosphorylation of Cdc13 and the increased abundance of Est1, both occurring in late S phase, restrict the association of functional telomerases to telomeres in that phase of the cell cycle (Chen et al., 2018; Li et al., 2009; Liu et al., 2014; Osterhage et al., 2006; Wu and Zakian, 2011). Telomere elongation by the telomerase is limited through the restoration the G-overhang and assembly of the CST complex on it (Gilson and Géli, 2007). The C-strand fill in synthesis finalizes telomere elongation and newly generated double-stranded TG-repeats are bound by Rap1 and cap the telomeres until the next replication round. The helicase Pif1 promotes the removal of the telomerase (Gilson and Géli, 2007).

2.4. The telomerase in *S. cerevisiae*

The telomerase represents an evolutionary conserved ribonucleoprotein (RNP) consisting of the telomerase RNA (*TLC1*) and accessory proteins, which was first identified in the model organism *Tetrahymena* in 1985 (Dandjinou et al., 2004; Greider and Blackburn, 1985). *TLC1* serves on the one hand as a scaffold on which the proteins assemble in an incompletely known order and it contains on the other hand a template sequence for telomere elongation (Singer and Gottschling, 1994; Zappulla and Cech, 2004). In yeast, the telomerase is constitutive present and consists of the Est and Pop proteins as well as the Sm-ring and possibly the Yku complex (Hughes et al., 2000; Lemieux et al., 2016; Lendvay et al., 1996; Lingner et al., 1997a; Peterson et al., 2001; Seto et al., 1999). Telomere elongation is facilitated by the reverse transcriptase action of Est2, which adds different numbers of $TG_{1\text{-}3}$ repeats to the telomeres at the end of the S phase (Blackburn, 1992; Lingner et al., 1997b; Marcand et al., 2000; Wellinger et al., 1993).

2.4.1. Telomerase RNA (*TLC1*)

TLC1 (TeLomerase Component 1) is located on chromosome II between the genes *EDS1* and *CHS2* on the sense strand and between the genes *SNR161* and *CSG2* on the antisense strand. Due to its size and genomic localization, *TLC1* belongs to the long non-coding RNAs and can be classified as intergenic as it does not overlap with adjacent genes. *TLC1* is transcribed by RNAP II and is expressed as an approximately 1.3 kb long transcript (Chapon et al., 1997; Singer and Gottschling, 1994). It is polyadenylated at its 3´-end and it receives a m^7G cap-structure at its 5´-end, as it is typical for mRNAs (Chapon et al., 1997; Seto et al., 1999). However, it also shares characteristics with snRNAs, because it contains a Sm-ring binding site and its m^7G cap is modified into a TMG-cap (Franke et al., 2008; Seto et al., 1999).

2.4.1.1. Structure and conserved regions of the telomerase RNA

Although the size of the telomerase RNA varies between different species between 150 nt in ciliates, 451 nt in human and 930 - 1300 nt in yeast, the template region and the core structures are conserved within several organisms (Figure 3), (Egan and Collins, 2012; Niederer and Zappulla, 2015). Conserved regions comprise the template region for repeat addition, the pseudoknot and template boundary element, as reserve transcriptase binding site, as well as the stem-terminus element for telomerase activity (Chen and Greider, 2004; Dandjinou et al., 2004; Egan and Collins, 2012; Lin et al., 2004).

Only 430 nucleotides of *TLC1* are essential, containing the template sequence, the Est1 and Est2 binding regions and the Sm-binding site (Coy et al., 2013; Hass and Zappulla, 2020; Livengood et al., 2002; Seto et al., 1999). Besides the Sm-binding site, other species-specific RNA stability elements can be found, such as the H/ACA motif in human cells (Figure 3), (Egan and Collins, 2012; Mitchell et al., 1999).

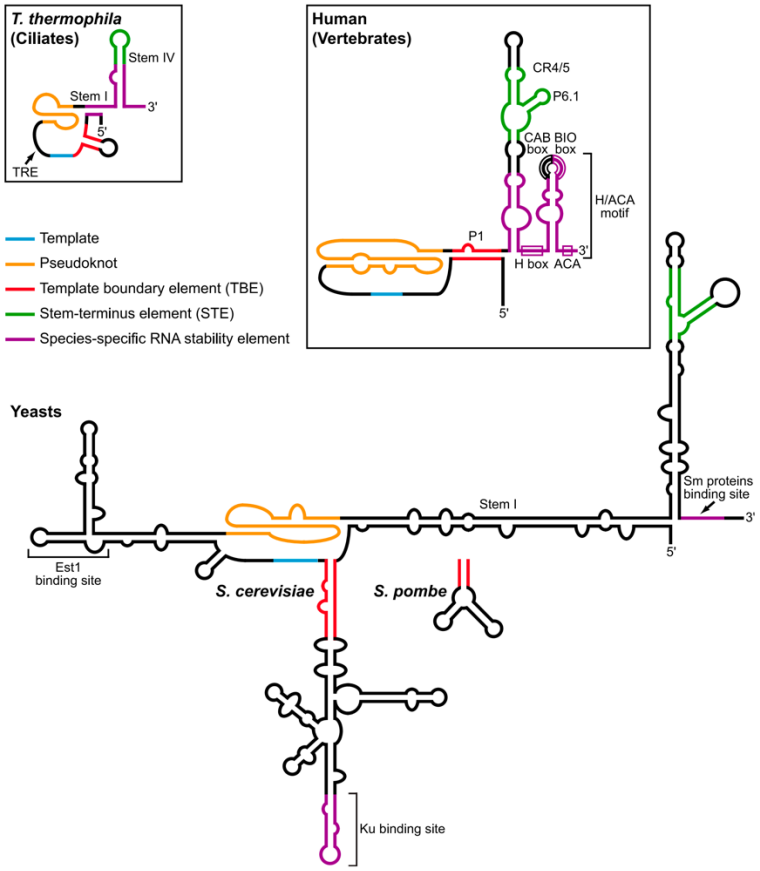

Figure 3: Secondary structure of ciliate, vertebrate and yeast telomerase RNA.
Structural elements are shown in orange and green. The reverse transcriptase binds to the pseudoknot (orange) and additionally to stem IV in ciliates and to the P6 stem in humans. The template region (blue), the template boundary element (red) and the protein binding sites as well as species specific RNA stability elements (purple) are indicated. Adopted from Egan and Collins (2012).

Only predicted secondary structure models are available for *TLC1* and the yeast telomerase, which suggest a flexible scaffold (Figure 4), (Dandjinou et al., 2004; Niederer and Zappulla, 2015; Zappulla and Cech, 2004, 2006). However, the Yku heterodimer was analyzed via crystallization and a part of *TLC1* was shown to participate in the Yku-*TLC1* interaction (Chen et al., 2018)

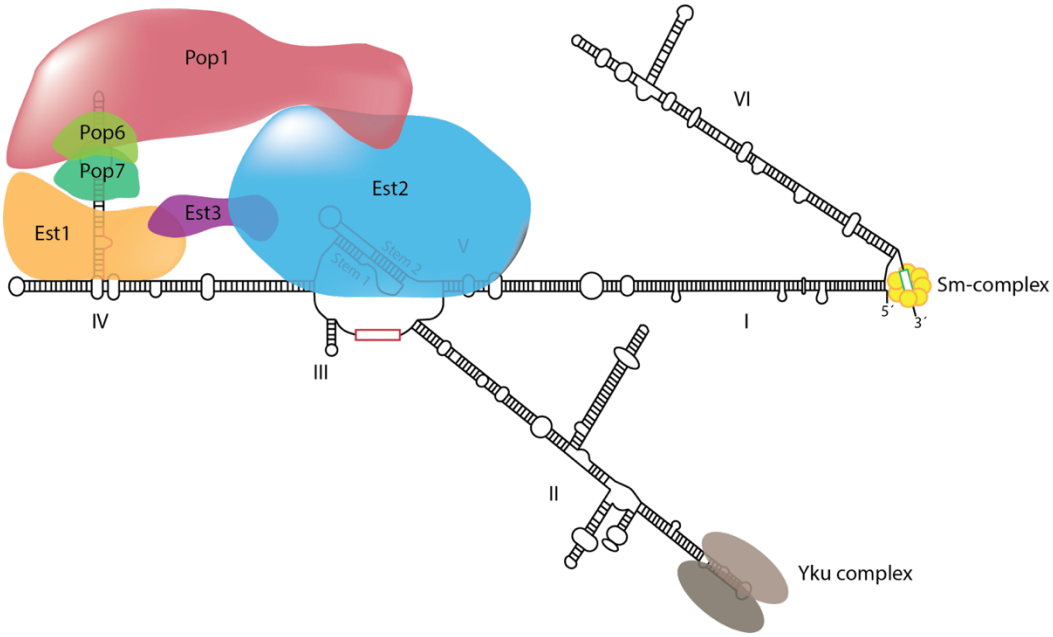

Figure 4: Predicted secondary structure of *TLC1* and the telomerase holoenzyme.
Binding of accessory proteins on the yeast telomerase is indicated. Overall, six stem domains (I – VI) are present in *TLC1*. Stem II is bound by the Yku heterodimer. The template region is indicated in red. Stem IV is essential for telomerase action *in vivo* as it severs as a binding platform for Est1. The catalytic center of *TLC1* is located in the pseudoknot, whose structure establishes interaction with Est2. For region VI, no interactions with proteins are known so far. The 3´-end of *TLC1* contains the Sm-binding site. Physical interactions of the Pop proteins with the Est proteins are hypothetical and modeled from interaction studies. Adapted from Laterreur et al.(2013) and Lemieux et al. (2016).

2.4.1.2. *TLC1* level and localization

TLC1 is a low abundant RNA with ~ 30 transcripts per cell (Mozdy and Cech, 2006). Transcription initiation of *TLC1* is cell-cycle regulated by both enhancer and suppressor elements that limit its expression to the transition between G1 and S phase (Chapon et al., 1997; Dionne et al., 2013). However, it is unclear whether the amount of *TLC1* varies between the cell-cycle phases (Fisher et al., 2004). *TLC1* is present in two distinct forms, a poly(A)$^+$ and a poly(A)$^-$ form, the latter of which is present in the functional telomerase, however the poly(A)$^+$ form may serve as precursor for the poly(A)$^-$ form (Chapon et al., 1997). Under normal conditions, about 80 to 90 % of *TLC1* are present in the mature, non-polyadenylated form (Chapon et al., 1997). Even though *TLC1* has a cytoplasmic phase during maturation, it is mainly present in the nucleus (Gallardo et al., 2008, 2011). In the G2 phase of the cell cycle *TLC1* is mainly located in the nucleolus to be separated from DNA repair mechanisms that occur in the G2/M phase (Ouenzar et al., 2017). So far it is unclear where, when and how the telomerase ends its life cycle (Vasianovich and Wellinger, 2017).

2.4.1.3. Transcription termination of RNAP II transcripts

In *S. cerevisiae*, transcription termination of RNAP II transcripts is mainly ensured by two termination machineries: The cleavage and polyadenylation factor (CPF)- cleavage factor (CFI)-complex, that is mainly responsible for the termination of mRNAs and transcripts larger than 1 kb and the Nrd1-Nab3-Sen1 (NNS) complex, mainly responsible for the termination of non-coding transcripts smaller than 1 kb (Birse et al., 1998; Connelly and Manley, 1988; Creamer et al., 2011; Jamonnak et al., 2011; Larochelle et al., 2018; Porrua and Libri, 2015; Proudfoot, 1989; Richard and Manley, 2009).

In the CPF-CFI complex mediated transcription termination, species specific sequences in a 3´ untranslated region of a transcript are recognized by components of the CPF-CFI complex. This results in RNAP II pausing and is followed by endoribonucleolytic cleavage of the nascent transcript via Ysh1 (Porrua and Libri, 2015). The upstream cleavage product leaves a free hydroxyl group at the 3´-end which is polyadenylated via Pab1 whereas the downstream cleavage product is degraded (Porrua and Libri, 2015).

In the NNS complex mediated transcription termination, the NNS complex is recruited to specific Nrd1 and Nab3 binding motifs of the transcript via interaction of Nrd1 with RNAP II (Conrad et al., 2000; Creamer et al., 2011; Porrua and Libri, 2015; Steinmetz et al., 2001). Sen1 is loaded independently onto the nascent transcript and through ATP hydrolysis catches up to RNAP II enabling the cleavage of the transcript (Porrua and Libri 2015). The Nrd1-Nab3 bound transcript subsequently interacts with the TRAMP (Trf4-Air2-Mtr4) complex which promotes oligoadenylation of the transcript and leads either to degradation or processing by the exosome (Han et al., 2020; LaCava et al., 2005; Porrua and Libri, 2015; Tudek et al., 2018; Vasiljeva and Buratowski, 2006; Villa et al., 2020; Wyers et al., 2005). Sen1 seems to be the limiting factor as its presence is cell cycle regulated (Mischo et al., 2018).

As *TLC1* possesses both termination site types (Figure 5), two different transcription termination models exist for *TLC1*. On the one hand mature poly(A)$^-$ *TLC1* might be generated via processing of the poly(A)$^+$ precursor, generated via CPF-CFI mediated transcription termination (Chapon et al., 1997; Coy et al., 2013). On the other hand poly(A)$^-$ *TLC1* might be generated directly via transcription termination by the NNS complex and might subsequently be assembled to a telomerase (Jamonnak et al., 2011; Noël et al., 2012). Up to date it is unclear which termination pathway leads to functional *TLC1*.

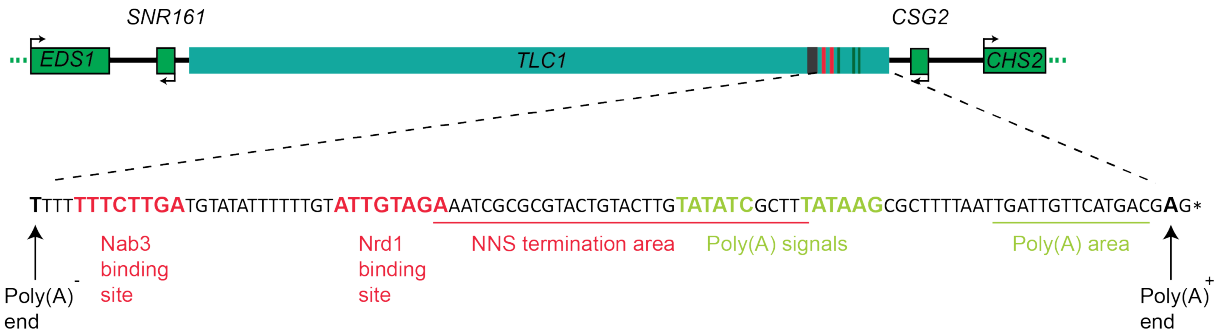

Figure 5: Genomic localization and transcription termination sites in *TLC1*.
TLC1 is localized between the genes *EDS1* and *CHS2* on the sense strand and between *SNR161* and *CSG2* on the antisense strand. Nab3 and Nrd1 binding sites of the NNS complex are indicated in red and are followed by the NNS termination area (adopted from Jamonnak et al. (2011)). Poly(A) signals are indicated in green and are followed by the poly(A) termination area (adopted from Chapon, Cech, and Zaug (1997)).

2.4.1.4. 5´- and 3´-end processing of *TLC1*

Both the 5´-end and the 3´-end of pre-*TLC1* are processed to obtain a mature TMG-capped, 1157 nt long *TLC1* transcript (Bosoy et al., 2003; Chapon et al., 1997; Coy et al., 2013; Franke et al., 2008; Hass and Zappulla, 2020; Seto et al., 1999). The m^7G cap at the 5´-end of nascent mRNAs and snRNAs is directly bound by the heterodimeric cap binding complex (CBC), consisting of Cbp20 and Cbp80 (Baejen et al., 2014; Izaurralde et al., 1995; Lewis and Izaurralde, 1997; Schwer et al., 2011). Additionally, loading of the guard protein Npl3 occurs co-transcriptional on mRNAs as it interacts with the RNAP II and the CBC (Lei et al., 2001; Shen et al., 2000). Both, the CBC and Npl3 function in mRNA control and direct the transcript to export or degradation (Das et al., 2000; Gilbert et al., 2004; Lei et al., 2001; Lewis and Izaurralde, 1997; Liu et al., 1999; Moehle et al., 2012; Shen et al., 2000; Zander et al., 2016). Although *TLC1* is like mRNAs produced by RNAP II and receives an m^7G cap, it is unclear whether *TLC1* contacts the CBC or Npl3.

In yeast, the hypermethylation of the m^7G cap to a 5'-2,2,7- trimethylguanosine (TMG) cap occurs via the trimethylguanosine synthase I (Tgs1) in the nucleolus (Franke et al., 2008; Mouaikel et al., 2002; Seto et al., 1999). So far it is assumed that TMG-capping occurs prior to export (Gallardo et al., 2008; Garcia et al., 2020; Wu et al., 2014). However, it was shown that preferentially monomethylated RNAs are contacted by the CBC, enabling export, and that the Sm-binding is important for the hypermethylation (Hamm and Mattaj, 1990; Mouaikel et al.,

2002; Plessel et al., 1994; Schwer et al., 2011). In fact, TMG-capping was recently shown to finalize maturation of snRNAs after a cytoplasmic loading of the Sm-ring and re-import into the nucleus (Becker et al., 2019), which might also be true for *TLC1*. In particular, the interaction between the Smb1 protein and Tgs1 *in vitro* and *in vivo* is suggested to guide the transcript into the nucleolus for TMG-cap formation (Becker et al., 2019; Mouaikel et al., 2002). Moreover, the telomere length is increased in *tgs1Δ* cells, which is associated with premature aging in yeast represented by a shortened replicative lifespan, and possibly with carcinogenesis in humans, highlighting the importance of this processing step (Austriaco and Guarente, 1997; Chen et al., 2020; Franke et al., 2008).

TLC1 is generated as a 3´-extended poly(A)$^+$ transcript which has to be trimmed up to the Sm-binding site, probably via the nuclear exosome, resulting in mature poly(A)$^-$ *TLC1* (Chapon et al., 1997; Coy et al., 2013; Hass and Zappulla, 2020; Seto et al., 1999). However, recent results suggested that the poly(A)$^-$ form might be generated directly by transcription termination of *TLC1* through the NNS complex (Jamonnak et al., 2011; Noël et al., 2012).

2.4.2. Accessory proteins

2.4.2.1. Est proteins

The "ever shorter telomeres" proteins, Est1, Est2 and Est3 are essential for the *in vivo* function of the telomerase, but Est2 is sufficient for telomerase action *in vitro* as it is the catalytically active subunit (Lendvay et al., 1996; Lingner et al., 1997b, 1997a). Loss of any Est protein or Cdc13 leads to progressive telomere shortening and senescence, but some cells escape by switching to a recombination-based telomere lengthening mechanism, after approximately 75 to 100 generations (Chen et al., 2001; Le et al., 1999; Lendvay et al., 1996; Lingner et al., 1997a; Lundblad and Szostak, 1989).

Est1 is a cell-cycle regulated protein, essential for the interaction of Est2 and Est3 with the telomerase (Osterhage et al., 2006; Taggart et al., 2002). The transcription of *Est1* is induced at the transition of G1 to S phase, as it is the case for *TLC1* (Chapon et al., 1997; Dionne et al., 2013; Taggart et al., 2002). Interestingly, the protein is regulated via proteasome-specific degradation during the G1 phase and thus restrict the association of Est1 with *TLC1* to the S phase (Lin et al., 2015; Osterhage et al., 2006; Taggart et al., 2002). Binding of Est1 to *TLC1* is likely stabilized by direct interaction of one or more Pop proteins (Garcia et al., 2020; Laterreur

et al., 2018; Lemieux et al., 2016). Although, overexpression of Est1 in G1 phase leads to formation of a *per se* functional telomerase RNP and recent studies suggest an early assembly of Est1 onto *TLC1*, no telomere elongation was observed, suggesting additional regulatory mechanisms that restrict telomere lengthening to S phase (Marcand et al., 2000; Osterhage et al., 2006; Tucey and Lundblad, 2013). Est1 interacts directly with Cdc13 which recruits the telomerase to telomere ends, which is crucial for telomere elongation (Churikov et al., 2013; Evans and Lundblad, 1999; Li et al., 2009; Wu and Zakian, 2011). However, the interaction between Est1 and Cdc13 occurs only after phosphorylation of Cdc13 in the S phase (Li et al., 2009; Liu et al., 2014).

The catalytically active subunit Est2 can interact with *TLC1* and with telomeres throughout the cell-cycle (Chan et al., 2008; Taggart et al., 2002; Vasianovich et al., 2019). In the G1 and G2 phase of the cell-cycle the interaction of the Est2 with the telomeres is transient and is facilitated through the interaction of Yku bound *TLC1* with the Sir complex (Chen et al., 2018; Ge et al., 2020; Vasianovich et al., 2019). The Est2-*TLC1* subcomplex is suggested to be activated by Est1 and Est3 binding in late S phase (Chen et al., 2018; Ge et al., 2020). However, the assembly of the telomerase was suggested to occur in the cytoplasm and re-import is facilitated as holoenzyme (Gallardo et al., 2008; Garcia et al., 2020; Wu et al., 2014).

Unlike Est1 and Est2, Est3 does not bind directly to *TLC1*, but interacts with Est2 and Est1 (Tuzon et al., 2011; Vasianovich et al., 2019). Thus the association of Est3 to the telomerase is indirectly limited to the S phase by the amount of Est1 (Hughes et al., 2000; Osterhage et al., 2006; Tucey and Lundblad, 2014; Tuzon et al., 2011; Vasianovich et al., 2019). The function of Est3 has not yet been fully elucidated (Vasianovich et al., 2019).

2.4.2.2. Pop proteins

The Pop proteins are well studied components of the conserved RNase MRP and the RNase P complexes required for rRNA and tRNA processing, respectively (Chamberlain et al., 1998; Chu et al., 1994; Esakova and Krasilnikov, 2010; Hopper and Nostramo, 2019; Lygerou et al., 1994). The RNase MRP and RNase P complexes contain seven Pop proteins (Salinas et al., 2005). Recently, an association of Pop1, Pop6 and Pop7 with the telomerase RNP was discovered (Laterreur et al., 2018; Lemieux et al., 2016). The Pop1 protein is mainly localized to the nucleolus, but nuclear staining and small cytoplasmic foci during mitosis were also observed

(Gill et al., 2006). This mainly nucleolar localization is most likely due to the function of RNase MRP in ribosome biogenesis. Binding of Pop6 and Pop7 to *TLC1* is facilitated via stem IV and may serve as binding platform for Pop1 (Figure 4), (Laterreur et al., 2018; Lemieux et al., 2016). Overall, the Pop proteins are required for a stable association of Est1 and Est2 on the telomerase and nuclear localization of *TLC1* (Garcia and Zakian, 2020; Garcia et al., 2020; Laterreur et al., 2018; Lemieux et al., 2016). However, they seem to be dispensable for the secondary structure of *TLC1* in contrast to the RNA of the RNase MRP complex (Garcia et al., 2020). Recently, a cytoplasmic mislocalization of *TLC1* was observed in *POP* deficient mutants, suggesting a cytoplasmic loading of the Pop proteins onto *TLC1* (Garcia et al., 2020). Whether they have additional functions in telomerase and telomere biology requires further investigation.

2.4.2.3. The Sm-ring in *TLC1* maturation and RNP biogenesis

The Sm-ring is a conserved heptametric complex (Sm_7 complex), which consist of the proteins Smb1, Smd1, Smd2, Smd3, Sme1, Smx2 and Smx3, and is essential for vegetative growth (Coy et al., 2013; Matera and Wang, 2014; Pettersson et al., 1984; Séraphin, 1995). The Sm-proteins contain an RNA-binding domain and a Sm-domain which has hydrophobic amino acids essential for protein-protein interactions (Camasses et al., 1998; Collins et al., 2003; Hermann et al., 1995; Li et al., 2016; Schwer et al., 2016). The Sm-ring assembly around the RNA occurs via both types of interactions, protein-protein and protein-RNA interactions (Collins et al., 2003; Li et al., 2016; Schwer et al., 2016). The loading of the Sm-ring onto snRNAs is facilitated in the cytoplasm and essential for functional snRNAs and spliceosome formation (Becker et al., 2019; Matera and Wang, 2014). Sm-ring loading is also a prerequisite for a functional telomerase, as loss of the proteins or the binding site leads to drastic reduction in *TLC1* level and telomere shortening (Coy et al., 2013; Seto et al., 1999). In addition, the Sm-ring binding site determines the 3´-end of mature *TLC1* (Hass and Zappulla, 2020). It has recently been suggested to associate also with *TLC1* in the cytoplasm (Vasianovich et al., 2020). In fact, the re-import of snRNAs proceeds through interaction of Smb1 with Cse1, which may also be true for *TLC1* (Becker et al., 2019).

2.5. Assumed lifecycle of *TLC1* and the telomerase

In current models, a cell cycle-dependent assembly of the telomerase is assumed, since telomerase activity occurs only in the late S phase, after conventional replication is accomplished (Diede and Gottschling, 1999; Dionne and Wellinger, 1998; Marcand et al., 2000; Taggart et al., 2002; Wellinger et al., 1993). Transcription initiation of *TLC1* is regulated by both enhancer and suppressor elements and occurs at G1 - S phase transition (Chapon et al., 1997; Dionne et al., 2013). Two opposing models are discussed for transcription termination. Either *TLC1* is generated as a ~ 1.3 kb long polyadenylated precursor, poly(A)$^+$, via termination by the CPF-CFI complex or directly as mature *TLC1* form, poly(A)$^-$, via termination by the NNS complex (Chapon et al., 1997; Coy et al., 2013; Jamonnak et al., 2011; Noël et al., 2012). After transcription, the pre-*TLC1* contains a m^{7}G cap at its 5'-end (Figure 6), (Seto et al., 1999). So far it was assumed that the Sm-ring loading occurs in the nucleus (Gallardo et al., 2008; Wu et al., 2014). Thereafter 3´-end processing by the nuclear exosome shortens the transcript, which is subsequently directed into the nucleolus, for TMG-capping (Franke et al., 2008; Gallardo et al., 2008; Mouaikel et al., 2002; Seto et al., 1999). Export of *TLC1* into the cytoplasm is mediated via Mex67-Mtr2 and Xpo1 (Gallardo et al., 2008; Wu et al., 2014). Loading of *TLC1* with the Est proteins occurs in the cytoplasm, as the absence of the Est proteins leads to mislocalization of *TLC1* to the cytoplasm and the absence of the *TLC1* export receptors leads to the mislocalization of Est1 and Est2 to the cytoplasm (Gallardo et al., 2008; Wu et al., 2014). Recently, it was suggested that loading of the Sm-ring and the Pop proteins might also occur in the cytoplasm, because *TLC1* mislocalizes to the cytoplasm in *POP* or Sm-protein deficient mutants (Garcia et al., 2020; Vasianovich et al., 2020). The compartment in which the Yku complex is loaded onto *TLC1* is unclear. After RNP formation, re-import is mediated via Mtr10 and Kap122 (Ferrezuelo et al., 2002; Gallardo et al., 2008). Functional telomerase are recruited to telomere ends through interaction between Cdc13 and Est1 that in turn interacts indirectly with Est2, which mediates telomere elongation through its reverse transcriptase function in late S phase of the cell-cycle (Li et al., 2009; Lingner et al., 1997b; Marcand et al., 2000; Taggart et al., 2002; Wu and Zakian, 2011)

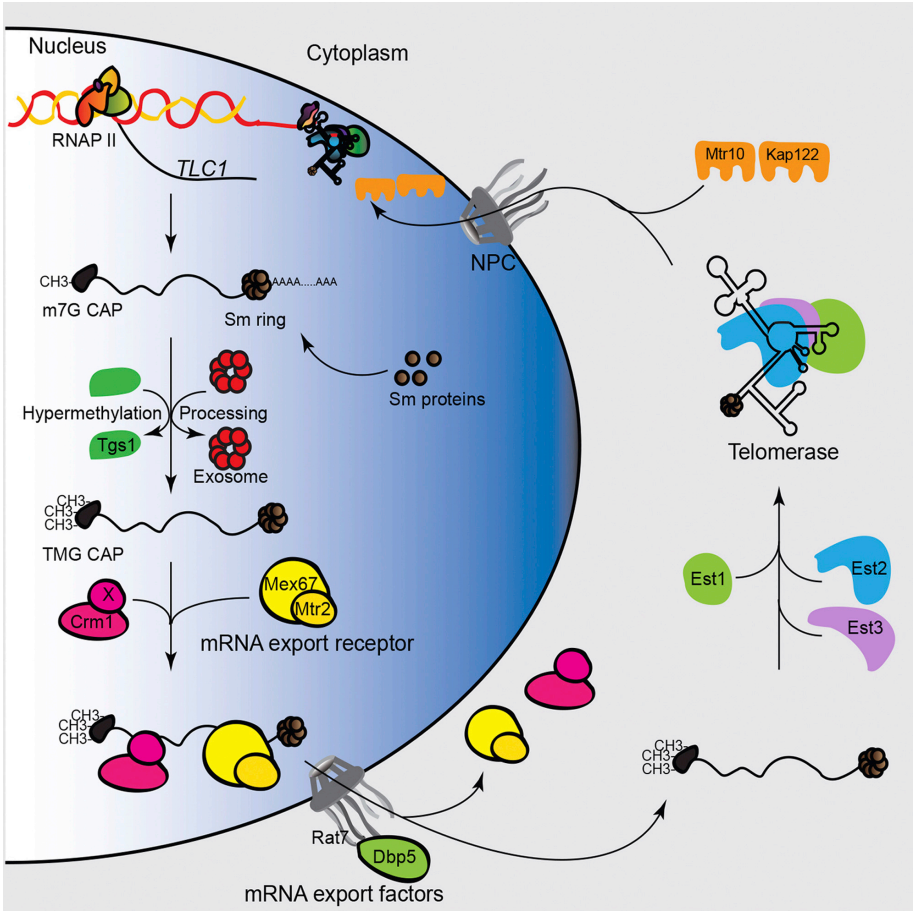

Figure 6: Current model of *TLC1* processing and telomerase assembly in *S. cerevisiae*.
TLC1 is generated by RNAP II. After transcription, the m^7G capped pre-*TLC1* is trimmed at its 3´-end via the nuclear exosome and is guided to the nucleolus for TMG-capping. In the model, Sm-ring loading is indicated to occur in the nucleus, however was recently suggested to occur in the cytoplasm (Vasianovich et al., 2020). The 3´-trimmed and 5´ TMG-capped RNA is exported to the cytoplasm by Mex67-Mtr2 and Xpo1 (Crm1). The export receptor Xpo1 associates with *TLC1* via a currently unknown protein (X). Dbp5 displaces the export receptor Mex67-Mtr2 at the cytoplasmic site of the NPC. Dissociation of Xpo1 from the cargo is facilitated via Ran-GTP hydrolysis. After cytoplasmic loading of the Est proteins the telomerase is re-imported by Mtr10 and possibly also Kap122. Adopted from Wu et al., (2014).

Even though the current model contains certain important points, there are still some open questions, in particular the precise order of the processing steps. To begin with, it is not known whether adaptor proteins between *TCL1* and Mex67 and Xpo1 are required for nuclear export. Mex67 can interact directly with RNAs under stress conditions, but contacts mRNAs through the SR-like proteins under normal circumstances (Hackmann et al., 2014; Zander and Krebber, 2017; Zander et al., 2016). Furthermore, Xpo1 (Crm1 in human) contacts either directly or indirectly the cap binding complex (CBC) for nuclear export of snRNAs in yeast, which in humans is facilitated via the adaptor protein PHAX (Becker et al., 2019; Izaurralde et al., 1995;

Ohno et al., 2000). So far, no PHAX homolog in *S. cerevisiae* is known. And additionally, it is not known whether *TLC1* binds to the CBC that contacts Xpo1. The CBC recognizes the m^7G-cap of RNAP II transcripts (Hamm and Mattaj, 1990; Izaurralde et al., 1995; Lewis and Izaurralde, 1997; Schwer et al., 2011). This argues for a TMG-capping after re-import as it would terminate repeated nuclear export via Xpo1. Additionally, the Sm-ring is essential for trimming of *TLC1* (Coy et al., 2013; Hass and Zappulla, 2020). Thus, it should be associated before the exosomal attack occurs. Moreover, the Sm-ring presumably guides the transcript to the nucleolus through interaction between Smb1 and Tgs1 (Becker et al., 2019; Mouaikel et al., 2002). In fact, for snRNAs, TMG-capping was recently shown to finalize maturation after a cytoplasmic loading of the Sm-ring and re-import into the nucleus (Becker et al., 2019). This could also be true for *TLC1*. The cytoplasmic loading of the Sm-ring was not reported in the beginning of this study, but a recent study of Vasianovich, Bajon, and Wellinger (2020) supports the idea of a cytoplasmic loading of the Sm-ring, which we suspected from the data of Becker et al. (2019) earlier. Additionally, this would suggest that 3´-trimming as well as TMG-capping occurs after re-import. Furthermore, the suggested cytoplasmic loading of the Pop proteins onto *TLC1* was not known in the beginning of this study and indicates a holoenzyme formation prior to re-import as suggested earlier (Garcia et al., 2020; Wu et al., 2014).

2.6. Recombination based telomere elongation

Absence of the telomerase leads to gradual telomere shortening and senescence (Lendvay et al., 1996; Lundblad and Szostak, 1989). However, loss of the telomerase is not lethal *per se*, instead, some cells escape senescence by using a recombination-based mechanism to lengthen telomere ends, termed Type I and Type II survivor (Figure 7), (Chen et al., 2001; Le et al., 1999; Lundblad and Blackburn, 1993; Teng and Zakian, 1999). In this process, factors that are normally used for DNA repair are utilized for telomere lengthening (Chen et al., 2001; Hu et al., 2013; Kockler et al., 2021; Nugent et al., 1998). Rad52 and its homolog Rad59 are essential for the generation of both types (Chen et al., 2001; Lundblad and Blackburn, 1993). The formation of Type I survivor starts with a Rad51/Rad52 dependent strand invasion and needs additionally Rad54 and Rad57 for Y´ element amplification, however leads to very short $TG_{1\text{-}3}$ repeats (Chen et al., 2001; Le et al., 1999; Teng and Zakian, 1999). In contrast, the

formation of Type II survivors depends on the helicase Sgs1, Rad50, Rad59 and the MRX complex, using the TG-repeats for recombination, resulting in a heterogenous pattern of long tracs of TG_{1-3} repeats and only slight Y´ amplification (Chen et al., 2001; Le et al., 1999; Teng and Zakian, 1999). Recently, it has been suggested that both pathways are consecutive steps in an unified survivor pathway which can lead to Type I/Type II hybrids (Kockler et al., 2021). Here, the Rad51-dependent strand invasion and DNA damage checkpoint activation leads to a pre-survivor precursor which is subsequently processed via an Rad59/Rad52-dependent pathway to stabilize the telomeres, resulting in either Type I or Type II survivors (Kockler et al., 2021). However, Type I survivors which have short telomere ends can also be elongated via the Rad59/Rad52 pathway leading to hybrid chromosome ends (Kockler et al., 2021). In human, survivor cells are called ALT (alternative lengthening of telomeres) cells, and resemble the yeast Type II survivors (Bryan et al., 1997; Nabetani and Ishikawa, 2011). Recombination and telomerase based telomere maintenance are both equally efficient in terms of cell survival and genome stability, yet telomerase deficient strains possess a shorter replicative life span (Chen et al., 2009).

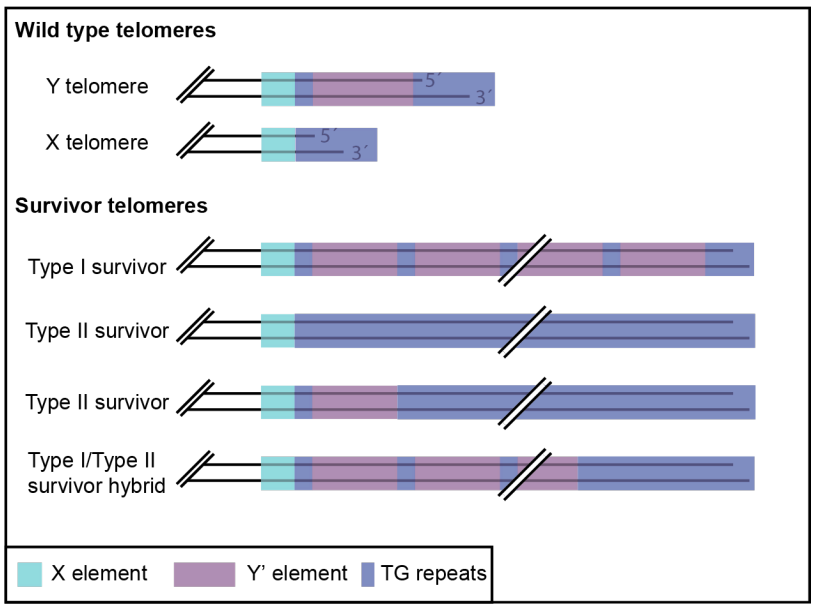

Figure 7: Different classes of functional telomeres in *S. cerevisiae*.
Natural occurring telomeres in wild type cells are X and Y telomeres that both contain one X element. Y´ telomeres contain 1 to 4 Y´ elements in addition to the X element. Upon depletion of a functional telomerase or capping of telomeres, Type I and Type II survivor cells can arise upon a recombination mediated telomere elongation. Type I survivor contain multiple Y´ elements whereas Type II survivor harbor increased TG-repeat sequences. The Type I/Type II hybrid can be formed via cooperative function of both recombination pathways. Adapted from Lydall (2003) and Kockler, Comeron, and Malkova (2021).

2.7. Nucleo-cytoplasmic transport

Nucleo-cytoplasmic transport occurs through bilateral gateways, the nuclear pore complexes (NPC) (Köhler and Hurt, 2007; Strambio-De-Castillia et al., 2010; Wälde and Kehlenbach, 2010). They have an octagonally symmetrical cylinder composed of multiple ring structures and possess a nuclear basket and cytoplasmic filaments. The interior of the NPC is highly hydrophobic, to prevent the diffusion of large cargos. Hydrophobicity is achieved by the FG (phenylalanine-glycine)-repeats of the nucleoporins (Nups) (Wälde and Kehlenbach, 2010). Small molecules can passively diffuse through the NPCs, whereas the transport of larger cargoes require transport receptors, either karyopherins, or Mex67-Mtr2 (Köhler and Hurt, 2007; Sloan et al., 2016; Wälde and Kehlenbach, 2010).

2.7.1. Mex67-Mtr2 mediated transport

The heterodimer Mex67-Mtr2 is conserved from yeast to human (Katahira et al., 1999). Mex67 (TAP in human), together with Mtr2 (p15 in human), contributes to the export of pre-ribosomal particles, mediates export of mRNAs and is involved in the export of the long non-coding RNA *TLC1* (Gallardo et al., 2008; Köhler and Hurt, 2007; Sloan et al., 2016; Wu et al., 2014). Mex67 can bind directly to mRNAs under stress conditions (Zander et al., 2016). However, mRNAs are normally loaded co-transcriptionally with quality control factors (Hackmann et al., 2014; Hurt et al., 2004; Lei et al., 2001; Zander et al., 2016). The SR-like proteins Npl3, Gbp2 and Hrb1, retain the RNA in the nucleus until the quality control of the RNA is completed (Hackmann et al., 2014; Zander et al., 2016). Faulty transcripts are then guided to degradation while correct mRNAs are exported through the binding of Mex67 to the SR-like proteins (Hackmann et al., 2014; Zander et al., 2016). Correctness of assembled mRNPs is controlled via Mlp1 that is located at the nuclear basket and export is only supported when the retention factors are covered with Mex67 (Zander and Krebber, 2017). On the cytoplasmic site, Mex67-Mtr2 is released from the mRNP by the DEAD box RNA helicase Dbp5/Rat8 via ATP-hydrolysis which creates directionality (Folkmann et al., 2011; Kelly and Corbett, 2009; Tieg and Krebber, 2013).

2.7.2. Karyopherin mediated transport

Transport of proteins is mediated by karyopherins which bind to specific localization signals present in the proteins. Proteins which harbor a nuclear localization signal (NLS) are imported via importins and proteins bearing a nuclear export signal (NES) are exported via exportins (Figure 8). Thus the karyopherins are classified according to the directionality in which they operate, however bidirectional transporters are also known (Becker et al., 2019; Yoshida and Blobel, 2001). Karyopherins share a similar architectural structure and harbor an N-terminal Ran-GTP (Gsp1-GTP in yeast) binding domain. They contain multiple HEAT repeats (huntingtin, elongation factor 3, the A subunit of PP2A, and TOR1) which are necessary for the interaction with the FG-repeats of the Nups (Macara, 2001). So far, 14 different karyopherins have been identified in yeast and 19 in mammalian cells (Chook and Süel, 2011; Güttler and Görlich, 2011). Directionality is mediated by a Ran-GTP/-GDP gradient, with high Ran-GTP and low Ran-GDP concentration in the nucleus and vice versa in the cytoplasm (Moore and Blobel, 1994; Sloan et al., 2016). The guanine nucleotide exchange factor (GEF), termed RCC1 (Prp20 in yeast) exchanges GDP with GTP in the nucleus (Bischoff and Ponstingl, 1991; Sloan et al., 2016). The GTPase activating protein (GAP), termed Ran-GAP (Rna1 in yeast) stimulates the hydrolysis of GTP to GDP in the cytoplasm (Bischoff et al., 1994, 1995; Hopper et al., 1990; Sloan et al., 2016). This, and the active re-import of Ran-GDP through NTF2 (Ntf2 in yeast), maintains a high Ran level in the nucleus and the GTP/GDP gradient (Ribbeck et al., 1998; Sloan et al., 2016).

For protein export, the exportin simultaneous binds the cargo and Ran-GTP in the nucleus. Interaction with FG-repeats of the inner hydrophobic layer allow the passage. CRM1 (Xpo1 in yeast) exports proteins with classical NES signals and is furthermore involved in the transport of the telomerase RNA *TLC1* in yeast (Fornerod et al., 1997; Wu et al., 2014). Cargo release is mediated via Ran-GAP stimulated Ran-GTP hydrolysis at the cytoplasmic site and remodeling of the complex via RanBP1 (Yrb1 in yeast) (Bischoff and Görlich, 1997; Kehlenbach et al., 1999; Sloan et al., 2016). The exportin translocates back to the nucleus and the re-import of Ran-GDP via NTF2 maintains the high Ran level in the nucleus (Görlich et al., 2003; Ribbeck et al., 1998).

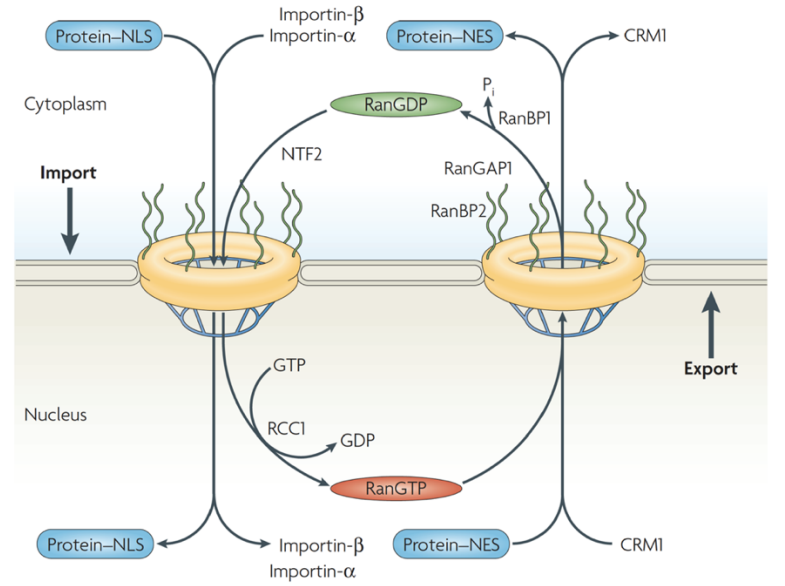

Figure 8: Karyopherin mediated nucleo-cytoplasmic transport and the Ran cycle.
High nuclear Ran-GTP concentration is generated by nucleotide exchange via RCC1 (yeast Prp20). For nuclear protein export Ran-GTP binds to a NES-containing protein and CRM1 (yeast Xpo1). Cargo release is facilitated at the cytoplasmic site via Ran-GAP (yeast Rna1) stimulated GTP hydrolysis and remodeling of the complex via RanBP1 and presumably RanBP2. The exportin is recycled and Ran-GDP is re-imported via NTF2 (Ntf2 yeast). Due to active re-import, the concentration of Ran is increased in the nucleus. For nuclear import, importin β binds to NLS containing proteins mostly using of importin α as adaptor protein. Binding of Ran-GTP to the import complex facilitates disassembly in the nucleus and re-export of importin α occurs via CAS (yeast Cse1) (not shown). Adopted from Clarke and Zhang (2008).

Most karyopherins do not need an adaptor protein but bind directly to their cargos, however protein import via importin β requires mostly the binding of importin α (Srp1 in yeast) as an adaptor (Conti et al., 1998; Görlich et al., 1996; Lott and Cingolani, 2011). After translocation and cargo release, Srp1 is recycled via Cse1 (CAS in human), which is associated with Gsp1-GTP in an open conformation in the nucleus (Hood and Silver, 1998; Kutay et al., 1997; Solsbacher et al., 1998). After transport to the cytoplasm, the complex of Cse1, Gsp1-GTP and Srp1 is resolved through GAP-stimulated hydrolysis of Gsp1-GTP, resulting in a closed conformation of Cse1 and release of its cargo (Cook et al., 2005; Sloan et al., 2016). So far, Cse1 has been described as classical export receptor that cannot interact with importin α in its cytoplasmic form in which it has an closed conformation (Cook et al., 2005; Hood and Silver, 1998; Solsbacher et al., 1998). However, Cse1 was recently shown to be involved in the re-import of snRNAs via interaction with Smb1, revealing a novel function as bidirectional transport factor (Becker et al., 2019).

The importin β like karyopherin, Mtr10 (Transportin SR in human) is involved in re-import of the SR-like protein Npl3 in yeast and shuttling SR-proteins in humans (Lai et al., 2000, 2001; Pemberton et al., 1997; Senger et al., 1998). In addition, it is known to be required for the re-import of *TLC1* and retrograde import of tRNAs in yeast (Ferrezuelo et al., 2002; Okamura et al., 2015).

2.7.3. Nucleo-cytoplasmic transport of *TLC1*

Nuclear export of *TLC1* is ensured by the Ran-dependent transport pathway, via the karyopherin Xpo1, and via the Mex67-Mtr2 mediated pathway (Gallardo et al., 2008; Wu et al., 2014). Xpo1 may contact either directly or indirectly the CBC for *TLC1* export, as it is known for snRNAs (Becker et al., 2019). So far, no adaptor protein is known for Mex67 to bind *TLC1*. Npl3 may be a possible adaptor for Mex67 in *TLC1* transport, as known for mRNAs (Köhler and Hurt, 2007; Zander et al., 2016). Additionally, Npl3 might participate in telomere maintenance, as it accelerates the senescence of *tlc1Δ* (Lee-Soety et al., 2012). However, there is no interaction known between Npl3 and *TLC1*. The karyopherin Mtr10 acts as re-import receptor of *TLC1*, but also Kap122 (Pdr6) was suggested earlier (Ferrezuelo et al., 2002; Gallardo et al., 2008; Vasianovich et al., 2020). Defects in Mex67, Xpo1 and Mtr10 lead to severe telomere shortening defects, whereas defects in Pdr6 only slightly affect the telomere length (Ferrezuelo et al., 2002; Vasianovich et al., 2020; Wu et al., 2014).

2.8. Aim of the study

Regulated maturation of *TLC1* (*hTR* in human) and correct assembly of the telomerase holoenzyme is a prerequisite for telomere length homeostasis from yeast to human. The telomerase functions in telomere elongation via the conserved reverse transcriptase Est2 (hTERT in human) using a template sequence of its scaffolding RNA (Schmidt and Cech, 2015; Vasianovich et al., 2019). The conserved function of the holoenzyme and the processing steps of telomerase RNA, provide key targets in the control of various hereditary diseases and carcinogenesis (Armanios and Blackburn, 2012; Blackburn, 1992; Collins and Mitchell, 2002; Egan and Collins, 2012; Nagpal and Agarwal, 2020; Schmidt and Cech, 2015; Vasianovich et al., 2019). Thus, understanding the order in which the steps occur is crucial. The current model was challenged though recent results in snRNA research. Here it was shown, that immature snRNA precursors are exported to the cytoplasm, where the loading of the Sm-ring occurs (Becker et al., 2019). Additionally, the re-import is dependent on the Sm-ring which is contacted by Cse1 (Becker et al., 2019). Maturation of snRNAs is finalized by TMG-capping, which could also be true for *TLC1* (Becker et al., 2019). In this work, we will investigate the individual steps of telomerase maturation. We chose the model organism *S. cerevisiae* for this purpose, because the telomerase is present in all cells.

3. Material and Methods

All solutions and media used in this study were prepared in the laboratory and were sterilized either by autoclaving at 121 °C for 20 min or by sterile filtration. Plastic material and glassware were autoclaved or sterilized at 180 °C for 6 h.

3.1. Chemicals and Consumables

Table 1: List of consumable materials

Materials	**Manufacturer/Source**
2-Mercapoethanol	Carl Roth (Karlsruhe/Germany)
Agarose NEEO Ultra	Carl Roth (Karlsruhe/Germany)
Amersham Hybond N+ Nylon Membrane	GE Healthcare (Freiburg/Germany)
Amersham Protran 0.45 µm nitrocellulose membrane	GE Healthcare (Freiburg/Germany)
Blocking Reagent	Roche (Mannheim/Germany)
cOmplete™, EDTA-free Protease Inhibitor	Roche (Mannheim/Germany)
CSPD	Roche (Mannheim/Germany)
Deionized Formamide	Applichem (München/Germany)
Difco Skim Milk	Applichem (München/Germany)
dNTPs	Thermo Fisher Scientific (Schwerte/Germany)
Dithiothreitol (DTT)	Nippon Genetics (Düren/Germany)
5-Fluoroortic acid (FOA)	Apollo Scientific (Derbyshire/UK)
Formaldehyde 37 %	AppliChem (München/Germany)
GFP-Trap® Beads	ChromoTek GmbH (Planegg-Martinsried/Germany)
GFP-Selector-beads	NanoTag Biotechnologies (Göttingen/Germany)
Gibson Assembly® Master Mix	New England Biolabs (Frankfurt/Germany)
Glass Beads Type S 0.4-0,6 mm	Carl Roth (Karlsruhe/Germany)
GlycoBlue™ Coprecipitant	Thermo Fisher Scientific (Schwerte/Germany)
HDGreen™ Plus DNA Stain	Intas Science Imaging (Göttingen/Germany)
Microscope slides, 12 well, 5.2 mm, PTFE-coating	Thermo Fisher Scientific (Schwerte/Germany)
MF-Millipore™ Membrane Filter, 0.025 µm pore size	Merck Millipore (Darmstadt/Germany)
MYC-Trap®-A Beads	ChromoTek GmbH (Planegg-Martinsried/Germany)
Oligonucleotides	Sigma-Aldrich (München/Germany)
Phenol/chloroform/isoamyl alcohol (25:24:1)	Carl Roth (Karlsruhe/Germany)

Table 1: List of consumable materials (continued)

Materials	**Manufacturer/Source**
Poly-L-lysine solution	Sigma-Aldrich (München/Germany)
qPCRBIO SyGreen Mix Lo-ROX	Nippon Genetics (Düren/Germany)
Rotiphorese Gel 30 (37.5:1) Acrylamide	Carl Roth (Karlsruhe/Germany)
RiboLock RNase Inhibitor	Thermo Fisher Scientific (Schwerte/Germany)
TRIzol™ Reagent	Thermo Fisher Scientific (Schwerte/Germany)
tRNA	Sigma-Aldrich (München/Germany)
Salmon Sperm-Carrier DNA (ssDNA)	Applichem (München/Germany)
WesternBright™ Quantum™ Western Blotting HRP Substrate	Advansta (San Jose,CA/USA)
Whatman® Blotting Paper	Hahnemühle (Dassel/Germany)

Table 2: Kits used in this study

Kit	**Supplier / Source**
DIG RNA labeling mix, 10x	Roche (Mannheim/Germany)
FastGene® Scriptase II cDNA Kit	Nippon Genetics (Düren/Germany)
MasterPure Yeast DNA Purification Kit	Lucigen/Biozym (Hessisch Oldendorf/Germany)
Maxima First Strand cDNA Synthesis Kit	Thermo Fisher Scientific (Schwerte/Germany)
NucleoSpin® Gel and PCR Clean-up	Macherey-Nagel (Düren/Germany)
NucleoSpin® Plasmid	Macherey-Nagel (Düren/Germany)
NucleoSpin® RNA	Macherey-Nagel (Düren/Germany)
TURBO DNA-free™ DNase Kit	Thermo Fisher Scientific (Schwerte/Germany)

Table 3: Enzymes used in this study

Enzyme	**Supplier / Source**
Conventional Restriction Enzymes	New England Biolabs (Frankfurt/Germany) and Thermo Fisher Scientific (Schwerte/Germany)
DreamTaq DNA-Polymerase	Thermo Fisher Scientific (Schwerte/Germany)
Phusion® High-Fidelity DNA polymerase	New England Biolabs (Frankfurt/Germany)
Q5® High-Fidelity DNA polymerase	New England Biolabs (Frankfurt/Germany)
RNase A	Qiagen (Hilden/Germany)
RNase-Free DNase	Qiagen (Hilden/Germany)
Taq Ligase	New England Biolabs (Frankfurt/Germany)
T5 Exonuclease	New England Biolabs (Frankfurt/Germany)
Zymolyase 20T	Zymo Research (Freiburg/Germany)
XhoI	Nippon Genetics (Düren/Germany)
DpnI	Nippon Genetics (Düren/Germany)

Table 4: Antibodies used in this study

Antibody	**Dilution**	**Supplier/Source**
Anti-Aco1 (rabbit)	1:2,000	Prof. Dr. U. Mühlenhoff (Marburg/Germany)
Anti-Hdf1 (Yku70) (mouse)	1:4,000	Santa Cruz (Heidelberg/Germany)
Anti-GFP (mouse)	1:5,000 (WB) 1:1,000 (IF)	Thermo Fisher Scientific (Schwerte/Germany)
Anti-GFP (rabbit)	1:4,000	ChromoTek GmbH (Planegg-Martinsried/Germany)
Anti-Grx4 (rabbit)	1:5,000	Prof. Dr. U. Mühlenhoff (Marburg/Germany)
Anti-Hem15 (rabbit)	1:5,000	Prof. Dr. U. Mühlenhoff (Marburg/Germany)
Anti-Myc (9E10) (mouse)	1:1,000	Santa Cruz (Heidelberg/Germany)
Anti-Myc (A-14) (rabbit)	1:1,000	Santa Cruz (Heidelberg/Germany)
Anti-Nop1 (mouse)	1:4,000	Santa Cruz (Heidelberg/Germany)
Anti-Npl3 (rabbit)	1:5,000	Prof. Dr. H. Krebber (Göttingen/Germany)
Anti-Zwf1 (rabbit)	1:4,000	Prof. Dr. U. Mühlenhoff (Marburg/Germany)
Anti-rabbit IgG-HRP (goat)	1:10,000	Dianova (Hamburg/Germany)
Anti-mouse IgG-HRP (goat)	1:10,000	Dianova (Hamburg/Germany)
Anti-Digoxigenin-AP (sheep)	1:10,000	Roche (Mannheim/Germany)
Anti-mouse IgG-FITC (sheep)	1:100 (IF)	Sigma-Aldrich (München/Germany)
Anti-2,2,7-Trimethylguanosine mouse mAB (NA02A) Agarose Conjugate	10 µl per RIP	Merck Millipore (Darmstadt/Germany)

Table 5: Marker and standards used in this study

Marker / Standard	**Supplier / Source**
GeneRuler 50 bp DNA Ladder	Thermo Fisher Scientific (Schwerte/Germany)
GeneRuler 1 kb DNA Ladder	Thermo Fisher Scientific (Schwerte/Germany)
Lambda DNA/EcoRI plus HindIII Marker	Thermo Fisher Scientific (Schwerte/Germany)
PageRuler™ Prestained Protein Ladder	Thermo Fisher Scientific (Schwerte/Germany)
PageRuler™ Unstained Protein Ladder	Thermo Fisher Scientific (Schwerte/Germany)
Cozy™ Prestained Protein Ladder	highQu (Kraichtal/Germany)

3.2. Equipment, Hardware and Software

Table 6: Equipment and hardware used in this study

Machine	**Supplier / Source**
AF6000 microscope with Leica DFC360 FX camera	Leica (Wetzlar/Germany)
Bio-Link 254 UV-crosslinking chamber	Vilber Lourmat (Eberhardzell/Germany)
CFX Connect 96FX2 qPCR cycler	Bio-Rad (München/Germany)
Eclipse E400 tetrad microscope	Nikon (Düsseldorf/Germany)
Electro Blotter PerfectBlue Semi-Dry, Sedec M	Peqlab (Erlangen/Germany)
FastPrep-24® Cell homogenizer	MP Biomedicals (Illkirch/France)
Fusion-SL-3500.WL	Vilber Lourmat (Eberhardzell/Germany)
Fusion FX	Vilber Lourmat (Eberhardzell/Germany)
Gene Pulser Xcell™ Electroporation System	Bio-Rad (München/Germany)
Heraeus™ Pico™ 21	Thermo Fisher Scientific (Schwerte/Germany)
Heraeus™ Fresco™ 21	Thermo Fisher Scientific (Schwerte/Germany)
Heraeus™ Multifuge™ X3 with TX-750 or F15-8x50cy rotor	Thermo Fisher Scientific (Schwerte/Germany)
Improved Neubauer counting chamber	Carl Roth (Karlsruhe/Germany)
Innova42R Incubator Shaker	Eppendorf (Hamburg/Germany)
INTAS UV gel detection system	INTAS (Göttingen/Germany)
Intelli Scan1600	Quato Technology (Braunschweig/Germany)
Milli-Q® Water purification system	Millipore (Eschborn/Germany)
Nano Drop 2000 spectrophotometer	Peqlab (Erlangen/Germany)
Primo Star light microscope	Zeiss (Jena/Germany)
T100™ Thermal Cycler	BioRad (Feldkirchen/Germany)

Table 7: Software used in this study

Software	**Supplier / Source**
Ape Plasmid Editor	M. Wayne Davis (University of Utah/USA)
CFX manager 3.1	BioRad (Feldkirchen/Germany)
Fusion Capt Software	Vilber Lourmat (Eberhardzell/Germany)
Illustrator CS6	Adobe Systems (San Jose/USA)
Leica AF 2.7.3.9723	Leica (Wetzlar/Germany)
Office® 2011/2019	Microsoft Corporation (Redmond/USA)
Photoshop CS6	Adobe Systems (San Jose/USA)
GraphPad Prism 5	GraphPad Software (San Diego/USA)
SilverFast Quato XFU	LaserSoft Imaging (Kiel/Germany)
Snapgene	GSL Biotech LLC (Chicago/USA)

3.3. Strains

3.3.1. *Escherichia coli*

Table 8: *Escherichia coli* strain used in this study

Strain	Genotype	Application
DH5α™	F⁻ Φ80*lac*ZΔM15 Δ(*lacZYA-argF*)U169 recA1 *endA1* hsdR17($r_K^- m_K^+$) *phoA supE44* λ– *thi-1 gyrA96 relA1*	Plasmid amplification

3.3.2. *Saccharomyces cerevisiae*

Table 9: *Saccharomyces cerevisiae* strains used in this study

Number	Genotype	Source	Parental strains
HKY36	*MATα ura3-52 leu2Δ1 his3Δ200*	(Winston *et al*., 1995)	
HKY37	*MATα ura3-52 leu2Δ1 his3Δ200 srp1-31*	(Loeb *et al.*, 1995)	
HKY46	*MATα ura3-52 lys2-301 ade2 mtr10-1*	(Liu *et al.,* 1999)	
HKY82	*MATα ura3 leu2 trp1 his3 ade2 Mtr10Δ pURA-Mtr10 (pRS316)*	(Senger *et al*., 1998)	
HKY208	*MATα ura3-52 ade2-101 his3-11,15, trp1-Δ901 cse1-1*	(Taura *et al*., 1998)	
HKY316	*MATα ura3-52 leu2Δ1 trp1Δ63 MTR10-9xMyc-TRP1*	Prof. Dr. H. Krebber	
HKY331	*MATα ura3 his3 leu2 met15 nrd1::KAN pJC719 nrd1-101 (LEU2)*	(Conrad *et al*., 2000)	
HKY332	*MATα ura3 his3 leu2 met15 nrd1::KAN pJC720 nrd1-103 (LEU2)*	(Conrad *et al*., 2000)	
HKY380	*MATa his3Δ1 leu2Δ0 met12Δ0 ura3Δ0 npl3::KanMX4*	Euroscarf	
HKY644	*MATα ade2, his3, leu2, trp1, ura3 mex67::HIS3 pUN100-mex67-5 (LEU2, CEN)*	(Segref *et al*., 1997)	
HKY1028	*MATα his3Δ1; leu2Δ0; lys2Δ0; ura3Δ0 rrp6::kanMX4*	Euroscarf	
HKY1073	*MATα his3Δ1; leu2Δ0; met15Δ0; ura3Δ0; yKu70::kanMX4*	Euroscarf	
HKY1079	*MATa his3Δ1 leu2Δ0 met15Δ0 ura3Δ0 RAP1-GFP:HIS3MX6*	(Huh *et al*., 2003)	
HKY1093	*MATa his3Δ1 leu2Δ0 met15Δ0 ura3Δ0 CDC13-GFP:HIS3MX6*	(Huh *et al*., 2003)	
HKY1193	*Tgs1::KanMX4/Tgs1::KanMX4 his3Δ1 / his3Δ1; leu2Δ0 / leu2Δ0; ura3Δ0 / ura3Δ0; lys2Δ0 / LYS2; MET15 / met15Δ0*	Euroscarf	

Table 9: *Saccharomyces cerevisiae* strains used in this study (continued)

Number	Genotype	Source	Parental strains
HKY1277	*MATa his3Δ1 leu2Δ0 met15Δ0 ura3Δ0 MTR10-GFP:HIS3MX6*	(Huh *et al.,* 2003)	
HKY1293	*MATa ura3-52 lys2-801 trp-Δ1 his3-Δ200 leu2-Δ1 tlc1-Δ::HIS pURA-TLC1*	(Lubin *et al*., 2012)	
HKY1353	*MATa ura3-52 mex67::HIS3 xpo1::TRP1 pUN100-mex67-5 (LEU2, CEN) xpo1-1::HIS3*	(Brune *et al*., 2005)	
HKY1596	*MATa his3Δ1 leu2Δ0 met15Δ0 ura3Δ0 CSE1-GFP:HIS3MX6*	(Huh *et al*., 2003)	
HKY1642	*MATa ura3-52 lys2-801 ade2-Δ trp1-Δ63 his3-Δ200 leu2-Δ1 Smb1::KAN pGal-TRP1-SMB1*	(Bordonné, 2000)	
HKY1689	*MATα rrp6::kanMX4 mex67::HIS3 pUN100-mex67-5 (LEU2, CEN)*	(Zander *et al.*2016)	
HKY1776	*MATa lys ura leu his mtr10:kanMX4*	Prof. Dr. H. Krebber	
HKY1799	*MATa his3Δ1 leu2Δ0 met15Δ0 ura3Δ0 CBP20-GFP:HISMX6*	Euroscarf	
HKY1815	*MATa ura leu POP1-GFP:HisMX6*	Euroscarf	
HKY2087	*MATα his ura KAN cse1-1 mtr10:kanMX4*	This study	HKY208 x HKY1776
HKY2093	*MATa ura cse1-1 POP1-GFP:HisMX6*	This study	HKY208 x HKY1815
HKY2101	*MATa leu2Δ1 ura3-52 MTR10-9xMyc-TRP1 POP1-GFP:HisMX6*	This study	HKY316 x HKY1815
HKY2153	*MATα ura POP1-GFP:HisMX6 mex67::HIS3 pUN100-mex67-5 (LEU2, CEN)*	This study	HKY644 x HKY1815
HKY2220	*MATα TLC1 poly(A)*::ura3-52 leu2Δ1 his3Δ200*	Prof. Dr. H. Krebber	HKY2204 after URA excision via Cre/LoxP
HKY2221	*MATα TLC1 NNS*::ura3-52 leu2Δ1 his3Δ200*	Prof. Dr. H. Krebber	HKY2203 after URA excision via Cre/LoxP
HKY2224	*MATα TLC1 poly(A) *::ura3-52 ade his3Δ200 trp cse1-1*	Prof. Dr. H. Krebber	HKY208 x HKY2210
HKY2225	*MATα TLC1 NNS*::ura3-52 ade trp his3Δ200 cse1-1*	Prof. Dr. H. Krebber	HKY208 x HKY2211
HKY 2245	*MATα TLC1 poly(A)* NNS*::ura3-52 leu2Δ1 his3Δ200*	Prof. Dr. H. Krebber	HKY2232 after URA excision via Cre/LoxP
HKY2246	*MATα TLC1 poly(A)* NNS*::ura3-52 leu2Δ1 his3Δ200 cse1-1*	Prof. Dr. H. Krebber	HKY2233 after URA excision via Cre/LoxP
HKY2259	*MATa ura3-52 ade2-101, trp1-Δ901 cse1-1 RAP1-GFP:HIS3MX6*	This study	HKY208 x HKY1079

Table 9: *Saccharomyces cerevisiae* strains used in this study (continued)

Number	Genotype	Source	Parental strains
HKY2261	*MATa leu2Δ0 met15Δ0 ura3Δ0 ade2-101 cse1-1 CDC13-GFP:HISMX6*	This study	HKY208 x HKY1093
HKY2289	*MATa ura3Δ leu2Δ his3Δ1 met15Δ sen1-1::KanMX*	(Li *et al.*, 2011)	
HKY2290	*MATa ura3Δ leu2Δ his3Δ1 met15Δ rna15-58::KanMX*	(Li *et al.*, 2011)	

3.4. Plasmids

Table 10: Plasmids used in this study

Number	Genotype	Source	Origin and construction
pHK87	*CEN LEU2 AMP$_R$*	(Sikorski and Hieter, 1989)	
pHK88	*CEN URA3 (pRS316), AMP$_R$*	(Sikorski and Hieter, 1989)	
pHK206	*CEN URA CSE1*	Prof. Dr. H. Krebber	
pHK640	*HIS3* GAL1-cre	Euroscarf	
pHK765	*CEN URA GFP-Npl3*	(Hackmann *et al*., 2011)	
pHK1469	*CEN URA SMB1-GFP*	(Becker *et al*., 2019)	
pHK1483	*CEN URA GFP-POP1*	(Gill *et al.*, 2006)	
pHK1589	*URA3 EST1-(Gly)6-(myc)12*	(Tucey and Lundblad, 2014)	
pHK1606	*CEN URA pAdh-EST1-GFP*	Prof. Dr. H. Krebber	
pHK1696	*CEN URA TLC1* NNS* T->C (1175); G->C (1196)	This study	Mutagenic PCR on pHK1700
pHK1697	*CEN URA TLC1 poly(A)** AT->GC (1222/23); AT->CC (1232/33); A->G (1244))	This study	Mutagenic PCR on pHK1700
pHK1700	*CEN URA TLC1*	(Lubin *et al*., 2012)	Isolated from HKY1293
pHK1725	pUC19 Cloning Vector	Prof. Dr. H. Krebber	
pHK1742	*CEN URA* TLC1 *poly(A)** AT->GC (1222/23); AT->CC (1232/33); A->G (1244)	Prof. Dr. H. Krebber	GA of pHK1725 with *TLC1 poly(A)** amplified of pHK1697 using HK4167 + HK4168
pHK1743	*CEN URA* TLC1 *NNS** T->C (1175); G->C (1196)	Prof. Dr. H. Krebber	GA of pHK1725 with *TLC1 NNS** amplified of pHK1696 using HK4167 + HK4168
pHK1753	*CEN URA* TLC1 *poly(A)* NNS**	Prof. Dr. H. Krebber	Mutagenic PCR on pHK1742 using HK3669 + HK3670

3.5. Oligonucleotides

Oligonucleotides were purchased from Sigma-Aldrich. They were shipped dried and then immersed in DEPC treated water to a concentration of 100 µM stock solution and stored at - 20 °C. Fluorescently labeled oligonucleotides were aliquoted after solubilization and stored at - 20 °C. The currently used fluorescently labeled oligonucleotide was stored at 4 °C in the dark.

Table 11: Oligonucleotides used in this study

Number	Sequence	Name
HK281	5´-AGCGCTTTGTTTTTATC-3´	Control Mtr10 reverse
HK421	5´-CGAGGCCGCGATTAAATTCC-3´	kanMX4 control forward
HK836	5´-CCAAGCCTCTTGTTTTTCGC-3´	Control Mtr10 forward
HK1384	5´-GCGGAAGGAACCGTGTGTTC-3´	*TLC1* immature fw
HK1385	5´-GAAGCCTACCATCACCACACC-3´	Internal *TLC1* fw
HK1386	5´-ACAGCGCTTAGCACCGTCTG-3´	Internal *TLC1* rev
HK1539	5´-DIG-CCACCACACACACCCACACCC-3´	5' DIG labeled – Telomeric repeat probe
HK1598	5´-GGCCCCAGGTAAGAAAGTCG-3´	*RPL8a* fw
HK1599	5´-GAAGGTTTCGGCAGCGGTG-3´	*RPL8a* rev
HK1738	5´-TGCAAACTCCTTGGTCACAC-3´	*U1* snRNA (snR19) fw
HK1739	5´-CCAGGCAGAAGAAACAAAGG-3´	*U1* snRNA (snR19) rev
HK1761	5´-CY3-GCGCACACACAAGCATCTACACTGACACCAGCATACTCGAAATTCTTTGG-CY3-3´	*TLC1* probe 1
HK1789	5´-CY3-CGATAAGATAGACATAAAGTGACAGCGCTTAGCACCGTCTGTTTGC-CY3-3´	*TLC1* probe 2
HK1790	5´-CY3-CCTACTCGTATTTTTCTCTGTCACATCGTTCGATGTACGGGGCACATTTGG-CY3-3´	*TLC1* probe 3
HK2154	5'-CCAGAACAATCCGTACACAAGG-3´	*Hem15* fw
HK2155	5´-GCAATTGTCTTCTGATACTTAGCAC-3´	*Hem15* rev
HK2859	5´-CAGCTTTACAGATCAATGGC-3´	*U5* snRNA (snR7-L) fw
HK2860	5´-TATGGCAAGCCCACAGTAA-3´	*U5* snRNA (snR7-L) rev
HK3089	5´-AGTTACGCTAGGGATAACAGGG-3´	*21S* rRNA fw
HK3090	5´-TGACGAACAGTCAAACCCTTC-3´	*21S* rRNA rev
HK3513	5´-ACGCGCGATTTCTACAATAC-3´	*TLC1* immature rev
HK3515	5´-TAAATATTAAGAGGCATACCTCC-3´	Long *TLC1* rev qPCR

Table 12: Oligonucleotides used for cloning and mutation via Mutagenic PCR

Number	Sequence	Name
HK3667	5´-ACTTGTGCATCGCTTTCCAAGCGCTTTTGATTGATTGTTCATGACGAGGA-3´	*TLC1* Mutagenic PCR *poly(A)** fw
HK3668	5´-GAACAATCAATCAAAAGCGCTTGGAAAGCGATGCACAAGTACAGTACGCGCGAT-3´	*TLC1* Mutagenic PCR *poly(A)** rev
HK3669	5´-CATTTTTTTTCCTGATGTATATTTTTTGTATTCTAGAAATCGCGCGTACTG-3´	*TLC1* Mutagenic PCR *NNS** fw
HK3670	5´-CGATTTCTAGAATACAAAAAATATACATCAGGAAAAAAAATGTTTCCAAAAATT-3´	*TLC1* Mutagenic PCR *NNS** rev
HK4167	5´-CAATTTCACACAGGAAACAGCTATGACCATGATTACGCCACTAGAGAGGAAGATAGGTACCCTATG-3´	Cloning *TLC1* into pHK1725 fw
HK4168	5´-ctcagATAACTTCGTATAGCATACATTATACGAAGTTATGTAAATATTAAGAGGCATACCTCCGCC-3´	Cloning into pHK1725 *TLC1* rev
HK4169	5´-CTAGAGAGGAAGATAGGTACCCTATG-3´	Cassette for HR *TLC1* fw
HK4170	5´-TATATTCTAAAAAGAAGAAGCCATTTGGTGGGCTTTATTAGTAAAACGACGGCCAGTGAATTC-3´	Cassette for HR *TLC1* rev

3.6. Cell biological methods

3.6.1. Cell cultivation

All media were autoclaved prior to usage and heat sensitive substances such as antibiotics were added subsequently to the media. For preparation of plates, 1.5 % agar was added to the appropriate medium for *Escherichia coli* (*E. coli*) and 1.8 % for *Saccharomyces cerevisiae* (*S. cerevisiae*). The use of synthetic selective media for *S. cerevisiae* required separate autoclaving of the solutions (Table 13) and subsequent combination of these.

3.6.1.1. Cultivation of *E. coli*

E. coli cells were cultivated in LB medium with the addition of the appropriate antibiotics as referred to Sambrook, Fritsch, and Maniatis (1989). Single colonies were picked and used as inoculum for the liquid cultures, that were grown at 37 °C over night.

LB medium	
Tryptone	1.0 % (w/v)
Yeast extract	0.5 % (w/v)
NaCl	0.5 % (w/v)
Ampicillin* (if added)	100 µg/ml
Agar-Agar (for plates only)	1.5 % (w/v)
*Ampicillin was added after autoclaving and cooling the medium to ~ 60 °C	

3.6.1.2. Cultivation of *S. cerevisiae*

All yeast strains were grown in full (YPD) or synthetic selective liquid medium according to standard protocols of Sherman (2002) (Table 13). Full medium was used for culturing strains, for which no selection for a specific marker gene was necessary. Strains which harbor a plasmid-encoded selection marker which complement an auxotrophy of the strain were grown and cultured in the respective synthetic selective medium. All strains were incubated at 25 °C unless indicated otherwise. For storage, the strains were plated on YPD or synthetic selective media plates and stored at 4 °C. Cells were suspended in 50 % glycerol for long term storage at - 80 °C. Depending on the experiment, 10 ml or 50 ml pre-cultures were inoculated with the necessary strain taken form the plate stock, and incubated over night under agitation. The cell density was determined by counting with a hemocytometer and diluted to 0.5 - 1x 10^7 cells/ml in the main-culture (see section 3.6.4). For all experiments 400 ml main-cultures were used unless otherwise stated. The cells were grown to mid log-phase (1 - 2x 10^7 cells/ml) and either shifted to the restrictive temperature if temperature sensitive mutants were used, or they were directly harvested via centrifugation at 4,000 x g for 5 min. The cell pellet was resuspended in 5 ml H_2O, transferred into a 15 ml falcon and centrifugated again. The supernatant was discarded and the pellet was frozen in liquid nitrogen and stored at - 20 °C.

Table 13: Yeast cultivation and mating media

YPD	
Yeast extract	1 % (w/v)
Peptone	2 % (w/v)
Glucose	2 % (w/v)
Agar-Agar	1.8 % (w/v)

Selective Media	
Nitrogen base	1.7 g/l
Ammonium sulphate	40 mM
Glucose*	2 % (w/v)
Agar-Agar*	1.8 % (w/v)
L-Alanine	80 mg/l
L-Arginine	80 mg/l
L-Asparagine	80 mg/l
L-Aspartic acid	80 mg/l
L-Cysteine	80 mg/l
L-Glutamine	80 mg/l
L-Glutamic acid	80 mg/l
L-Glycine	80 mg/l
Inositol	80 mg/l
L-Isoleucine	80 mg/l
L-Methionine	80 mg/l
Para-aminobenzoic acid	8 mg/l
L-Phenylalanine	80 mg/l
L-Proline	80 mg/l
L-Serine	80 mg/l
L-Threonine	80 mg/l
L-Tyrosine	80 mg/l
L-Valine	80 mg/l
optional metabolites according to selectivity	
L-Adenine	20 mg/l
L-Histidine	80 mg/l
L-Leucine	400 mg/l
L-Lysine	80 mg/l
L-Tryptophan	80 mg/l
Uracil	80 mg/l

Sporulation medium	
Yeast extract	0.25 % (w/v)
Potassium acetate	150 mM
Glucose**	0.05 % (w/v)
Uracil**	40 mg/l
Adenine**	40 mg/l
Tyrosine**	40 mg/l
Histidine**	20 mg/l
Leucine**	20 mg/l
Lysine**	20 mg/l
Tryptophan**	20 mg/l
Methionine**	20 mg/l
Arginine**	20 mg/l
Phenylalanine**	100 mg/l
Threonine**	350 mg/l

B-plates	
Nitrogen Base	0.17 % (w/v)
Ammonium sulphate	3 mM
Agar-Agar*	3 % (w/v)
Glucose*	2 %

FOA plates	
Drop out mix (-URA)	0.2 %
Uracil	0.005 %
Nitrogen Base	0.17 %
Ammonium sulphate	0.51 %
5-fluoroorotic acid	0.1 %
Agar-Agar	1.8 %

(Sherman, 2002; Sprague, 1991); modified
*components were autoclaved separately
**components were sterile filtered (0.2 µm)

5-Fluoorotic acid (FOA) plates were used to select for the loss of an *URA3* gene-containing plasmid (Table 13). Here, the drop out mix contains every amino acid and nucleobase except uracil. Cells that still contain a *URA3* gene will die, because 5-Fluoorotic acid is decarboxylated by the *URA3* encoded Orotidine 5´-phosphate decarboxylase, and results in production of the toxic metabolite 5-fluorouracil.

3.6.2. Transformation of *E. coli*

For multiplication of an existing plasmid, *E. coli* were transformed by heat shock transformation according to Inoue, Nojima, and Okayama (1990). In case a new plasmid was generated by via site directed mutagenesis or Gibson assembly (GA), the protocol according to Dower, Miller, and Ragsdale (1988) was used for the *E. coli* transformation, which introduces the plasmid DNA by electroporation.

3.6.2.1. Transformation of *E. coli* via heat shock

Chemically ultra-competent *E. coli* cells, produced by the protocol provided by Inoue, Nojima, and Okayama (1990), were transformed with plasmid DNA, via heat shock transformation. An aliquot of 100 µl of chemically competent *E. coli* was thawed on ice and mixed with 200 - 300 ng plasmid DNA. The cell suspension was incubated for 30 min on ice and afterwards heat shock was carried out at 42 °C for 2 min. Subsequently 1 ml LB medium was added and cells were incubated for 45 - 60 min at 37 °C under agitation. The cells were collected by centrifugation at 4,000 x g for 1 min and resuspended in 1 ml H_2O. Again, the cells were collected by centrifugation and the supernatant was discarded. The pellet was dissolved in 100 µl H_2O and plated on LB plates containing the respective antibiotics. The plate was incubated over night at 37 °C.

3.6.2.2. Transformation of *E. coli* via electroporation

Electrocompetent cells were produced according to Dower, Miller, and Ragsdale (1988). Transformation via electroporation has a higher transformation efficiency for low yield plasmids. Using this method, the plasmid or GA mix has to be dialyzed, to make sure that no free ions would elicit a bypass during the electroporation. The plasmid DNA or the GA mix was dialyzed on a nitrocellulose membrane placed in a tray with deionized water for at least 30 min. Afterwards the mix was collected and mixed with 50 µl electrocompetent *E. coli* cells. The cell suspension was pipetted into a pre-cooled electroporation cuvette (1 mm gap). Using the Bio-Rad Laboratories electroporator, a pulse of 155 V, 50 µF, 150 Ω was generated for penetrating the cell wall allowing uptake of plasmid DNA. After electroporation cells were

directly taken up in 1ml LB media and transferred into a new reaction tube. Cell recovery and subsequent plating was carried out as described in section 3.6.2.1.

3.6.3. Passaging of yeast cells

The passaging of cells was used for subsequent Southern blot experiments to analyze the length and structure of telomeres in yeast cells. Two variations of cell passaging were carried out. Either, the cells were passaged in liquid culture or on solid agar plates. Telomere shortening occurs gradually from generation to generation. Therefore, a freshly generated deletion strain should be used. However, in this study strains were directly taken from a - 80 °C stock which already replicated multiple times and, therefore, already might exhibit telomere shortening at this point. For each replication of the experiment the desired strains were freshly re-streaked from the - 80 °C freezer stocks onto YPD plates. For liquid culture passaging, a singe colony was used as inoculum for a 50 ml YPD liquid cultures and incubated for 3 days under agitation. The cell density was determined using the hemocytometer and adjusted to 1x 10^5 cells/ml in 20 ml cultures. A volume of 14 ml of the pre-culture was harvested via centrifugation for 5 min at 4,000 x g. The supernatant was discarded and the pellet was resuspended in 1 ml H_2O and transferred into a screw top tube. The cells were centrifuged again for 5 min at 4,000 x g, the supernatant was discarded and the tubes were frozen in liquid nitrogen and stored at - 20°C. The first harvesting time point is referred to point “0”. Afterwards the liquid culture was again grown for 3 days at 20 °C as semi-permissive temperatures for the *cse1-1* strain. The cultures were harvested after the cell density of 1x 10^8 cells/ml was reached, which correspond to 10 generation doublings. This procedure was repeated until 80 to 125 generations were reached.

Passaging on solid plates was achieved in such a way that after 3 days of incubation at 25 °C, a single colony was streaked onto a new plate and incubated for 2 - 3 days. One repassing corresponds to ~ 25 generations (Lundblad and Blackburn, 1993). After each passage, a single colony was picked and used as inoculum for a liquid culture. The cells were grown to mid-log phase and harvested by centrifugation. The pellet was frozen in liquid nitrogen and stored at - 20 °C.

3.6.4. Measurement of yeast cell density in liquid culture

The cell density of yeast cells grown in liquid culture was determined using a hemocytometer. A sample of the culture was diluted depending on the optical cell density and counted on a light microscope. The cell density was calculated using the formula:

$$1x10^4\ x\ dilution\ factor\ x\ counted\ cells = cells/ml$$

3.6.5. Transformation of *S. cerevisiae*

The transformation of yeast cells was achieved by lithium acetate treatment and heat shock following the protocol of Gietz *et al.* (1992). A pre-culture of cells was grown over night. On the following day the cells were diluted and harvested upon a cell density of 1- 2x 10^7 cells/ml by centrifugation at 4,000 x g for 5 min. The pellet was washed once with H_2O and once with TE lithium acetate buffer (10 mM Tris/Cl, 1 mM EDTA, 100 mM lithium acetate, pH 7.5) and was collected via centrifugation at 4,000 x g for 5 min. The pellet was resuspended in 100 µl TE lithium acetate buffer and subsequently, 50 µl of this suspension (~ 0.5x 10^8 cells) were used for each transformation. The cell suspension was combined with 1 µg plasmid DNA, 50 µg *salmon sperm* carrier DNA (AppliChem GmbH), which was boiled for 5 min at 95 °C and subsequent cooled on ice for 5 min, and 300 µl PEG-TE lithium acetate buffer (10 mM Tris, pH 7.5, 1 mM EDTA, 100 mM lithium acetate, 40 % (v/v) poly ethylene glycol 4000). The cell suspension was incubated for 30 min at 25 °C under agitation. Afterwards the heat-shock was carried out for 15 min at 42 °C. The cells were collected by centrifugation at 4,000 x g for 5 min and the pellet was washed once with H_2O. After centrifugation and discarding the supernatant, the pellet was resuspended in 100 µl H_2O and plated onto the required selective media plate.

3.6.6. Crossing of *S. cerevisiae* strains

New yeast strains were generated in such a way that two haploid strains of the opposite mating types (*MATa* or *MATα*) were mated according to standard protocols of Sherman (2002) and Sprague (1991). The resulting diploid strain can sporulate under nutrient depletion and will generate four haploid spores in an ascus after meiosis. The desired strains were streaked out and mixed on a YPD plate and incubated for 2 - 3 days. Diploid selection was achieved by replica plating onto the respective selective media plates according to the selection markers of the parental strains. After 2 - 3 days of growth on the selection plate only the mixed area containing diploid strains should be able to grow, which is only possible if different selection markers are present in the parental strains. The resulting diploid strain was forced to sporulate under nutrient depletion through cultivation in 5 ml Super Spo medium (Table 13). The cells were incubated for 5 - 8 days on a rotator. If the asci formation could be detected 100 µl of the cell suspension was harvested by centrifugation at 4,000 x g for 1 min and washed once with 1 ml H_2O and resuspended in 50 µl P-solution (0.1 M phosphate buffer - pH 6.5, 1.2 M sorbitol). For digestion of the ascus wall, the cells were treated with 1 µg/µl Zymolyase (Zymo Research) for 5 - 10 min at room temperature. After centrifugation at 4,000 x g for 1 min the cells were washed once with 1 ml P-solution and finally resuspended in 200 µl P-solution. A volume of 1 - 5 µl of this cell suspension was mixed with 150 µl H_2O and pipetted onto a YPD plate. The spores were separated using a tetrade microscope. Each spore of an ascus was separated and after 3 days of incubation the single strains were re-streaked on YPD plates. The resulting strains were transferred in a 96-well plate with 200 µl of 50 % glycerol per well. For long term storage they were kept at - 80 °C. Based on the 96-well plate, cell material was stamped onto YPD and selective plates to analyze the genotypes of the strains. Testing for temperature sensitivity was conducted using YPD plates and cultivation at 16 °C and 37 °C. Antibiotic resistance was tested using 100 µl geneticin (40 µg/µl) for KanMX4 resistance or the respective antibiotics which was distributed onto YPD plates. To identify the mating type of the newly generated strain, the spores were stamped onto *MATa* or *MATα* plates respectively. After one day of growth at 25 °C they were replica stamped onto selective B-plates and further incubated. The *MATa* and *MATα* strains were isoleucine and valine auxotroph, which was only complemented by the tested strain with the opposite mating type.

3.6.7. Growth analysis of yeast strains

The growth at different temperatures or on certain media was analyzed by serial dilution assay of the respective strains. The strains were inoculated in 10 ml YPD or synthetic selective media and incubated over night. The cell density was determined as described in section 3.6.4 and serially diluted from 1x 10^7 to 1x 10^3 cells/ml. A volume of 10 µl of each dilution was pipetted onto YPD or selective media plates and incubated for 2 - 3 days. Plates were documented via scanning with Intelli Scan1600 (Quato Technology).

3.7. DNA methods

3.7.1. Isolation of chromosomal DNA from yeast

Yeast chromosomal DNA was extracted with modifications as described earlier by Rose, Winston, and Hieter (1990). Yeast cells were grown in a pre-culture to saturation over night in the corresponding medium. 10 ml of the culture were collected by centrifugation at 4,000 x g for 5 min. The supernatant was removed and the pellet was resuspended in 1 ml H_2O and transferred into a 2 ml screw top tube. After centrifugation the supernatant was removed and 500 µl of detergent lysis buffer (2 % Triton X-100, 1 % SDS, 100 mM NaCl, 10 mM Tris pH 8, 1 mM EDTA), 500 µl phenol and 300 µl glass beads (0.4 - 0.6 mm) were added. The cells were homogenized using the Fast prep machine twice at 5 m/s for 20 sec. The samples were centrifuged for 5 min at 11,600 x g to separate the aquatic and the organic phase. The aquatic, upper phase, in which the hydrophilic DNA remains, was transferred into a fresh 1.5 ml tube and mixed with the equal amount of phenol by vigorously shaking. For phase separation the tube was centrifuged again for 5 min at top speed. The procedure was repeated with the usage of phenol-chloroform-isoamyl alcohol and afterwards with chloroform-isoamyl alcohol prior to DNA precipitation. For precipitation 1/10 volume of 3 M sodium acetate (pH 5.2) and 2.5 volumes of 100 % ethanol were added to the aquatic phase and mixed by inversion. The samples were incubated over night at - 20 °C for precipitation of the DNA. After precipitation the samples were centrifuged for 30 min at top speed at 4 °C. The supernatant was removed and the DNA pellet was washed twice with 70 % ethanol. The pellet was dried for 5 min at 65 °C and afterwards resolved in 100 µl H_2O under gentle shaking at 50 °C.

3.7.2. Isolation of high-quality chromosomal DNA from yeast for Southern blotting

Lucigen's MasterPure Yeast DNA Purification Kit was used to isolate highly pure, unsheared chromosomal DNA for Southern blotting experiments. Yeast cells were grown and harvested as described in section 3.6.3. The cell pellet was resuspended with 300 µl Yeast Cell lysis solution with addition of 1 µl (5 µg/µl) RNase A and incubated at 65 °C for 15 min. Samples were subsequently cooled for 5 min on ice and 150 µl of MPC Protein Precipitation Reagent was added. Samples were vortexed for 10 sec and centrifuged at 16,200 x g for 10 min. The supernatant was transferred into a fresh reaction tube and was mixed with 500 µl isopropanol. After repeated inversions, the DNA was precipitated overnight at - 20 °C. On the next day the DNA was pelleted via centrifugation for 10 min at 16,200 x g, the supernatant was discarded, and the pellet was dried at room temperature and then resuspended in 100 µl H_2O.

3.7.3. Isolation of plasmid DNA from *E. coli*

Plasmid DNA was purified using the NucleoSpin Plasmid purification kit (Macherey-Nagel) following the manufacturer's instructions. *E. coli* cells were grown in 10 ml LB as described in section 3.6.1.1. DNA was purified according to the manufacturer's instructions and the yield was determined by photometric analysis, see section 3.7.4.

3.7.4. Measurement of DNA and RNA concentration

The concentration of nucleic acids was determined using the NanoDrop spectrophotometer. The NanoDrop measured the absorbance of light at 260 nm wavelength and the concentration was calculated, using a modification of the Beer-Lambert equation. The calculation includes the absorbance at 260 nm, the wavelength-dependent extinction coefficient and a normalization / baseline correction (340 nm). The extinction coefficient for double-stranded DNA is 50 ng-cm/µl, 33 ng-cm/µl for single-stranded DNA and 40 ng-cm/µl for RNA.

3.7.5. Polymerase chain reaction

The polymerase chain reaction (PCR) is a molecular biological method to amplify precise DNA fragments. It is based on three general steps: Denaturation, primer annealing and elongation. The denaturation of double stranded DNA takes place at 95 - 98 °C. The annealing of the primers depends on the melting temperature of the used primers and was carried out between ~ 55 - 65 °C. The elongation takes place at 72 °C and the duration is based on the processivity of the polymerase and the length of the fragment which is synthesized. The DreamTaq polymerase was used for analytical purposes and the Q5 or Phusion were used for cloning strategies and site directed mutagenesis, as those are proof-reading polymerases. The reaction mixes and cycling conditions are based on the supplied protocol of the respective polymerase (Table 14 and Table 15). The PCR products were analyzed using agarose gel electrophoresis, see section 3.7.7.

Table 14: PCR reaction mix composition

Polymerase	**DreamTaq**	**Phusion**	**Q5**
dNTPs	200 µM each	200 µM each	200 µM each
Primers	0.2 µM each	0.5 µM each	0.5 µM each
Polymerase	0.025 U/µl	0.02 U/µl	0.02 U/µl

Table 15: PCR protocols

Polymerase	**DreamTaq**	**Phusion**	**Q5**
Initial denaturation	95 °C - 3 min	98 °C - 30 sec	98 °C - 30 sec
Denaturation	95 °C - 30 sec	98 °C - 10 sec	98 °C - 10 sec
Annealing	55 - 65 °C - 30 sec	55 - 65 °C - 30 sec	55 - 65 °C - 30 sec
Elongation	72 °C - 1 min/kb	72 °C - 30 sec/kb	72 °C - 30 sec/kb
		35 cycles	
Final elongation	72 °C - 10 min	72 °C - 10 min	72 °C - 10 min

3.7.6. Cleavage of DNA by restriction digestion

Restriction digestion was applied either on plasmid DNA for cloning strategies or on chromosomal DNA for downstream Southern blot experiments. For plasmid DNA digestion, 0.5 µg of the plasmid was mixed with 5 units of the required enzyme in the respective buffers according to the manufacturer's description, and incubated at 37 °C for 4 - 15 h. Here, standard restriction enzymes were used (Table 3). Chromosomal DNA was digested with the

enzyme XhoI (Nippon Genetics) according to the manufacturer's description. For this, 5 units of the enzyme per µg of genomic DNA and the 10x FastGene Buffer IV were used and incubated for 1 h at 37 °C. The enzyme was then inactivated by heat at 80 °C for 20 min and digested DNA was available for downstream applications.

3.7.7. Agarose gel electrophoresis

DNA samples, prepared by restriction digestion or PCR, were separated according to their size on an agarose gel. For the preparation of the gels 1 % (w/v) agarose was dissolved in TAE buffer (40 mM Tris base, 0.1 (v/v) Acetic acid, 1 mM EDTA, pH 8.5). The mixture was boiled with the TAE buffer in a regular microwave until the agarose was totally dissolved. The solution was cooled down to approximately 60 °C at room temperature under constant stirring using a magnetic stirrer prior adding 5 µl/100 ml HDGreen Plus DNA Stain (Intas Science Imaging). The solution was poured into a gel tray and a sample comb was added. The gel was solidified at room temperature and either used directly or stored at 4 °C. The gel was completely covered with TAE buffer in an agarose gel running chamber. Prior loading the DNA samples into the gel pockets, they were mixed with 6x loading buffer (10 mM Tris pH 7.6, 60 mM EDTA, 60% (v/v) glycerol, 0.03/ (w/v) bromophenol blue). Separation of the DNA fragments was achieved by applying voltage. After running 30 - 90 min at 120 V, DNA bands were visualized under a UV transilluminator at 320 nm and excised from the gel for preparative purposes.
Agarose gels for Southern blotting were made with TAE or TBE buffer (13 mM Tris pH 7.6, 45 mM boric acid, 2.5 mM EDTA), according to the running time of the gel. TBE gels were used for separation of fragments for over 4 h up to 16 h at 4°C and TAE gels were used for separation of fragments over 1 - 4 h at 120 V at 4 °C.

3.7.8. DNA extraction from agarose gels

If a preparative agarose gel was conducted, DNA fragments were excised from the gel and purified using the NucleoSpin Gel and PCR Clean-up kit (Macherey-Nagel). The purification is based on silica membranes and was carried out following the manufacturer's instructions. The DNA was finally eluted in H_2O.

3.7.9. Site directed mutagenesis by Quick Change PCR

The Quick Change PCR was used for a site directed mutagenesis of plasmid DNA, in which the desired mutation(s) were integrated into a newly synthesized plasmid via primers. The primers need to contain the desired mutation(s) and they need overlapping sequences to the plasmid DNA at those sequences where the mutations should be inserted. Based on the primers the whole plasmid was newly synthesized via PCR using a proof-reading polymerase. The elongation time depends on the amount of amplified base pairs. Subsequently the whole sample was digested with the restriction enzyme DpnI, that specifically recognizes methylated adenosine sites and cleaves the sequence 5´ - GATC - 3´. Since only the template plasmid, isolated from *E. coli*, harbors methylated adenosine sites only this plasmid will be digested. Digestion was carried out over night at 37 °C. Afterwards the reaction mixture was pipetted on a 0.025 µm MCE membrane (Merck Millipore) and dialyzed with H_2O for 30 min and subsequently *E. coli* were transformed with the mix, see section 3.6.2.2.

3.7.10. Endogenous mutation of *TLC1* transcription termination sites

For the analysis of the transcription termination of *TLC1*, mutations in the transcription factor binding sites were analyzed in endogenously mutated strains. For this purpose, first, plasmids carrying *TLC1* harboring the desired mutations followed by a loxP embedded *URA3* marker gene were first generated via Gibson Assembly (Gibson et al., 2009). Therefore, DNA fragments with 30 - 40 nt overlapping regions were synthesized by PCR, controlled on an agarose gel, purified and inserted into a digested vector plasmid. For this purpose, 100 - 150 ng of the digested vector were mixed with 2 - 3 times the molar amount of the insert DNA in a total volume of 10 µl. This was further mixed with 10 µl of 2x self-made Gibson Assembly Master Mix (Table 16). The samples were incubated at 50 °C for 1 h. During the reaction, the 5' exonuclease trims the 5' ends and generates a 3' overhang. The overlapping regions of the insert allow annealing of the fragments. Gaps of the annealed fragments are filled by a polymerase and a ligase establishes the final phosphodiester bond, with both enzymes present in the GA mix (Gibson et al., 2009). Subsequently *E. coli* were transformed wit half of the reaction mix as described in section 3.6.2.2.

In the next step, the respective regions on the plasmids were then amplified by PCR with a genomic overlap and transformed via homologues recombination into *S. cerevisiae* as described in section 3.6.5. The *URA3* gene was used as a marker for the successful integration of the regions into *S. cerevisiae* and was subsequently removed from the strains by the Cre/Lox system. Therefore, a plasmid-encoded Cre recombinase under a galactose-inducible promoter was used. After transformation of desired strains with the Cre recombinase, the expression of the Cre recombinase was induced in YP + galactose (2 % peptone, 1% yeast extract, 2 % sterile-filtered galactose after autoclavation) for 24 h, 10 - 100 µl of the cell suspension were plated on FOA plates. After 2 - 3 days at 25 °C, individual clones were picked and successful excision was verified by PCR. Furthermore, the subsequent loss of the Cre-recombinase plasmid was checked by incubating the strains in YPD and in selective medium. A single Lox site located downstream of the termination region remained in the generated strains. The *TLC1* termination site mutant plasmids for genomal integration and the endogenously mutated strains were created under my supervision by the student Jan-Philipp Lamping during an internship.

Table 16: Gibson Assembly reaction buffers

Solution	**5x Iso buffer**	**2x GA mastermix**
Composition	500 mM Tris pH 7.5	100 µl 5x Iso buffer
	50 mM $MgCl_2$	2 µl T5 Exonuclease (1 U/µl) (NEB)
	1 mM each of the four dNTPs	6.3 µl Phusion Polymerase (2 U/µl) (NEB)
	50 mM DTT	50 µl Taq Ligase (40 U/µl) (NEB)
	25 % PEG 8000	Ad. 375 µl DEPC dH_2O
	5 mM NAD^+	

3.7.11. Sequencing

To verify newly assembled DNA constructs the Sanger sequencing method was used, carried out by LGC Genomics.

3.8. Molecular biological methods with yeast

3.8.1. RNA extraction from yeast

In this study two different methods for the RNA extraction were used:
For total RNA extraction the NucleoSpin RNA Kit (Macherey-Nagel) was used unless stated otherwise, following the manufacturer's instructions. Two steps were carried out differently in contrast to the protocol. The DNA digestion on the column was carried out for 1 h and after RNA elution a second DNA digestion was carried out in the eluate for 1 h at 37 °C. After the second DNA digestion a sodium acetate ethanol precipitation was achieved by using 0.1 volumes 3 M sodium acetate pH 5.2, 2.5 volumes 100 % ethanol and 1 µl glycoblue over night at - 20 °C.
RNA extraction after RIP experiments was accomplished via phenol extraction using TRIzol Reagent (Invitrogen). The prepared samples were mixed with 1 ml TRIzol and incubated for 10 min at 65 °C on the shaker at 1300 rpm. Afterwards 200 µl chloroform were added to the samples and mixed thoroughly. The phases were separated through centrifugation for 15 min at 16,200 x g. The upper, aquatic phase was transferred into a fresh tube and mixed with 0.1 volumes sodium acetate pH 5.2, 2.5 volumes cold 100 % ethanol and 1 µl glycoblue. The precipitation was completed over night at - 20 °C.

3.8.2. Complementary DNA (cDNA) synthesis

In regard to the lower stability of RNA and for further downstream analysis, 100 ng to 500 ng of the isolated RNA was reverse transcribed in complementary DNA (cDNA). Either the Maxima First Strand cDNA Synthesis Kit (Thermo Fisher Scientific) or the FastGene Scriptase II Kit (Nippon Genetics), were used following the manufacturer's instructions. In all experiments random hexamer primers were used for cDNA synthesis, except for the RNA of the Cbp20 RIPs in which oligo(dT) primers were used. Reverse transcription was carried out at 50 °C with the Maxima First Strand cDNA Synthesis Kit, or at 42 °C with the FastGene Scriptase II Kit. As a negative control to monitor DNA contaminations, all samples were treated twice the same way. However, reverse transcriptase was added to only one of them. After reverse transcription, the cDNA was diluted with DEPC treated H_2O to a final concentration of 0.5 ng/µl. For each qPCR 2 ng of cDNA were used per well.

3.8.3. Quantitative Real time PCR (qPCR)

The qPCR is a PCR-based method that allows the user to indirectly measure relative and absolute amounts of RNA, depending on the procedure, in a sample in real time. A two-step qPCR was used in this work, in which the cDNA synthesis is separated from the qPCR. The cDNA serves as a template for the qPCR, which amplifies the target via specific primers.
A fluorescence dye, in this case SYBR Green, was added to the reaction, which interacts with dsDNA. SYBR Green is excited with 494 nm light and emits light at 521 nm, which is measured after each PCR cycle. The amount of the generated product depends on the amount of cDNA and efficiency of the primers used in the qPCR. Under optimal conditions the product is doubled in each cycle and leads to an exponential curve of emitted light. The evaluation is based on dividing the fluorescent signal by the number of cycles. As soon as the exponential phase occurs a program-controlled threshold is exceeded indicating the required number of cycles by the Cq-value (quantification cycle). The raw data was further processed using the $2^{-\Delta\Delta C}{}_T$ method (Livak and Schmittgen, 2001). All measurements and evaluations in this work deal with relative quantification of the targets. Each target was tested at least in three technical and a minimum of three biological replicates with the reaction mixture and cycler program listed in Table 17 and Table 18. The precipitated RNA in RIP experiments was used in equal amounts. In addition, concerning RIP experiments, the enrichments or depletions of the RNAs in the pull down are related to the total RNA level of the lysates.

Table 17: qPCR reaction mixture

Components	**Volume per reaction**
cDNA	4 µl
2x SyGreen Mix Lo-ROX (Nippon Genetics)	5
Forward Primer 10 mM	0,08 µl
Reverse Primer 10 mM	0,08 µl
DEPC treated H_2O	0,84

Table 18: qPCR cycler program

Hot start	**Denaturing**	**Annealing**	**Elongation**	**Plate read**	**Melting**
95 °C	95 °C	60 °C	72 °C		65 → 95 °C
5 min	5 s	20 s	40 s		5 s = 0.5 °C
	<----------50x----------				

3.8.4. Nucleo-cytoplasmic fractionation experiments

The nucleo-cytoplasmic fractionation was used for the isolation of the cytoplasmic fraction of a cell lysate and was carried out with modifications, but in general according to Sklenar and Parthun (2004). First, the cytoplasmic fraction was isolated and second, for normalization and control, also the total fraction was isolated from the same initial culture. After preparing a pre-culture of the desired strains in 50 ml, a main-culture was inoculated in 400 ml and cells were grown to mid-log phase (2x 10^7 cells/ml). The cells were harvested by centrifugation at 4000 x g for 5 min, the pellet was resuspended in 5 ml H_2O and transferred to a 15 ml falcon tube. The cell suspension was centrifuged again, the supernatant was discarded and the pellet was washed once in 1 ml YPD, 1 M sorbitol, 2 mM DTT and transferred into a fresh 2 ml tube. The cells were centrifuged, the supernatant was discarded and the pellet was resuspended in 1 ml YPD, 1 M sorbitol, 1 mM DTT. The cell suspension was mixed with 1 mg Zymolyase and incubated until 70 % of the cells were spheroblasted. Digestion was carried out for 30 - 60 min at room temperature. Afterwards the cells were transferred into 50 ml YPD/1 M sorbitol and incubated for 30 min under constant shaking. The strains were shifted to the restrictive temperature of 16 °C for 1 h 15 min or 1 - 2 h at 37 °C, depending on the temperature sensitivity of the used strain. Afterwards, the cells were collected by centrifugation for 10 min at 2000 x g. A volume of 10 ml of the culture served as total RNA and total protein control and 40 ml were used for the nucleo-cytoplasmic fractionation experiment. For total RNA and total protein controls, the pellet of the 10 ml fraction was resuspended in 1ml H_2O. For total RNA isolation 700 µl of the 1 ml were used and 300 µl served as the total protein control. The samples were collected in 2 ml screw top tubes for cell lysis with the fast prep and were treated as described in section 3.8.1 and 3.10.1.

For the nucleo-cytoplasmic fractionation, the supernatant of the 40 ml samples was discarded after centrifugation and the pellet was resuspended in 500 µl Lysis buffer (18 % Ficoll 400, 10 mM HEPES pH 6.0) plus 1 µl Ribolock and transferred into a fresh 1.5 ml tube. A volume of 1 ml Buffer A (50 mM NaCl, 1 mM $MgCl_2$, 10 mM HEPES pH 6.0) was added and the tube was vortexed thoroughly. To separate the cytosolic fraction the tube was centrifuged at 1,500 x g at 4 °C for 15 min. The supernatant, containing the cytosolic fraction, was collected. A volume of 1 ml was used for RNA extraction and 100 µl were used as a cytosolic protein control. RNA extraction was carried out as described in 3.8.1. The protein control samples were mixed with

2x SDS sample buffer (125 mM Tris pH 6.8, 4 % SDS, 20 % (v/v) glycerol, 0.05 % (w/v) Bromophenol blue, 5 % (v/v) 2-mercaptoethanol). A control Western blot was carried out using specific antibodies detecting the cytoplasmic protein Zwf1, glucose-6-phosphate dehydrogenase, and the nucleolar protein Nop1, histone glutamine methyltransferase, as described in section 3.10.3 and 3.10.4.

3.8.5. Southern blot analysis

In this study the Southern blot analysis was used to investigate the length and structure of the telomeric DNA of *S. cerevisiae*. The basic principle of Southern blotting is based on the separation of digested chromosomal DNA on an agarose gel, subsequent transfer of the DNA to a carrier membrane and visualization of the DNA via a chemiluminescence reaction. For detection a specific probe complementary to the desired target, a secondary antibody coupled to alkaline phosphatase and the substrate CSPD (Roche) were used.

3.8.5.1. Telomere restriction fragment (TRF) analysis

The technique of telomere-restriction-fragments (TRF) is a modified version of a southern blot, in which the terminal-restriction-fragments of the heterogeneous telomere ends are analyzed and visualized using specific digoxigenin-labeled DNA-probes (Sigma Aldrich) which are complementary to the TG-repeats of the telomeres (Meyne et al., 1989).
The cell cultures were passaged and harvested as described in section 3.6.3. High-quality chromosomal DNA was isolated as described in section 3.7.2. DNA concentration was measured as described in 3.7.4 and 100 µg DNA per strain were digested with XhoI for 1 h at 37 °C, as described in section 3.7.6. The overall experimental set-up was modified, in particular non-radioactive probes were used, but was carried out in accordance to Xia et al. (2000). Per lane 20 µg XhoI digested DNA were loaded onto a 1 % agarose TBE or TAE gel containing 5 µl/100 ml HdGreen (Intas Science Imaging). By applying a voltage, the DNA fragments were separated based on their size, see 3.7.7. The fragments were separated for 4 h to 24 h at 120 to 25 volts respectively. A size standard was loaded to document the separation of the DNA via the UV Gel detection system after running the gel. After gel-electrophoresis, the gel was subsequently processed by depurination (250 mM HCl) for 15 min, denaturation (1.5 M NaCl,

0.5 M NaOH) for 30 min, neutralization (1.5 M NaCl, 0.5 M Tris-HCl, pH 7.5) for 30 min, and finally equilibration with 20x SSC (0.3 M Tri-sodium citrate, 3 M NaCl, pH 7.0) for 15 min: Each step was done under constitutive shaking. A capillary blot was used to transfer the DNA fragments from the gel onto a positively charged nylon membrane HybondN$^+$ (GE Healthcare). Therefore, the gel was placed on a glass plate and the boundaries of the gel were covered with parafilm. The membrane was placed on top of the gel followed by 3 whatman paper and a bunch of paper towels. On top of that, a glass plate covered with a heavy weight (500 – 750 g) was placed, to allow a capillary transfer of the DNA to the membrane. The DNA transfer was carried out over night. Subsequently the membrane was exposed to UV light for 7 min at 254 nm, 12,0000 µJ/cm^2, and afterwards heated to 80 °C for 2 h, to crosslink the DNA with the membrane. The pre-hybridization of the membrane was carried out for 1 h at 68 °C in hybridization buffer (0.5 M sodium phosphate buffer pH 7.5, 7% (w/v) SDS, 1mM EDTA). After pre-hybridization, 50 pmol of the digoxygenin-labeled probe (Sigma Aldrich) were first denatured at 95 °C for 10 min and subsequently added to the hybridization buffer. The membrane was incubated over night at 68 °C under agitation.

On the next day, 15 minutes washing steps were carried out, once with 2x SSC, 0.1 % SDS, followed by 1x SSC, 0.1 % SDS at room temperature. Afterwards, the membrane was washed twice with 0.5 x SSC, 0.1 % SDS for each 15 min at 37 °C and finally for 5 min in washing buffer (Table 19). The membrane was blocked for 30 min in blocking buffer. Detection was achieved by using an anti-digoxygenin antibody coupled to an alkaline phosphatase (Roche), diluted 1:10.000 in blocking buffer and incubated for 30 min. The membrane was washed twice with washing buffer for 15 min each time. Afterwards, the membrane was equilibrated in detection buffer for 5 min. Finally, 1 ml CSPD (Roche), which activates the chemiluminescent reaction, was added to the membrane and incubated for 10 min at 37 °C in the dark. For detection the Fusion FX (Vilber) was used.

Table 19: Southern blot detection solutions

Solution	Composition
Hybridization buffer	0.5 M Na-Phosphate pH 7.2 7 % SDS 1 mM EDTA
1M Na-phosphate buffer pH 7.2	68.4 ml 1 M Na_2HPO_4 31.6 ml 1 M NaH_2PO_4
5x Maleic acid buffer	0.5 M Maleic acid 0.75 M NaCl pH was adjusted to pH 7.5 using solid NaOH
Blocking buffer	1x Blocking reagent (Roche) 1x Maleic acid buffer
Washing buffer	1x Maleic acid buffer 0.3 % Tween-20
10x Detection buffer pH 9.5	1 M Tris 1 M NaCl
CSPD	1:100 CSPD (Roche) in detection buffer

3.9. Microscopic studies

3.9.1. Fluorescence *in situ* hybridization experiments (FISH)

Fluorescence *in situ* hybridization (FISH) experiments were used as a molecular biological method for visualization of individual RNA species. The FISH experiments were carried out as described in Hackmann et al. (2014). The detection of *TLC1* was conducted by three at the 3'- and the 5'-end Cy3-labled DNA probes (Sigma Aldrich) which are complementary to *TLC1*. The microscopic analysis of *TLC1* localization was achieved by stacking pictures of 10 layers (0.2 µm each) of the cell using the Leica DMI6000B fluorescence microscope with the Leica DFC360 FX camera, which was finally deconvoluted using the LAS AF1.6.2 software. Used solutions are listed in Table 20.

Desired strains were grown to mid-log phase (1x 10^7 cells/ml) at 25 °C prior to a temperature shift to the restrictive temperature, if a temperature sensitive mutant was used. Afterwards, the cells were fixed by adding formaldehyde to a final concentration of 4 %. Fixation was carried out for 60 min under agitation and subsequently cells were collected by centrifugation for 1 min at 4000 x g at 4 °C. The supernatant was discharged and the pellet was washed three times in each 1 ml P-solution. The pellet was finally resuspended in 100 µl P-solution, mixed with 1 µl 1 M DTT and incubated for 10 min at room temperature. The cells were spheroblasted using Zymolyase treatment to allow the probes to penetrate the cell wall.

Therefore, 10 µl of Zymolyase (10 mg/ml) were added to the cell suspension and samples incubated for 5 - 30 min until 70 % of the cells were spheroblasted. Cells were collected by centrifugation at 2000 x g for 5 min and resuspended in 1 ml P-solution. A volume of 20 µl of the cell suspension was spotted onto a Poly-L-lysine coated slide and incubated for 1 h in a humidified chamber. Subsequently cells were permeabilized using P-solution with 0.5 % Triton X-100 for 10 min. The excess was gently aspirated, the wells were rinsed once with P-solution and equilibrated with freshly prepared 0.1 M TEA pH 8.0 for 2 min at room temperature. To block polar groups the cells were treated with 0.25 % acetic anhydride in 0.1 M TEA for 10 min at room temperature. Finally, the slide was rinsed with P-solution and the pre-hybridization was carried out. For the pre-hybridization *salmon sperm* DNA was boiled for 5 min at 95 °C and afterwards chilled for another 5 min on ice. The pre-hybridization mix was prepared, and 20 µl per well were added, including 19.8 µl HybMix, 0.1 µl tRNA (10 mg/ml) and 0.1 µl *salmon sperm* carrier DNA. The pre-hybridization mix was incubated for 1 h at 37 °C in a humidified chamber.

Finally, the pre-hybridization mix was aspirated and the hybridization mix was applied. The hybridization mix contains HybMix, tRNA and *salmon sperm* carrier DNA in the same concentrations. Furthermore, the Cy3-labeled probes were added in a 1:200 dilution. The slides were incubated over night at 37 °C in a humidified chamber. On the next day, the slides were washed each for 1 h with 2x SSC and with 1x SSC at room temperature. Afterwards the slides were washed with pre-warmed 0.5x SSC at 37 °C for 30 min and once with 0.5x SSC at room temperature for 30 min.

For nuclear staining Hoechst (1:10,000 diluted in 1x PBS) solution or DAPI (1:8,000 diluted in 1x PBS) was applied on the wells and incubated for 2 min in the dark. The cells were subsequently washed once with 1x PBS, 0.1 % Tween-20 for 5 min and twice with 1x PBS for each 5 min. All of these steps were carried out at room temperature. The slides were dried in the dark and finally mounted. Slides were stored at - 20 °C.

Table 20: Solutions for microscopic analysis

Solution	Composition
1x PBS pH 7.4	137 mM NaCl 2,7 mM KCl 10 mM Na_2HPO_4 1.8 mM KH_2PO_4
P-solution	0.1 M phosphate buffer pH 6.5 1.2 M sorbitol
HybMix	50 % deionized formamide 25 % 20x SSC made with DEPC treated H_2O 1 % 500mM EDTA pH 8.0 1 % Tween-20 (10%) 2 % 50x Denhardt's 1 % Heparin, 10mg/ml
50x Denhardt´s solution	1 % Ficoll 1 % Polyvinylpyrrolidone 1% BSA (Pentax Fraction V)
Mounting medium	2 % (w/v) n-propyl gallate 80 % (v/v) glycerol 20 % (v/v) PBS pH 8.0

3.9.2. GFP-Microscopy

The localization of GFP-tagged proteins, either encoded on a plasmid or in the genome, was visualized using the GFP-microscopy protocol as described in Hackmann et al. (2014). Cells were grown, and prepared as described in the FISH experiments, but fixation was carried out in a final concentration of 2,5 % formaldehyde for 1 min. The cells were collected by centrifugation at 4000 x g for 1 min and subsequently washed once with 1 ml 0.1 M phosphate buffer pH 6.5 and once with 1 ml P-solution. The pellet was resuspended in 100 µl to 1 ml P-solution depending on the size of the harvested pellet. A volume of 20 µl of each cell suspension was applied on a Poly-L-lysine coated slide and incubated for 15 min at room temperature. Permeabilization of the cells was achieved by treating them with P-solution, 0.5 % Triton X-100 in for 5 min at room temperature. Afterwards, the cells were washed twice with P-solution, the nucleus was stained and the slides were mounted as described in 3.9.1.

3.9.3. Immunofluorescence experiments

In this method, tagged proteins are visualized by an antigen-antibody reaction. The interaction of the primary antibody which recognizes the tag of the protein and a secondary antibody which is coupled with a fluorochrome allows direct detection and thus cellular localization of the tagged protein *in vivo*. The experiments were carried out as described in H. Wu, Becker, and Krebber (2014), except that the incubation time with the primary antibody was changed and that the washing steps were modified.

Cells were grown to mid-log phase in a volume of 10 ml and were shifted to the restrictive temperature of the strain, if a temperature-sensitive mutant was used. Fixation of the cells was carried out in a final concentration of 4 % formaldehyde for 10 min at the restrictive temperature followed by 50 min at 25 °C. Cells were collected via centrifugation for 2 min at 4000 x g at 4 °C and subsequently washed three times with 1 ml of P-solution. The pellet was resuspended in 100 µl of P-solution and incubated with 1 µl of DTT for 10 min at room temperature. The cells were spheroblasted using 10 µl of Zymolyase (10 mg/ml) for 5 - 15 min at room temperature. The prepared cells were placed on a Poly-L-lysine coated slide and incubated for 30 - 60 min at 4 °C. The supernatant was aspirated and the cells were permeabilized with 0.5 % Triton X-100 in P-solution for 5 min. Afterwards, the cells were blocked for 1 h in antibody blocking buffer (0.1 M Tris pH 9.0, 0.2 M NaCl, 5 % heat-inactivated FCS, 0.3 % tween) (ABB). The ABB was finally removed and the cells were covered with an appropriate primary antibody diluted in ABB and incubated for 2 h at room temperature (Table 4). Subsequently, the cells were washed twice shortly with 1x PBS + 0.5 % tween and once for 30 min with 1x PBS + 0.5 % tween. This was followed by two 15 min washing steps with 1x PBS and one washing step with ABB for 30 min. The secondary antibody was diluted in ABB and incubated on the cells for 1 h at room temperature (Table 4). The cells were quickly washed once with 1x PBS + 0.5 % tween and again for 30 min with 1x PBS + 0.5 % tween. Subsequently, cells were washed two times with 1x PBS for 15 min. The nucleus was stained and the slides were mounted as described in 3.9.1.

3.10. Biochemical methods

3.10.1. Preparation of yeast cell lysate

For the preparation of cell lysates, the respective strains were grown to mid-log phase, shifted to the restrictive temperature if required, and harvested by centrifugation at 4000 x g for 5 min at 4 °C. Subsequently, depending on the culture volume, they were transferred to 2 ml or 15 ml screw top tubes and stored on ice for direct use or stored at - 20 °C after treatment with liquid nitrogen. Depending on the following experiment, the pellet was lysed in the appropriate buffer, see 3.10.2 for Immunoprecipitation experiments and see 3.10.5 for RNA Co-Immunoprecipitation experiments, and by addition of glass beads. The volume of the buffer and of the glass beads (0.4 – 0.6 mm) were equal to the volume of the corresponding cell pellet. The pellet was lysed using the FastPrep machine three times for 30 sec at 4 m/s with 5 min incubation on ice in-between. The lysate was cleared of cell debris by centrifugation for 10 min at 16.000 x g at 4 °C and used according to the experimental protocols.

3.10.2. Immunoprecipitation (IP) experiments

To analyze protein-protein interactions, immunoprecipitation (IP) experiments were essentially carried out as published earlier Zander et al. (2016). GFP-tagged proteins were purified using the GFP-Selector-beads (NanoTag) or GFP-trap beads (ChromoTek) and Myc-tagged proteins with Myc-trap beads (ChromoTek). Ready to use beads were prepared according to manufacturer's instructions and washed three times with 1 ml PBSKM-T buffer (1x PBS (137 mM NaCl, 2.7 mM KCl, 1.8 mM KH_2PO_4, 10 mM Na_2HPO_4) pH 7.4, 2.5 mM $MgCl_2$, 3 mM KCl, 0.5 % Triton X-100, and protease inhibitor added freshly each time (5µl per 100 µl pellet; cOmplete™ EDTA-free Protease Inhibitor Cocktail, Roche)). After each washing step they were centrifuged for 1 min at 400 x g. For one IP sample a pellet of a 400 ml culture was resuspended in the same volume (~ 500 µl) of cooled PBSKM-T buffer. Cell lysates were generated as described in 3.10.1. For IP experiments with Mtr10 a concentration of 1 % Triton X-100 was used during cell lysis which was diluted after homogenization to a final volume of 0.5 % Triton X-100. For total protein control, 30 - 100 µl of the pre-cleared lysates were mixed with 2 x SDS sample buffer (125 mM Tris pH 6.8, 4 % SDS, 20 % (v/v) glycerol, 0.05 % (w/v)

Bromophenol blue, 5 % (v/v) 2-mercaptoethanol). For the IP, 1ml of the pre-cleared lysate was incubated with the respective PBSKM-T adjusted, beads under agitation for 1 h at 4 °C. Subsequently, the beads were washed 5 times with PBSKM-T buffer with a final concentration of 0.5 % Triton X-100. After the last washing step, the supernatant was discarded leaving approximately 30 µl of residual liquid in the tube without losing the beads. The sample including the beads is now termed “eluate”. The eluate was mixed with 30 µl 2 x SDS sample buffer. Prior to loading on a SDS gel, the samples were boiled for 5 min at 95 °C.

3.10.3. SDS-Polyacrylamide gel-electrophoresis (SDS-PAGE)

In this study the standard, vertical, discontinuous Polyacrylamide gel electrophoresis was carried out to separate proteins according to their size (Garfin, 2009). The stacking and the separation gel compositions are listed in Table 21. First, the separation gel mix was prepared, poured between two 25 x 20 cm glass plates with 2 mm thick spacers and was covered with a layer of isopropanol to generate an even surface of the gel. The isopropanol was removed after polymerization of the separation gel. The stacking gel mix was poured onto the separation gel and a comb was immediately inserted to generate sample pockets. After polymerization of the stacking gel, it was put in a running chamber and the reservoirs of the chamber were filled with SDS running buffer (25 mM Tris Base, 0.1 % SDS, 190 mM glycine). Air bubbles underneath the gel were removed using a syringe and the comb was removed from the gel. The prepared samples, as well as a protein maker with appropriate marker sizes (Table 5) were loaded onto the gel. The power source was coupled with the two electrodes of the chamber and the gel run was carried out for approximately 16 h at 10 mA.

Table 21: Composition of SDS Polyacrylamide gels

Components	**Stacking gel**	**Separation gel**
Bis-/Acrylamide mixture 37,5:1	5 % (v/v)	10 % (v/v)
Tris/HCl pH 8.8	-	375 mM
Tris/HCl pH 6.8	125 mM	-
SDS	0.1 % (w/v)	0.1 % (w/v)
APS	0.1 % (w/v)	0.1 % (w/v)
TEMED	0.1 % (v/v)	0.04 % (v/v)

3.10.4. Western blot analysis

After successful SDS-PAGE, the proteins were transferred onto a Amersham Protran 0.45 µm nitrocellulose membrane (GE Healthcare Life Sciences) by semi-dry blotting procedure according to Towbin, Staehelin, and Gordon (1979). For the transfer, the anode plate was covered with blotting buffer (25 mM Tris Base, 192 mM glycine, 20 % (v/v) methanol). A pre-soaked whatman paper was put onto the anode, followed by the membrane, the SDS-Gel and finally by another pre-soaked whatman paper. Air bubbles were eliminated and additional blotting buffer was poured onto the stack. Finally, the cathode was placed on top and fixed by screws. Depending on the size of the membrane the mA for transfer was calculated (1.2 mA/cm^2) and the transfer took place for 2 h. After transfer, the membrane was blocked in 5 % (w/v) milk powder in TBS-T (50 mM Tris pH 7.4, 150 mM NaCl, 0.1 % (v/v) Tween 20) for 1 h at room temperature under constant shaking. After blocking the primary antibody was diluted in 2 % milk powder in TBS-T and added to the membrane (Table 4). The primary antibody was incubated over night at 4 °C under constant shaking. After removal of the primary antibody the membrane was washed three times with TBS-T for 5 min each and afterwards incubated with the secondary antibody. Depending on the primary antibody, anti-mouse or anti-rabbit secondary antibodies, which are coupled to the horseradish peroxidase (HRP), were used. The secondary antibody was diluted in TBS-T with 2 % milk powder and incubated for 2 h at room temperature under constant shaking (Table 4). The membrane was washed three times with TBS-T for 5 min each and rinsed once with water. The membrane was covered with ECL substrate solution (WesternBright Quantum, Advansta) and put into a plastic sheet. The excess liquid was removed and the signals were detected in a chemiluminescence imaging system (Fusion SL and Fusion FX (Vilber)).

3.10.5. RNA Co-Immunoprecipitation (RIP) experiments

To investigate RNA-Protein interactions, RNA Co-Immunoprecipitation (RIP) experiments were carried out. They were conducted essentially as published earlier in Zander et al. (2016). For one RIP sample a pellet of a 400 ml culture was used. For lysates and beads preparation freshly prepared RIP buffer (25 mM Tris/HCl pH 7.5, 150 mM NaCl, 2 mM $MgCl_2$, 0.2 mM PMSF, 0.5 mM DTT, 0.2 % (v/v) Triton X-100) with protease inhibitor (5 µl per 100 µl cell pellet; cOmplete™, EDTA-free Protease Inhibitor Cocktail, Roche) and RNase inhibitor (0.6 µl / 500 µl pellet-volume RiboLock, Thermo Scientific)) was used. The lysis and pre-clearance of the lysates was carried out as described in section 3.10.1. Besides 30 - 100 µl for protein lysate control also 100 µl for RNA lysate control were taken before the RIP experiment started. Protein control samples were mixed with 2 x SDS buffer and kept at - 20 °C before usage as lysate control for Western blot analysis. The RNA lysate control was treated with 10 µl DNAse (Qiagen) for 1 h at 4 °C under agitation. GFP-tagged proteins were purified using the GFP-Selector-beads (NanoTag) or GFP-trap beads (ChromoTek) and Myc-tagged proteins with Myc-trap beads (ChromoTek). Ready to use beads were prepared according to manufacturer's instructions and washed three times with pre-cooled RIP buffer. For one RIP, 10 µl beads were mixed with 1 ml of pre-cleared lysate (equal volume for all tested strains). The RIP was carried out with the addition of 10 µl DNase (Qiagen) for 1 h at 4 °C under agitation. After incubation the RIP samples were washed 5 times in 1 ml pre-cooled RIP buffer and centrifugated at 400 x g at 4 °C for 1 min between the washing steps. Prior to the last washing step, the RIP sample was separated into two portions, 300 µl of 1 ml served as protein eluate control, for Western blot analysis, and 700 µl were used for RNA isolation. After removal of the supernatant, the protein samples were mixed with 2x SDS loading buffer and further analyzed using the Western blot analysis. The RNA lysate control and the RIP samples containing the co-precipitated RNA were mixed with 1 ml TRIzol and RNA Isolation was carried out as described in section 3.8.1. Afterwards, DNA digestion was carried out with the TurboDNAse Kit according to the manufacturer's description, but the digest was incubated for 1 h at 37 °C. Subsequently, the RNA was precipitated via sodium acetate ethanol precipitation as described in section 3.8.1. The RNA concentration was measured, 100 - 500 ng RNA were reverse transcribed into cDNA and finally analyzed using qPCR as described in section 3.7.4, 3.8.2 and 3.8.3.

Furthermore, a special form of RIP experiments was carried out, in which the trimethylguanosine modification of nascent RNA species is used for precipitation purpose. For TMG-cap RIP, total RNA was isolated from yeast cell lysates via TRIzol-chloroform extraction. Afterwards, 50 µg of total RNA was adjusted to a volume of 300 µl with RIP buffer and was incubated with 10 µl of an anti-2,2,7-trimethylguanosine antibody (Calbiochem Milipore) coupled to agarose beads for 1 h at 4 °C under agitation. Subsequently, the beads were washed 5 times with RIP buffer and the co-precipitated RNA was extracted via TRIzol-chloroform extraction and afterwards precipitated by sodium acetate precipitation as described in section 3.8.1. The RNA was reverse transcribed into cDNA and finally analyzed using qPCR as described in section 3.8.2 and 3.8.3.

3.11. Quantification and statistical analysis

All experiments were carried out in at least three independent biological replicates, and qPCR additionally in three technical replicates. Statistical significance was evaluated using an unpaired, one-tailed or two-tailed, unequal variance student´s t-test. The p-values are indicated by * ($p < 0.05$), ** ($p < 0.01$) and *** ($p < 0.001$). Error bars represent the standard deviation. The amount of the *21S* rRNA, *25S* rRNA or the house keeping gene *RPL8a* served for normalization of the qPCR experiments.

4. Results

4.1. The *TLC1* amount increases in mutants of the NNS complex

The genomic sequence of the 3´-region of *TLC1* possesses termination motifs typical for both termination pathways, the CPF-CFI-mediated and the NNS-mediated termination (Figure 5 and Figure 9). So far it is unclear which pathway led to functional *TLC1* that is incorporated into the telomerase.

To gain insight into which transcription termination pathway is primarily used, we analyzed the change in the relative amount of *TLC1* in different termination factor mutants. A mutant of *RNA15*, encoding a core subunit of the cleavage factor IA, was used for CPF-CFI-mediated termination defects. This protein is essential for poly(A) signal site recognition and cleavage of the targeting RNA. In order to analyze the NNS-mediated termination, mutants of Nrd1 as well as a mutant of the helicase Sen1 were used. These proteins are essential for target recognition and cleavage at the NNS termination area. By choosing specific primers, both the total *TLC1* and the immature form were examined. Notably the pool of the total *TLC1* includes the immature form, as the primers can amplify both (Figure 9). Moreover, the amplification of total *TLC1* and immature *TLC1* is independent of the termination machinery used, because the reverse primer for the immature form is located upstream of the first termination area (Figure 9).

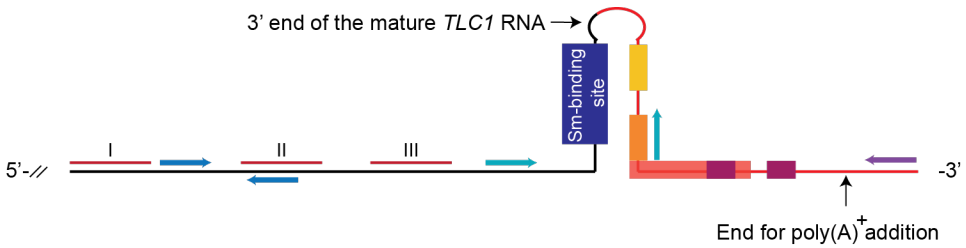

Primers used for qPCR	Probes used for FISH experiments	Termination factor binding sites
Total *TLC1* forward Total *TLC1* reverse Immature *TLC1* forward Immature *TLC1* reverse Long *TLC1* reverse	FISH probe I - 222-271 50bp FISH probe II- 617-662 46bp FISH probe III- 836-886 51bp	Nab3 binding site Nrd1 binding site NNS termination area Poly(A) signal sites

Figure 9: Schematic representation of the *TLC1* RNA with the indicated termination factor binding sites. Used primers and probes are shown.

The indicated strains were shifted to the restrictive temperature for 2 h before the cells were lysed. The total RNA was isolated, reverse transcribed and subsequently analyzed via qPCR. The analysis revealed that neither *rna15-58* nor *nrd1-101* mutants seriously affected the amount of *TLC1,* even though a very slight decrease of total *TLC1* was observed in the *nrd1-101* mutant (Figure 10). Thus, the specific mutations in *rna15-58* and *nrd1-101* mutants are not likely to affect the transcription termination of *TLC1* or the generated transcripts are processed normally (Figure 10). In contrast, the *nrd1-102* and *sen1-1* mutants, which are both defective in the RNA recognition of the nascent transcript (Conrad et al., 2000; Hazelbaker et al., 2013), showed an increased amount of both the total *TLC1* and the immature *TLC1* (Figure 10). This indicates a read-through of transcription, which is for *nrd1-102* supported by published data (Noël et al., 2012). Furthermore, it indicates that the *TLC1* RNA is stabilized when the NNS-pathway is not functional, which could indicate that NNS-transcripts are normally more degraded than processed.

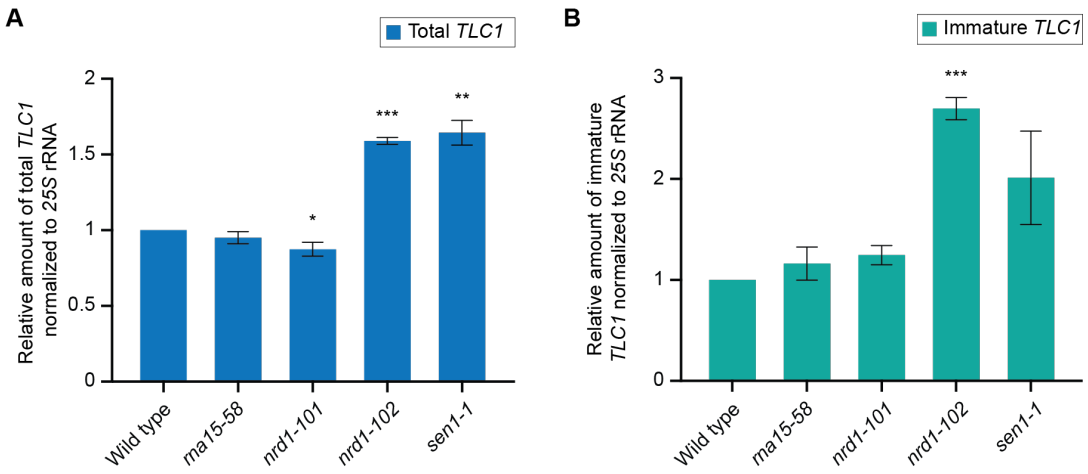

Figure 10: *nrd1-102* and *sen1-1* mutants lead to an increased *TLC1* amount.
The indicated strains were grown to mid-log phase prior to the 2 h incubation at their restrictive temperatures. The temperatures of 30 °C, 35 °C and 37 °C were used for the *sen1-1*, the *rna15-58* and the *nrd1* mutants respectively. After cell lysis, the total RNA was isolated, reverse transcribed into cDNA and analyzed via qPCR. qPCR data of **(A)** the total or **(B)** the immature *TLC1* was obtained using specific primers. The error bars represent the standard deviation, p-values were calculated by unpaired two-tailed unequal variance student´s t-test (* = p< 0.05, ** = p< 0.01, *** = p< 0.001); n=3.

4.1.1. The *poly(A)*, NNS** and *poly(A)*NNS** termination site mutants show an altered *TLC1* abundance *in vivo*

Mutation of the poly(A) signal (PAS) sites did not result in telomeric shortening in a plasmid based approach, which was interpreted as this pathway being not essential for *TLC1* termination (Noël et al., 2012). Furthermore, mutation of the NNS sites in the 3´-end region of a reporter construct resulted in defective termination and a read-through of the NNS-site (Noël et al., 2012). Based on this data, it was hypothesized the NNS complex is vital for the termination of the *TLC1* RNA, which is incorporated into the telomerase (Noël et al., 2012). However, the NNS mutations were not analyzed directly in the termination of *TLC1* and thus the study lacks the information of the essentiality of the termination sites. Thus, additional research is needed and we started this analysis by endogenous mutating both sites (Figure 11).

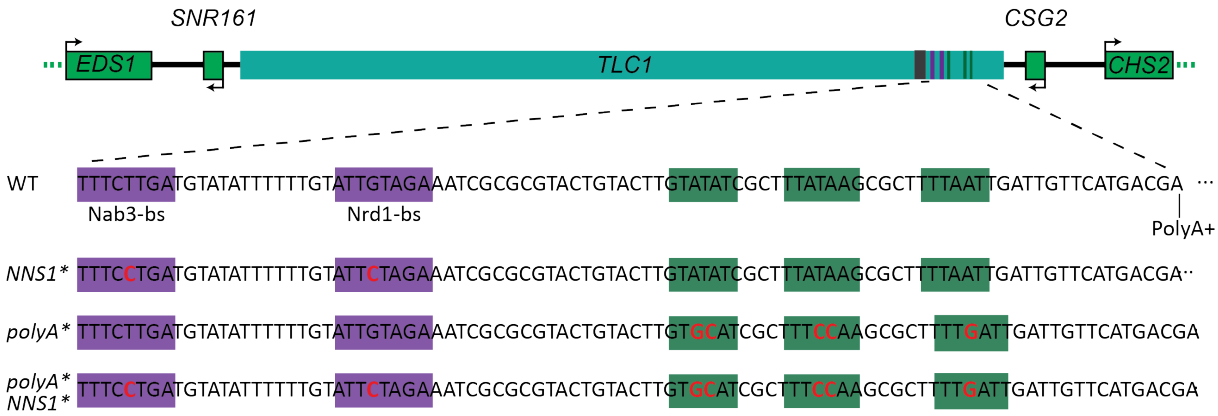

Figure 11: *TLC1* termination site mutants used in this study.
Schematic representation of inserted point mutations, highlighted in red, in the *NNS**, *poly(A)** and *poly(A)*NNS** mutants. Nab3 and Nrd1 binding sites are highlighted in purple and poly(A) signal sites in green.

The indicated termination site mutants were grown to mid-log phase and cells were harvested and lysed. The total RNA was isolated, reverse transcribed and subsequently analyzed via qPCR.

We observed a decrease in the total *TLC1* amount for all mutations tested to approximately 55 % compared to the wild type (Figure 12 A). This indicates that both termination sites are used under normal conditions. For detection of transcription read-through, primers amplifying a long *TLC1* form were used in which the reverse primer is complementary to the end of the *TLC1* locus (Figure 9). Compared to wild type, mutation of the PAS site and

simultaneous mutation of both the PAS and the NNS sites in the *poly(A)*NNS** led to an ~ 500 % and an ~ 200 % increased abundance of long *TLC1* respectively (Figure 12 B). This indicates that mutation of the PAS sites leads to read-though and that downstream termination sites are present. In contrast, we observed a decreased abundance of long *TLC1* in the *NNS** mutant to 37 % compared to wild type (Figure 12 B). This might indicate that transcription of *TLC1* is terminated in the *NNS** mutant by the CPF-CFI complex at the PAS site, limiting the formation of long *TLC1.* This would imply a read-through of the NNS site but a termination at the PAS site in the *NNS** mutant.

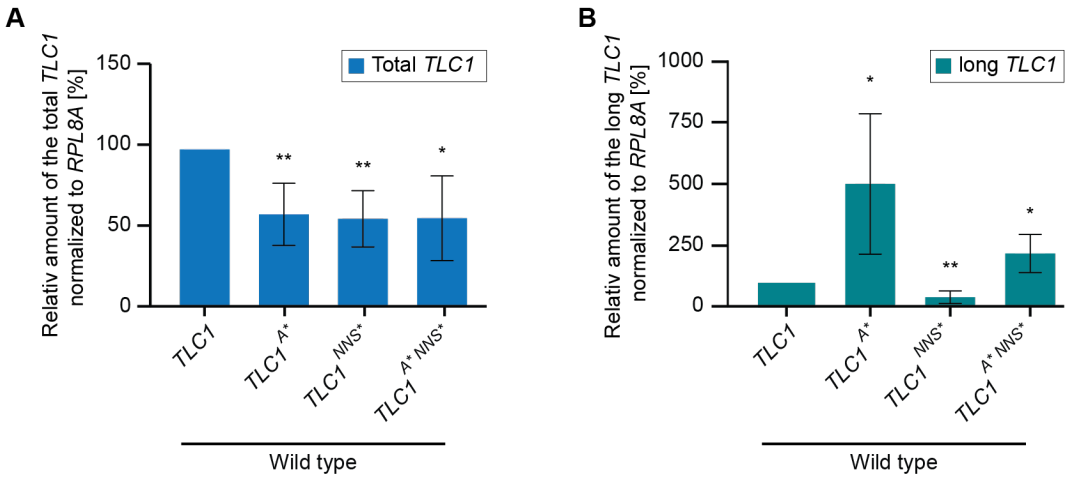

Figure 12: Mutation of the PAS site and the NNS binding site led to a decreased abundance of total *TLC1* but read-through transcripts occur in upon PAS mutation *in vivo*.
After cell lysis, the total RNA was isolated from the indicated transcription termination mutants and subsequently analyzed via qPCR. **(A)** Total *TLC1* and **(B)** long *TLC1* were amplified using specific primers. The error bars represent the standard deviation, p-values were calculated by unpaired two-tailed unequal variance student´s t-test (* = p< 0.05, ** = p< 0.01, *** = p< 0.001); n= 5.

4.1.2. Cytoplasmic accumulation of *TLC1* in transcription termination mutants

To gain further insight into which termination pathway may lead to functional *TLC1*, the localization of *TLC1* was analyzed in the termination mutants via Fluorescence *in situ* hybridization (FISH) and nucleo-cytoplasmic fractionation experiments.

FISH experiments were used to determine the localization of endogenously expressed *TLC1* via detection with three Cy3-labeled probes. In wild type cells *TLC1* predominantly localizes to the nucleus and served as a control. The mutation of the PAS termination site did not alter the localization of *TLC1* compared to wild type (Figure 13). In contrast, we detected a

mislocalization of *TLC1* to the cytoplasm in the *NNS** and the *poly(A)*NNS** mutants (Figure 13). The cytoplasmic mislocalization of *TLC1* was visible in approximately 80 % of the *NNS** cells, in which 379 cells were counted. In the in *polyA*NNS** mutant, in which 221 cells were counted, approximately 90 % of the cells showed a cytoplasmic mislocalization of *TLC1*. This indicates the production of a stable transcript in the *NNS** and the *poly(A)*NNS** mutants which most likely escape degradation.

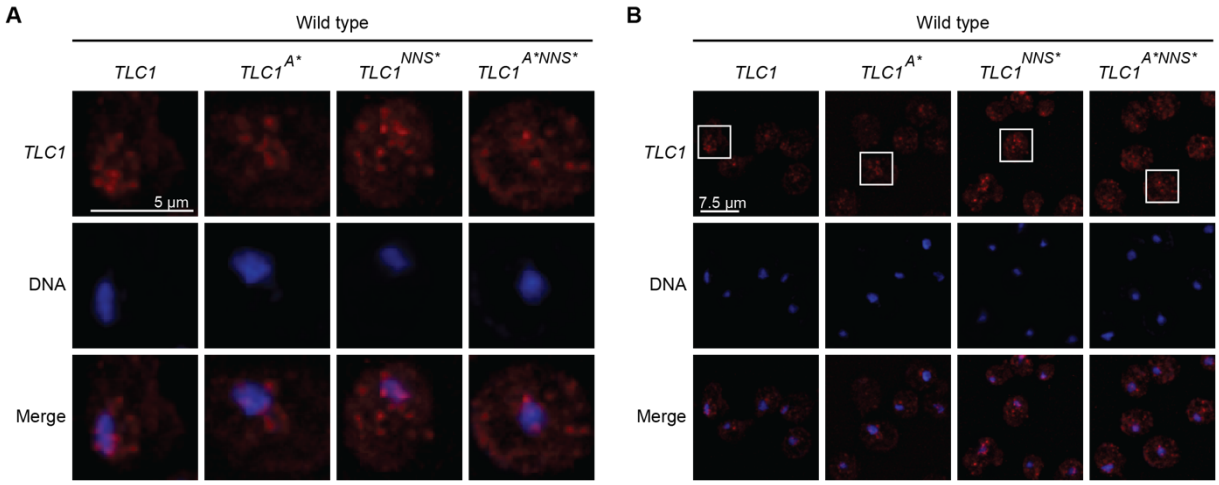

Figure 13: FISH analysis revealed a mislocalization of *TLC1* to the cytoplasm in the *NNS and the *poly(A)*NNS** mutants compared to wild type.**

FISH analysis of the indicated strains was carried out. Three sequence-specific Cy3-labelled probes were used to detect *TLC1* (red). DNA was stained with Hoechst (blue) **(A)** Single cell images of the indicated cells in (B) are shown. **(B)** Overview of several cells is shown of which the framed ones are depicted in (A). n=3.

Although the FISH experiments revealed a mislocalization of *TLC1* in the *NNS** and *poly(A)*NNS** mutated cells, it is unclear which *TLC1* transcripts mislocalize. To investigate this, nucleo-cytoplasmic fractionation experiments were carried out. In addition to the wild type background, experiments were conducted in the *cse1-1* mutant. The *cse1-1* mutant was chosen since recently a function of Cse1 as re-import factor of snRNAs and *TLC1* was identified (see section 4.4 and Becker et al. (2019)).

The indicated strains were shifted to the restrictive temperature for 1 h and 15 min before the cytoplasmic fraction was purified. The total RNA of the cytoplasmic fraction was isolated and subsequently analyzed via qPCR. As controls for successful nucleo-cytoplasmic fractionation, both the cytoplasmic protein Zwf1, and the nucleolar protein Nop1 were detected via Western blot analysis using protein specific antibodies (Figure 14 A).

In the *cse1-1* mutant, total *TLC1* was enriched in the cytoplasm compared to wild type. This suggests that Cse1 has a function in the re-import of *TLC1*. In the *poly(A)** and *poly(A)*NNS**

mutants a decreased amount of total *TLC1* was detected in the cytoplasm, both in the wild type and the *cse1-1* background. This again indicates, that the PAS mutation has a negative effect on transcription termination of *TLC1* and that its effect is dominant over the *NNS** mutant in regard to total *TLC1.* In addition, in the *NNS** mutant we observed an increased amount of *TLC1* in the cytoplasm in wild type cells and in the *cse1-1* mutant (Figure 14 B). This indicates that stable transcripts accumulate in the cytoplasm even when the re-import is not hindered.

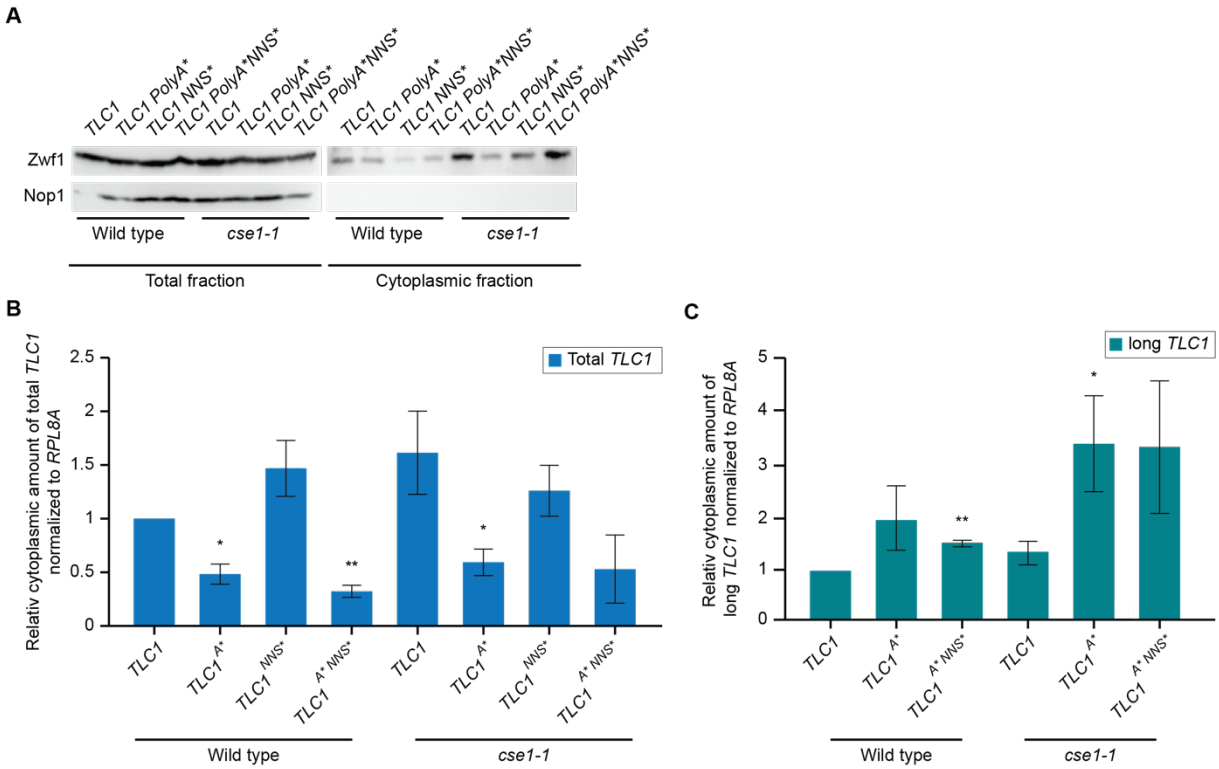

Figure 14: Nucleo-cytoplasmic fractionation experiment revealed altered localization of *TLC1* in the termination site mutants.

Nucleo-cytoplasmic fractionation experiments were carried out with the indicated strains. The strains were shifted to 16 °C for 1h and 15 min prior to cell lysis and isolation of the cytoplasmic fraction. Total RNA was isolated, reverse transcribed and analyzed via qPCR. **(A)** Western blot analysis of nucleo-cytoplasmic fractionation experiments is shown (B and C). The total and cytoplasmic fractions were controlled by detecting the cytoplasmic protein Zwf1 (Glucose-6-phosphate dehydrogenase) and the nucleolar protein Nop1 (Histone glutamine methyltransferase). **(B)** and **(C)** qPCR data of **(B)** total *TLC1* amplifying primers and **(C)** long *TLC1* amplifying primers of the cytoplasmic fraction are shown. The error bars indicate the standard deviation, p-values were calculated by unpaired two-tailed unequal variance student´s t-test (* = p< 0.05, ** = p< 0.01, *** = p< 0.001); n= 3; except wild type *NNS** n=4.

Analyzing the mutants in which a long *TLC1* form was present (Figure 12), we observed a cytoplasmic enrichment of these long read-though transcripts in all mutants tested

(Figure 14 C). First, this reveals downstream termination sites are used concerning all termination site mutants. In addition, altering the PAS termination resulted in a longer *TLC1* transcript which reached the cytoplasm and seemed to be processed normally, as it was not mislocalized in the FISH experiments, in contrast to altering the NNS termination pathway (Figure 14 C and Figure 13). Second, in the *cse1-1* mutant the abundance of long *TLC1* increases in the *poly(A)** and the *poly(A)*NNS** mutant background compared to the wild type, indicating that the long *TLC1* form is a target of Cse1 mediated re-import. We cannot clarify at this point which pathway leads to functional *TLC1* incorporated in the telomerase or whether both pathways are capable of generating a functional transcript. But we have shown that altering both termination pathways affect the abundance of *TLC1* and that only limiting NNS termination results in mislocalization of total *TLC1 in vivo*.

4.2. The Cap-binding complex component Cbp20 and *TLC1* physically interact

RNAP II transcripts harbor a m^7G-cap, which is recognized by the cap binding complex (CBC) consisting of Cbp20 and Cbp80 (Hamm and Mattaj, 1990; Izaurralde et al., 1995; Lewis and Izaurralde, 1997; Schwer et al., 2011). To investigate whether the Xpo1 mediated export of *TLC1* might involve binding to the CBC, we wished to analyze if Cbp20 as part of the CBC contacts immature *TLC1*. For this purpose, RNA Co-Immunoprecipitation (RIP) experiments were carried out. After cell lysis, Cbp20-GFP was precipitated via GFP-beads and the co-immunoprecipitated RNA was isolated, reverse transcribed and analyzed via qPCR. Successful precipitation of Cbp20-GFP was controlled by Western blot analysis. Both the pull down and a control protein were detected (Figure 15 A). The control mRNA, *Rpl8A*, showed an ~ 18-fold enrichment in Cbp20 binding. Specific primers were chosen to detect the immature form of *TLC1*, which was ~ 5-fold enriched compared to no tag. This indicates that *TLC1* and Cbp20 physically interact (Figure 15 B). Thus, in analogy to mRNAs also *TLC1* is bound and protected by the CBC.

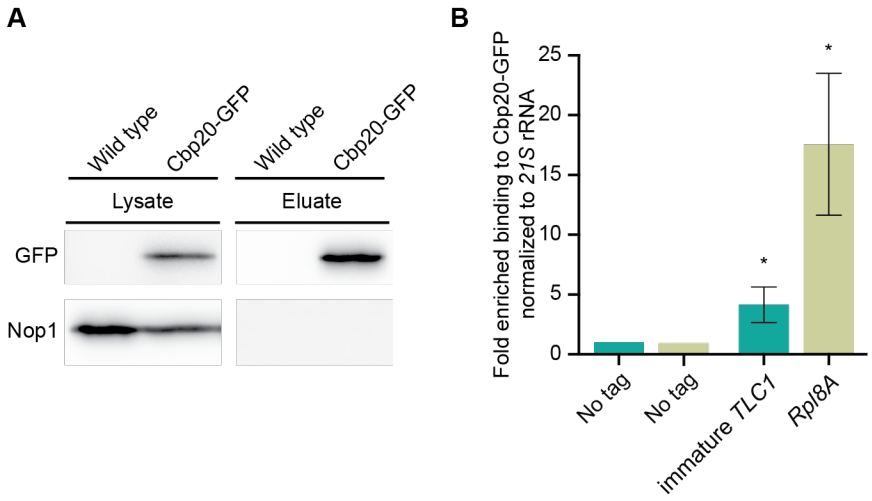

Figure 15: Cbp20 and *TLC1* physically interact.
The indicated strains were grown to mid-log phase prior cell lysis. Cbp20-GFP was precipitated with GFP-beads. Co-immunoprecipitated RNA was isolated, reverse transcribed and analyzed via qPCR. **(A)** A Western blot shows an example IP of immunoprecipitated Cbp20-GFP from the RIP experiments shown in (B). Nop1 served as a control for unspecific protein binding to the GFP-beads. Cbp20-GFP was detected with a GFP-specific antibody. **(B)** qPCR data from RIP experiments is shown. Primer amplifying immature *TLC1* and the *Rpl8A* control mRNA were used. The error bars indicate the standard deviation, p-values were calculated by unpaired one-tailed unequal variance student´s t-test (* = p< 0.05, ** = p< 0.01, *** = p< 0.001); n=3. (Part of the bioRxiv article Hirsch et al. (2021)).

4.3. Loading of the Sm-ring onto immature *TLC1* occurs in the cytoplasm

One characteristic feature of *TLC1* shared with snRNAs is the presence of a Sm-binding site (Seto et al., 1999). For snRNAs a cytoplasmic loading of the Sm-ring on unprocessed snRNAs has recently been shown and was suggested also for *TLC1* (Becker et al., 2019; Vasianovich et al., 2020). To analyze whether the Smb1 protein of the Sm-ring is loaded onto *TLC1* in the nucleus prior to export, RIP experiments were conducted in the export factor mutant *mex67-5 xpo1-1* in which RNA accumulates in the nucleus after temperature shift (Becker et al., 2019).

First, we precipitated Smb1-GFP from wild type cell lysates and showed an interaction between *TLC1* and Smb1 *in vivo*, as *TLC1* was ~ 300-fold enriched compared to when no tag was used (Figure 16).

In a second experiment the wild type and the *mex67-5 xpo1-1* mutant were shifted to the restrictive temperature for 1 h before the cells were lysed and GFP-tagged Smb1 was precipitated via GFP-beads. Protein precipitation was controlled by Western blot analysis and

showed a lower pull down in *mex67-5 xpo1-1* compared to wild type (Figure 16 C). Co-immunoprecipitated RNA was isolated and equal amounts of the RNA were subsequently reverse transcribed into cDNA and analyzed via qPCR. We observed a ~ 80 % depletion in the amount of *TLC1* bound to Smb1 in the *mex67-5 xpo1-1* mutant compared to wild type (Figure 16 D), suggesting that the loading of Smb1 onto *TLC1* occurs after export.

To test this directly, RIP experiments were carried out in the import factor mutant *mtr10Δ*, in which *TLC1* accumulates in the cytoplasm (Ferrezuelo et al., 2002; Gallardo et al., 2008).

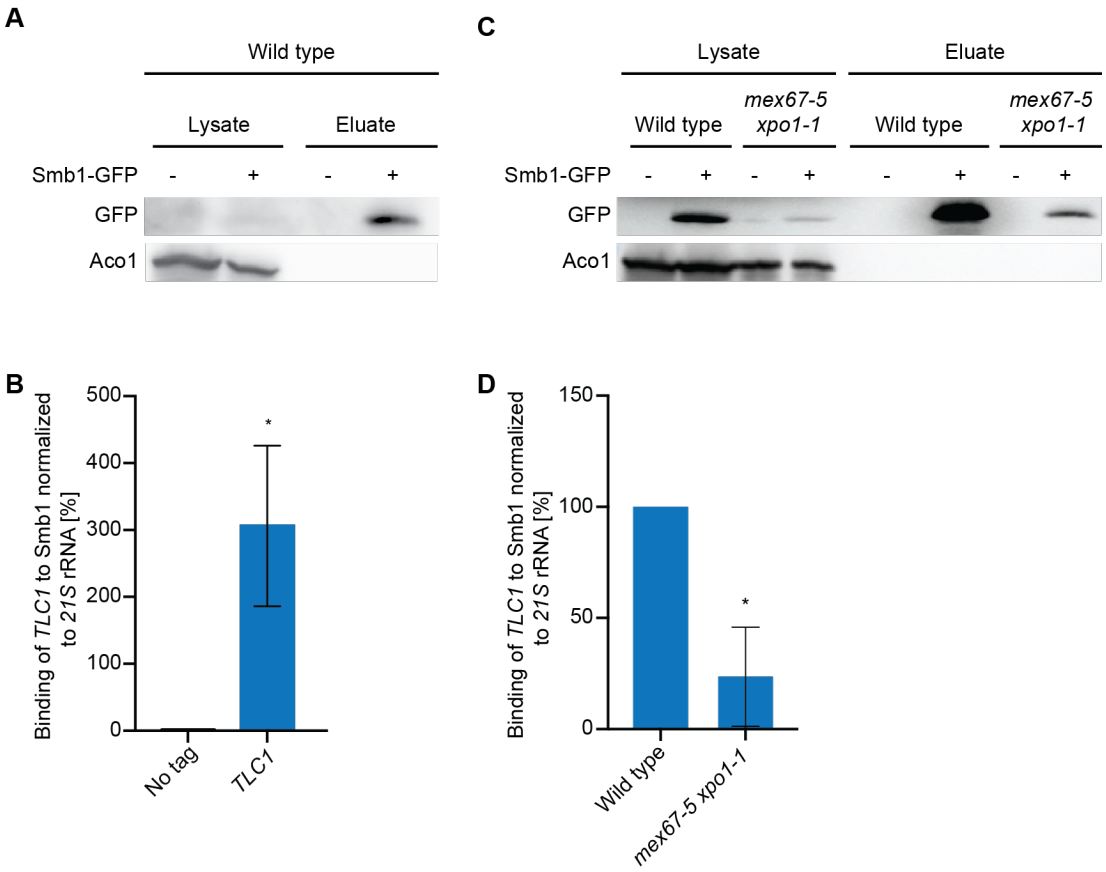

Figure 16: Decreased binding of *TLC1* to Smb1-GFP in *mex67-5 xpo1-1* mutants.
Indicated strains were grown to mid-log phase and either lysed directly (A) and (B) or shifted to the restrictive temperature of 37 °C for 1 h prior lysis (C) and (D). For protein precipitation GFP-beads were used. Co-immunoprecipitated RNA was isolated, reverse transcribed and analyzed via qPCR. **(A)** and **(C)** Western blot analysis of immunoprecipitated Smb1-GFP form the RIP experiments shown in (B) and (D) respectively. Aco1 (Aconitase 1) served as control for unspecific protein binding to the GFP-beads. Smb1-GFP was detected with a GFP-specific antibody. **(B)** qPCR data from RIP experiments showing the binding of *TLC1* to Smb1-GFP compared to no tag; n=4. **(D)** qPCR data from RIP experiments showing the binding of *TLC1* to Smb1-GFP in *mex67-5 xpo1-1* compared to wild type; n=3. The error bars represent the standard deviation, p-values were calculated by unpaired two-tailed unequal variance student´s t-test (* = p< 0.05, ** = p< 0.01, *** = p< 0.001). (Part of the bioRxiv article Hirsch et al. (2021)).

After cell lysis of wild type and *mtr10Δ* cells, Smb1-GFP precipitation was controlled by Western blot analysis (Figure 17 A). Analysis of the co-precipitated RNA via qPCR showed an approximately 170 % increased binding of total *TLC1* and an approximately 200 % increased binding of the immature *TLC1* to Smb1 in the *mtr10Δ* mutant compared to the wild type (Figure 17 B and C). We conclude that the Sm-ring loading onto immature *TLC1* takes place in the cytoplasm.

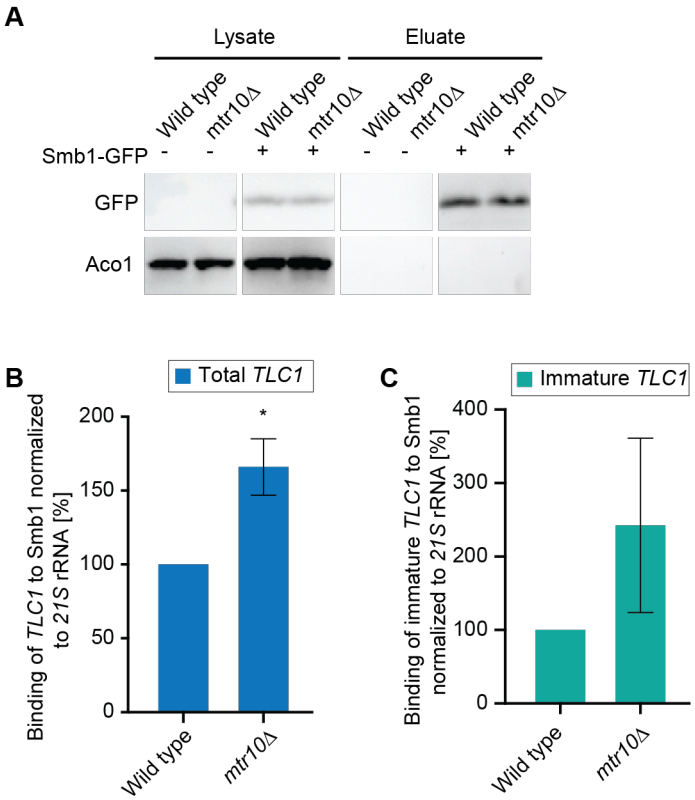

Figure 17: Increased binding of *TLC1* to Smb1-GFP in *mtr10Δ*.
The indicated strains were grown to mid-log phase prior cell lysis. For protein precipitation GFP-beads were used. Co-immunoprecipitated RNA was isolated, reverse transcribed and analyzed via qPCR. **(A)** A Western blot shows an example IP of immunoprecipitated Smb1-GFP form RIP experiments shown in (B) and (C). Aco1 served as control for unspecific protein binding to the GFP-beads. Smb1-GFP was detected using a GFP-specific antibody. **(B)** and **(C)** qPCR data from RIP experiments showing the binding of **(B)** the total *TLC1* and **(C)** the immature *TLC1* to Smb1-GFP in *mtr10Δ* compared to wild type. The error bars represent the standard deviation, p-values were calculated by unpaired two-tailed unequal variance student´s t-test (* = p< 0.05, ** = p< 0.01, *** = p< 0.001); n=3. (Part of the bioRxiv article Hirsch et al. (2021)).

4.4. Cse1 is involved in the nuclear import of *TLC1*

Recently, a physical interaction of snRNAs with Cse1 and Mtr10 and a mislocalization of snRNAs in the cytoplasm in the *cse1-1* mutant has been observed (Becker et al., 2019). Therefore, we wondered whether Cse1 might impact the localization of *TLC1* as well.

To investigate this, FISH experiments were carried out in the *cse1-1* and *cse1-1 mtr10Δ* mutants. The *mtr10Δ* mutant served as control and was shifted to 37 °C for 1 h. The *cse1-1* and *cse1-1-mtr10Δ* mutants were shifted to 16 °C for 1 h and 15 min, which was found as the optimal shifting period to preserve a severe phenotype.

Endogenously expressed total *TLC1* was detected via three Cy3-labeled probes (Figure 18). In wild type cells *TLC1* localizes predominantly to the nucleus whereas a mislocalization to the cytoplasm was shown in the *mtr10Δ* mutant (Ferrezuelo et al., 2002; Gallardo et al., 2008). We observed that *TLC1* mislocalizes to the cytoplasm in the *cse1-1* and in the *cse1-1 mtr10Δ* mutants (Figure 18). However, the signal was decreased in the double mutant, which may be due to the presence of a reduced amount of *TLC1* in this mutant. The increased cytoplasmic presence of *TLC1* in the *cse1-1* mutant suggests that this karyopherin is important for the nuclear re-import of *TLC1*.

We wondered if mostly the immature form of *TLC1* is exported to the cytoplasm and is accumulating upon re-import block. In order to analyze this, nucleo-cytoplasmic fractionation experiments were carried out in import factor mutants. The cytoplasmic fraction of the indicated strains was isolated after temperature shift to the restrictive temperature for 1 h and 15 min. The successful isolation of the cytoplasmic fraction was controlled by Western blot analysis (Figure 19 A). The total RNA of the cytoplasmic fraction was isolated, reverse transcribed into cDNA and analyzed via qPCR.

Total *TLC1* accumulated in the cytoplasm in the *cse1-1* mutant whereas the immature *TLC1* accumulated in the cytoplasm in all tested mutants (Figure 19 B and C). This suggests that *TLC1* is exported as immature transcript which accumulates in the cytoplasm in both import factor mutants. In addition, the ratio of immature to total *TLC1* present in the cytoplasm was significantly enriched in the *mtr10Δ* mutant but only slightly in the *cse1-1* mutant (Figure 19 D). This suggests, that Mtr10 is the major import factor. However, the ratio of immature to total *TLC1* in the cytoplasm was also significantly enriched in the *cse1-1 mtr10Δ*

mutant, indicating that both factors cooperate in the re-import of *TLC1* (Figure 19 D). The cytoplasmic enrichment of the total *U1* and the immature *U1* snRNA in the *cse1-1* and *mtr10Δ* mutants is consistent with published data (Becker et al. 2019). In addition, we observed an additive effect in the enrichment of the total *U1* and the immature *U1* snRNA in the *cse1-1 mtr10Δ* mutant (Figure 19 E and F). Together this suggests the immature forms of *TLC1* and of *U1* snRNA accumulate upon blocking their re-import and that Cse1 and Mtr10 cooperate in the re-import of theses ncRNAs.

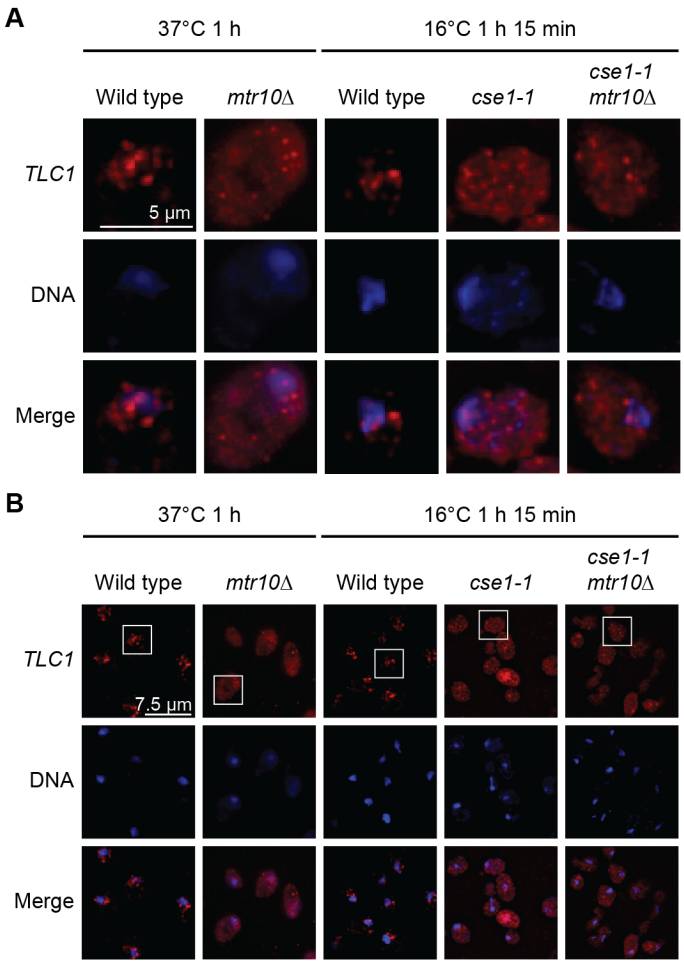

Figure 18: *TLC1* mislocalizes to the cytoplasm in the *cse1-1* and *cse1-1 mtr10Δ* mutants.
FISH analysis was carried out after shifting the *mtr10Δ* mutant and the *cse1-1* mutants to 37 °C and 16 °C respectively, for the indicated times. Three sequence-specific Cy3-labelled probes were used to detect *TLC1* (red). DNA was stained with Hoechst (blue). **(A)** Single cell images of the indicated cells in (B) are shown. **(B)** Overview of several cells is shown of which the framed ones are depicted in (A). Images of *mtr10Δ* were carried out by Dr. Daniel Becker; n=3. (Part of the bioRxiv article Hirsch et al. (2021)).

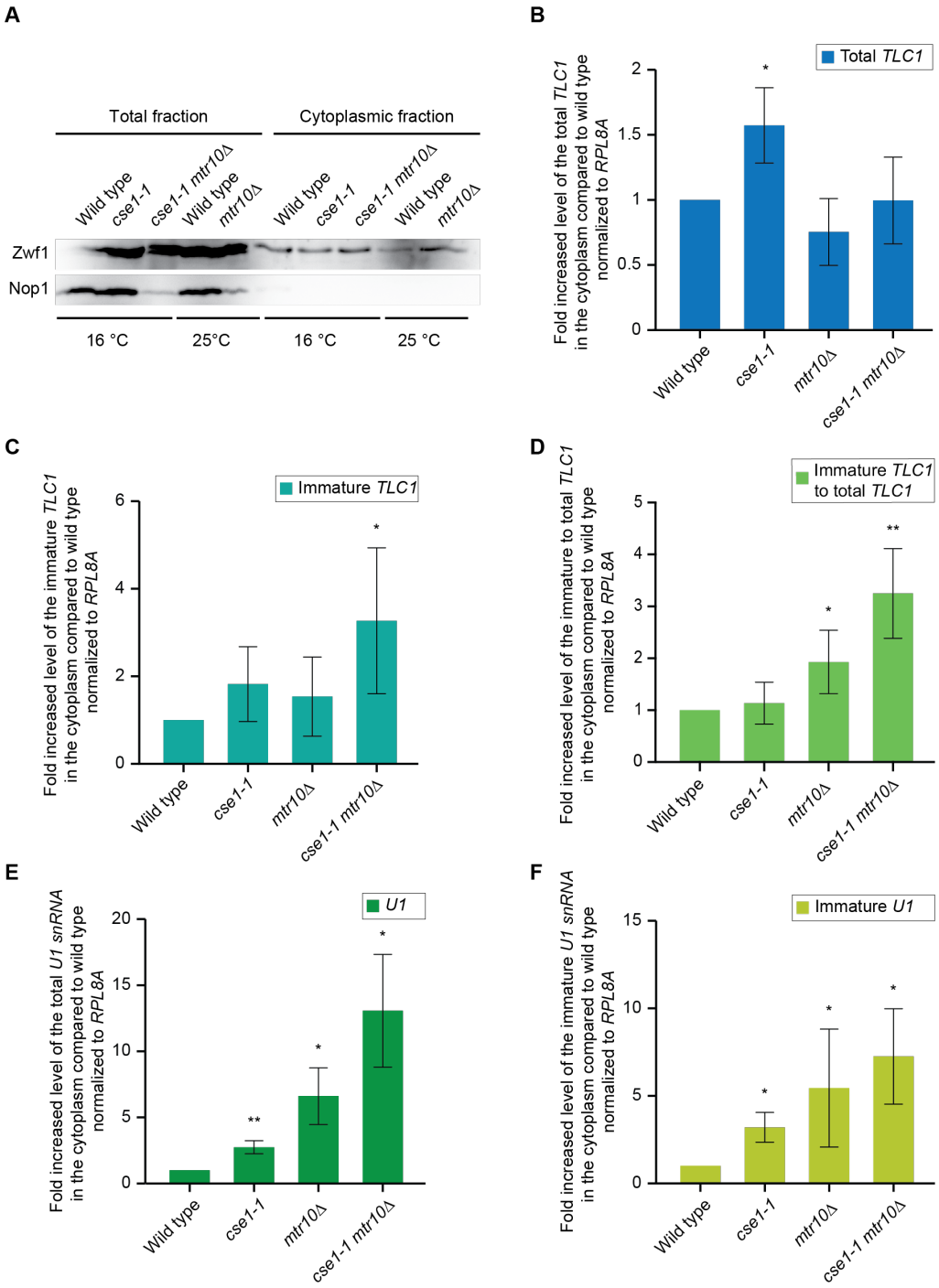

Figure 19: Immature *TLC1* accumulates in the cytoplasm upon re-import block.
Indicated strains were shifted to 16 °C for 1h and 15 min prior to isolation of the cytoplasmic fraction. The total RNA of the cytoplasmic fraction was isolated, reverse transcribed and analyzed via qPCR. **(A)** A Western blot shown an example of nucleo-cytoplasmic fractionation experiments shown in (B - F). Total and cytoplasmic fractions were controlled by detecting the cytoplasmic protein Zwf1 and the nucleolar protein Nop1. **(B - F)** qPCR data showing the cytoplasmic level of **(B)** total *TLC1* **(C)** immature *TLC1* **(D)** the ratio of immature to total *TLC1* level **(E)** *U1* snRNA and **(F)** immature *U1* snRNA. The error bars represent the standard deviation, p-values were calculated by unpaired two-tailed unequal variance student´s t-test in (* = p< 0.05, ** = p< 0.01, *** = p< 0.001); n= 5, except for *U1* n=4. (Part of the bioRxiv article Hirsch et al. (2021)).

4.5. Cse1 and Mtr10 physically interact with *TLC1*

A physical interaction of snRNAs with both import receptors was described to occur *in vivo* (Becker et al., 2019) and due to shared similarities of both RNA types, we wondered whether this might also be true for *TLC1*. Therefore, RIP experiments were carried out in which endogenously expressed, GFP-tagged proteins were precipitated from cell lysates via GFP-beads (Figure 20). Successful precipitation was controlled via Western blot and the co-immunoprecipitated RNA was isolated, reverse transcribed into cDNA and analyzed via qPCR. Compared to the precipitation without the use of a tagged protein, we observed a 2-fold increase in the binding of *TLC1* to Mtr10 and a 1.5-fold increase in the binding to Cse1 (Figure 20 B). The *U1* and *U5* snRNA were used as an internal positive control. Both snRNAs showed a comparable binding rate to the import receptors as published previously (Becker et al., 2019). Although low, the binding of *TLC1* to the import receptors was still significant.

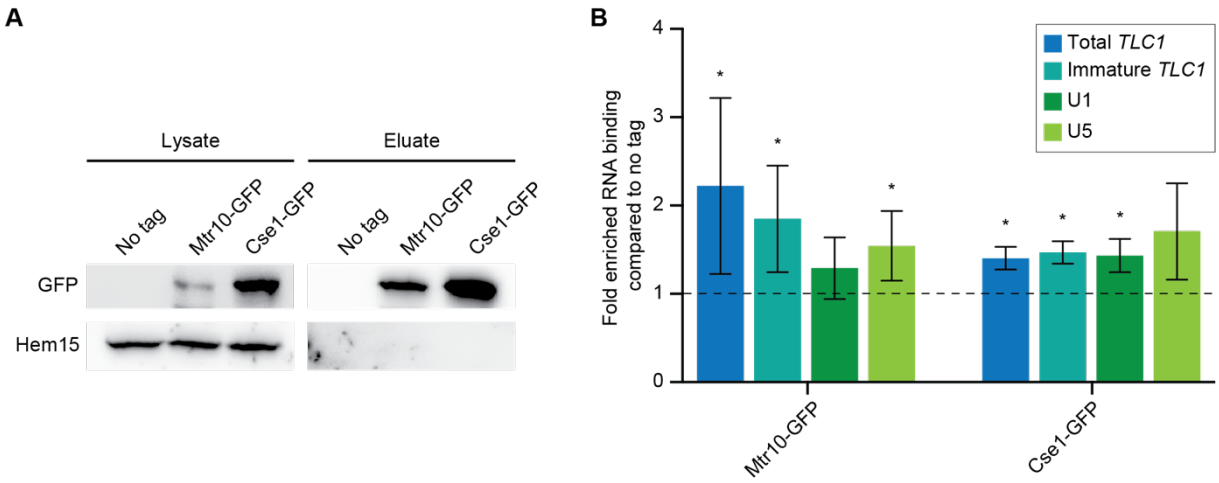

Figure 20: Mtr10 and Cse1 physically interact with *TLC1*.
Indicated strains were grown to mid-log phase and GFP-tagged proteins were precipitated with GFP-beads after cell lysis. Co-immunoprecipitated RNA was isolated, reverse transcribed into cDNA and subsequently used for qPCR analysis. **(A)** A Western blot shows an example IP of immunoprecipitated proteins form RIP experiments shown in (B). Hem15 (Ferrochelatase) served as control for unspecific protein binding to the GFP-beads. Cse1-GFP and Mtr10-GFP were detected with a GFP-specific antibody. **(B)** qPCR data show the binding of the indicated target RNAs to Mtr10 and Cse1. The error bars represent the standard deviation, p-values were calculated by unpaired one-tailed unequal variance student´s t-test (* = p< 0.05, ** = p< 0.01, *** = p< 0.001); For Mtr10-GFP RIPs n=4, for Cse1-GFP RIPs n=3. (Part of the bioRxiv article Hirsch et al. (2021)).

4.6. The *cse1-1* mutation does not affect the overall level of total *TLC1 in vivo*

To analyze whether *MTR10* and *CSE1* act together in the re-import of their cargos, we analyzed whether they genetically interact.

For this purpose, a *mtr10Δ* strain was crossed with the temperature sensitive *cse1-1* mutant and a growth analysis of the resulting double mutant was carried out. The serial drop dilution assay showed no growth for *cse1-1* at its restrictive temperature of 16 °C and a growth defect compared to wild type at all tested temperatures (Figure 21) and (Xiao et al. 1993). The *mtr10Δ* mutant exhibited a defect at all tested temperatures compared to the wild type (Figure 21). The genetic interaction of the two factors became apparent at temperatures of 20 °C and higher, where the double mutant revealed a growth defect compared to the wild type and the parental strains (Figure 21).

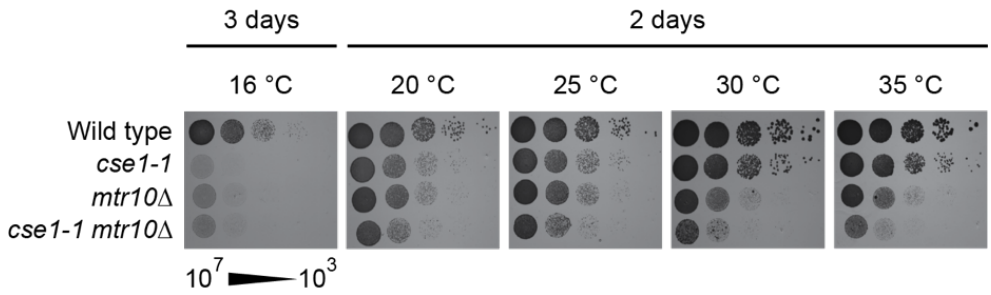

Figure 21: Growth analysis revealed a genetic interaction between *MTR10* and *CSE1*.
Serial dilution of the indicated strains were spotted on YPD plates and incubated for 2 to 3 days at the indicated temperatures. n=3. (Part of the bioRxiv article Hirsch et al. (2021); the analyses were partly carried out by Jan-Philipp Lamping).

To gain insight into the relative cellular amount of *TLC1* in the mutants, the total and immature *TLC1* forms were analyzed in cell lysates. The indicated strains were grown to mid-log phase and lysed after a temperature shift to their restrictive temperatures. In case of the *cse1-1* and the *cse1-1 mtr10Δ* mutants a cold shock for 1 h and 15 min to 16 °C was carried out and the *mtr10-1* mutant was shifted to 37 °C for 1 h. The cells were lysed and the total RNA was isolated, reverse transcribed into cDNA and analyzed via qPCR.

The deletion of *MTR10* or the mutation of *mtr10-1* led to a significant reduction to half of the total *TLC1* level (Figure 22 A) and (Ferrezuelo et al., 2002; Gallardo et al., 2008). In contrast, the total *TLC1* level was not altered significantly in the *cse1-1* mutant (Figure 22 A). In the double mutant, the total *TLC1* level was reduced to ~ 40 %, which is comparable to the

mtr10-1 mutant (Figure 22 A). The decreased abundance of *TLC1* in mutants that lack Mtr10 suggests that Mtr10 is the major import factor of *TLC1* which is degraded upon re-import block (Figure 22 A).

Interestingly, the immature form of *TLC1* was not significantly altered in this experimental set-up compared to the wild type (Figure 22 B). However, the ratio of immature to total *TLC1* was significantly enriched in the *cse1-1 mtr10Δ* mutant compared to wild type (Figure 22 C). This demonstrates that both import factors cooperate in the re-import of immature *TLC1* as the mutation of both factors led to a stronger import block (Figure 22 C). In addition to Mtr10 as major import factor, Cse1 seems to have a supporting function in the re-import of *TLC1*.

We demonstrated a genetic interaction between *CSE1* and *MTR10* and have shown that mutation of both import factors led to an increased ratio of immature to total *TLC1*. However, mutation of *MTR10* but not *CSE1* affected the overall level of *TLC1 in vivo.*

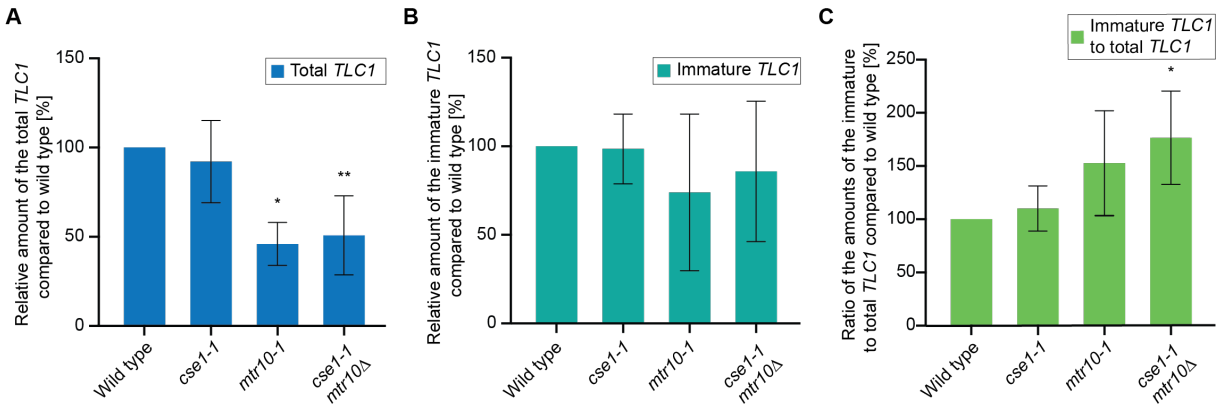

Figure 22: Mutation of *MTR10* but not of *CSE1* affects the total *TLC1* level, but the combination of both leads to an accumulation of immature *TLC1*.

Indicated strains were grown to mid-log phase and lysed after shifting the cells to their restrictive temperature. The *mtr10-1* mutant was shifted to 37 °C for 1h while the *cse1-1* and the *cse1-1 mtr10Δ* mutants were shifted to 16 °C for 1h and 15 min. The total RNA was isolated, reverse transcribed into cDNA and subsequent analyzed via qPCR. *TLC1* levels were analyzed using primers that amplify **(A)** total *TLC1* or **(B)** the immature *TLC1* forms. **(C)** The ratio of immature *TLC1* to total *TLC1* is shown. The error bars represent the standard deviation, p-values were calculated by unpaired two-tailed unequal variance student´s t-test in (* = p< 0.05, ** = p< 0.01, *** = p< 0.001); For *cse1-1* n=6; *mtr10-1* n=3; for *cse1-1 mtr10Δ* n=5. (Part of the bioRxiv article Hirsch et al. (2021)).

4.7. Cse1 stabilizes the interaction of immature *TLC1* and Smb1 prior to the re-import

As shown earlier, the binding of immature *TLC1* to the Sm-ring is increased when the re-import was inhibited in the *mtr10Δ* mutant (Figure 17). To investigate whether this is also true for the new *TLC1* import mutant *cse1-1* and whether their effects are additive, RIP experiments were carried out in the *cse1-1* and *cse1-1 mtr10Δ* mutants. The indicated strains were grown to mid-log phase and lysed after a temperature shift to the restrictive temperature of 16 °C for 1 h and 15 min. GFP-tagged proteins were precipitated by using GFP-beads and an equal pull down in all used strains was observed by Western blot analysis (Figure 23 A). Co-immunoprecipitated RNA was isolated, reverse transcribed and analyzed by qPCR using *TLC1* specific primers.

Compared to the wild type, we observed a decreased binding of *TLC1* to Smb1 in the *cse1-1* mutant and an even stronger effect concerning the *cse1-1 mtr10Δ* double mutant, in which the interaction of *TLC1* and Smb1-GFP dropped to ~ 10 % (Figure 23 B). Furthermore, we observed a decreased binding of the immature form of *TLC1* to Smb1 to ~ 60 % in the *cse1-1* mutant and to ~ 14 % in the *cse1-1 mtr10Δ* mutant (Figure 23 C).

In contrast to the increased binding of *TLC1* to Smb1 in the absence of Mtr10, this interaction was decreased in the *cse1-1* and the *cse1-1 mtr10Δ* mutants, suggesting that Cse1 is involved in stabilization of the Sm-ring binding onto *TLC1* (Figure 17 and Figure 23). Nevertheless, the ratio of the immature *TLC1* to the total *TLC1* form bound to Smb1-GFP was increased in the *cse1-1 mtr10Δ* mutant (Figure 23 D). This implies that the immature *TLC1* form is mostly bound to Smb1-GFP in the *cse1-1 mtr10* mutant when *TLC1* is accumulating in the cytoplasm (Figure 18, Figure 19 and Figure 23). These findings confirm a cytoplasmic loading of the Sm-ring onto immature *TLC1* and reveal a stabilizing function of Cse1 for the interaction between *TLC1* and the Sm-ring.

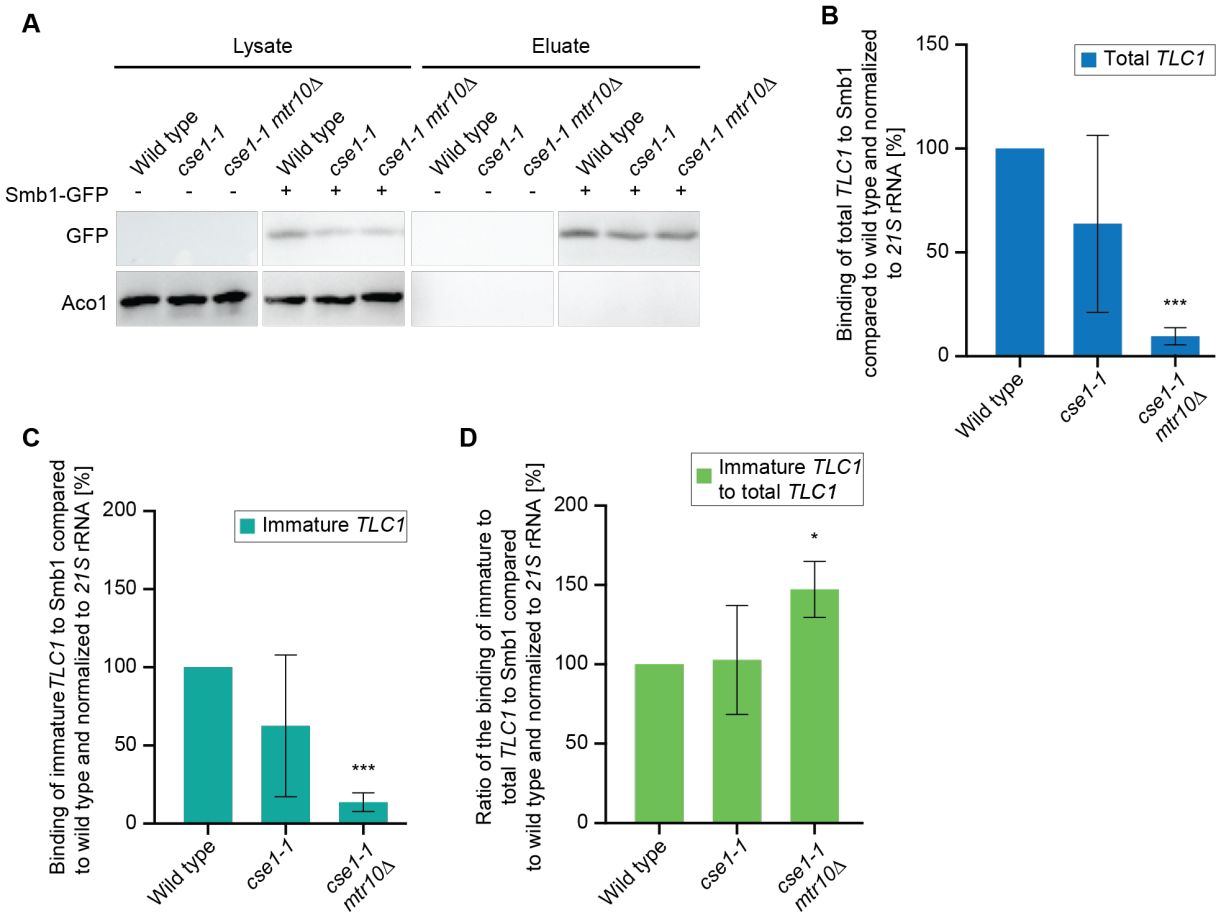

Figure 23: The Sm-ring loading onto *TLC1* occurs in the cytoplasm and is stabilized via Cse1.
The indicated strains were grown to mid-log phase and shifted to the restrictive temperature of 16 °C for 1 h and 15 min. Smb1-GFP was precipitated with GFP-beads after cell lysis. Co-immunoprecipitated RNA was isolated, reverse transcribed and analyzed via qPCR. **(A)** A Western blot shows an example IP of the precipitated Smb1-GFP from RIP experiment shown in (B - D). Aco1 served as control for unspecific protein binding to the GFP-beads. Smb1-GFP was detected with a GFP-specific antibody. **(B - D)** qPCR data from RIP experiments showing the interaction between Smb1-GFP and **(B)** total *TLC1* **(C)** immature *TLC1* **(D)** the ratio of immature *TLC1* to total *TLC1*. The error bars represent the standard deviation, p-values were calculated by unpaired two-tailed unequal variance student´s t-test (* = p< 0.05, ** = p< 0.01, *** = p< 0.001); For *cse1-1* n=3; for *cse1-1 mtr10Δ* n=4. (Part of the bioRxiv article Hirsch et al. (2021)).

4.8. The import factor Mtr10 contacts the Smb1 protein presumably for re-import

The re-import of the *TLC1* requires Cse1 and Mtr10 (Figure 18) and (Ferrezuelo et al., 2002). In addition, we have shown that especially the immature *TLC1* requires both karyopherins Cse1 and Mtr10 for the re-import (Figure 19). Cse1 was shown to contact the Sm-ring (Becker et al., 2019). For Mtr10 it is currently unknown how it contacts *TLC1*. Therefore, we investigated the interaction of Mtr10 to proteins of the telomerase holoenzyme, which may function as adaptor protein between *TLC1* and Mtr10.

Indicated GFP- or Myc-tagged proteins were precipitated via GFP- or Myc-beads after cell lysis of the indicated strains. As no RNase was added to the immunoprecipitation experiments, a potential indirect interaction via an RNA cannot be excluded. No physical interaction was observed between Mtr10 and Pop1, Est1 or Yku70. But we observed a physical interaction between Smb1 and Mtr10, indicating that Mtr10 might contact the RNP via the Sm-ring for nuclear re-import (Figure 24).

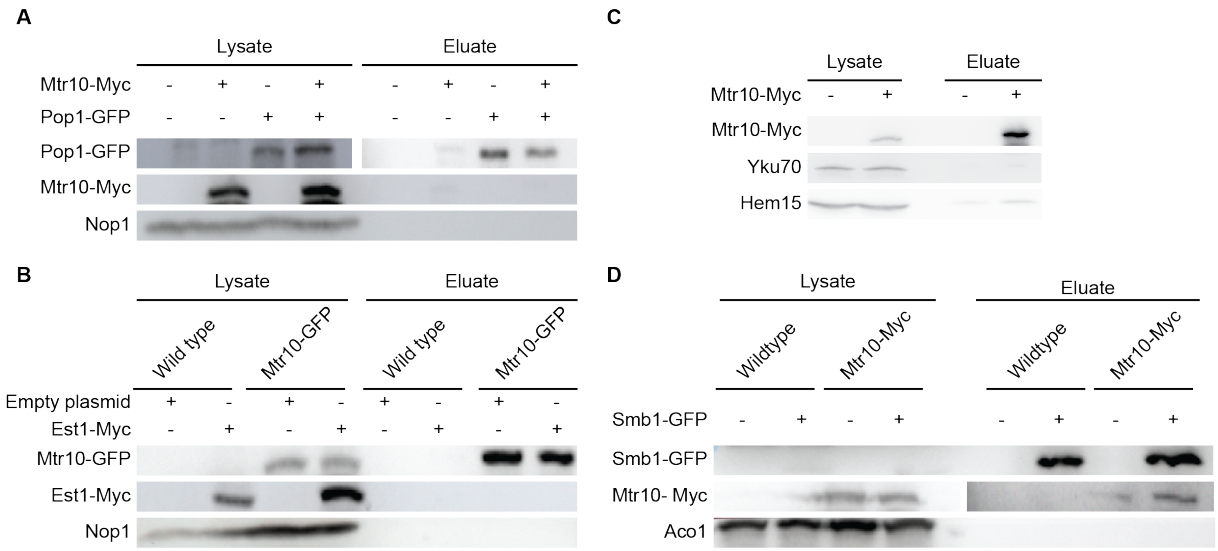

Figure 24: Mtr10 physically interacts with Smb1.
In all IP experiments indicated proteins were precipitated with GFP- or Myc-beads and were detected either with a GFP-specific antibody or a Myc-specific antibody. Nop1, Hem15 and Aco1 served as control for unspecific protein binding to the GFP- and Myc-beads. The detected proteins are arranged as follows: (top) pull-down, (middle) analyzed protein to be co-precipitated, (bottom) unspecific protein binding control. **(A)** Western blot analysis of IP experiments with Pop1-GFP and Mtr10-Myc. **(B)** Western blot analysis of IP experiments with Mtr10-GFP and Est1-Myc. **(C)** Western blot analysis of IP experiments with of Mtr10-Myc and Yku70. Yku70 was detected using a Hdf1 (Yku70) antibody. **(D)** Western blot analysis of IP experiments with Smb1-GFP and Mtr10-Myc revealing a physical interaction of both proteins. n=3. (Part of the bioRxiv article Hirsch et al. (2021)).

4.9. The re-import of *TLC1* is independent of the importin α pathway

Cse1 is involved in the re-export of Srp1, which in turn is involved in the nuclear import of Est1 (Hawkins and Friedman, 2014; Hood and Silver, 1998; Solsbacher et al., 1998). Thus, it is possible that the observed mislocalization of *TLC1* in the *cse1-1* mutant is a secondary effect, because it was shown that the nuclear localization of Est1 is disturbed in *srp1* mutants, that are defective in the import of classical NLS-containing proteins (Hawkins and Friedman, 2014). Although the Est1 mislocalization might be due to secondary effects, we wished to investigate if the re-import of *TLC1* depends on Srp1.

Therefore, we analyzed the localization of *TLC1* in the *srp1-31* mutant via FISH experiments. The indicated strains were shifted to the restrictive temperature of 37 °C for 1 h. Endogenously expressed total *TLC1* was detected via three Cy3-labeled probes.

In wild type cells, *TLC1* localizes to the nucleus at 25 °C and 37 °C (Figure 25) and (Gallardo et al. 2008). The localization of *TLC1* was not affected in the *srp1-31* mutant, distinct *TLC1* foci were visible in the nucleus (Figure 25) and (Gallardo et al. 2008). Thus, we can conclude that the mislocalization of *TLC1* in *cse1-1* is not caused by the importin α pathway.

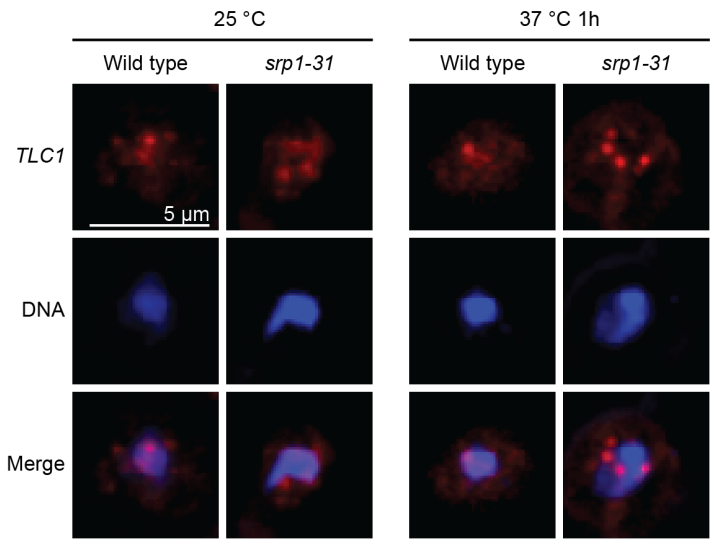

Figure 25: Localization of *TLC1* is not affected in the *srp1-31* mutant.
FISH analysis of the indicated strains were carried out before and after shifting them to the restrictive temperature of 37 °C for 1 h. Three sequence-specific Cy3-labelled probes were used to detect *TLC1* (red). DNA was stained with Hoechst (blue). Single cell images of are shown. n=3. (Part of the bioRxiv article Hirsch et al. (2021)).

To investigate whether Pop1, which harbors a predicted NLS sequence (Lee et al., 2006), also mislocalizes in a *srp1* mutant we carried out immunofluorescence experiments. The *srp1-31* mutant was transformed with the Pop1-GFP plasmid and cells were grown to mid-log phase prior to shifting them to the restrictive temperature of 37 °C for 1 h. In agreement with the mislocalization of Est1 in the *srp1-31* mutant (Hawkins and Friedman, 2014), Pop1 also mislocalizes to the cytoplasm in the *srp1-31* mutant (Figure 26). The mislocalization of Pop1 implies a role of Srp1 in the nuclear import of the unbound protein. Proper localization of *TLC1* in *srp1-31* suggests no limitation of the association of the proteins that form the matured RNP.

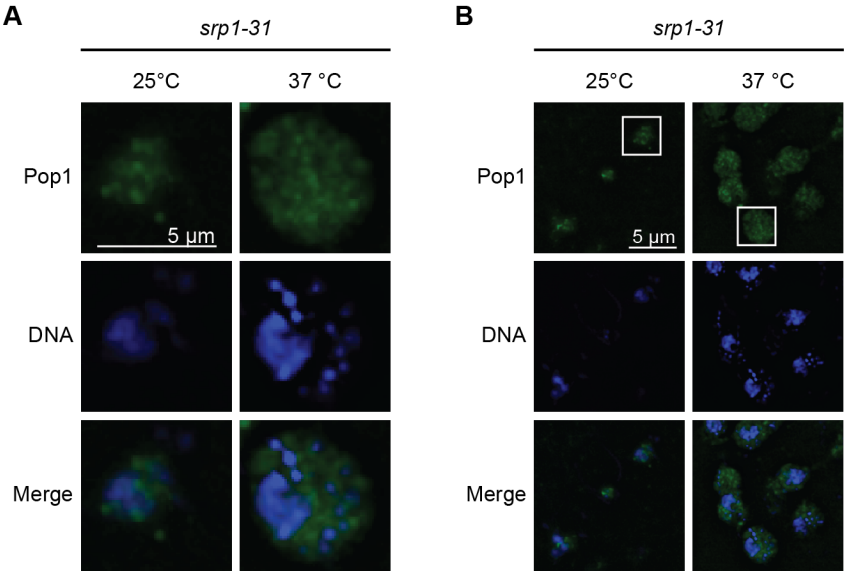

Figure 26: Pop1-GFP mislocalizes to the cytoplasm in the *srp1-31* mutant.
The *srp1-31* mutant was grown to mid-log phase prior to a temperature shift to 37 °C for 1 h. Immunofluorescence experiments were carried out for signal enhancement. Pop1-GFP was detected with a primary anti-GFP and a secondary anti-mouse-FITC antibody. Images are shown after deconvolution. **(A)** Single cell images of the indicated cells in (B) are shown. **(B)** Overview of several cells is shown of which the framed ones are depicted in (A). n=3.

4.10. Southern blot analysis revealed an altered telomere structure with amplified Y´ elements in the *cse1-1* mutant

Impairment of the export factors Mex67 and Xpo1 as well as of the import factor Mtr10 leads to a progressive shortening of the telomere ends (Ferrezuelo et al., 2002; Wu et al., 2014). Because we have shown that Cse1 is involved in the re-import of *TLC1*, we investigated the length of telomere ends in the *cse1-1* mutant.

Indicated strains were freshly taken from a - 80 °C stock, which were already replicated multiple times and therefore could exhibit telomere shortening at generation "0". Nevertheless, cell passaging was carried out in liquid culture under constant incubation at the semi-permissive temperature or on solid plates until 80 to 125 generations were reached. Chromosomal DNA was isolated, digested with XhoI and analyzed via Southern blot experiments. For detection of the terminal fragment and also indirectly for the Y´ elements, a probe binding to the TG-repeats was used (Figure 27).

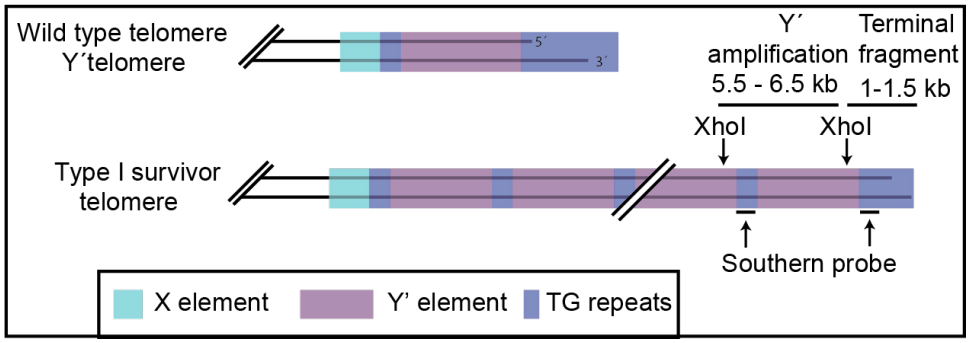

Figure 27: Schematic representation of yeast wild type Y´ telomere and Type I survivor telomere. Probe targeting the TG-repeats of the telomeres is indicated as Southern probe.

Analysis of the telomere-restriction fragments after XhoI digestion via Southern blot analysis revealed no shortening of the terminal telomere fragment in the *cse1-1* mutant. However, a highly amplified band with the size of approximately 5.5 kb appeared in the *cse1-1* mutant (Figure 28). The *cse1-1 mtr10Δ* mutant has shortened telomere ends, which is consistent with the phenotype of *mtr10Δ* (Ferrezuelo et al., 2002). No amplification of the Y´ element was observed in the *cse1-1 mtr10Δ* mutant, suggesting that the loss of Mtr10 is dominant. The *tlc1Δ* mutant was used as a control of the passaging process and showed a shortening of the terminal fragment at the beginning and switched after approximately 80 generations to the

phenotype of a Type II survivor (Figure 28) and (Chen et al., 2001; Grandin and Charbonneau, 2007).

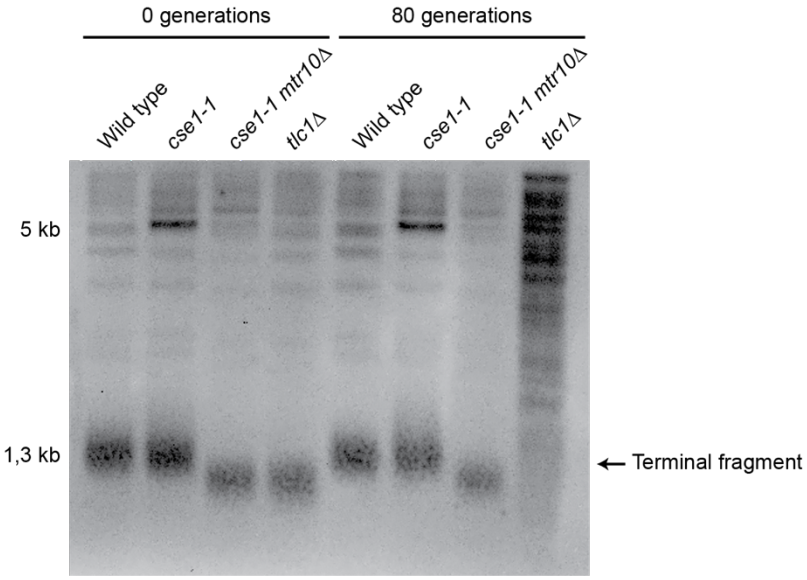

Figure 28: Southern blot analysis of XhoI digested chromosomal DNA revealed no telomere shortening defect for *cse1-1* but amplification of an approximately 5.5 kb fragment.
Cell passaging of the indicated strains was carried out in liquid culture at semi-permissive temperature of 20 °C. Chromosomal DNA was isolated, digested with XhoI and separated on a TBE gel. A telomeric-repeat specific probe was used for detection. (Part of the bioRxiv article Hirsch et al. (2021)).

To verify that the highly amplified band in the *cse1-1* mutant resembles the same pattern as described for the Type I survivor in the *tlc1Δ* mutant (Grandin and Charbonneau, 2007; Teng and Zakian, 1999), the following strains were passaged on solid YPD plates. Thereby, the slower growing Type I survivor is less likely to be overgrown by Type II survivor cells (Grandin and Charbonneau, 2007). Furthermore, we analyzed whether the phenotype in the *cse1-1* strain, the appearance of the 5.5 kb band in particular, can be reversed by introducing a wild type *CSE1* encoded on a plasmid.

Telomere shortening is observed in a telomerase deficient mutant with switch to a Type I survivor phenotype after approximately 75 - 100 generations (Bosoy et al., 2003; Grandin and Charbonneau, 2007; Makovets et al., 2008; Teng and Zakian, 1999). Compared to the generated Type I survivor phenotype in the *tlc1Δ* mutant, the generated band in the *cse1-1* strain was detected at the same height, using the same probe that binds the TG-repeats (Figure 29). In addition, we observed that the introduction of a *CSE1* containing plasmid rescued the phenotype of the *cse1-1* mutant (Figure 29). This indicates that the mutation of *CSE1* specifically leads to the Y´ amplification. Interestingly, the overall telomere length in the *cse1-1* mutant might be increased in comparison to wild type telomeres as the Y´ elements

are amplified in addition to a normal length of the terminal fragment. This implies, that even if *TLC1* mislocalizes to the cytoplasm, enough telomerases reach the nucleus for telomere elongation. Additionally, homologues recombination seems to be used in the *cse1-1* mutant, leading Y´ element amplification. This is a special phenotype in which telomerase dependent lengthening and recombination events might act simultaneously, resulting in the observed phenotype. Because the *cse1-1* strain does not show the shortening of the terminal fragment which is a characteristic for Type I survivors, the observed phenotype was named “Type I like survivor” (Hirsch et al., 2021). However, “Amplified Y´ element mutant” or “Long telomere mutant” might be more suitable.

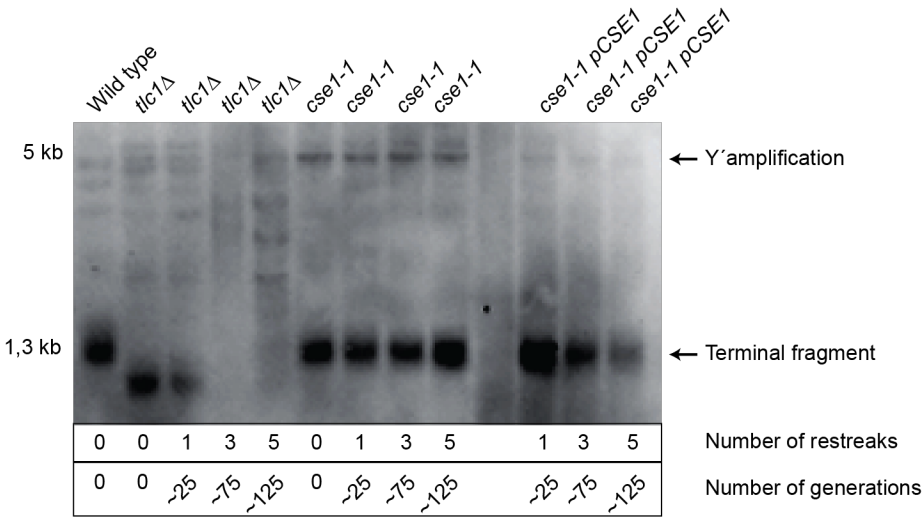

Figure 29: The Y´ elements are amplified in the *cse1-1* mutant, which is reversible by complementation with *CSE1*.

Cell passaging was carried out on solid YPD plates at 25 °C. Chromosomal DNA was isolated, digested with XhoI and separated on an TAE gel. A telomeric-repeat specific probe was used for detection. (Part of the bioRxiv article Hirsch et al. (2021)).

4.11. Mutation of *CSE1* altered the localization Rap1

Although *TLC1* is mislocalized to the cytoplasm in both the *cse1-1* mutant (Figure 18) and the *mtr10Δ* mutant (Figure 18) and (Ferrezuelo et al., 2002), the Southern blot analysis revealed a different telomere structure for both mutants (Figure 28) and (Ferrezuelo et al., 2002). Besides the telomerase, also the nature of the telomere cap structure is important for correct telomere elongation. Both very short and uncapped telomeres are prone to recombination (Blackburn, 2000; McEachern and Iyer, 2001; Teixeira et al., 2004). Therefore, we wondered whether telomere capping factors may mislocalize in the *cse1-1* mutant and thus elicit this special phenotype. For this purpose, we chose two important telomere proteins and analyzed their localization in the *cse1-1* mutant by immunofluorescence experiments.

The single-stranded telomeric DNA-binding protein Cdc13 regulates telomere replication and elongation and has both positive and negative regulatory functions on telomere length (Churikov et al., 2013; Li et al., 2009; Liu et al., 2014). In wild type, Cdc13 is mainly localized in the nucleus (Ouenzar et al., 2017). This is not altered in the *cse1-1* mutant (Figure 30), indicating that Cse1 did not function in the localization of Cdc13.

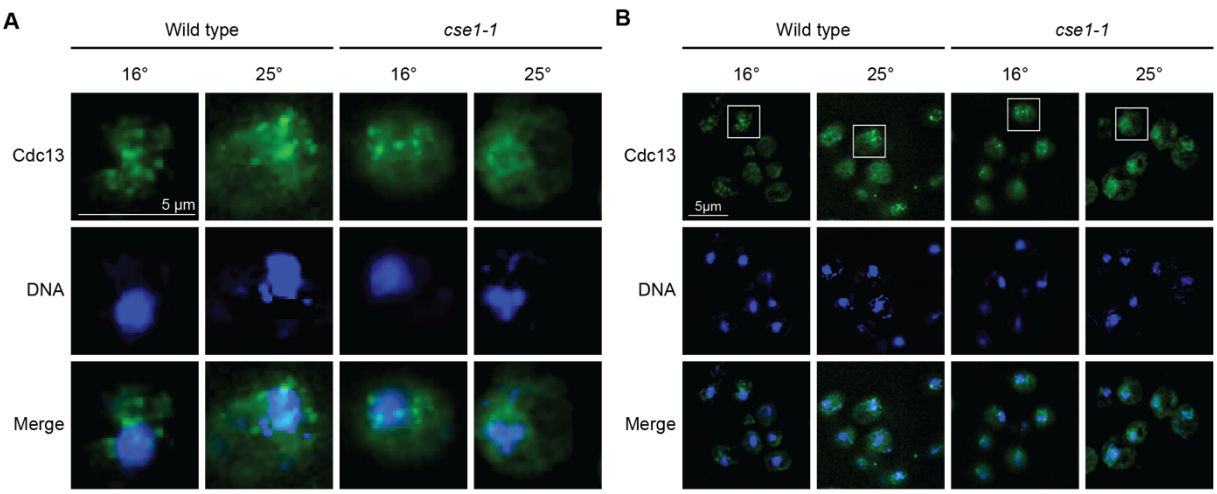

Figure 30: Cdc13-GFP is not mislocalized in the *cse1-1* mutant.
Indicated strains were grown to mid-log phase prior to shifting them to 16 °C for 1 h and 15 min. Cdc13-GFP was detected with a primary anti-GFP and a secondary anti-mouse-FITC antibody to enhance the otherwise faint signal and the recorded image stacks were used for deconvolution. DNA was stained with Hoechst. **(A)** Single cell images of the indicated cells in (B) are shown. **(B)** Overview of several cells is shown of which the framed ones are depicted in (A). n=3.

Rap1 is an essential dsDNA-binding protein that functions in telomere length maintenance and chromatin silencing, and is mainly localized in the nucleus as it directly binds to telomeric repeat DNA (Gilson and Géli, 2007; Gotta et al., 1996; Klein et al., 1992; Marcand et al., 1997). Even without shifting *cse1-1* to the restrictive temperature, we observed a presumably more nucleolar localization of Rap1 (Figure 31). Shifting *cse1-1* to the restrictive temperature resulted in a weaker, more diffuse GFP signal that was detectable in the cytoplasm. This suggests a function of Cse1 in the re-import of Rap1. Overall, this might lead to partially uncapped telomeres which are hence more accessible for homologues recombination events.

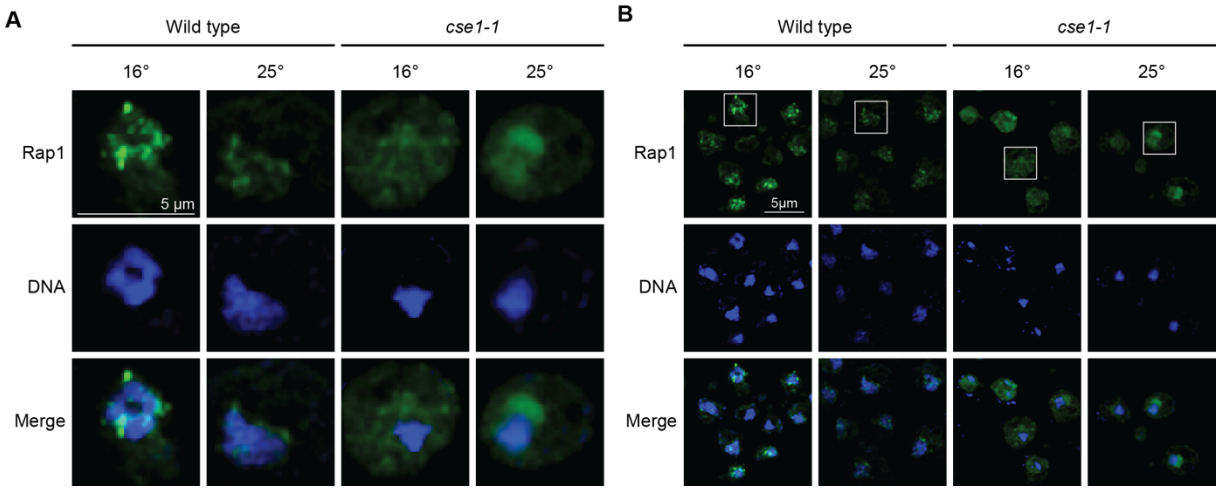

Figure 31: Rap1-GFP mislocalizes in the *cse1-1* mutant.
Indicated strains were grown to mid-log phase prior to the temperature shift to 16 °C for 1h and 15 min. Rap1-GFP was detected with a primary anti-GFP and a secondary anti-mouse-FITC antibody to enhance the otherwise faint signal and recorded image stacks were used for deconvolution. DNA was stained with Hoechst. **(A)** Single cell images of the indicated cells in (B) are shown. **(B)** Overview of several cells is shown of which the framed ones are depicted in (A). n=3.

4.12. Loading of the Est and Pop proteins occurs in the cytoplasm

Another essential step in *TLC1* biogenesis is the assembly of the telomerase holoenzyme. Est1 is loaded onto *TLC1* in the cytoplasm (Gallardo et al., 2008; Wu et al., 2014). Pop1 stabilizes the Est1 binding on the RNP and was recently sugessted to be loaded on *TLC1* in the cytoplasm (Garcia et al., 2020; Laterreur et al., 2018; Lemieux et al., 2016). We analyzed directly whether Pop1 is loaded onto the telomerase in the cell nucleus prior export or in the cytoplasm after export, by using GFP microscopy and RIP experiments. The localization of Est1 served as control in GFP microscopy experiments.

Est1-GFP localizes to the nucleus in wild type cells and is loaded onto *TLC1* in the cytoplasm, which is reflected in its mislocalization in the export- and import-mutants, including *cse1-1* (Figure 32 B) and (Gallardo et al., 2008; Wu et al., 2014). This indicates that Cse1 supports in the re-import of Est1, which is presumably bound to *TLC1*. In addition, we observed a partial mislocalization of Est1-GFP to the cytoplasm in the *tlc1Δ* mutant (Figure 32 B). This suggests that Est1 might also be imported into the nucleus independently of the telomerase.

Pop1-GFP is localized to the nucleus and the nucleolus in wild type cells (Gill et al., 2006). We observed a mislocalization of Pop1-GFP to the cytoplasm in all mutants tested (Figure 32 A). The cytoplasmic mislocalization of Pop1-GFP in the *tlc1Δ* strain confirms that *TLC1* is indeed a target of Pop1 (Figure 32 A) and (Garcia et al., 2020; Laterreur et al., 2018; Lemieux et al., 2016). Furthermore, we observed a mislocalization of Pop1-GFP to the cytoplasm in the export mutants *mex67-5* and *mex67-5 xpo1-1* (Figure 32 A). This mislocalization could be due to the missing target, *TLC1*, which is retained in the nucleus of these mutants (Wu et al., 2014). The observed mislocalization of Pop1 to the cytoplasm in the import factor mutants *cse1-1* and *mtr10-1* could be due to the cytoplasmic mislocalization of *TLC1* in these mutants (Figure 32 A and Figure 18). Taken together this suggests, that Pop1 is loaded onto *TLC1* in the cytoplasm.

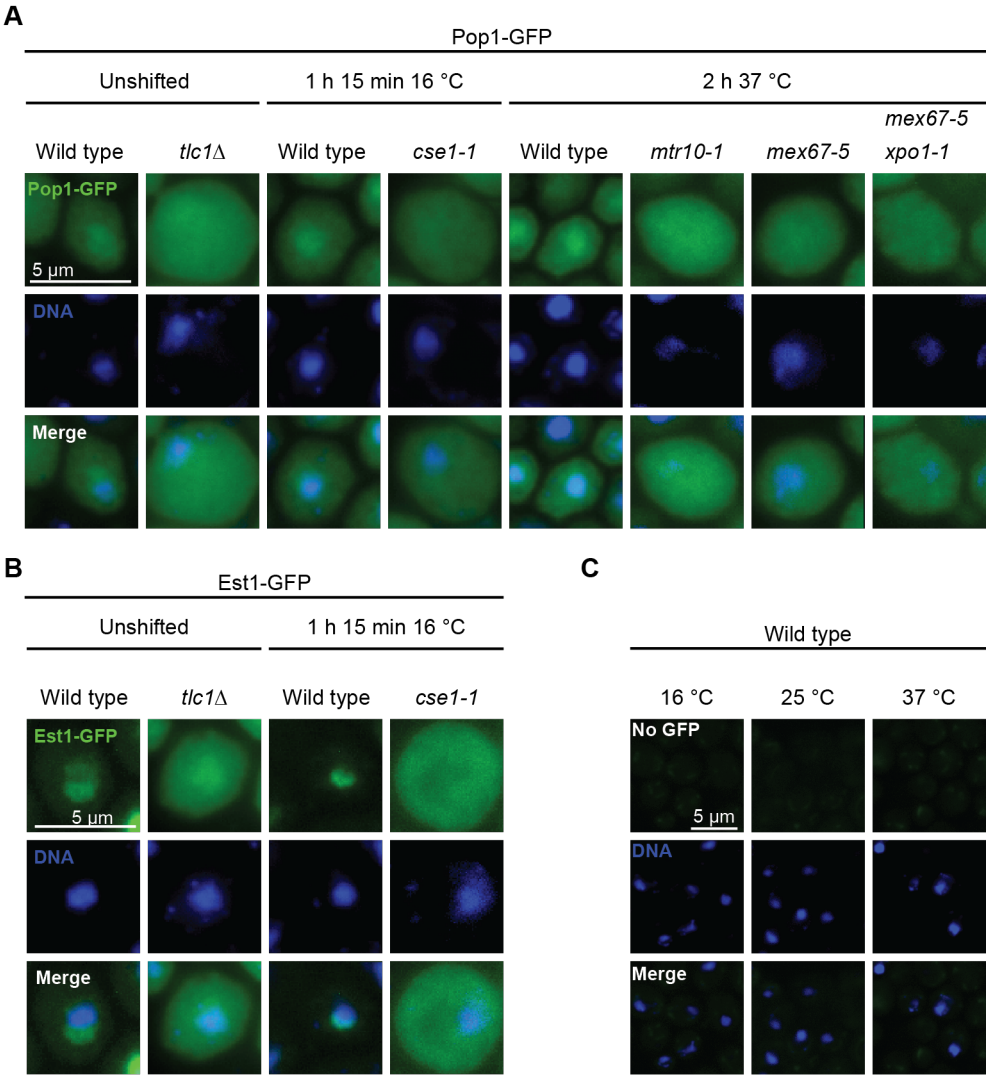

Figure 32: *TLC1* export and import factor mutants affect the localization of Pop1 and Est1.
Indicated strains were grown to mid-log phase prior to a temperature shift to 16 °C or 37 °C, respectively. **(A)** Pop1-GFP and **(B)** Est1-GFP localization is shown. **(C)** Negative control is shown. n=3. (Part of the bioRxiv article Hirsch et al. (2021); the analyses were partly carried out by Jan-Philipp Lamping).

Since Pop1 is present in the telomerase and in the RNAse P / MRP complexes (Lemieux et al., 2016; Lygerou et al., 1994), we analyzed the binding of *TLC1* to Pop1-GFP directly in import and export factor mutants by RIP experiments. The *mex67-5* and *cse1-1* mutants were shifted to their restricted temperatures of 37 °C and 16 °C, respectively. Cells were lysed, Pop1-GFP was precipitated via GFP-beads and co-immunoprecipitated RNA was isolated, reverse transcribed into cDNA and analyzed via qPCR. Successful precipitation of Pop1-GFP was controlled by Western blot analysis (Figure 33 A, C).

We observed a decreased binding of *TLC1* to Pop1-GFP in the *mex67-5* mutant and an increased binding of *TLC1* to Pop1-GFP in the *cse1-1* mutant (Figure 33 B, D). The increased

interaction between immature *TLC1* and Pop1 in the *cse1-1* mutant supports the model in which the loading of the proteins occurs in the cytoplasm on an untrimmed *TLC1* precursor. This result is in agreement with recent findings that revealed a mislocalization of *TLC1* in Pop protein deficient mutants (Garcia et al., 2020).

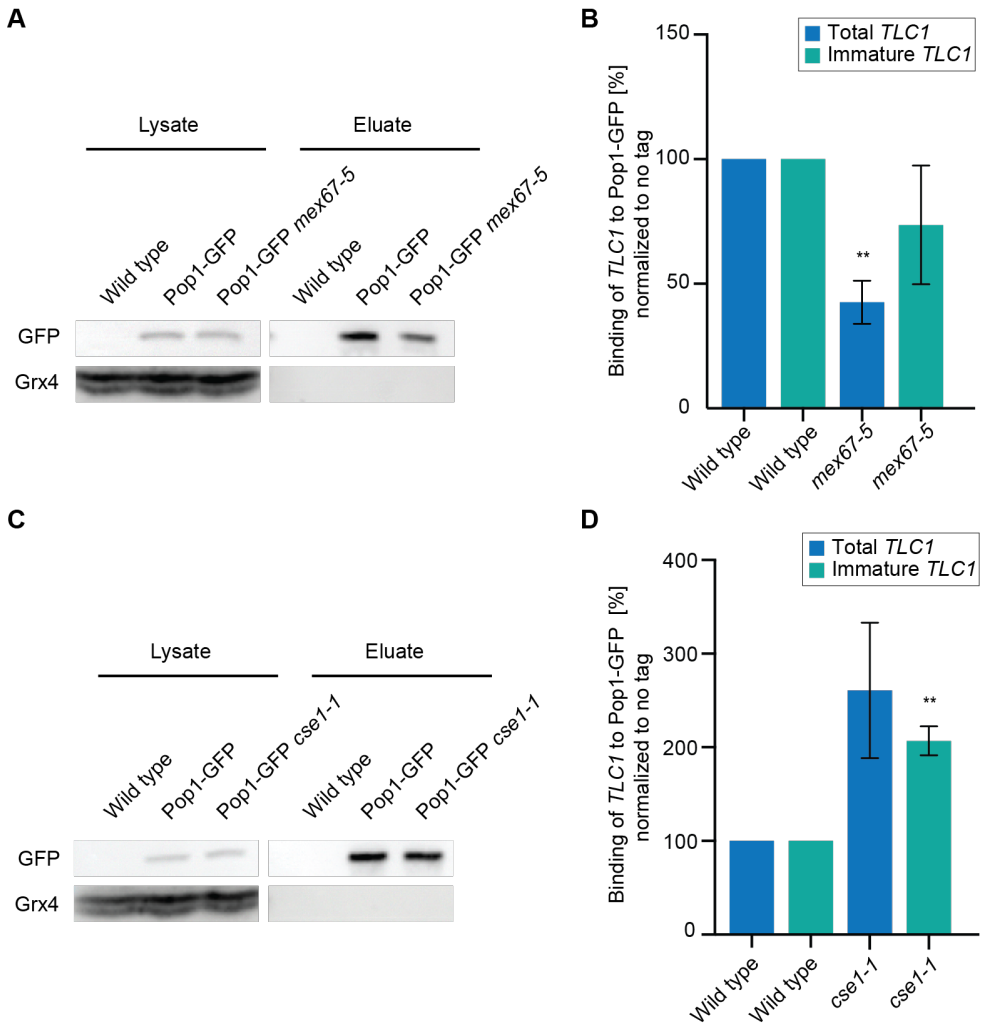

Figure 33: Pop1-GFP loading onto *TLC1* occurs in the cytoplasm.
Indicated strains were shifted to the restrictive temperature (A) and (B) to 37 °C for 2 h or (C) and (D) to 16 °C for 1 h and 15 min. Cells were lysed and Pop1-GFP was precipitated with GFP-beads. Co-immunoprecipitated RNA was isolated, reverse transcribed and analyzed via qPCR. **(A)** and **(C)** A Western blot shows an example IP of immunoprecipitated proteins form the RIP experiments shown in (B) and (D) respectively. Grx4 (Glutathione-dependent oxidoreductase) served as control for unspecific protein binding to the GFP-beads. Pop1-GFP was detected with a GFP-specific antibody. **(B)** qPCR data from RIP experiments showing a decreased binding of the total and the immature *TLC1* to Pop1-GFP in the *mex67-5* mutant. **(D)** qPCR data from RIP experiments showing the increased binding of the total and the immature *TLC1* to Pop1-GFP in the *cse1-1* mutant. The error bars represent the standard deviation, p-values were calculated by unpaired two-tailed unequal variance student´s t-test (* = p< 0.05, ** = p< 0.01, *** = p< 0.001); n=3. (Part of the bioRxiv article Hirsch et al. (2021)).

4.13. TMG-cap formation and trimming of immature *TLC1* is facilitated after re-import of *TLC1* into the nucleus

In addition to the maturation of the RNP complex via protein loading, *TLC1* undergoes two additional processing steps: First, the ~ 1.3 kb long immature transcript is trimmed at its 3´-end to 1157 nt (Bosoy et al., 2003; Chapon et al., 1997; Coy et al., 2013; Hass and Zappulla, 2020). Second, the monomethylguanosine (m^7G) cap at its 5'-end is trimethylated to a 2,2,7-trimethylguanosine (TMG)-cap, which is present in the active telomerase (Franke et al., 2008; Seto et al., 1999). The TMG-cap is also characteristic for snRNAs where TMG-capping occurs after the re-import (Becker et al., 2019). Currently TMG-capping is suggested to occur before export (Gallardo et al., 2008; Garcia et al., 2020). Interestingly, Smb1 is suggested to support TMG-capping by interaction with Tgs1 *in vitro* and *in vivo* (Becker et al., 2019; Mouaikel et al., 2002). Since we and others have shown the Sm-ring loading onto *TLC1* occurs after export to the cytoplasm (Figure 17 and Figure 23) and (Hirsch et al., 2021; Vasianovich et al., 2020), it seems likely that TMG-capping occurs after re-import. To investigate this, we carried out RIP experiments in the import factor mutants with an antibody that targets the TMG-cap. Since the antibody binds both trimethylated caps and also partially monomethylated caps, the *tgs1Δ* mutant was used as a control to represent the baseline for the experimental setup, because it is the only methyltransferase in yeast for TMG-capping (Franke et al., 2008; Mouaikel et al., 2002).

Approximately 25 % of TMG-capped *TLC1* was present in *tgs1Δ* compared to wild type. (Figure 34). This marks the baseline for unspecific binding. We observed a reduction of TMG-capped *TLC1* in the import mutants *mtr10Δ* and *cse1-1* as well as the double mutant *cse1- 1 mtr10Δ* to similar levels compared to *tgs1Δ* (Figure 34). This finding indicates that TMG-capping occurs after re-import into the nucleus, however we cannot distinguish whether this step is prior or after trimming of *TLC1*.

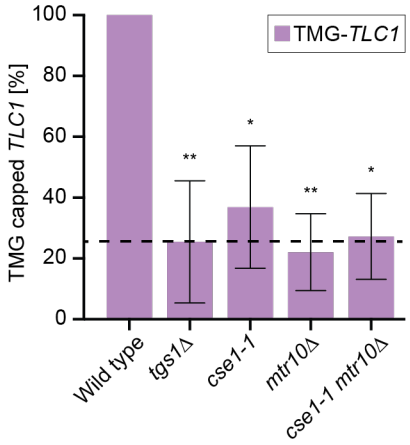

Figure 34: TMG-capping of *TLC1* is reduced in import factor mutants.
Purified total RNA from the indicated strains after a 1 h and 15 min shift to the restrictive temperature of 16 °C was used for the co-precipitation with an anti-2,2,7- trimethyl-guanosine-antibody coupled to agarose beads. Co-precipitated RNA was isolated via Trizol-chloroform isolation and analyzed via qPCR. The amount of TMG-capped *TLC1* is shown in the indicated strains relative to wild type. The error bars represent the standard deviation, p-values were calculated by unpaired two-tailed unequal variance student´s t-test in (* = p< 0.05, ** = p< 0.01, *** = p< 0.001); *tgs1Δ* and *mtr10Δ* n=4; *cse1-1* and *cse1-1 mtr10Δ* n=3. (Part of the bioRxiv article Hirsch et al. (2021)).

Furthermore, it was assumed that the 3´-trimming of the immature *TLC1* up to the Sm-ring binding sites occurs in the nucleus prior to export (Garcia et al., 2020; Noël et al., 2012; Wu et al., 2014). However, the Sm-ring loading onto immature *TLC1* occurs in the cytoplasm (Figure 17 and Figure 23) and (Hirsch et al., 2021; Vasianovich et al., 2020), which protects the RNA from complete degradation (Coy et al., 2013; Hass and Zappulla, 2020). In addition, the immature form accumulates in the re-import mutants (Figure 19). Therefore, 3´-trimming might occur after nuclear re-import of immature *TLC1*. To finally exclude a trimming beforehand, we analyzed the forms of *TLC1* in a double mutant of the nuclear exosome component Rrp6 and the export mutant *mex67-5*, both known to cause accumulation of poly(A)$^+$ *TLC1* when mutated individually (Coy et al., 2013; Segref et al., 1997). Cells were harvested in mid-log phase after a temperature shift to 37 °C for 2 h, total RNA was isolated, reverse transcribed into cDNA and subsequent analyzed via qPCR.

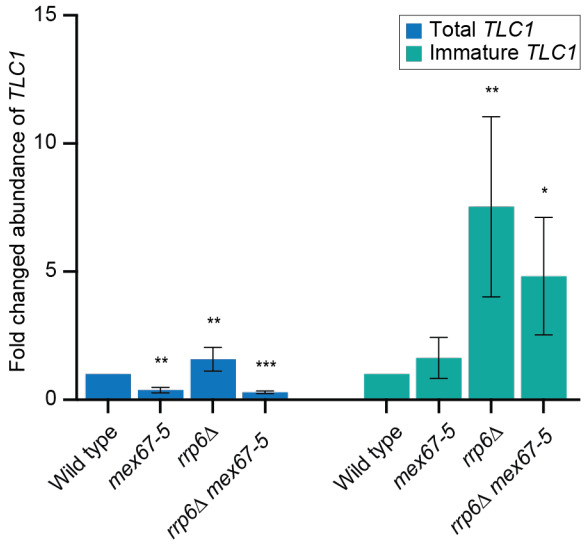

Figure 35: 3´-end processing of *TLC1* occurs in the nucleus after *TLC1* re-import.
Indicated strains were shifted to 37 °C for 2 h prior to harvest. After cell lysis, the total RNA was isolated, reverse transcribed and subsequently analyzed via qPCR. Total and immature *TLC1* were amplified using specific primers. The error bars represent the standard deviation, p-values were calculated by unpaired two-tailed unequal variance student´s t-test in (* = p< 0.05, ** = p< 0.01, *** = p< 0.001). For *mex67 -5* and *rrp6Δmex67-5* n= 4. For *rrp6Δ* n=8. (Part of the bioRxiv article Hirsch et al. (2021)).

We observed a ~ 2-fold increase of total *TLC1* and a ~ 7-fold increase of the immature *TLC1* form in the *rrp6Δ* strain compared to the wild type (Figure 35). This indicates that Rrp6 and thus the nuclear exosome is indeed involved in trimming of *TLC1* (Figure 35) and (Coy et al., 2013). In the *mex67-5* and in the *mex67-5 rrp6Δ* mutants, we observed a decreased abundance of total *TLC1* suggesting that the export block leads to the degradation of transcripts. However, we observed a ~ 1.6-fold and a ~ 5-fold increase of the immature form of *TLC1* in the *mex67-5* mutant and the *rrp6Δ mex67-5* mutant, respectively (Figure 35). These findings suggest that Mex67 may function in the stabilization of transcripts (Vasianovich et al., 2020). However, as the immature form of *TLC1* is rather stabilized and only the total *TLC1* that includes mostly the mature form is degraded, we suggest that pre-*TLC1* is particularly protected by additional factors, possibly Npl3.
Overall, our data suggest that 3´-trimming of the transcript occurs via the exosome after re-import.

4.14. The guard protein Npl3 physically interacts with *TLC1*

Guard proteins like Npl3 are co-transcriptionally loaded onto the RNA for quality control and Mex67-recruitment (Lei et al., 2001; Zander et al., 2016). To investigate whether Npl3 and *TLC1* physically interact RIP experiments were carried out.

After cell lysis, Npl3-GFP was precipitated via GFP-beads and co-immunoprecipitated RNA was isolated, reverse transcribed analyzed via qPCR. Successful precipitation of Npl3-GFP was controlled by Western blot analysis (Figure 36 A). A control mRNA, *Hem15*, showed a ~ 3-fold enrichment compared to the no tag. Internal *TLC1* primers showed a ~ 6-fold enrichment of the total *TLC1* binding to Npl3-GFP compared to the no tag control, indicating that *TLC1* and Npl3 physically interact (Figure 36 B). Furthermore, we detected an ~ 7-fold enriched binding of immature *TLC1* to Npl3-GFP compared to the no tag control, indicating that Npl3 and *TLC1* interact before the 3´-end of *TLC1* is trimmed. This binding might protect the immature form of *TLC1* from degradation prior to nuclear export and may serve as an adaptor protein for Mex67 mediated nuclear export.

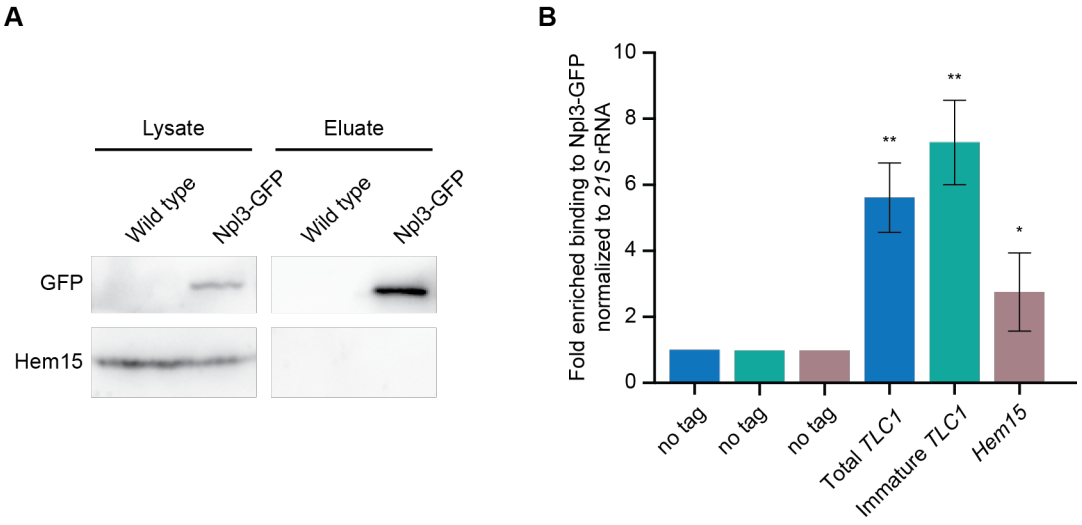

Figure 36: Npl3 and immature *TLC1* physically interact.
Indicated strains were harvested in mid-log phase, lysed and Npl3-GFP was precipitated with GFP-beads**.** Co-immunoprecipitated RNA was isolated, reverse transcribed and analyzed via qPCR. **(A)** A Western blot shows an example IP of immunoprecipitated Npl3-GFP from RIP experiments shown in (B). Hem15 served as control for unspecific protein binding to the GFP-beads. Npl3-GFP was detected with a GFP-specific antibody. **(B)** qPCR data from RIP experiments showing a interaction between Npl3-GFP and total and immature *TLC1* compared to no tag. The error bars represent the standard deviation, p-values were calculated by unpaired one-tailed unequal variance student´s t-test in (* = p< 0.05, ** = p< 0.01, *** = p<0.001). n=4. (Part of the bioRxiv article Hirsch et al. (2021)).

5. Discussion

Functional telomerases and telomere length homeostasis are essential for regulating the replicative life span in yeast (Austriaco and Guarente, 1997; Chen et al., 2009; Romano et al., 2013). Dysfunction is associated with carcinogenesis and pre-mature aging in human (Armanios and Blackburn, 2012; Calado and Young, 2009; Epel and Lithgow, 2014; McNally et al., 2019; Nagpal and Agarwal, 2020; Smogorzewska and De Lange, 2004). Research on telomeres and the telomerase was highlighted by the award of the Nobel Prize to Elizabeth H. Blackburn, Carol W. Greider and Jack W. Szostak in 2009, and still represents a main focus in cancer research. The function and essential features of the enzymatic complex are generally conserved. However, several functional aspects and details in the maturation pathway are unclear and we choose the simple eukaryote *S. cerevisiae* to investigate the life cycle of the telomerase RNA *TLC1* and assembly of the telomerase.

5.1. Transcription termination of *TLC1* involves the CPF-CFI complex and the NNS complex

Regulated gene expression is essential for cellular fitness and often achieved on a transcriptional level. Recent studies revealed pervasive transcription of the genome, suggesting that transcript abundance is regulated mostly by degradation rather than by transcription initiation (Dijk et al., 2011; Jensen et al., 2013; Larochelle et al., 2018; Neil et al., 2009; Porrua and Libri, 2015; Wyers et al., 2005; Xu et al., 2009). RNAP II is mainly responsible for the synthesis of protein-coding RNAs, but also for a variety of non-coding RNAs, such as snRNAs, snoRNAs, Cryptic Unstable Transcripts (CUTs) and Stable Unannotated Transcripts (SUTs), and for the lncRNA *TLC1* (Chapon et al., 1997; Porrua and Libri, 2015; Tuck and Tollervey, 2013; Xu et al., 2009). Interestingly, *TLC1* harbors transcription termination sites for the CPF-CFI complex and the NNS complex mediated termination (Figure 5, Figure 9 and Figure 37). It is currently unclear if both or only one of the sites is used for generating functional *TLC1*. To examine which *TLC1* termination pathways are used we surveyed the *TLC1* levels in mutants of both termination pathways. We observed that the amount of total and immature *TLC1* increases in mutants of the NNS pathway, such as the *nrd1-102* mutant and the *sen1-1*

mutant (Figure 10). This may reflect an increased abundance of polyadenylated, ~ 1.3 kb long poly(A)$^+$ *TLC1* which was observed in the *nrd1-102* mutant (Noël et al., 2012). In addition, due to the usage of a different *sen1* mutant which is defective in the RNA binding instead of the NTP binding (Hazelbaker et al., 2013; Noël et al., 2012), we were able to show that the same enrichment of immature *TLC1* is true for the *sen1-1* mutant (Figure 10). In contrast, the *nrd1-101* mutant did only slightly affect the *TLC1* level (Figure 10). In the *nrd1-101* mutant contact with RNAP II is disrupted (Conrad et al., 2000), yet the NNS complex appears to be functional and correctly positioned by other mechanisms. Together, this suggests that under normal conditions more *TLC1* is transcribed which is eliminated by the NNS pathway.

In fact, *TLC1* is a low abundant RNA with about 30 molecules per cell (Mozdy and Cech, 2006). Too little or too much are critical for the cell and leads to telomere defects (Austriaco and Guarente, 1997; Mozdy and Cech, 2006; Singer and Gottschling, 1994; Teixeira, 2013). Furthermore, the *TLC1* level was not affected by the *rna15-58* mutant (Figure 10). Even if the *rna15-58* mutant is defective in RNAP II termination, the mutant still retains the ability to polyadenylate improperly processed transcripts (Hammell et al., 2002). Thus, the recognition of binding motifs might be reduced but does not affect the overall *TLC1* level (Figure 10). This may indicate that improperly processed transcripts are subsequently processed to mature *TLC1.* While the *rna15-58* mutant does not impact the *TLC1* level, the decreased abundance of Rna14 and Rna15 of the CPF-CFI complex lead to telomere shortening (Ungar et al. 2009). Thus, the CPF-CFI complex is important for telomere length homeostasis. Nevertheless, the observed telomere shortening in the study of Ungar et al. (2009) may occur indirectly as the termination of essential telomerase subunits and other factors might be disturbed.

Two opposing models exist for transcription termination of *TLC1*: On the one hand mature poly(A)$^-$ *TLC1* might be generated via processing of the poly(A)$^+$ precursor, generated via CPF-CFI mediated transcription termination (Chapon et al., 1997; Coy et al., 2013). On the other hand poly(A)$^-$ *TLC1* might be generated directly via transcription termination by the NNS complex (Jamonnak et al., 2011; Noël et al., 2012). Two publications have questioned the importance of the CPF-CFI pathway in transcription termination of *TLC1* by showing that Nrd1 and Nab3 of the NNS complex bind in the 3' region of *TLC1*, that read-though occurs in a reporter assay when these binding sites are mutated, and that no telomere shorting occurs upon PAS mutation (Jamonnak et al., 2011; Noël et al., 2012). We wanted to analyze this question in greater detail and mutated the binding sites of both termination pathways

endogenously (Figure 11). Upon endogenous mutation of the NNS and the PAS sites, we observed a reduction of the total *TLC1* level in cell lysates, indicating that both termination pathways are used *in vivo* (Figure 12). By using a reverse primer at the 3´-end region of *TLC1* we were able to detect read-through transcripts, called long *TLC1*. We detected an increased abundance of long *TLC1* upon PAS mutation, but a decreased abundance upon NNS mutation (Figure 12 B). This might indicate that the NNS deficient mutant is presumably terminated via the CPF-CFI complex, preventing the formation of long *TLC1* but instead might generate transcripts ending at the poly(A)$^+$ end (Figure 37). This hypothesis is supported by the finding that the abundance of poly(A)$^+$ *TLC1* is increased in the *nrd1-102* mutant (Noël et al., 2012). Nevertheless, this would imply a read-through of the NNS site but a termination at the poly(A) signal area in the *NNS** mutant, suggesting that these transcripts are normally targeted for degradation. However, the decreased presence of total *TLC1* in the *NNS** mutant needs further investigation but may depend on the near proximity of the PAS signals and thus may affect also the PAS termination, in contrast to the *nrd1-102* mutant. Whether *TLC1* is terminated at the poly(A) signal area or if it is terminated at a different site in the *NNS** mutant should be analyzed in greater detail for example using the 3´ RACE method.

The increased presence of the long *TLC1* upon PAS mutation is in agreement with the finding that an 3´-extended polyadenylated *TLC1* transcript occurs upon PAS mutation in an plasmid based approach (Figure 12) and (Chapon et al., 1997; Noël et al., 2012). This indicates that downstream termination sites exist which may serve as fail-safe mechanism for *TLC1* termination via the CPF-CFI pathway (Figure 37) and (Chapon et al., 1997). Interestingly, for each termination pathway the opposite termination pathway is discussed to serve as a fail-safe mechanism (Ghazal et al., 2009; Grzechnik and Kufel, 2008; Rondón et al., 2009). Nevertheless, it is possible that yet unknown fail-safe NNS termination sites downstream of *TLC1* exist. Taken together our first finding is that both termination pathways are used *in vivo* and that mechanisms exists that secure the transcription termination of both pathways in *TLC1* transcription termination.

To gain a better understanding of the underlying context, we investigated where the *TLC1* transcripts localize in the PAS and the NNS mutants. Overall, the localization of *TLC1* was not altered upon PAS mutation (Figure 13). But, by using a more sensitive method we observed an increased abundance of long *TLC1* in the cytoplasm in the *poly(A)** mutant (Figure 14). This might suggest that long *TLC1* is processed more slowly during RNP formation and re-import.

In addition, we observed that the long *TLC1* form accumulates in the cytoplasm upon *CSE1* mutation, indicating that the re-import of long *TLC1* is also dependent on Cse1 (Figure 14).

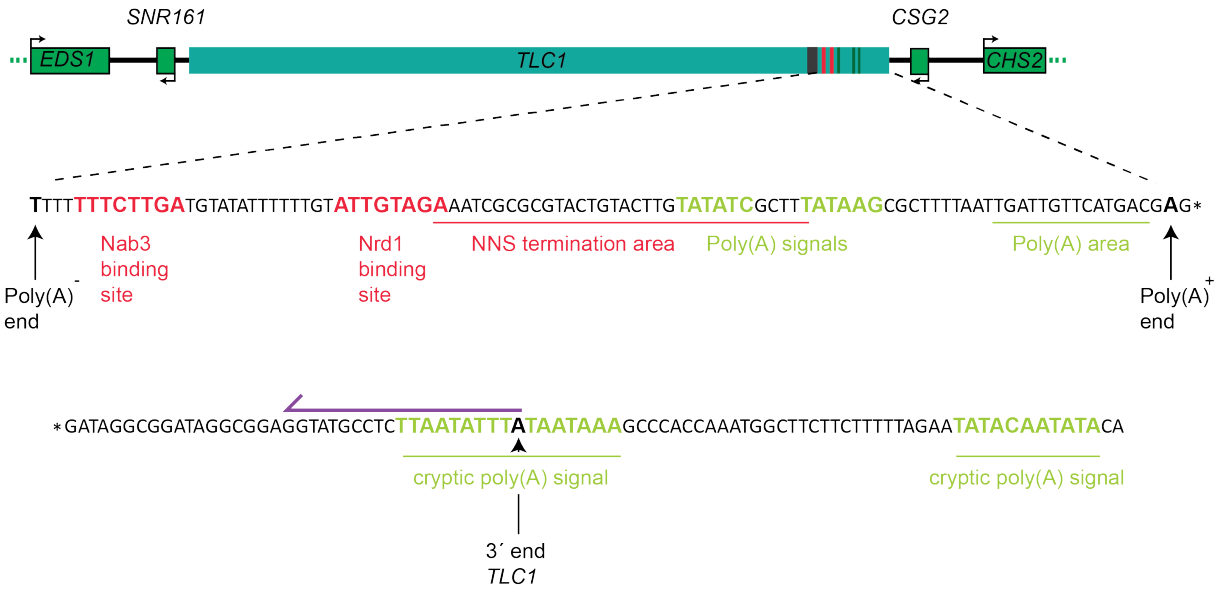

Figure 37: Termination factor binding sites in *TLC1*.
Binding sites of Nrd1 and Nab3 (red) are followed by the NNS termination area, adopted from Jamonnak et al. (2011) and Noël et al. (2012). Poly(A) signals (green) are followed by the poly(A) area, adopted from Chapon, Cech, and Zaug (1997). Cryptic poly(A) signals (green), adopted from Chapon, Cech, and Zaug (1997), may serve as fail safe transcription termination sites. The originally published mature poly(A)$^-$ end, the poly(A)$^+$ end and the 3´end region of *TLC1* are indicated (Bosoy et al., 2003; Chapon et al., 1997). Reverse primer amplifying the long *TLC1* (purple) is indicated.

In the *NNS** and *poly(A)*NNS** mutants, we detected a mislocalization of *TLC1* to the cytoplasm in about 80 or 90 % of the cells, respectively (Figure 13). In addition, we have shown a cytoplasmic accumulation of *TLC1* in the *NNS** mutant in an asynchronous grown culture through nucleo-cytoplasmic fractionation experiments (Figure 14). This indicates a leakage of stable transcripts into the cytoplasm. These transcripts might be terminated via the CPF-CFI complex, either at the PAS site in the *NNS** mutant or at additional downstream termination sites in the *poly(A)*NNS** mutant. Thus, these transcripts might be polyadenylated and furthermore contacted by the *TLC1* export machineries. The cytoplasmic accumulation may be due to incompletely assembled holoenzymes that are not targeted for import. In addition, the timing of the different termination complexes may be relevant. In particular, the Sen1 expression is cell cycle regulated and is high in the transition of the S and G2 phase (Mischo et al., 2018). This might limit the NNS termination to a cell cycle phase in which presumably no *TLC1* is needed for producing a functional telomerase. This question could be analyzed in synchronized cells. Taken together, this suggests that the termination of *TLC1* depends on

both the CPF-CFI and the NNS complex but might lead to different transcript fates depending on the used complex. Nevertheless, we cannot exclude that NNS terminated transcripts are in principle exported to the cytoplasm and are incorporated into the telomerase RNP. However, it seems less likely that the NNS complex is the main pathway to generate functional *TLC1* because transcript stability upon NNS termination presumably requires stability elements in the RNA or co-transcriptional loading of stabilizing factors because termination and 3´-end processing is coupled (Grzechnik et al., 2018; Richard and Manley, 2009; Villa et al., 2020).
Non-coding RNAs which are terminated via the NNS complex are oligoadenylated by TRAMP complex which are thus targeted to the nuclear exosome (Han et al., 2020; LaCava et al., 2005; Vanacova et al., 2005; Wyers et al., 2005). In this way CUTs are eliminated (Neil et al., 2009; Wyers et al., 2005; Xu et al., 2009). Co-transcriptional cleavage of snoRNAs by Rnt1 and co-transcriptional assembly of the snoRNP core by loading accessory proteins onto the snoRNAs ensures the stability and processing of snoRNAs (Caffarelli et al., 1996; Grzechnik and Kufel, 2008; Grzechnik et al., 2018; Gudipati et al., 2012). In the case of snRNAs, a stem loop, which is later cleaved by Rnt1, may prevent the complete degradation of the transcripts after NNS termination (Allmang et al., 1999; Seipelt et al., 1999). Furthermore, it was shown that the cleavage by Rnt1 and 3´-trimming of pre-snRNPs occurs after re-import and stops at the Sm-ring (Becker et al., 2019; Coy et al., 2013). Also *TLC1* is protected via the Sm-ring, however this is loaded in the cytoplasm (Coy et al., 2013; Hirsch et al., 2021; Vasianovich et al., 2020). Thus, the Sm-ring cannot stabilize the RNA during transcription termination via the NNS complex. The Nrd1-binding itself was discussed to function as a stop signal for the nuclear exosome (Steinmetz and Brow, 1998; Steinmetz et al., 2001; Vasiljeva and Buratowski, 2006). By eliminating the binding of Nrd1 to the transcript one would suggest a drastic decreased abundance of *TLC1* and telomere shortening effects if the NNS complex is used exclusively to obtain a functional *TLC1* transcript. Indeed, we observed a decreased presence of *TLC1* in the *NNS** mutant (Figure 12) but an increased abundance of poly(A)$^+$ *TLC1* transcripts was observed in the *nrd1-102* mutant (Noël et al., 2012). This again suggests that *TLC1* is terminated via the CPF-CFI pathway in NNS deficient mutants and that NNS terminated transcripts are rather targeted for degradation. In addition no telomere defects are known for NNS complex mutants (Askree et al., 2004; Gatbonton et al., 2006; Ungar et al., 2009). Again, the decreased presence of *TLC1* in the *NNS** mutant needs further investigation but may depend on the near proximity of the PAS signals and thus may affect also the PAS termination.

Overall, this suggests that the coupling between the NNS complex and the exosome is normally used for degradation of these transcripts. This may counteract the transcript abundance through the pervasive transcription of the genome and fine tune the *TLC1* level. Nevertheless, one cannot exclude that unknown motifs may be present protecting *TLC1* from degradation by the nuclear exosome. Furthermore, this suggests that the CPF-CFI pathway functions as main termination pathway for generating functional *TLC1*. This is in agreement with previous publications which revealed that the 3´-extended precursor upon PAS mutation is capable to interact with Est2 *in vitro*, suggesting that that poly(A)$^+$ precursor might be incorporated into the telomerase (Chapon et al., 1997; Coy et al., 2013).

Interestingly, high-throughput data detected more transcripts that end after the poly(A) termination area than after the NNS termination area, indicating that the poly(A) termination area is used more frequently (Schmid et al., 2018) and (Figure 38). This confirms that approximately 90 % of *TLC1* transcripts end after the Sm-binding site, as originally termed the poly(A)$^-$ *TLC1* (Chapon et al., 1997). This method would be an excellent tool for analyzing the 3´-ends in the *poly(A)** and *NNS** deficient mutants in synchronized cells.

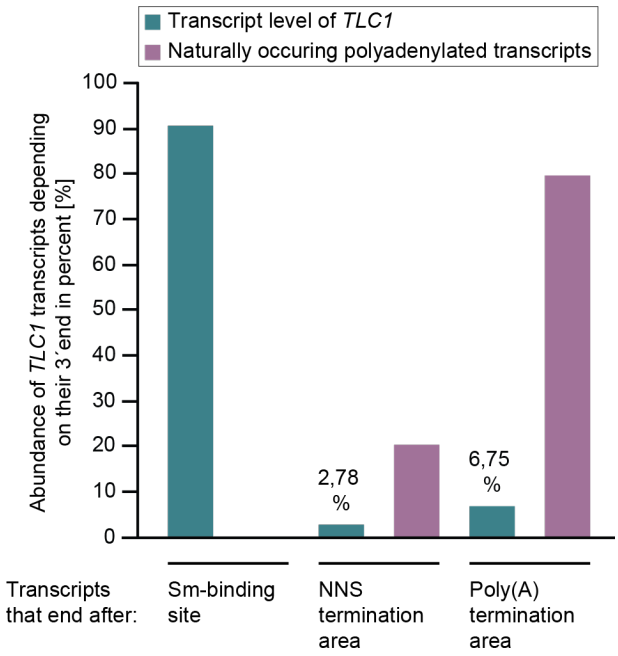

Figure 38: Abundance of *TLC1* transcripts according their 3´-end.
Transcripts were measured via 3´-end sequencing after using 4-thiouracil (4tZ) labeling. Samples were sequenced directly, revealing the naturally occurring polyadenylated transcripts (pink) or after artificially adding a poly(A) tail through *E.coli* pA polymerase (E-PAP), revealing all transcripts (dark green). The data used for this figure are from Schmid et al., (2018).

In comparison to yeast, a similar mechanism for transcription termination was shown for the human telomerase RNA (*hTR*). *hTR* always originates from a 3' extended precursor, which is either directly processed via 3'-5'exonucleolytic trimming to the mature form, which is possible through its co-transcriptional assembly with proteins of the snoRNP family, or it is first polyadenylated and then degraded or processed to the mature *hTR* (Roake et al., 2019).
So far, it was assumed that only one of the termination pathways is essential and used for transcription termination of *TLC1*. However, mutations in both pathways (*poly(A)*NNS**) led to a mixed phenotype which did not resemble the *tlc1Δ* phenotype, suggesting the use of other termination sites. Furthermore, this might imply that the two pathways have different functions regarding the transcript fate of *TLC1*.

5.2. *TLC1* interacts with the cap binding complex component Cbp20 and the guard protein Npl3

The maturation of *TLC1* involves a cytoplasmic step and the export from the nucleus to the cytoplasm is mediated by the export receptors Xpo1 and Mex67 (Ferrezuelo et al., 2002; Gallardo et al., 2008; Wu et al., 2014). While Mex67-Mtr2 contacts mRNAs mostly via an adaptor protein, Xpo1 contacts the CBC either directly or indirectly via a yet unknown adaptor protein in yeast (Becker et al., 2019; Köhler and Hurt, 2007; Zander et al., 2016). In human cells, Crm1 (Xpo1) contacts the CBC via the adaptor protein PHAX for nuclear export of snRNAs (Ohno et al., 2000). Interestingly, in yeast no PHAX homolog was identified. Although immature *TLC1* contains an m^7G-cap it was unclear if the CBC contacts *TLC1*.
Through RIP experiments, we demonstrated a physical interaction between immature *TLC1* and Cbp20 (Figure 15). Because we detected the immature *TLC1* form in this RIP, we suggest that this interaction takes place prior to trimming of *TLC1,* which is facilitated after re-import (Figure 35). The CBC contacts pre-mRNAs, preferentially interacts with m^7G cap transcripts and Cbp80 contacts Xpo1 for export of snRNA (Baejen et al., 2014; Becker et al., 2019; Schwer et al., 2011). Thus, we suggest that the contact of immature m^7G capped *TLC1* with the CBC could facilitate export of *TLC1* to the cytoplasm via Xpo1 (Hirsch et al., 2021). Nevertheless, it is still unclear whether a yet unknown adaptor protein is missing, which bridges the contact between the CBC and Xpo1.

Another protein which is involved in nuclear export is the guard protein Npl3, as it acts as retention factor for RNAs until Mex67 binds to enable export (Zander et al., 2016). The loading of Npl3 onto nascent transcripts occurs co-transcriptionally, because Npl3 interacts with the RNAP II and the CBC (Lei et al., 2001; Shen et al., 2000). We have shown that *TLC1* and especially the immature form interacts physically with Npl3 *in vivo* (Figure 36). Whether Npl3 only serves as an adaptor for nuclear export or whether it additionally functions as quality control factor or as stabilizing factor before the transcript is exported, needs further research. One aspect that suggests a stabilizing role for Npl3 is, that the loss of functional Mex67 in *mex67-5* did not eliminate the presence of immature *TLC1* (Figure 35) and (Hirsch et al., 2021). Whether the other guard proteins Hrp1 and Gbp2 might also contact *TLC1*, as known for mRNAs, would be beneficial to analyze as this may serve as quality control step prior nuclear export (Hackmann et al., 2014; Zander et al., 2016). Although Gbp2 and Hrb1 are quality control and splicing factors of mRNAs, they have been shown to interact with the 5´-end of lncRNAs (Baejen et al., 2014; Hackmann et al., 2014; Tuck and Tollervey, 2013). However, what function they might fulfill in lncRNA biogenesis needs further investigation.

5.3. Telomerase holoenzyme assembly occurs in the cytoplasm

The telomerase consists of the Est and Pop proteins as well as the Sm-ring and possibly the Yku complex (Hughes et al., 2000; Lemieux et al., 2016; Lendvay et al., 1996; Lingner et al., 1997a; Peterson et al., 2001; Seto et al., 1999). However, the order in which the proteins assemble has not been fully elucidated. The loading of the Est proteins onto *TLC1* occurs in the cytoplasm (Gallardo et al., 2008; Wu et al., 2014). Simultaneous to our studies, it was suggested that the loading of the Pop proteins as well as the Sm-ring onto *TLC1* are cytoplasmic events (Garcia et al., 2020; Hirsch et al., 2021; Vasianovich et al., 2020). In contrast to this, the 3´-processing and 5´-TMG-capping were suggested to occur prior to nuclear export (Gallardo et al., 2008; Garcia et al., 2020; Wu et al., 2014). In the telomerase RNP, Pop6 and Pop7 are acting as a binding platform for Pop1, which in turn seems to stabilize Est1 binding to the RNP, arguing for a cytoplasmic loading of the Pop proteins (Laterreur et al., 2018; Lemieux et al., 2016). Since Pop1 is not only present in the telomerase but also in the RNAse P and the RNAse MRP complex (Lemieux et al., 2016; Lygerou et al., 1994), we investigated the loading of the Pop1 protein onto *TLC1* directly via RIP experiments. We have shown a

decreased interaction between *TLC1* and Pop1 in the *mex67-5* mutant and a highly increased interaction between immature *TLC1* and Pop1-GFP in *cse1-1* mutant (Figure 33). Additionally, we have shown that blocking nucleo-cytoplasmic transport pathways or the loss of *TLC1* led to a cytoplasmic mislocalization of Pop1 (Figure 32).These findings suggest that Pop1 is loaded in the cytoplasm onto the immature *TLC1* and that the re-import of the telomerase is facilitated as holoenzyme (Hirsch et al., 2021). This is consistent with recent findings that *TLC1* mislocalizes to the cytoplasm in *POP1* and *POP6* deficient mutants (Garcia et al., 2020). As Pop1 binding depends on Pop6 and Pop7, they are most likely loaded first (Lemieux et al., 2016).

We identified Cse1 as a novel re-import factor of pre-*TLC1* (Figure 18 and Figure 19) and (Hirsch et al., 2021). Cse1 is known as export factor for Srp1, yeast importin α (Hood and Silver, 1998; Solsbacher et al., 1998). Earlier studies suggested that Est1 might be imported via the importin α /ß pathway (Hawkins and Friedman, 2014). In fact, we observed a cytoplasmic mislocalization of Est1-GFP in the *cse1-1* mutant (Figure 32). This finding is reassuring for the cytoplasmic loading of Est1 onto the RNP and supports the model in which the holoenzyme assembly occurs in the cytoplasm as suggested earlier (Gallardo et al., 2008; Wu et al., 2014). The re-import of the telomerase as holoenzyme is further supported by the fact that the re-import of *TLC1* is independent of Srp1 (Gallardo et al., 2008) and (Figure 25). We suggest, that the importin α pathway might be a way to import additional Est1 into the nucleus, independent from its telomerase associated import. This hypothesis can be strengthened by the observation that Est1 is only partially mislocalized in the *tlc1Δ* mutant (Figure 32). In addition, the telomerase independent import pathway does not seem to be that important because only a mild telomere shortening effect was observed in the *srp1-54* mutant without survivor cell formation (Hawkins and Friedman, 2014). In contrast to that, *estΔ* or *tlc1Δ* mutant strains show severe telomere shortening defects and survivor type formation (Lundblad and Blackburn, 1993; Lundblad and Szostak, 1989; Singer and Gottschling, 1994; Teng and Zakian, 1999). Furthermore, in immunofluorescence experiments we have shown that proper nuclear localization of Pop1 is also dependent on the importin α pathway (Figure 26). Thus, telomerase independent nuclear import of associated proteins of the complex could either indicate independent nuclear function of these proteins or it may suggest that defective components of the telomerase can be exchanged. Since the re-import of *TLC1* is independent of the importin α pathway and because Est1 and Pop1 mislocalize upon *TLC1* deletion we

assume that only proper assembled RNPs are re-imported independent of the importin α pathway (Gallardo et al., 2008; Garcia et al., 2020; Hirsch et al., 2021; Wu et al., 2014).

5.4. Nuclear import of immature *TLC1* is facilitated by Cse1 and Mtr10 in dependence of the Sm-ring

After pre-*TLC1* was exported to the cytoplasm, re-import is mandatory because the telomerase functions in the nucleus. After RNP formation, re-import is mediated via Mtr10, but Kap122 has also been suggested as import factor (Ferrezuelo et al., 2002; Gallardo et al., 2008; Vasianovich et al., 2020). However, we never observed an effect of *kap122* on the localization of *TLC1* and *kap122* only slightly effects the telomere length (unpublished data Krebber lab and Vasianovich, Bajon, and Wellinger (2020)). Recently Cse1 was described as snRNA re-import factor, which contacts the Sm-ring for the re-import of snRNAs (Becker et al., 2019). This is also the case for *TLC1* which was shown in Fish experiments (Figure 18) and (Hirsch et al., 2021). Furthermore, we show that the transcripts that accumulate in the cytoplasm upon re-import block are still immature (Figure 19), suggesting that 3´-end processing occurs after re-import. We suggest that both factors, Cse1 and Mtr10, cooperate in the re-import of immature *TLC1* because an additive effect was observed when both factors were mutated (Figure 19).

In addition, we found that Cse1 and Mtr10 both interact physically with *TLC1* (Figure 20). Because transport via both karyopherins is dependent on the Ran gradient, the mild enrichment of the interaction between *TLC1* and Mtr10 and Cse1 observed in the co-immunoprecipitation could be explained by the experimental setup. Through cell lysis, the Gsp1 (Ran in human) gradient breaks down and might induce disassembly of the import-cargo complexes, resulting in lower *TLC1* co-purification. Crosslinking the cells with UV light or formaldehyde prior to cell lysis might preserve the interactions but it could also lead to stronger non-specific binding and lower the quality of the co-precipitated RNA.

For snRNA, the cytoplasmic loading of the Sm-ring is a prerequisite for re-import (Becker et al., 2019). To investigate whether this is also the case for *TLC1*, we analyzed how the physical interaction of *TLC1* and Smb1 changes in import and export factor mutants. Indeed, we have shown that the interaction between *TLC1* and Smb1-GFP decreases in the export factor mutant *mex67-5* and increases in the import factor mutant *mtr10Δ*, indicating that the Sm-

ring loading to *TLC1* occurs in the cytoplasm (Figure 16 and Figure 17) and (Hirsch et al., 2021). In parallel to our experiments, another group analyzed a *tlc1* mutant harboring a defective Sm-ring binding site, which was additionally tagged with an MS2-tag and expressed via an inducible promoter (Vasianovich et al., 2020). Using an MS2-specific FISH probe, they have shown that the newly synthesized defective *TLC1* accumulated in the cytoplasm, indicating a cytoplasmic loading of the Sm-ring (Vasianovich et al., 2020). This is in agreement with a cytoplasmic mislocalization of *TLC1* in *smb1 smd* mutants and confirms a cytoplasmic loading of the Sm-ring on *TLC1* (Hirsch et al., 2021). While Vasianovich and colleges could not distinguish which form of *TLC1* is contacted by the Sm-ring we have shown that the Sm-ring assembles onto immature pre-*TLC1* (Hirsch et al., 2021; Vasianovich et al., 2020).

CSE1 and *MTR10* genetically interact (Figure 21) and cooperate in the reimport of pre-*TLC1*, as the ratio of immature to total *TLC1* is significantly increased in the *cse1-1 mtr10Δ* mutant compared to the single mutants (Figure 19). Interestingly, both factors seem to have additional functions in the stabilization of *TLC1*. Mutation in *CSE1* did not alter the overall *TLC1* level (Figure 22), but led to an increased presence of immature *TLC1* in the cytoplasm. (Figure 19). Furthermore, the interaction between *TLC1* and Smb1 decreases in the *cse1-1* mutant (Figure 23). This is also the case in the *cse1-1 mtr10Δ* double mutant. This indicates a stabilizing function of Cse1 in RNP formation and suggests that only properly assembled holoenzymes may be re-imported (Figure 23) and (Hirsch et al., 2021). In contrast to this, mutation or loss of *MTR10* led to a decreased level of total *TLC1* (Figure 22) and (Ferrezuelo et al., 2002). This suggests that the transcripts might be degraded when the re-import is blocked. However, we observed an increased ratio of immature *TLC1* in relation to the total *TLC1* (Figure 19 and Figure 22) and an increased interaction between *TLC1* with Smb1 in the *mtr10Δ* mutant (Figure 17). These findings suggest that although both karyopherins were identified to support the nuclear re-import of pre-*TLC1*, Mtr10 functions as the major import factor, supported by Cse1. The accumulation of pre-*TLC1* in the cytoplasm of *cse1-1* might rather indicate processing defects, because the Sm-ring is not properly attached (Figure 23). In contrast, in *mtr10Δ* readily assembled pre-telomerases accumulate as shown by the increased presence of Sm-ring containing particles (Figure 17). Thus, Cse1 might stabilize the Sm-ring on pre-*TLC1* (Figure 19, Figure 23) and (Hirsch et al., 2021).

Interestingly, Cse1 possess a closed conformation in its cargo free state and opens up in the presence of Ran-GTP allowing binding of importin α and subsequent transport to the

cytoplasm (Cook et al., 2005; Hood and Silver, 1998). Whether *TLC1* or the snRNA interrupt the closed conformation and how the import is facilitated will be interesting to address.

Cse1 does not bind snRNAs *in vitro* but physically interacts with Smb1 *in vivo*, suggesting that Smb1 might function as adaptor protein for *TLC1* in nuclear re-import (Becker et al., 2019). Due to structural similarities of Cse1 and Mtr10 and because Mtr10 belongs to the group of importin β like karyopherins which have a highly hydrophobic core it seems convincing that Mtr10 needs an adaptor protein for cargo import (Güttler and Görlich, 2011; Ström and Weis, 2001). Therefore, we investigated whether Mtr10 interacts with proteins of the telomerase holoenzyme, which may also provide docking points for *TLC1* contact. Through IP experiments we revealed a physical interaction between Mtr10 and Smb1 which presumably facilitates the re-import of *TLC1* as holoenzyme (Figure 24). Thus, both karyopherins contact the Sm-ring for import of their cargos. However, it is possible that the interaction of Mtr10 and Smb1 occurs directly or indirectly. This question should be analyzed via *in vitro* binding studies.

Additionally, Mtr10 functions in the re-import of Npl3 (Pemberton et al., 1997; Senger et al., 1998). We observed a physical interaction of Npl3 and immature *TLC1* in RIP experiments (Figure 36). Whether Npl3 is loaded co-transcriptionally prior to export, establishes contact with *TLC1* only in the cytoplasm, or whether binding persists until re-import needs to be determined by further experiments. However, it is conceivable that Npl3 may function as an adaptor protein for Mex67-mediated *TLC1* export, because it contacts mRNAs co-transcriptionally and mRNA bound Npl3 is released by Mtr10 in the cytoplasm (Lei et al., 2001; Windgassen et al., 2004). However, Npl3 is also re-imported by Mtr10 and is released from Mtr10 through binding of RNA to Npl3 and Ran-GTP to Mtr10, but not RNA and Ran-GDP *in vitro* (Senger et al., 1998). Because Mtr10 contacts also *TLC1* for re-import it is still possible that Npl3 might persist on *TLC1* until the re-import is facilitated.

Overall, we have shown a physical interaction between the Smb1 protein and immature *TLC1,* and that the presence of both import factors facilitate the nuclear re-import in dependence of the Sm-ring, which is stabilized via Cse1 (Hirsch et al., 2021).

5.5. A novel role of Cse1 in telomere biology

Telomere length homeostasis is a dynamic system of temporarily uncapped and capped telomere ends allowing coordinated telomere elongation in late S phase and otherwise providing protection from detection as double strand break (Blackburn, 2001; Kupiec, 2014; Marcand et al., 2000; Teixeira et al., 2004; Wellinger and Zakian, 2012). Both, a functional telomerase and an intact telomere cap is crucial for telomere length homeostasis. Telomerase negative cells undergo gradual telomere shortening and senescence upon critically short telomeres (Lendvay et al., 1996; Lundblad and Szostak, 1989; Singer and Gottschling, 1994). Changing the telomeric structure and telomere shortening in the absence of the telomerase stimulate different cellular responses, as partially uncapped telomeres are normally prone to accelerated senescence (Chang et al., 2011; Nugent et al., 1998; Teixeira, 2013). Both uncapped and critically short telomeres are sensed by components of DNA repair pathways and lead to DNA damage checkpoint activation (Ijpma and Greider, 2003; Teixeira, 2013). The signaling slightly differs as uncapped telomeres can be sensed by the DNA repair pathway throughout the cell cycle (Teixeira, 2013). However, the outcome of senescence and escaping this status by survivor type formation is the same. In rare cases switch to homologous recombination based telomere elongation can occur leading to Type I and Type II survivor cells (Chen et al., 2001; Lundblad and Blackburn, 1993; Teng and Zakian, 1999). Both survivor types depend on Rad52, however are further generated via distinct pathways (Chen et al., 2001; Teng and Zakian, 1999). This view was recently modified through analysis of survivor types by ultra-long sequencing and population genetics, suggesting that both pathways are consecutive steps in an overall pathway, leading in rare cases to a Type I/Type II survivor hybrid (Kockler et al., 2021). Three genome-wide studies revealed that over 270 non-essential genes and 87 essential genes affect the telomere length in yeast (Askree et al., 2004; Gatbonton et al., 2006; Ungar et al., 2009). However this studies seem to be incomplete as they did not identify Mtr10, Mex67, and Xpo1, known to negatively affect the telomere length in yeast when mutated (Ferrezuelo et al., 2002; Wu et al., 2014). We found that Cse1 is involved in the re-import of *TLC1* into the nucleus (Figure 18 and Figure 19). Interestingly, Southern blot analysis indicated normal telomere length in the *cse1-1* mutant but an altered telomere structure, with an amplification of the Y´ elements (Figure 28 and Figure 29). Y´ element amplification is a typical feature of Type I survivor cells (Lundblad and Blackburn,

1993; Teng and Zakian, 1999). Strikingly, the Y´ element amplification occurs without the presence of telomere shortening. Thus, Cse1 was presumably not identified in the screen of Ungar et al. (2009) because they looked for short and long terminal telomere fragments. Complementation with *CSE1* reverted the Y´ amplification in the *cse1-1* mutant (Figure 29), reassuring that the observed phenotype depends on the mutation of *CSE1*. Normally, Type I survivors exhibit very short terminal fragments due to loss of the telomerase and highly amplified Y´ elements due telomere elongation via recombination of Y´ elements (Lundblad and Blackburn, 1993; Teng and Zakian, 1999). In the *cse1-1* mutant we observed normal lengthened terminal telomere ends but amplification of the Y´ elements. Therefore, we termed the phenotype observed in *cse1-1* "Type I-like survivor" (Hirsch et al., 2021), however "Amplified Y´ element mutant" or "Long telomere mutant" might be more suitable.

The normal length of the terminal telomere fragment in the *cse1-1* might be generated by two possibilities: First, even if some *TLC1* is mislocalized to the cytoplasm (Figure 18), enough telomerase molecules can enter the nucleus that lengthen the telomeres (Figure 28). Secondly, Y´ tandems are formed early on eroded telomeres, including long telomeres (Churikov et al., 2014). They could switch to a Type I/Type II survivor hybrid by the use of both replication machineries (Kockler et al., 2021). This could result in amplified Y´ elements and additionally lengthened terminal fragments. However, because the terminal fragments are not over elongated in the *cse1-1* mutant, its phenotype might represent a stable intermediate prior to Type I/Type II hybrid formation. Furthermore, it is well possible that other proteins important for telomere lengthening are mislocalized in *cse1-1*, which might support the Y´ amplification. The double mutant *cse1-1 mtr10Δ* shows a telomere shortening defect comparable to the *mtr10Δ* mutant (Figure 28) and (Ferrezuelo et al. 2002). In addition, we observed no survivor formation or Y´ amplification in the *cse1-1 mtr10Δ* mutant (Figure 28). This indicates that loss of *MTR10* is crucial and that Mtr10 might additionally import proteins necessary for recombination events such as Rad52.

In addition to the presence of a functional telomerase, the telomere cap structure is an essential checkpoint to decide which elongation pathway is used. As both very short or uncapped telomeres are prone to recombination events, we suppose that mutations in *CSE1* additionally impact the cap structure of telomere ends (Blackburn, 2000; McEachern and Iyer, 2001; Teixeira et al., 2004). Therefore, we localized Cdc13 and Rap1, which both function in telomere capping, via Immunofluorescence experiments in the *cse1-1* mutant. While

localization of Cdc13 was not affected in the *cse1-1* mutant (Figure 30), Rap1 partially mislocalized to the nucleolus at the permissive temperature and the cytoplasm at the non-permissive temperature (Figure 31). The nature of *cse1-1* mutation itself is not clear and it would be interesting to analyze whether the protein is mis-folded or degraded. Further investigations are needed to distinguish whether Cse1 transports Rap1 directly or indirectly. The mislocalization of Rap1 might be an indirect effect of *the cse1-1* mutant, which might depend on a mislocalization of silencing factors in the *cse1-1* mutant as mislocalization of Sir3 and Sir4 in the *sir2Δ* mutant additionally express a diffuse localization of Rap1 (Gotta et al., 1996, 1997). Therefore, it might be possible that mostly the Rap1/Sir complex but not the Rap1/Rif1/Rif2 (telosome) complex is mislocalized in the *cse1-1* mutant. This would maintain a telomerase mediated lengthening in dependence of the Rap1/Rif1/Rif2 proteins, favoring short telomeres for lengthening via a counting mechanism (Krauskopf and Blackburn, 1996; Levy and Blackburn, 2004; Marcand et al., 1997; Teixeira et al., 2004; Wotton and Shore, 1997). However, internal Rap1-bound TG_{1-3} repeats facilitate Y´ recombination between internal and terminal TG_{1-3} repeats by homologous recombination (Churikov et al., 2014). Thus, it would be interesting to analyze how the Y´ elements are amplified in the *cse1-1* mutant.

Subtelomeric regions, as the Y´ elements, can be used for telomere maintenance and are discussed as telomere capping factor, in case of a non-functional telomerase or cap structure (Dorer and Henikoff, 1997). Homologous recombination is as efficient as telomerase based telomere maintenance in regard to cell survival and overall genome stability (Chen et al., 2009). However, telomerase deficient strains possess a shorter replicative life span (Chen et al., 2009). Thus, it would be interesting to analyze whether the replicative life span is changed in the *cse1-1* mutant. Additionally, it would be exciting to analyze whether the normal lengthened telomere ends and Y´ amplification in the *cse1-1* mutant might delay or bypass a senescence phenotype, which normally occurs prior to switching to recombination based telomere lengthening (Makovets et al., 2008).

Overall, we assume that the partial mislocalization of telomerase has a minor impact on the phenotype. Altering the cap structure indicated by Rap1 mislocalization seems to initiate the use of homologues recombination in *cse1-1* mutant in addition to telomerase mediated lengthening, leading to this special phenotype.

5.6. 3´-end processing of *TLC1* occurs after re-import and processing is finalized by TMG-cap formation as prerequisite for telomerase function

Recent studies assume that 3´-trimming and TMG-capping of *TLC1* occurs prior to nuclear export (Gallardo et al., 2008; Garcia et al., 2020; Wu et al., 2014). However, Sm-ring loading is a prerequisite for 3´-end processing facilitated via the nuclear exosome (Coy et al., 2013; Hass and Zappulla, 2020). Additionally, the interaction of Smb1 and Tgs1 is suggested to guide snRNAs to the nucleolus for TMG-capping (Becker et al., 2019; Mouaikel et al., 2002). We and others have shown that the Sm-ring loading onto *TLC1* occurs in the cytoplasm (Figure 16 and Figure 17) and (Vasianovich, Bajon, and Wellinger 2020; Hirsch et al. 2021). In particular we have shown that the immature *TLC1* is the target of Sm-ring loading (Figure 17 and Figure 23). This suggests that the 3´-trimming and TMG-capping occur after re-import. Further evidence comes from studies in which the double mutant *rrp6Δ mex67-5* was used. We and others have shown that mutation of the export factor alone led to an overall decreased abundance of *TLC1,* indicating that nuclear export is important for the generation of mature *TLC1* (Figure 35) and (Vasianovich, Bajon, and Wellinger 2020). Thus, Mex67 has a stabilizing function for pre-*TLC1* (Figure 35) and (Vasianovich, Bajon, and Wellinger 2020). Also, it would not be surprising if transcripts are partially degraded when retained in the *mex67-5* mutant, as the protecting Sm-ring is not yet bound (Figure 16) and (Vasianovich, Bajon, and Wellinger 2020; Hirsch et al. 2021). Interestingly, we found that the relative level of the immature *TLC1* is not affected by the absence of functional Mex67 (Figure 35), suggesting that additional factors protect the nascent transcripts from degradation. One of them might be the guard protein Npl3 that physically interacts with immature *TLC1* and in this way might protect it (Figure 36). Furthermore, we and others have shown that the total, the immature and the poly(A)$^+$ *TLC1,* is increased in the *rrp6Δ* mutant compared to wild type, indicating that Rrp6 is involved in 3´-end processing of *TLC1* (Figure 35) and (Coy et al., 2013). Interestingly, we observed an overall reduction in the total *TLC1* level but an ~ 5-fold increase in the immature *TLC1* in the *rrp6Δ mex67-5* mutant (Figure 35). The increased amount of immature *TLC1* in the *rrp6Δ mex67-5* mutant is consistent with recent data in which a restoration of newly synthesized MS2 tagged *TLC1* was observed in an *rrp6Δ mex67-5* mutant (Vasianovich, Bajon, and Wellinger 2020). In addition our data suggest that nucleo-cytoplasmic shuttling is mandatory for the overall *TLC1* level even if the nuclear degradation of immature *TLC1* is

limited (Hirsch et al., 2021). This highlights the importance of nucleo-cytoplasmic shuttling to generate mature *TLC1* and hence a functional telomerase as shown earlier (Wu et al., 2014). Taken together, the relative increase of immature *TLC1* in the *rrp6Δ mex67-5* mutant and the accumulation of immature *TLC1* in re-import mutants indicate that the 3´-end processing occurs after the re-import via the nuclear exosome (Figure 35 and Figure 19) and (Hirsch et al., 2021). This is reasonable in regard to the cytoplasmic loading of the Sm-ring onto *TLC1*, which protects *TCL1* from full degradation (Coy et al., 2013; Hass and Zappulla, 2020; Hirsch et al., 2021; Vasianovich et al., 2020). These findings are in agreement with previous studies in which the poly(A)$^+$ *TLC1* level was shown to be recovered in an Sm-binding site mutant in which additionally the exosome component *rrp47* was missing (Coy et al., 2013). This again also suggests a precursor function of the poly(A)$^+$ form for mature *TLC1* (Coy et al., 2013).

Besides 3'-trimming by the exosome, another processing step of *TLC1* is the TMG-capping (Franke et al., 2008; Seto et al., 1999). We observed a decreased level of TMG-capped *TLC1* in the import factor mutants which is comparable to the level in *tgs1Δ* (Figure 34), where no TMG-capping of *TLC1* occurs (Franke et al., 2008). Therefore, we conclude, that TMG-capping of *TLC1* is facilitated after re-import (Hirsch et al., 2021). It is convincing that TMG-capping occurs after re-import, as the CBC binds preferentially monomethylated RNAs for export via Xpo1 (Becker et al., 2019; Schwer et al., 2011). Thus, TMG capping after re-import could serve as a nuclear retention signal as suggested earlier (Becker et al., 2019). Additionally, is not known whether a re-export of the assembled telomerase via Mex67-Mtr2 is possible, as Mex67-Mtr2 is released from the mRNP at the cytoplasmic site of the NPC after cargo transport (Folkmann et al., 2011; Kelly and Corbett, 2009; Tieg and Krebber, 2013). Nevertheless, it would be of interest to investigate whether TMG-capped *TLC1* is transported out of the nucleus again, as it may be necessary for degradation of the telomerase.

Overall, our data indicate that 3´-end processing and TMG-capping of *TLC1* occurs in the nucleus after re-import (Hirsch et al., 2021). Especially the TMG-capping after re-import may resemble a mechanism to prevent leakage of the functional telomerase. Recent studies have shown that deletion of *TGS1* leads to nucleolar accumulation of the *U1* snRNA which is also true for *TLC1* (Gallardo et al., 2008; Mouaikel et al., 2002). Additionally, over-elongated telomeres are present in the *tgs1Δ* mutant in *S. cerevisiae*, leading to a shortened replicative life span (Austriaco and Guarente, 1997; Franke et al., 2008). Also in human, the nuclear localized TGS1-SF is involved in the trimethylation of snoRNAs and thus presumably also *hTR*

(Girard et al., 2008). Lack of TGS1 leads to the mislocalization of *hTR* into nucleoli and the cytoplasm as well as a general increase in the *hTR* level and telomere elongation which is associated with cancer formation (Chen et al., 2020). Thus, controlling the maturation of *TLC1* and *hTR* via 3´-end processing and TMG-capping seems to be a conserved mechanism essential from yeast to human.

5.7. Novel model of *TLC1* maturation and Telomerase assembly in *S. cerevisiae*

Based on the results of this work, we postulate the following model for the maturation pathway of the long non-coding RNA *TLC1* and its assembly into the telomerase RNP (Figure 39). First, *TLC1* is transcribed by RNAP II leading to a 5´ m^7G capped immature pre-*TLC1*. Transcription termination of *TLC1* might be carried out by the NNS complex and by the CPF-CFI complex, presumably resulting either in degradation of the transcript or in the generation of functional *TLC1*, respectively. Loading of Npl3 onto *TLC1* presumably occurs co-transcriptionally, because Npl3 interacts with immature *TLC1*. The export of immature *TLC1* is facilitated via Mex67-Mtr2 and Xpo1 (Gallardo et al., 2008; Wu et al., 2014). Thereby Npl3 may serve as adaptor protein for the export receptor Mex67. The m^7G cap of *TLC1* is, like that of mRNAs bound by the CBC, which protects the RNA from 5´-degradation and provides the docking site for Xpo1, either directly or indirectly or via an unknown adaptor protein. Mex67-Mtr2 is dissociated from the mRNP by the DEAD box RNA helicase Dbp5/Rat8 via ATP-hydrolysis (Folkmann et al., 2011; Kelly and Corbett, 2009; Tieg and Krebber, 2013). Xpo1 is released via Gsp1-GTP hydrolysis at the cytoplasmic site of the NPC (Sloan et al., 2016). The Est and Pop proteins as well as the Sm-ring are loaded in the cytoplasm onto the immature *TLC1* (Gallardo et al., 2008; Garcia et al., 2020; Hirsch et al., 2021; Vasianovich et al., 2020; Wu et al., 2014). Subsequently Cse1 and Mtr10 bind to the Sm-ring (Becker et al., 2019; Hirsch et al., 2021). The re-import of immature *TLC1* is carried out cooperatively via both import factors, Mtr10 and Cse1. While binding of Cse1 stabilizes the Sm-ring on immature *TLC1*, the binding of Mtr10 supports nuclear import (Ferrezuelo et al., 2002; Hirsch et al., 2021). In fact, mutation of *cse1-1* led to a decreased interaction between *TLC1* and Smb1. This resembles a quality control step which assures that only properly covered telomerases are re-imported (Hirsch et al., 2021). After re-import of the RNP into the nucleus, the 3'-end of *TLC1* is trimmed up to the Sm-binding site by the nuclear exosome (Coy et al., 2013; Hass and Zappulla, 2020; Hirsch et

al., 2021). Maturation of *TLC1* is finalized by trimethylation of the 5'-end via Tgs1 in the nucleolus (Hirsch et al., 2021). TMG-capping prevents re-export of *TLC1* because the CBC cannot bind anymore to contact Xpo1 as suggested earlier (Becker et al., 2019; Schwer et al., 2011). Therefore, TMG-capping may resemble another quality control step for nuclear retention of *TLC1* localization in yeast. Likewise, the Yku complex has an essential role in the retention of telomerase in the nucleus (Fisher et al., 2004; Laroche et al., 1998; Peterson et al., 2001). However, it is not known at which point the Yku complex is loaded onto the RNP. The functional telomerase elongates telomeres in late S phase of the cell cycle (Marcand et al., 2000). In which compartment the telomerase is disassembled and degraded has not yet been clarified.

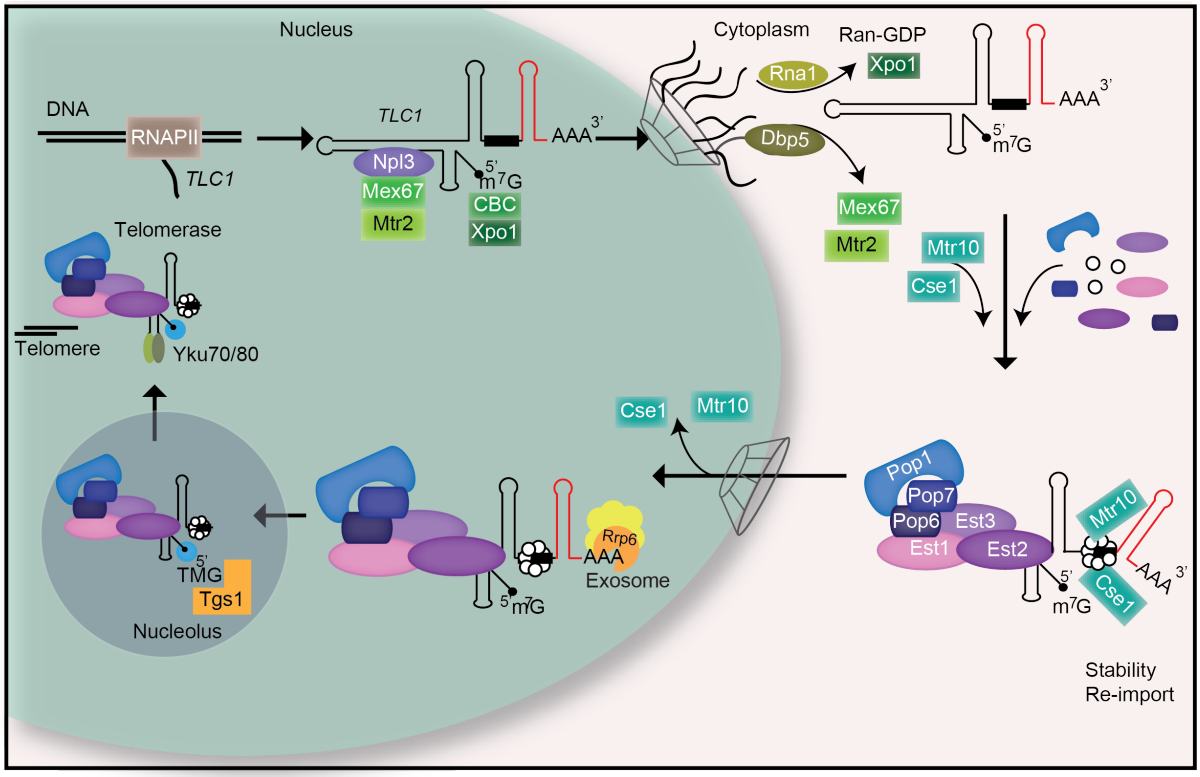

Figure 39: Model for *TLC1* and telomerase maturation in *S. cerevisiae*.
The life cycle of *TLC1* starts with its transcription via RNAP II. Npl3 is loaded co-transcriptionally onto *TLC1* and functions as adaptor protein for Mex67-Mtr2. Besides Mex67, Xpo1 functions in the export of *TLC1*. Xpo1 contacts the CBC which interacts with the m^7G cap of *TLC1*. After export, Mex67-Mtr2 is released from the RNP at the cytoplasmic site of the NPC through DEAD box RNA helicase Dbp5/Rat8 via ATP-hydrolysis. Xpo1 is released via Gsp1-GTP hydrolysis at the cytoplasmic site of the NPC via Rna1. In the cytoplasm, the Pop and Est proteins and the Sm-ring are loaded onto pre-*TLC1*. The resulting RNP is re-imported via Mtr10 and Cse1. The interaction of Mtr10 and Cse1 with *TLC1* occurs via the Sm-ring. Back in the nucleus, the 3´-end of *TLC1* is trimmed by the exosome and the trimethylation of the m^7G cap by Tgs1 finalizes the maturation. At some point in its maturation the Yku70/80 complex is loaded onto *TLC1*. After maturation the telomerase can elongate the telomere ends.

In addition to the role of Cse1 in telomerase maturation it may function in formation of functional capped telomeres, as Rap1 partially mislocalize upon *CSE1* mutation. Surprisingly, altering *CSE1* leads to an additional use of recombination-based Y´ amplification for telomere lengthening, which represents a special phenotype (Figure 40) and (Hirsch et al., 2021).

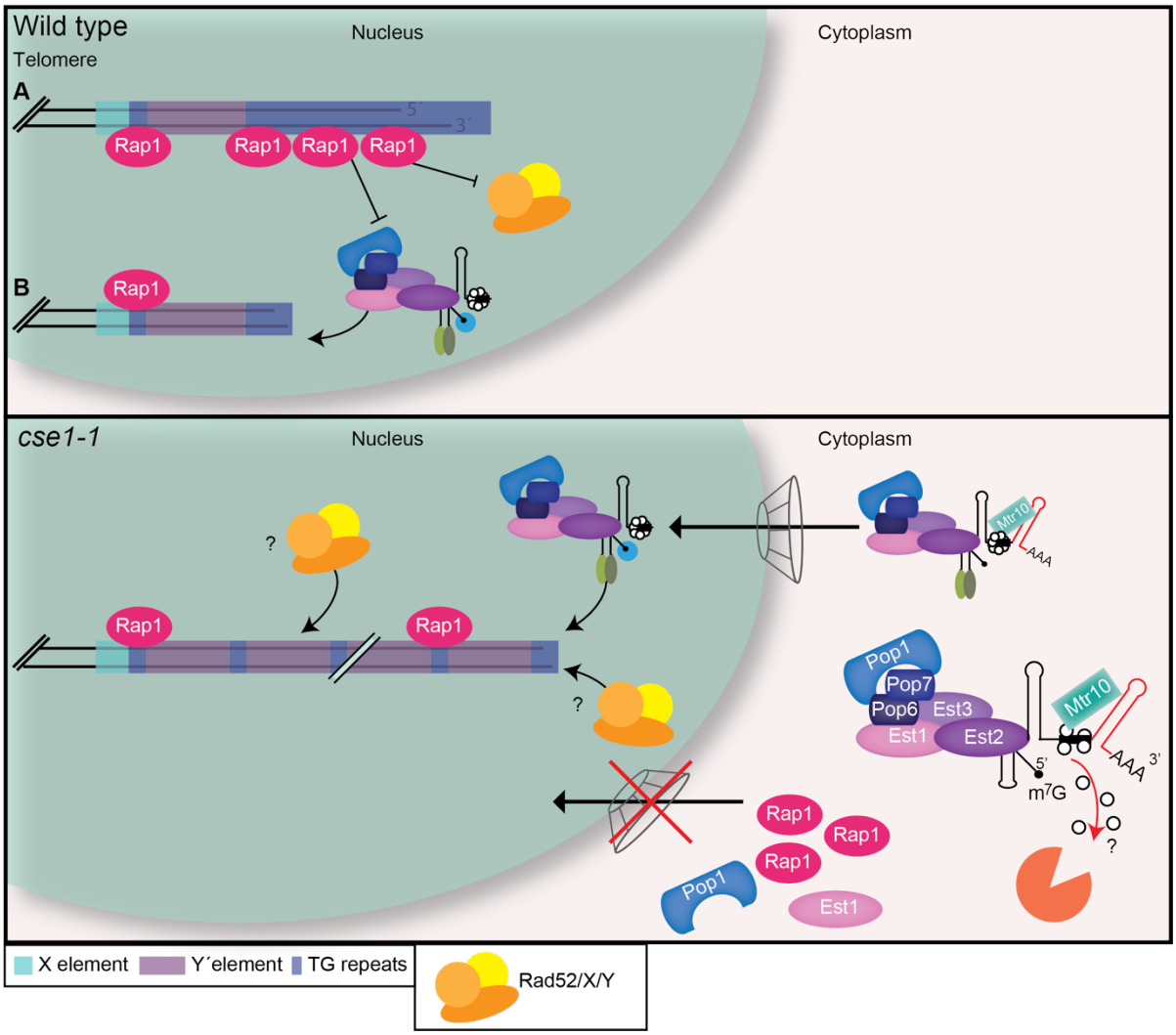

Figure 40: Model for *TLC1* maturation and telomere elongation in *S. cerevisiae* in the *cse1-1* mutant. In wild type cells (upper panel) **(A)** properly long and capped telomeres are usually not elongated via the telomerase, which favors **(B)** short telomeres for elongation. This is achieved via a Rap1 counting mechanism in which additional factors (not shown) participate. A proper cap structure restricts homologous recombination-based telomere elongation. In the *cse1-1* mutant (lower panel), the interaction between *TLC1* and Smb1 is reduced compared to wild type. However, some telomerase molecules seem to enter the nucleus and can elongate short telomere ends. Incubation of *cse1-1* at its restrictive temperature led to a cytoplasmic mislocalization of Rap1. This may uncover TG-repeat regions which could serve as template for strand invasion and homologous recombination, indicated by the complex for homologous recombination. In addition, in the *cse1-1* mutant presumably telomerase unbound Pop1 and Est1 are mislocalized to the cytoplasm.

6. References

Allmang, C., Kufel, J., Chanfreau, G., Mitchell, P., Petfalski, E., and Tollervey, D. (1999). Functions of the exosome in rRNA, snoRNA and snRNA synthesis. EMBO J. *18*, 5399–5410.

Armanios, M., and Blackburn, E.H. (2012). Telomere syndrome. Nat Rev Genet *13*, 693–704.

Armstrong, C.A., and Tomita, K. (2017). Fundamental mechanisms of telomerase action in yeasts and mammals: Understanding telomeres and telomerase in cancer cells. Open Biol. *7*.

Askree, S.H., Yehuda, T., Smolikov, S., Gurevich, R., Hawk, J., Coker, C., Krauskopf, A., Kupiec, M., and Mceachern, M.J. (2004). A genome-wide screen for Saccharomyces cerevisiae deletion mutants that affect telomere length. Proc. Natl. Acad. Sci. U. S. A. *101*, 8658–8663.

Auriche, C., Gino, E., Domenico, D., and Ascenzioni, F. (2008). Budding yeast with human telomeres : A puzzling structure. *90*, 108–115.

Austriaco, N.R., and Guarente, L.P. (1997). Changes of telomere length cause reciprocal changes in the lifespan of mother cells in Saccharomyces cerevisiae. Genetics *94*, 9768–9772.

Baejen, C., Torkler, P., Gressel, S., Essig, K., Söding, J., and Cramer, P. (2014). Transcriptome Maps of mRNP Biogenesis Factors Define Pre-mRNA Recognition. Mol. Cell *55*, 745–757.

Becker, D., Hirsch, A.G.A.G., Bender, L., Lingner, T., Salinas, G., and Krebber, H. (2019). Nuclear Pre-snRNA Export Is an Essential Quality Assurance Mechanism for Functional Spliceosomes. Cell Rep. *27*, 3199–3214.

Birse, C.E., Minvielle-Sebastia, L., Lee, B.A., Keller, W., and Proudfoot, N.J. (1998). Coupling termination of transcription to messenger RNA maturation in yeast. Science (80-.). *280*, 298–301.

Bischoff, R.F., and Görlich, D. (1997). RanBP1 is crucial for the release of RanGTP from importin β-related nuclear transport factors. FEBS Lett. *419*, 249–254.

Bischoff, R.F., and Ponstingl, H. (1991). Catalysis of guanine nucleotide exchange on Ran by the mitotic regulator RCC1. Lett. to Nat. *354*.

Bischoff, R.F., Klebe, C., Kretschmer, J., Wittinghofer, A., and Ponstingl, H. (1994). RanGAP1 induces GTPase activity of nuclear Ras-related Ran. Proc. Natl. Acad. Sci. U. S. A. *91*, 2587–2591.

Bischoff, R.F., Krebber, H., Kempf, T., Hermes, I., and Ponstingl, H. (1995). Human RanGTPase-activating protein RanGAPi is a homologue of yeast Rnalp involved in mRNA processing and transport. Biochemistry *92*, 1749–1753.

Blackburn, E.H. (1992). Telomerases. Ann. Rev. Biochem 113–129.

Blackburn, E.H. (2000). Telomere states and cell fates. Nature *408*, 53–56.

Blackburn, E.H. (2001). Switching and Signaling at the Telomere. Cell *106*, 661–673.

Bordonné, R. (2000). Functional Characterization of Nuclear Localization Signals in Yeast Sm Proteins. Mol. Cell. Biol. *20*, 7943–7954.

Bosoy, D., Peng, Y., Mian, I.S., and Lue, N.F. (2003). Conserved N-terminal motifs of telomerase reverse transcriptase required for ribonucleoprotein assembly in vivo. J. Biol. Chem. *278*, 3882–3890.

Boulton, S.J., and Jackson, S.P. (1996a). Saccharomyces cerevisiae Ku70 potentiates illegitimate DNA double-strand break repair and serves as a barrier to error-prone DNA repair pathways. EMBO J. *15*, 5093–5103.

Boulton, S.J., and Jackson, S.P. (1996b). Identification of a Saccharomyces cerevisiae Ku80 homologue: Roles in DNA double strand break rejoining and in telomeric maintenance. Nucleic Acids Res. *24*, 4639–4648.

Boulton, S.J., and Jackson, S.P. (1998). Components of the Ku-dependent non-homologous end-joining pathway are involved in telomeric length maintenance and telomeric silencing. EMBO J. *17*, 1819–1828.

Bourns, B.D., Alexander, M.K., Smith, A.M., and Zakian, V.A. (1998). Sir Proteins, Rif Proteins, and Cdc13p BindSaccharomyces Telomeres In Vivo. Mol. Cell. Biol. *18*, 5600–5608.

Brune, C., Munchel, S.E., Fischer, N., Podtelejnikov, A. V., and Weis, K. (2005). Yeast poly(A)-binding protein Pab1 shuttles between the nucleus and the cytoplasm and functions in mRNA export. Rna *11*, 517–531.

Bryan, T.M., Englezou, A., Dalla-Pozza, L., Dunham, M.A., and Reddel, R.R. (1997). Evidence for an alternative mechanism for maintaining telomere length in human tumors and tumor-derived cell lines. Nat. Med. *3*, 1271–1274.

Caffarelli, E., Fatica, A., Prislei, S., De Gregorio, E., Fragapane, P., and Bozzoni, I. (1996). Processing of the intron-encoded U16 and U18 snoRNAs: The conserved C and D boxes control both the processing reaction and the stability of the mature snoRNA. EMBO J. *15*, 1121–1131.

Calado, R.T., and Young, N.S. (2009). Telomere Diseases. N. Engl. J. Med. *361*, 2353–2365.

Camasses, A., Bragado-Nilsson, E., Martin, R., Séraphin, B., and Bordonné, R. (1998). Interactions within the Yeast Sm Core Complex: from Proteins to Amino Acids. Mol. Cell. Biol. *18*, 1956–1966.

Chakhparonian, M., and Wellinger, R.J. (2003). Telomere maintenance and DNA replication: How closely are these two connected?

Chamberlain, J.R., Lee, Y., Lane, W.S., and Engelke, D.R. (1998). Purification and characterization of the nuclear RNase P holoenzyme complex reveals extensive subunit overlap with RNase MRP. Genes Dev. *12*, 1678–1690.

Chan, C.S.M., and Tye, B.K. (1983a). Organization of DNA sequences and replication origins at yeast telomeres. Cell *33*, 563–573.

Chan, C.S.M., and Tye, B.K. (1983b). A family of Saccharomyces cerevisiae repetitive autonomously replicating sequences that have very similar genomic environments. J. Mol. Biol. *168*, 505–523.

Chan, A., Boulé, J.B., and Zakian, V.A. (2008). Two pathways recruit telomerase to Saccharomyces cerevisiae telomeres. PLoS Genet. *4*.

Chang, M., Dittmar, J.C., and Rothstein, R. (2011). Long Telomeres are Preferentially Extended During Recombination-Mediated Telomere Maintenance. Nat Struct Mol Biol *18*, 451–456.

Chapon, C., Cech, T.R., and Zaug, A.J. (1997). Polyadenylation of telomerase RNA in budding yeast. RNA *3*, 1337–1351.

Chen, J.-L., and Greider, C.W. (2004). An emerging consensus for telomerase RNA structure. PNAS *101*, 10–13.

Chen, H., Xue, J., Churikov, D., Hass, E.P., Shi, S., Lemon, L.D., Luciano, P., Bertuch, A.A., Zappulla, D.C., Géli, V., et al. (2018). Structural Insights into Yeast Telomerase Recruitment to Telomeres. Cell *172*, 331-343.e13.

Chen, L., Roake, C.M., Galati, A., Bavasso, F., Micheli, E., Saggio, I., Schoeftner, S., Cacchione, S., Gatti, M., Artandi, S.E., et al. (2020). Loss of Human TGS1 Hypermethylase Promotes Increased Telomerase RNA and Telomere Elongation. Cell Rep. *30*, 1358-1372.e5.

Chen, Q., Ijpma, A., and Greider, C.W. (2001). Two Survivor Pathways That Allow Growth in the Absence of Telomerase Are Generated by Distinct Telomere Recombination Events. Mol. Cell. Biol. *21*, 1819–1827.

Chen, X.-F., Meng, F.-L., and Zhou, J.-Q. (2009). Telomere recombination accelerates cellular aging in Saccharomyces cerevisiae. PLoS Genet. *5*.

Chook, Y.M., and Süel, K.E. (2011). Nuclear import by karyopherin-βs: Recognition and inhibition. Biochim. Biophys. Acta - Mol. Cell Res. *1813*, 1593–1606.

Chu, S., Archer, R.H., Zengel, J.M., and Lindahl, L. (1994). The RNA of RNase MRP is required for normal processing of ribosomal RNA. *91*, 659–663.

Churikov, D., Corda, Y., Luciano, P., and Géli, V. (2013). Cdc13 at a crossroads of telomerase action. Front. Oncol. *3*, 1–7.

Churikov, D., Charifi, F., Simon, M.N., and Géli, V. (2014). Rad59-Facilitated Acquisition of Y' Elements by Short Telomeres Delays the Onset of Senescence. PLoS Genet. *10*.

Clarke, P.R., and Zhang, C. (2008). Spatial and temporal coordination of mitosis by Ran GTPase. Nat. Rev. Mol. Cell Biol. *9*, 464–477.

Collins, K., and Mitchell, J.R. (2002). Telomerase in the human organism. Oncogene *21*, 564–579.

Collins, B.M., Cubeddu, L., Naidoo, N., Harrop, S.J., Kornfeld, G.D., Dawes, I.W., Curmi, P.M.G., and Mabbutt, B.C. (2003). Homomeric ring assemblies of eukaryotic Sm proteins have affinity for both RNA and DNA: Crystal structure of an oligomeric complex of yeast SmF. J. Biol. Chem. *278*, 17291–17298.

Connelly, S., and Manley, J.L. (1988). A functional mRNA polyadenylation signal is required for transcription termination by RNA polymerase II. Genes Dev. *2*, 440–452.

Conomos, D., Pickett, H.A., and Reddel, R.R. (2013). Alternative lengthening of telomeres: Remodeling the telomere architecture. Front. Oncol. *3*, 1–7.

Conrad, M.N., Wright, J.H., Wolf, A.J., and Zakian, V.A. (1990). RAP1 protein interacts with yeast telomeres in vivo: Overproduction alters telomere structure and decreases chromosome stability. Cell *63*, 739–750.

Conrad, N.K., Wilson, S.M., Steinmetz, E.J., Patturajan, M., Brow, D.A., Swanson, M.S., and Corden, J.L. (2000). A Yeast Heterogeneous Nuclear Ribonucleoprotein Complex Associated With RNA Polymerase II. Genetics *154*, 557–571.

Conti, E., Uy, M., Leighton, L., Blobel, G., and Kuriyan, J. (1998). Crystallographic analysis of the recognition of a nuclear localization signal by the nuclear import factor karyopherin α. Cell *94*, 193–204.

Cook, A., Fernandez, E., Lindner, D., Ebert, J., Schlenstedt, G., and Conti, E. (2005). The structure of the nuclear export receptor Cse1 in its cytosolic state reveals a closed conformation incompatible with cargo binding. Mol. Cell *18*, 355–367.

Coy, S., Volanakis, A., Shah, S., and Vasiljeva, L. (2013). The Sm Complex Is Required for the Processing of Non-Coding RNAs by the Exosome. PLoS One *8*.

Creamer, T.J., Darby, M.M., Jamonnak, N., Schaughency, P., Hao, H., Wheelan, S.J., and Corden, J.L. (2011). Transcriptome-wide binding sites for components of the Saccharomyces cerevisiae non-poly(A) termination pathway: Nrd1, Nab3, and Sen1. PLoS Genet. *7*.

D'mello, N.P., and Jazwinski, S.M. (1991). Telomere Length Constancy during Aging of Saccharomyces cerevisiae. J. Bacteriol. *173*, 6709–6713.

Dandjinou, A.T., Lévesque, N., Larose, S., Lucier, J.F., Elela, S.A., and Wellinger, R.J. (2004). A phylogenetically based secondary structure for the yeast telomerase RNA. Curr. Biol. *14*, 1148–1158.

Das, B., Guo, Z., Russo, P., Chartrand, P., and Sherman, F. (2000). The Role of Nuclear Cap Binding Protein Cbc1p of Yeast in mRNA Termination and Degradation. Mol. Cell. Biol. *20*, 2827–2838.

Denchi, E.L., and De Lange, T. (2007). Protection of telomeres through independent control of ATM and ATR by TRF2 and POT1. Nature *448*, 1068–1071.

Dewar, J.M., and Lydall, D. (2012). Similarities and differences between "uncapped" telomeres and DNA double-strand breaks. Chromosoma *121*, 117–130.

Diede, S.J., and Gottschling, D.E. (1999). Telomerase-Mediated Telomere Addition in Vivo Requires DNA Primase and DNA Polymerases. Cell *99*, 723–733.

Dijk, E.L. Van, Chen, C.L., d' Aubenton-Carafa, Y., Gourvennec, S., Kwapisz, M., Roche, V., Bertrand, C., Silvain, M., Legoix-Ne, P., Loeillet, S., et al. (2011). XUTs are a class of Xrn1-sensitive antisense regulatory non-coding RNA in yeast. Nature *475*, 114–119.

Dionne, I., and Wellinger, R.J. (1998). Processing of telomeric DNA ends requires the passage of a replication fork. Nucleic Acids Res. *26*.

Dionne, I., Larose, S., Dandjinou, A.T., Elela, S.A., and Wellinger, R.J. (2013). Cell cycle-dependent transcription factors control the expression of yeast telomerase RNA. RNA *19*, 992–1002.

Dorer, D.R., and Henikoff, S. (1997). Transgene repeat arrays interact with distant heterochromatin and cause silencing in cis and trans. Genetics *147*, 1181–1190.

Dower, W.J., Miller, J.F., and Ragsdale, C.W. (1988). High efficiency transformation of E.coli by high voltage electroporation. Nucleic Acids Res. *16*, 6127–6145.

Egan, E.D., and Collins, K. (2012). Biogenesis of telomerase ribonucleoproteins. RNA *18*, 1747–1759.

Epel, E.S., and Lithgow, G.J. (2014). Stress biology and aging mechanisms: Toward understanding the deep connection between adaptation to stress and longevity. Journals Gerontol. - Ser. A Biol. Sci. Med. Sci. *69*, S10–S16.

Esakova, O., and Krasilnikov, A.S. (2010). Of proteins and RNA: The RNase P/MRP family. Rna *16*, 1725–1747.

Evans, S.K., and Lundblad, V. (1999). Est1 and Cdc13 as Comediatoas of Telomerase Access. Science (80-.). *286*, 117–120.

Fell, V.L., and Schild-Poulter, C. (2015). The Ku heterodimer: Function in DNA repair and beyond. Mutat. Res. - Rev. Mutat. Res. *763*, 15–29.

Ferrezuelo, F., Steiner, B., Aldea, M., and Futcher, B. (2002). Biogenesis of Yeast Telomerase Depends on the Importin Mtr10. Mol. Cell. Biol. *22*, 6046–6055.

Fisher, T.S., Taggart, A.K.P., and Zakian, V.A. (2004). Cell cycle-dependent regulation of yeast telomerase by Ku. Nat. Struct. Mol. Biol. *11*, 1198–1205.

Folkmann, A.W., Noble, K.N., Cole, C.N., and Wente, S.R. (2011). Dbp5, Gle1-IP6 and Nup159: A working model for mRNP export. Nucleus *2*, 540–548.

Fornerod, M., Ohno, M., Yoshida, M., and Mattaj, I.W. (1997). CRM1 is an export receptor for leucine-rich nuclear export signals. Cell *90*, 1051–1060.

Frank, C.J., Hyde, M., and Greider, C.W. (2006). Regulation of Telomere Elongation by the Cyclin-Dependent Kinase CDK1. Mol. Cell *24*, 423–432.

Franke, J., Gehlen, J., and Ehrenhofer-Murray, A.E. (2008). Hypermethylation of yeast Telomerase RNA by the snRNA and snoRNA methyltransferase Tgs1. J. Cell Sci. *121*, 3553–3560.

Gallardo, F., Olivier, C., Dandjinou, A.T., Wellinger, R.J., and Chartrand, P. (2008). TLC1 RNA nucleo-cytoplasmic trafficking links telomerase biogenesis to its recruitment to telomeres. EMBO J. *27*, 748–757.

Gallardo, F., Laterreur, N., Cusanelli, E., Ouenzar, F., Querido, E., Wellinger, R.J., and Chartrand, P. (2011). Live cell imaging of telomerase RNA dynamics reveals cell cycle-dependent clustering of telomerase at elongating telomeres. Mol. Cell *44*, 819–827.

Garcia, P.D., and Zakian, V.A. (2020). A new role for proteins subunits of RNase P : stabilization of the telomerase holoenzyme. *7*, 250–254.

Garcia, P.D., Leach, R.W., Wadsworth, G.M., Choudhary, K., Li, H., Aviran, S., Kim, H.D., and Zakian, V.A. (2020). Stability and nuclear localization of yeast telomerase depend on protein components of RNase P/MRP. Nat. Commun. *11*, 1–19.

Garfin, D.E. (2009). One-Dimensional Gel Electrophoresis. Methods Enzymol. *182*, 497–513.

Gatbonton, T., Imbesi, M., Nelson, M., Akey, J.M., Ruderfer, D.M., Kruglyak, L., Simon, J.A., and Bedalov, A. (2006). Telomere length as a quantitative trait: Genome-wide survey and genetic mapping of telomere length-control genes in yeast. PLoS Genet. *2*, 0304–0315.

Ge, Y., Wu, Z., Chen, H., Zhong, Q., Shi, S., Li, G., Wu, J., and Lei, M. (2020). Structural insights into telomere protection and homeostasis regulation by yeast CST complex. Nat. Struct. Mol. Biol.

Ghazal, G., Gagnon, J., Jacques, P.É., Landry, J.R., Robert, F., and Abou Elela, S. (2009). Yeast RNase III Triggers Polyadenylation-Independent Transcription Termination. Mol. Cell *36*, 99–109.

Gibson, D.G., Young, L., Chuang, R.Y., Venter, J.C., Hutchison, C.A., and Smith, H.O. (2009). Enzymatic assembly of DNA molecules up to several hundred kilobases. Nat. Methods *6*, 343–345.

Gietz, D., Jean, A.S., Woods, R.A., and Schiestl, R.H. (1992). Improved method for high efficiency transformation of intact yeast cells. Nucleic Acids Res. *20*, 1425.

Gilbert, W., Guthrie, C., and Francisco, S. (2004). The Glc7p Nuclear Phosphatase Promotes mRNA Export by Facilitating Association of Mex67p with mRNA University of California at San Francisco. Mol. Cell *13*, 201–212.

Gill, T., Aulds, J., and Schmitt, M.E. (2006). A specialized processing body that is temporally and asymmetrically regulated during the cell cycle in Saccharomyces cerevisiae. J. Cell Biol. *173*, 35–45.

Gilson, E., and Géli, V. (2007). How telomeres are replicated. Nat. Rev. Mol. Cell Biol. *8*, 825–838.

Gilson, E., Roberge, M., Giraldo, R., Rhodes, D., and Gasser, S.M. (1993). Distortion of the DNA double helix by RAP1 at silencers and multiple telomeric binding sites. J. Mol. Biol. *231*, 293–310.

Girard, C., Verheggen, C., Neel, H., Cammas, A., Vagner, S., Soret, J., Bertrand, E., and Bordonné, R. (2008). Characterization of a short isoform of human Tgs1 hypermethylase associating with small nucleolar ribonucleoprotein core proteins and produced by limited proteolytic processing. J. Biol. Chem. *283*, 2060–2069.

Görlich, D., Henklein, P., Laskey, R.A., and Hartmann, E. (1996). A 41 amino acid motif in importin-α confers binding to importin-β and hence transit into the nucleus. EMBO J. *15*, 1810–1817.

Görlich, D., Seewald, M.J., and Ribbeck, K. (2003). Characterization of Ran-driven cargo transport and the RanGTPase system by kinetic measurements and computer simulation. EMBO J. *22*, 1088–1100.

Gotta, M., Laroche, T., Formenton, A., Maillet, L., Scherthan, H., and Gasser, S.M. (1996). The Clustering of Telomeres and Colocalization with Rapl, Sir3, and Sir4 Proteins in Wild-Type Saccharomyces cerevisiae. J. Biol. Chem. *134*, 1349–1363.

Gotta, M., Strahl-Bolsinger, S., Renauld, H., Laroche, T., Kennedy, B.K., Grunstein, M., and Gasser, S.M. (1997). Localization of Sir2p: The nucleolus as a compartment for silent information regulators. EMBO J. *16*, 3243–3255.

Grandin, N., and Charbonneau, M. (2007). Control of the yeast telomeric senescence survival pathways of recombination by the Mec1 and Mec3 DNA damage sensors and RPA. Nucleic Acids Res. *35*, 822–838.

Grandin, N., Reed, S.I., and Charbonneau, M. (1997). Stn1, a new Saccharomyces cerevisiae protein, is implicated in telomere size regulation in association with CDc13. Genes Dev. *11*, 512–527.

Grandin, N., Damon, C., and Charbonneau, M. (2001a). Cdc13 prevents telomere uncapping and Rad50-dependent homologous recombination. EMBO J. *20*, 6127–6139.

Grandin, N., Damon, C., and Charbonneau, M. (2001b). Ten1 functions in telomere end protection and

length regulation in association with Stn1 and Cdc13. EMBO J. *20*, 1173–1183.

Gravel, S., Larrivee, M., Labrecque, P., and Wellinger, R.J. (1998). Yeast Ku as Regulator of Chromosomal DNA End Structure. *280*, 741–744.

Greider, C.W., and Blackburn, E.H. (1985). Identification of a specific telomere terminal transferase activity in tetrahymena extracts. Cell *43*, 405–413.

Greider, C.W., and Blackburn, E.H. (1989). A telomeric sequence in the RNA of Tetrahymena telomerase required for telomere repeat synthesis. Nature *337*, 331–337.

Grzechnik, P., and Kufel, J. (2008). Polyadenylation Linked to Transcription Termination Directs the Processing of snoRNA Precursors in Yeast. Mol. Cell *32*, 247–258.

Grzechnik, P., Szczepaniak, S.A., Dhir, S., Pastucha, A., Parslow, H., Matuszek, Z., Mischo, H.E., Kufel, J., and Proudfoot, N.J. (2018). Nuclear fate of yeast snoRNA is determined by co-transcriptional Rnt1 cleavage. Nat. Commun. *9*.

Gudipati, R.K., Xu, Z., Lebreton, A., Séraphin, B., Steinmetz, L.M., Jacquier, A., and Libri, D. (2012). Extensive Degradation of RNA Precursors by the Exosome in Wild-Type Cells. Mol. Cell *48*, 409–421.

Güttler, T., and Görlich, D. (2011). Ran-dependent nuclear export mediators: A structural perspective. EMBO J. *30*, 3457–3474.

Hackmann, A., Gross, T., Baierlein, C., and Krebber, H. (2011). The mRNA export factor Npl3 mediates the nuclear export of large ribosomal subunits. EMBO Rep. *12*, 1024–1031.

Hackmann, A., Wu, H., Schneider, U.M., Meyer, K., Jung, K., and Krebber, H. (2014). Quality control of spliced mRNAs requires the shuttling SR proteins Gbp2 and Hrb1. Nat. Commun. *5*, 1–14.

Hamm, J., and Mattaj, I.W. (1990). Monomethylated cap structures facilitate RNA export from the nucleus. Cell *63*, 109–118.

Hammell, C.M., Gross, S., Zenklusen, D., Heath, C. V, Stutz, F., Moore, C., and Cole, C.N. (2002). Coupling of Termination , 3 Processing , and mRNA Export. *22*, 6441–6457.

Han, Z., Jasnovidova, O., Haidara, N., Tudek, A., Kubicek, K., Libri, D., Stefl, R., and Porrua, O. (2020). Termination of non-coding transcription in yeast relies on both an RNA Pol II CTD interaction domain and a CTD-mimicking region in Sen1. EMBO J. *39*, 1–22.

Harley B., C., Futcher B., A., and Greider W., C. (1990). Telomeres shorten during ageing of human fibroblasts. Nature *345*, 458–460.

Hass, E.P., and Zappulla, D.C. (2020). Repositioning the sm-binding site in saccharomyces cerevisiae telomerase rna reveals RNP organizational flexibility and sm-directed 3'-End formation. Non-Coding RNA *6*, 1–15.

Hawkins, C., and Friedman, K.L. (2014). Normal telomere length maintenance in Saccharomyces cerevisiae requires nuclear import of the ever shorter telomeres 1 (Est1) protein via the importin alpha pathway. Eukaryot. Cell *13*, 1036–1050.

Hayflick, L. (1965). The limited in vitro lifetime of human diploid cell strains. Exp. Cell Res. *37*, 614–636.

Hazelbaker, D.Z., Marquardt, S., Wlotzka, W., and Buratowski, S. (2013). Article Kinetic Competition between RNA Polymerase II and Sen1-Dependent Transcription Termination. Mol. Cell *49*, 55–66.

Hermann, H., Fabrizio, P., Raker, V.A., Foulaki, K., Hornig, H., Brahms, H., and Luhrmann, R. (1995). snRNP Sm proteins share two evolutionarily conserved sequence motifs which are involved in Sm protein-protein interactions. EMBO J. *14*, 2076–2088.

Hirsch, A.G., Becker, D., Lamping, J.-P., and Krebber, H. (2021). Unraveling the stepwise maturation of the yeast telomerase. BioRxiv. Https://Doi.Org/10.1101/2021.04.30.442090.

Hiyama, E., and Hiyama, K. (2007). Telomere and telomerase in stem cells. Br. J. Cancer *96*, 1020–1024.

Hood, J.K., and Silver, P.A. (1998). Cse1p is required for export of Srp1p/importin-α from the nucleus in Saccharomyces cerevisiae. J. Biol. Chem. *273*, 35142–35146.

Hopper, A.K., and Nostramo, R.T. (2019). TRNA processing and subcellular trafficking proteins multitask in pathways for other RNAs. Front. Genet. *10*.

Hopper, A.K., Traglia, H.M., and Dunst, R.W. (1990). The yeast RNA1 gene product necessary for RNA processing is located in the cytosol and apparently excluded from the nucleus. J. Cell Biol. *111*, 309–321.

Horowitz, H., Thorburn, P., and Haber, J.E. (1984). Rearrangements of highly polymorphic regions near telomeres of Saccharomyces cerevisiae. Mol. Cell. Biol. *4*, 2509–2517.

Hu, Y., Tang, H.B., Liu, N.N., Tong, X.J., Dang, W., Duan, Y.M., Fu, X.H., Zhang, Y., Peng, J., Meng, F.L., et al. (2013). Telomerase-Null Survivor Screening Identifies Novel Telomere Recombination Regulators. PLoS Genet. *9*.

Hughes, T.R., Evans, S.K., Weilbaecher, R.G., and Lundblad, V. (2000). The Est3 protein is a subunit of yeast telomerase. Curr. Biol. *10*, 809–812.

Huh, W., Falvo, J. V, Gerke, L.C., Carroll, A.S., Howson, R.W., Weissman, J.S., and Shea, E.K.O. (2003). Gobal analysis of protein localization in budding yeast. Nat. Publ. Gr. *425*, 686–691.

Hurt, E., Luo, M.J., Röther, S., Reed, R., and Sträßer, K. (2004). Cotranscriptional recruitment of the serine-arginine-rich (SR)-like proteins Gbp2 and Hrb1 to nascent mRNA via the TREX complex. Proc. Natl. Acad. Sci. U. S. A. *101*, 1858–1862.

Ijpma, A.S., and Greider, C.W. (2003). Short Telomeres Induce a DNA Damage Response in Saccharomyces cerevisiae. Mol. Biol. Cell *14*, 987–1001.

Inoue, H., Nojima, H., and Okayama, H. (1990). High efficiency transformation of Escherichia coli with plasmids. Gene *96*, 23–28.

Izaurralde, E., Lewis, J., Gamberi, C., Jarmolowski, A., McGuigan, C., and Mattaj, I.W. (1995). A cap-binding protein complex mediating U snRNA export. Nature *376*, 709–712.

Jamonnak, N., Creamer, T.J., Darby, M.M., Schaughency, P., Wheelan, S.J., and Corden, J.L. (2011). Yeast Nrd1, Nab3, and Sen1 transcriptome-wide binding maps suggest multiple roles in post-transcriptional RNA processing. Spring 2011–2025.

Jensen, T.H., Jacquier, A., and Libri, D. (2013). Dealing with pervasive transcription. Mol. Cell *52*, 473–484.

Katahira, J., Sträßer, K., Podtelejnikov, A., Mann, M., Jung, J.U., and Hurt, E. (1999). The Mex67p-mediated nuclear mRNA export pathway is conserved from yeast to human. EMBO J. *18*, 2593–2609.

Kehlenbach, R.H., Dickmanns, A., Kehlenbach, A., Guan, T., and Gerace, L. (1999). A Role for RanBP1 in the Release of CRM1 from the Nuclear Pore Complex in a Terminal Step of Nuclear Export. J. Cell Biol. *145*, 645–657.

Kelly, S.M., and Corbett, A.H. (2009). Messenger RNA export from the nucleus: A series of molecular wardrobe changes. Traffic *10*, 1199–1208.

Klein, F., Laroche, T., Cardenas, M.E., Hofmann, J.F.X., Schweizer, D., and Gasser, S.M. (1992). Localization of RAP1 and topoisomerase II in nuclei and meiotic chromosomes of yeast. J. Cell Biol. *117*, 935–948.

Kockler, Z.W., Comeron, J.M., and Malkova, A. (2021). A unified alternative telomere-lengthening pathway in yeast survivor cells. Mol. Cell *81*.

Köhler, A., and Hurt, E. (2007). Exporting RNA from the nucleus to the cytoplasm. Nat. Rev. Mol. Cell Biol. *8*, 761–773.

Krauskopf, A., and Blackburn, E.H. (1996). Control of telomere growth by interactions of RAP1 with the most distal telomeric repeats. Nature 354–357.

Kupiec, M. (2014). Biology of telomeres: Lessons from budding yeast. FEMS Microbiol. Rev. *38*, 144–171.

Kutay, U., Ralf Bischoff, F., Kostka, S., Kraft, R., and Görlich, D. (1997). Export of importin α from the nucleus is mediated by a specific nuclear transport factor. Cell *90*, 1061–1071.

Kyrion, G., Liu, K., and Lustig, A.J. (1993). RAP1 and telomere structure regulate telomere position effects in Saccharomyces cerevisiae. Genes Dev. *7*, 1146–1159.

LaCava, J., Houseley, J., Saveanu, C., Petfalski, E., Thompson, E., Jacquier, A., and Tollervey, D. (2005). RNA degradation by the exosome is promoted by a nuclear polyadenylation complex. Cell *121*, 713–724.

Lai, M.C., Lin, R.I., Huang, S.Y., Tsai, C.W., and Tarn, W.Y. (2000). A human importin-β family protein, transportin-SR2, interacts with the phosphorylated RS domain of SR proteins. J. Biol. Chem. *275*, 7950–7957.

Lai, M.C., Lin, R.I., and Tarn, W.Y. (2001). Transportin-SR2 mediates nuclear import of phosphorylated SR proteins. Proc. Natl. Acad. Sci. U. S. A. *98*, 10154–10159.

de Lange, T., Shiue, L., Myers, R.M., Cox, D.R., Naylor, S.L., Killery, A.M., and Varmus, H.E. (1990). Structure and variability of human chromosome ends. Mol. Cell. Biol. *10*, 518–527.

Laroche, T., Martin, S.G., Gotta, M., Gorham, H.C., Pryde, F.E., Louis, E.J., and Gasser, S.M. (1998). Mutation of yeast Ku genes disrupts the subnuclear organization of telomeres. Curr. Biol. *8*, 653–657.

Larochelle, M., Robert, M.A., Hébert, J.N., Liu, X., Matteau, D., Rodrigue, S., Tian, B., Jacques, P.É., and Bachand, F. (2018). Common mechanism of transcription termination at coding and noncoding RNA genes in fission yeast. Nat. Commun. *9*.

Laterreur, N., Eschbach, S.H., Lafontaine, D.A., and Wellinger, R.J. (2013). A new telomerase RNA element that is critical for telomere elongation. Nucleic Acids Res. *41*, 7713–7724.

Laterreur, N., Lemieux, B., Neumann, H., Berger-Dancause, J.-C., Lafontaine, D., and Wellinger, R.J. (2018). The yeast telomerase module for telomere recruitment requires a specific RNA architecture. RNA *24*, 1067–1079.

Le, S., Moore, J.K., Haber, J.E., and Greider, C.W. (1999). RAD50 and RAD51 Define Two Pathways That Collaborate to Maintain Telomeres in the Absence of Telomerase. Genetics *152*, 143–152.

Lee-Soety, J.Y., Jones, J., MacGibeny, M.A., Remaly, E.C., Daniels, L., Ito, A., Jean, J., Radecki, H., and Spencer, S. (2012). Yeast hnRNP-related proteins contribute to the maintenance of telomeres. Biochem. Biophys. Res. Commun. *426*, 12–17.

Lee, B.J., Cansizoglu, A.E., Süel, K.E., Louis, T.H., Zhang, Z., and Chook, Y.M. (2006). Rules for Nuclear Localization Sequence Recognition by Karyopherinβ2. Cell *126*, 543–558.

Lei, E.P., Krebber, H., and Silver, P.A. (2001). Messenger RNAs are recruited for nuclear export during transcription. Genes Dev. *15*, 1771–1782.

Lemieux, B., Laterreur, N., Perederina, A., Noël, J.F., Dubois, M.L., Krasilnikov, A.S., and Wellinger, R.J. (2016). Active Yeast Telomerase Shares Subunits with Ribonucleoproteins RNase P and RNase MRP. Cell *165*, 1171–1181.

Lendvay, T.S., Morris, D.K., Sah, J., Balasubramanian, B., and Lundblad, V. (1996). Senescence mutants of Saccharomyces cerevisiae with a defect in telomere replication identify three additional EST genes. Genetics *144*, 1399–1412.

Levy, D.L., and Blackburn, E.H. (2004). Counting of Rif1p and Rif2p on Saccharomyces cerevisiae Telomeres Regulates Telomere Length. Mol. Cell. Biol. *24*, 10857–10867.

Levy, M.Z., Allsopp, R.C., Futcher, A.B., Greider, C.W., and Harley, C.B. (1992). Telomere end-replication problem and cell aging. J. Mol. Biol. *225*, 951–960.

Lewis, J.D., and Izaurralde, E. (1997). The role of the cap structure in RNA processing and nuclear export. Eur. J. Biochem. *247*, 461–469.

Li, J., Leung, A.K., Kondo, Y., Oubridge, C., and Nagai, K. (2016). Re-refinement of the spliceosomal U4 snRNP core-domain structure. Acta Crystallogr. Sect. D Struct. Biol. *72*, 131–146.

Li, S., Makovets, S., Matsuguchi, T., Blethrow, J.D., Shokat, K.M., and Blackburn, E.H. (2009). Cdk1-Dependent Phosphorylation of Cdc13 Coordinates Telomere Elongation during Cell-Cycle Progression. Cell *136*, 50–61.

Li, Z., Vizeacoumar, F.J., Bahr, S., Li, J., Warringer, J., Vizeacoumar, F.S., Min, R., Vandersluis, B., Bellay, J., Devit, M., et al. (2011). Systematic exploration of essential yeast gene function with temperature-sensitive mutants. Nat. Biotechnol. *29*.

Lim, C.J., and Cech, T.R. (2021). Shaping human telomeres: from shelterin and CST complexes to telomeric chromatin organization. Nat. Rev. Mol. Cell Biol. *22*, 283–298.

Lin, J.J., and Zakian, V.A. (1996). The Saccharomyces CDC13 protein is a single-strand TG1-3 telomeric DNA-binding protein in vitro that affects telomere behavior in vivo. Proc. Natl. Acad. Sci. U. S. A. *93*, 13760–13765.

Lin, J., Hussain, A., Abraham, M., Pearl, S., Tzfati, Y., Parslow, T.G., and Blackburn, E.H. (2004). Structure Includes Structured Motifs Required for Binding the. Proc. Natl. Acad. Sci. *101*, 14713–14718.

Lin, K.W., McDonald, K.R., Guise, A.J., Chan, A., Cristea, I.M., and Zakian, V.A. (2015). Proteomics of yeast telomerase identified Cdc48-Npl4-Ufd1 and Ufd4 as regulators of Est1 and telomere length. Nat. Commun. *6*.

Lindsey, J., McGill, N.I., Lindsey, L.A., Green, D.K., and Cooke, H.J. (1991). In vivo loss of telomeric repeats with age in humans. Mutat. Res. DNAging *256*, 45–48.

Lingner, J., Cooper, J.P., and Cech, T.R. (1995). Telomerase and DNA End Replication: No Longer a Lagging Strand Problem? Science (80-.). *269*, 1533–1534.

Lingner, J., Cech, T.R., Hughes, T.R., and Lundblad, V. (1997a). Three ever shorter telomere (EST) genes are dispensable for in vitro yeast telomerase activity. Proc. Natl. Acad. Sci. U. S. A. *94*, 11190–11195.

Lingner, J., Hughes, T.R., Shevchenko, A., Mann, M., Lundblad, V., and Cech, T.R. (1997b). Reverse Transcriptase Motifs in the Catalytic Subunit of Telomerase. Science (80-.). *276*, 561–567.

Liu, C.-C., Gopalakrishnan, V., Poon, L.-F., Yan, T., and Li, S. (2014). Cdk1 Regulates the Temporal Recruitment of Telomerase and Cdc13-Stn1-Ten1 Complex for Telomere Replication. Mol. Cell. Biol. *34*, 57–70.

Liu, Y., Guo, W., Tartakoff, P.Y., and Tartakoff, A.M. (1999). A Crm1p-independent nuclear export path for the mRNA-associated protein, Npl3p/Mtr13p. Proc. Natl. Acad. Sci. U. S. A. *96*, 6739–6744.

Livak, K.J., and Schmittgen, T.D. (2001). Analysis of Relative Gene Expression Data Using Real- Time Quantitative PCR and the 2 2???CT Method. Methods *25*, 402–408.

Livengood, A.J., Zaug, A.J., and Cech, T.R. (2002). Essential Regions of Saccharomyces cerevisiae Telomerase RNA: Separate Elements for Est1p and Est2p Interaction. Mol. Cell. Biol. *22*, 2366–2374.

Loeb, J.D.J., Schlenstedt, G., Pellman, D., Kornitzer, D., Silver, P.A., and Fink, G.R. (1995). The yeast nuclear import receptor is required for mitosis. Proc. Natl. Acad. Sci. U. S. A. *92*, 7647–7651.

Lott, K., and Cingolani, G. (2011). The importin β binding domain as a master regulator of nucleocytoplasmic transport. BBA - Mol. Cell Res. *1813*, 1578–1592.

Lowell, J.E., and Pillus, L. (1998). Telomere tales: Chromatin, telomerase and telomere function in Saccharomyces cerevisiae. Cell. Mol. Life Sci. *54*, 32–49.

Lubin, J.W., Tucey, T.M., and Lundblad, V. (2012). The interaction between the yeast telomerase RNA and the Est1 protein requires three structural elements. Rna *18*, 1597–1604.

Lundblad, V., and Blackburn, E.H. (1993). An Alternative Pathway for Yeast Telomere Maintenance Rescues estl-Senescence. Cell *73*, 347–360.

Lundblad, V., and Szostak, J.W. (1989). A mutant with a defect in telomere elongation leads to senescence in yeast. Cell *57*, 633–643.

Lydall, D. (2003). Hiding at the ends of yeast chromosomes: Telomeres, nucleases and checkpoint pathways. J. Cell Sci. *116*, 4057–4065.

Lygerou, Z., Mitchell, P., Petfalski, E., Séraphin, B., and Tollervey, D. (1994). The POP1 gene encodes a protein component common to the RNase MRP and RNase P ribonucleoproteins. Genes Dev. *8*, 1423–1433.

Macara, I.G. (2001). Transport into and out of the Nucleus. Microbiol. Mol. Biol. Rev. *65*, 570–594.

Maciejowski, J., and De Lange, T. (2017). Telomeres in cancer: tumor suppression and genome instability. Nat Rev Mol Cell Biol *18*, 175–186.

Makovets, S., Williams, T.L., and Blackburn, E.H. (2008). The telotype defines the telomere state in Saccharomyces cerevisiae and is inherited as a dominant non-Mendelian characteristic in cells lacking telomerase. Genetics *178*, 245–257.

Marcand, S., Gilson, E., and Shore, D. (1997). A protein-counting mechanism for telomere length regulation in yeast. Science (80-.). *275*, 986–990.

Marcand, S., Brevet, V., Mann, C., and Gilson, E. (2000). Cell cycle restriction of telomere elongation. Curr. Biol. 487–490.

Matera, A.G., and Wang, Z. (2014). A day in the life of the spliceosome. Nat. Rev. Mol. Cell Biol. *15*.

McEachern, M.J., and Iyer, S. (2001). Short telomeres in yeast are highly recombinogenic. Mol. Cell *7*, 695–704.

McNally, E.J., Luncsford, P.J., and Armanios, M. (2019). Long telomeres and cancer risk: The price of cellular immortality. J. Clin. Invest. *129*, 3474–3481.

Mekhail, K., and Moazed, D. (2010). The nuclear envelope in genome organization, expression and stability. Nat. Rev. Mol. Cell Biol. *11*, 317–328.

Meyerson, M., Counter, C.M., Ng Eaton, E., Ellisen, L.W., Steiner, P., Dickinson Caddle, S., Ziaugra, L., and Beijersbergen, R.L. (1997). hEST2, the Putative Human Telomerase Catalytic Subunit Gene, Is Up-Regulated in Tumor Cells and during Immortalization. Cell *90*, 785–795.

Meyne, J., Ratliff, R.L., and Moyzis, R.K. (1989). Conservation of the human telomere sequence (TTAGGG)n among vertebrates. Proc. Natl. Acad. Sci. U. S. A. *86*, 7049–7053.

Mischo, H.E., Chun, Y., Harlen, K.M., Smalec, B.M., Dhir, S., Churchman, L.S., and Buratowski, S. (2018). Cell-Cycle Modulation of Transcription Termination Factor Sen1. Mol. Cell *70*, 312–326.

Mishra, K., and Shore, D. (1999). Yeast Ku protein plays a direct role in telomeric silencing and counteracts inhibition by Rif proteins. Curr. Biol. *9*, 1123–1126.

Mitchell, J.R., Cheng, J., and Collins, K. (1999). A box H/ACA small nucleolar RNA-like domain at the human telomerase RNA 3' end. Mol. Cell. Biol. *19*, 567–576.

Moehle, E.A., Ryan, C.J., Krogan, N.J., Kress, T.L., and Guthrie, C. (2012). The Yeast SR-Like Protein Npl3 Links Chromatin Modification to mRNA Processing. PLoS Genet. *8*.

Moore, M.S., and Blobel, G. (1994). A G protein involved in nucleocytoplasmic transport: the role of Ran. Trends Biochem. Sci. *19*, 211–216.

Mouaikel, J., Verheggen, C., Bertrand, E., Tazi, J., and Bordonné, R. (2002). Hypermethylation of the cap structure of both yeast snRNAs and snoRNAs requires a conserved methyltransferase that is localized to the nucleolus. Mol. Cell *9*, 891–901.

Mozdy, A.D., and Cech, T.R. (2006). Low abundance of telomerase in yeast: Implications for telomerase haploinsufficiency. RNA *12*, 1721–1737.

Nabetani, A., and Ishikawa, F. (2011). Alternative lengthening of telomeres pathway: Recombination-mediated telomere maintenance mechanism in human cells. J. Biochem. *149*, 5–14.

Nagpal, N., and Agarwal, S. (2020). Telomerase RNA processing: Implications for human health and disease. Stem Cells *38*, 1532–1543.

Neil, H., Malabat, C., D'Aubenton-Carafa, Y., Xu, Z., Steinmetz, L.M., and Jacquier, A. (2009). Widespread bidirectional promoters are the major source of cryptic transcripts in yeast. Nature *457*, 1038–1042.

Niederer, R.O., and Zappulla, D.C. (2015). Refined secondary-structure models of the core of yeast and human telomerase RNAs directed by SHAPE. Rna *21*, 254–261.

Noël, J.F., Larose, S., Elela, S.A., and Wellinger, R.J. (2012). Budding yeast telomerase RNA transcription termination is dictated by the Nrd1/Nab3 non-coding RNA termination pathway. Nucleic Acids Res. *40*, 5625–5636.

Nugent, C.I., Hughes, T.R., Lue, N.F., and Lundblad, V. (1996). Cdc13p: A single-strand telomeric DNA-binding protein with a dual role in yeast telomere maintenance. Science (80-.). *274*, 249–252.

Nugent, C.I., Bosco, G., Ross, L.O., Evans, S.K., Salinger, A.P., Moore, J.K., Haber, J.E., and Lundblad, V. (1998). Telomere maintenance is dependent on activities required for end repair of double-strand breaks. Curr. Biol. *8*, 657–662.

Ohno, M., Segref, A., Bachi, A., Wilm, M., and Mattaj, I.W. (2000). PHAX, a mediator of U snRNA nuclear export whose activity is regulated by phosphorylation. Cell *101*, 187–198.

Okamura, M., Inose, H., and Masuda, S. (2015). RNA export through the NPC in eukaryotes. Genes (Basel). *6*, 124–149.

Olovnikov, A.M. (1973). A theory of marginotomy. The incomplete copying of template margin in enzymic synthesis of polynucleotides and biological significance of the phenomenon. J. Theor. Biol. *41*, 181–190.

Osterhage, J.L., Talley, J.M., and Friedman, K.L. (2006). Proteasome-dependent degradation of Est1p regulates the cell cycle-restricted assembly of telomerase in Saccharomyces cerevisiae. Nat. Struct. Mol. Biol. *13*, 720–728.

Ouenzar, F., Lalonde, M., Laprade, H., Morin, G., Gallardo, F., Tremblay-Belzile, S., and Chartrand, P. (2017). Cell cycle-dependent spatial segregation of telomerase from sites of DNA damage. J. Cell Biol. *216*, 2355–2371.

Palm, W., and De Lange, T. (2008). How shelterin protects mammalian telomeres. Annu. Rev. Genet. *42*, 301–334.

Pemberton, L.F., Rosenblum, J.S., and Blobel, G. (1997). A Distinct and Parallel Pathway for the Nuclear Import of an mRNA-binding Protein. J. Cell Biol. *139*, 1645–1653.

Pennock, E., Buckley, K., and Lundblad, V. (2001). Cdc13 delivers separate complexes to the telomere for end protection and replication. Cell *104*, 387–396.

Perrem, K., Colgin, L.M., Neumann, A.A., Yeager, T.R., and Reddel, R.R. (2001). Coexistence of Alternative Lengthening of Telomeres and Telomerase in hTERT-Transfected GM847 Cells. Mol. Cell. Biol. *21*, 3862–3875.

Peterson, S.E., Stellwagen, A.E., Diede, S.J., Singer, M.S., Haimberger, Z.W., Johnson, C.O., Tzoneva, M., and Gottschling, D.E. (2001). The function of a stem-loop in telomerase RNA is linked to the DNA repair protein Ku. Nat. Genet. *27*, 64–67.

Pettersson, I., Hinterberger, M., Mimori, T., Gottlieb, E., and Steitz, J.A. (1984). The structure of mammalian small nuclear ribonucleoproteins. Identification of multiple protein components reactive with anti(U1)ribonucleoprotein and anti-Sm autoantibodies. J. Biol. Chem. *259*, 5907–5914.

Plessel, G., Fischer, U., and Lührmann, R. (1994). m3G cap hypermethylation of U1 small nuclear ribonucleoprotein (snRNP) in vitro: evidence that the U1 small nuclear RNA-(guanosine-N2)-methyltransferase is a non-snRNP cytoplasmic protein that requires a binding site on the Sm core domain. Mol. Cell. Biol. *14*, 4160–4172.

Polotnianka, R.M., Li, J., and Lustig, A.J. (1998). The yeast ku heterodimer is essential for protection of the telomere against nucleolytic and recombinational activities. Curr. Biol. *8*, 831–835.

Porrua, O., and Libri, D. (2015). Transcription termination and the control of the transcriptome: Why, where and how to stop. Nat. Rev. Mol. Cell Biol. *16*, 190–202.

Proudfoot, N.J. (1989). How RNA polymerase II terminates transcription in higher eukaryotes. Trends Biochem. Sci. *14*, 105–110.

Rhodes, D., and Giraldo, R. (1995). Telomere structure and function. Curr. Opin. Struct. Biol. *5*, 311–322.

Ribbeck, K., Lipowsky, G., Kent, H.M., Stewart, M., and Gö Rlich, D. (1998). NTF2 mediates nuclear import of Ran. EMBO J. *17*, 6587–6598.

Richard, P., and Manley, J.L. (2009). Transcription termination by nuclear RNA polymerases. Genes Dev. *23*, 1247–1269.

Roake, C.M., Chen, L., Chakravarthy, A.L., Ferrell, J.E., Raffa, G.D., and Artandi, S.E. (2019). Disruption of Telomerase RNA Maturation Kinetics Precipitates Disease. Mol. Cell *74*, 688–700.

Romano, G.H., Harari, Y., Yehuda, T., Podhorzer, A., Rubinstein, L., Shamir, R., Gottlieb, A., Silberberg, Y., Pe'er, D., Ruppin, E., et al. (2013). Environmental Stresses Disrupt Telomere Length Homeostasis. PLoS Genet. *9*.

Rondón, A.G., Mischo, H.E., Kawauchi, J., and Proudfoot, N.J. (2009). Fail-Safe Transcriptional Termination for Protein-Coding Genes in S. cerevisiae. Mol. Cell *36*, 88–98.

Rose, M., Winston, F., and Hieter, P. (1990). Methods in Yeast Genetics -- A Laboratory Course Manual. In Cold Spring Harbor Laboratory Press, p. pp 198.

Salinas, K., Wierzbicki, S., Zhou, L., and Schmitt, M.E. (2005). Characterization and purification of Saccharomyces cerevisiae RNase MRP reveals a new unique protein component. J. Biol. Chem. *280*, 11352–11360.

Sambrook, J., Fritsch, E.F., and Maniatis, T. (1989). Molecular cloning: a laboratory manual. Cold Spring Harb. Lab.

Schmid, M., Tudek, A., and Jensen, T.H. (2018). Simultaneous Measurement of Transcriptional and Post-transcriptional Parameters by 3' End RNA-Seq. Cell Rep. *24*, 2468-2478.e4.

Schmidt, J.C., and Cech, T.R. (2015). Human telomerase: biogenesis, trafficking, recruitment, and activation. Genes Dev. *29*, 1095–1105.

Schwer, B., Erdjument-Bromage, H., and Shuman, S. (2011). Composition of yeast snRNPs and snoRNPs in the absence of trimethylguanosine caps reveals nuclear cap binding protein as a gained U1 component implicated in the cold-sensitivity of tgs1δ cells. Nucleic Acids Res. *39*, 6715–6728.

Schwer, B., Kruchten, J., and Shuman, S. (2016). Structure-function analysis and genetic interactions of the SmG, SmE, and SmF subunits of the yeast Sm protein ring. Cold Spring Harb. Lab. Press RNA Soc.

22, 1320–1328.

Segref, A., Sharma, K., Doye, V., Hellwig, A., Huber, J., Lührmann, R., and Hurt, E. (1997). Mex67p, a novel factor for nuclear mRNA export. Binds to both poly(A)+ RNA and nuclear pores. EMBO J. *16*, 3256–3271.

Seipelt, R.L., Zheng, B., Asuru, A., and Rymond, B.C. (1999). U1 snRNA is cleaved by RNase III and processed through an Sm site-dependent pathway. Nucleic Acids Res. *27*, 587–595.

Senger, B., Simos, G., Bischoff, F.R., Podtelejnikov, A., Mann, M., Hurt, E., Heidelberg, B.-Z., and Feld, I.N. (1998). Mtr10p functions as a nuclear import receptor for the mRNA-binding protein Npl3p. EMBO J. *17*, 2196–2207.

Séraphin, B. (1995). Sm and Sm-like proteins belong to a large family: Identification of proteins of the U6 as well as the U1, U2, U4 and U5 snRNPs. EMBO J. *14*, 2089–2098.

Seto, A.G., Zaug, A.J., Sobel, S.G., Wolin, S.L., and Cech, T.R. (1999). Saccharomyces cerevisiae telomerase is an Sm small nuclear ribonucleoprotein particle. Nature *401*, 177–180.

Shampay, J., Szostak, J.W., and Blackburn, E.H. (1984). DNA sequences of telomeres maintained in yeast. Nature *310*, 154–157.

Shen, E.C., Stage-Zimmermann, T., Chui, P., and Silver, P.A. (2000). 7The yeast mRNA-binding protein Np13p interacts with the cap-binding complex. J. Biol. Chem. *275*, 23718–23724.

Sherman, F. (2002). Getting started with yeast. Methods Enzymol. *350*, 3–41.

Sikorski, R.S., and Hieter, P. (1989). A System of Shuttle Vectors and Yeast Host Strains Designed for Efficient Manipulation of DNA in Saccharomyces cerevisiae. Genet. Soc. Am. 19–27.

Singer, M.S., and Gottschling, D.E. (1994). TLC1: Template RNA component of Saccharomyces cerevisiae telomerase. Science (80-.). *266*, 404–409.

Sklenar, A.R., and Parthun, M.R. (2004). Characterization of yeast histone H3-specific type B histone acetyltransferases identifies an ADA2-independent Gcn5p activity. BMC Biochem. *5*, 1–12.

Sloan, K.E., Gleizes, P.-E.E., and Bohnsack, M.T. (2016). Nucleocytoplasmic Transport of RNAs and RNA-Protein Complexes. J. Mol. Biol. *428*, 2040–2059.

Smogorzewska, A., and De Lange, T. (2004). Regulation of Telomerase by Telomeric Proteins. Annu. Rev. Biochem. *73*, 177–208.

Solsbacher, J., Maurer, P., Bischoff, F.R., and Schlenstedt, G. (1998). Cse1p Is Involved in Export of Yeast Importin α from the Nucleus. Mol. Cell. Biol. *18*, 6805–6815.

Sprague, G.F. (1991). Assay of yeast mating reaction. Methods Enzymol. *194*, 77–93.

Steinmetz, E.J., and Brow, D.A. (1998). Control of pre-mRNA accumulation by the essential yeast protein Nrd1 requires high-affinity transcript binding and a domain implicated in RNA polymerase II association. Proc. Natl. Acad. Sci. U. S. A. *95*, 6699–6704.

Steinmetz, E.J., Conrad, N.K., Brow, D.A., and Corden, J.L. (2001). RNA-binding protein Nrd1 directs poly(A)-independent 3'-end formation of RNA polymerase II transcripts. Nature *413*, 327–331.

Strahl-Bolsinger, S., Hecht, A., Luo, K., and Grunstein, M. (1997). SIR2 and SIR4 interactions differ in core and extended telomeric heterochromatin in yeast. Genes Dev. *11*, 83–93.

Strambio-De-Castillia, C., Niepel, M., and Rout, M.P. (2010). The nuclear pore complex: Bridging nuclear transport and gene regulation. Nat. Rev. Mol. Cell Biol. *11*, 490–501.

Ström, A., and Weis, K. (2001). Importin-beta-like nuclear transport receptors. Genome Biol. *2*.

Taggart, A.K.P., Teng, S.C., and Zakian, V.A. (2002). Est1p as a cell cycle-regulated activator of telomere-bound telomerase. Science (80-.). *297*, 1023–1026.

Taura, T., Krebber, H., and Silver, P.A. (1998). A member of the Ran-binding protein family, Yrb2p, is

involved in nuclear protein export. Proc. Natl. Acad. Sci. U. S. A. *95*, 7427–7432.

Teixeira, M.T. (2013). Saccharomyces cerevisiae as a model to study replicative senescence triggered by telomere shortening. Front. Oncol. *3*.

Teixeira, M.T., Arneric, M., Sperisen, P., and Lingner, J. (2004). Telomere length homeostasis is achieved via a switch between telomerase- extendible and -nonextendible states. Cell *117*, 323–335.

Teng, S.-C., and Zakian, V.A. (1999). Telomere-Telomere Recombination Is an Efficient Bypass Pathway for Telomere Maintenance in Saccharomyces cerevisiae. Mol. Cell. Biol. *19*, 8083–8093.

Tieg, B., and Krebber, H. (2013). Dbp5 — From nuclear export to translation. Biochim. Biophys. Acta *1829*, 791–798.

Towbin, H., Staehelin, T., and Gordon, J. (1979). Electrophoretic transfer of proteins from polyacrylamide gels to nitrocellulose sheets: procedure and some applications. 1979. Proc. Natl. Acad. Sci. U. S. A. *76*, 4350–4354.

Tucey, T.M., and Lundblad, V. (2013). A Yeast Telomerase Complex Containing the Est1 Recruitment Protein Is Assembled Early in the Cell Cycle Timothy. Biochemistry *52*, 1131–1133.

Tucey, T.M., and Lundblad, V. (2014). Regulated assembly and disassembly of the yeast telomerase quaternary complex. Genes Dev. *28*, 2077–2089.

Tuck, A.C., and Tollervey, D. (2013). A transcriptome-wide atlas of RNP composition reveals diverse classes of mRNAs and lncRNAs. Cell *154*, 996–1009.

Tudek, A., Lloret-llinares, M., and Jensen, T.H. (2018). The multitasking polyA tail : nuclear RNA maturation , degradation and export. Philos. Trans. R. Soc. B *373*.

Tuzon, C.T., Wu, Y., Chan, A., and Zakian, V.A. (2011). The saccharomyces cerevisiae telomerase subunit Est3 binds telomeres in a cell cycle- and Est1-dependent manner and interacts directly with Est1 in vitro. PLoS Genet. *7*.

Ungar, L., Yosef, N., Sela, Y., Sharan, R., Ruppin, E., and Kupiec, M. (2009). A genome-wide screen for essential yeast genes that affect telomere length maintenance. Nucleic Acids Res. *37*, 3840–3849.

Vanacova, S., Wolf, J., Martin, G., Blank, D., Dettwiler, S., Friedlein, A., Langen, H., and Keith, GerardKeller, W. (2005). A New Yeast Poly (A) Polymerase Complex Involved in RNA Quality Control. PLoS Biol. *3*.

Vasianovich, Y., and Wellinger, R.J. (2017). Life and Death of Yeast Telomerase RNA. J. Mol. Biol. *429*, 3242–3254.

Vasianovich, Y., Krallis, A., and Wellinger, R. (2019). Telomerase in Space and Time: Regulation of Yeast Telomerase Function at Telomeres and DNA Breaks. In: Morrish TA (ed) Telomerase and Non-Telomerase Mechanisms of Telomere Maintenance, (IntechOpen)

Vasianovich, Y., Bajon, E., and Wellinger, R.J. (2020). Telomerase biogenesis requires a novel Mex67 function and a cytoplasmic association with the Sm 7 complex. eLife; 10.7554/eLife.60000

Vasiljeva, L., and Buratowski, S. (2006). Nrd1 interacts with the nuclear exosome for 3' processing of RNA polymerase II transcripts. Mol. Cell *21*, 239–248.

Villa, T., Barucco, M., Martin-Niclos, M.J., Jacquier, A., and Libri, D. (2020). Degradation of Non-coding RNAs Promotes Recycling of Termination Factors at Sites of Transcription. Cell Rep. *32*.

Vodenicharov, M.D., and Wellinger, R.J. (2006). DNA Degradation at Unprotected Telomeres in Yeast Is Regulated by the CDK1 (Cdc28/Clb) Cell-Cycle Kinase. Mol. Cell *24*, 127–137.

Wälde, S., and Kehlenbach, R.H. (2010). The Part and the Whole: Functions of nucleoporins in nucleocytoplasmic transport. Trends Cell Biol. *20*, 461–469.

Watson, J.D. (1972). Origin of Concatemeric T7 DNA. Nat. New Biol. *239*.

Wellinger, R.J., and Zakian, V.A. (2012). Everything you ever wanted to know about Saccharomyces cerevisiae telomeres: Beginning to end. Genetics *191*, 1073–1105.

Wellinger, R.J., Wolf, A.J., and Zakian, V.A. (1993). Saccharomyces Telomeres Acquire Single-Strand TG1-3 Tails Late in S Phase.

Windgassen, M., Sturm, D., Cajigas, I., González, C., Seedorf, M., Bastians, H., and Krebber, H. (2004). Yeast shuttling SR-proteins Npl3p, Gbp2p and Hrb1p are part of the translating mRNPs and Npl3p can function as a translational repressor. Mol. Cell. Biol. 10479–10491.

Winston, F., Dollard, C., and Ricupero-Hovasse, S.L. (1995). Construction of a set of convenient saccharomyces cerevisiae strains that are isogenic to S288C. Yeast *11*, 53–55.

Wotton, D., and Shore, D. (1997). A novel Rap1p-interacting factor, Rif2p, cooperates with Riflp to regulate telomere length in Saccharomyces cerevisiae. Genes Dev. *11*, 748–760.

Wright, J.H., Gottschling, D.E., and Zakian, V.A. (1992). Saccharomyces telomeres assume a non-nucleosomal chromatin structure. Genes Dev. *6*, 197–210.

Wu, Y., and Zakian, V.A. (2011). The telomeric Cdc13 protein interacts directly with the telomerase subunit Est1 to bring it to telomeric DNA ends in vitro. Proc. Natl. Acad. Sci. U. S. A. *108*, 20362–20369.

Wu, H., Becker, D., and Krebber, H. (2014). Telomerase RNA TLC1 shuttling to the cytoplasm requires mRNA export factors and is important for telomere maintenance. Cell Rep. *8*, 1630–1638.

Wyers, F., Rougemaille, M., Badis, G., Rousselle, J.C., Dufour, M.E., Boulay, J., Régnault, B., Devaux, F., Namane, A., Séraphin, B., et al. (2005). Cryptic Pol II transcripts are degraded by a nuclear quality control pathway involving a new poly(A) polymerase. Cell *121*, 725–737.

Wynford-Thomas, D., and Kipling, D. (1997). Cancer and the knockout mouse. Nature *389*, 551–552.

Xia, J., Peng, Y., Mian, I.S., and Lue, N.F. (2000). Identification of Functionally Important Domains in the N-Terminal Region of Telomerase Reverse Transcriptase. Mol. Cell. Biol. *20*, 5196–5207.

Xiao, Z., McGrew, J.T., Schroeder, A.J., and Fitzgerald-Hayes, M. (1993). CSE1 and CSE2, two new genes required for accurate mitotic chromosome segregation in Saccharomyces cerevisiae. Mol. Cell. Biol. *13*, 4691–4702.

Xu, Z., Wei, W., Gagneur, J., Perocchi, F., Clauder-Münster, S., Camblong, J., Guffanti, E., Stutz, F., Huber, W., and Steinmetz, L.M. (2009). Bidirectional promoters generate pervasive transcription in yeast. Nature *457*, 1033–1037.

Yi, X., Shay, J.W., and Wright, W.E. (2001). Quantitation of telomerase components and hTERT mRNA splicing patterns in immortal human cells. Nucleic Acids Res. *29*, 4818–4825.

Yoshida, K., and Blobel, G. (2001). The karyopherin Kap142p/Msn5p mediates nuclear import and nuclear export of different cargo proteins. J. Cell Biol. *152*, 729–739.

Zander, G., and Krebber, H. (2017). Quick or quality? How mRNA escapes nuclear quality control during stress. RNA Biol. *14*, 1642–1648.

Zander, G., Hackmann, A., Bender, L., Becker, D., Lingner, T., Salinas, G., and Krebber, H. (2016). mRNA quality control is bypassed for immediate export of stress-responsive transcripts. Nature *540*, 593–596.

Zappulla, D.C., and Cech, T.R. (2004). Yeast telomerase RNA: A flexible scaffold for protein subunits. Proc. Natl. Acad. Sci. U. S. A. *101*, 10024–10029.

Zappulla, D.C., and Cech, T.R. (2006). RNA as a flexible scaffold for proteins: Yeast telomerase and beyond. Cold Spring Harb. Symp. Quant. Biol. *71*, 217–224.

7. Acknowledgement

Zu guter Letzt möchte ich mich an dieser Stelle bei allen bedanken, die mich bei der Anfertigung dieser Arbeit unterstützt haben.
Allen voran möchte ich Prof. Dr. Heike Krebber dafür danken, dass Sie mir die Möglichkeit gegeben hat in Ihrem Labor diese Dissertation anzufertigen. Darüber hinaus möchte ich Ihr auch dafür danken, dass ich an diversen spannenden Themen arbeiten konnte sowie für die Unterstützung, das Vertrauen und die enge Betreuung. Herzlichen Dank dafür.
Weiterhin danke ich den Mitgliedern meines *Thesis committees,* Prof. Dr. Ralph Kehlenbach und Prof. Dr. Jörg Großhans, die mich während meiner Doktorandenzeit mit anregenden Diskussionen und wertvollen Ratschlägen begleitet haben. Ganz besonders danke ich Prof. Dr. Ralph Kehlenbach für die Übernahme des Zweitgutachtens.
Herzlich danken möchte ich auch allen weiteren Mitgliedern meines *Examination boards,* Prof. Dr. Kai Heimel, Prof. Dr. Ralf Ficner und PD Dr. Wilfried Kramer.

Besonders möchte ich mich auch bei allen aktuellen und ehemaligen Mitgliedern der AG Krebber und AG Bastians für die tolle Arbeitsatmosphäre, ihre Hilfsbereitschaft und die zahlreichen Diskussionen und Anregungen bedanken.
Bei Ivo Coban möchte ich mich für den tollen gemeinsamen Start im Thema der long non-coding RNAs und im Doktorandenleben bedanken. Dr. Daniel Becker danke ich für die tolle Zusammenarbeit im snRNA Bereich und Dr. Ulla Schneider für den kleinen aber wertvollen Exkurs in die vielfältigen Wirkungsbereiche von Npl3 sowie natürlich auch für unsere gemeinsamen Unternehmungen. Dr. Wilfried Kramer danke ich für seine Ratschläge und das Teilen seines großen Hefe-Wissens. Lena Söldner danke ich für die große Unterstützung im allgemeinen Laborbetrieb sowie ihre herzliche und aufgeschlossene Art. Ein großer Dank gilt auch Jan-Philipp Lamping, der im Zuge seiner *Lab rotations*, der Bachelorarbeit und Masterarbeit an vielen Stellen Teil des *TLC1* Projekts geworden ist. Yen-Yun Lu möchte ich für die tolle gemeinsame Zeit und vor allem auch für die motivierenden Worte während unserer finalen Phase danken.

Für das Korrekturlesen dieser Arbeit bedanke ich mich herzlich bei Prof. Dr. Heike Krebber, Dr. Sebastian Grosse, Ivo Coban, Jan-Philipp Lamping, Anne-Sophie Lindemann, Markus Röder und Theresa Binder.

Abschließend möchte ich mich bei meinen Eltern, Brüdern und Freunden bedanken, die mir in jeder Lebenslage den Rücken gestärkt, mich motiviert und an mich geglaubt haben. Von ganzem Herzen lieben Dank dafür.

8. Curriculum Vitae

Anna Greta Hirsch

Date of birth: 21.05.1990

Place of birth: Berlin, Germany

2017 – present	Georg-August-Universität Göttingen Member of GGNB graduate school – Molecular Biology of Cells PhD student in the group of Prof. Dr. Heike Krebber, Department of Molecular Genetics; Institute for Microbiology and Genetics
2014-2017	Technische Universität Braunschweig Master of Science (M.Sc.) in Biology Master Thesis in the group of Prof. Dr. André Fleißner, Genetics of filamentous fungi, Institute for Genetics “Expression und Lokalisierung des “Multidrug Resistance“-Transporters CDR4 während der Kolonieentwicklung von *Neurospora crassa*“
2011-2014	Technische Universität Braunschweig Bachelor of Science (B.Sc.) in Biology Bachelor Thesis in the group of Prof. Dr. Ralf Schnabel and Prof. Dr. Henning Schmidt, Developmental Genetics, Institute for Genetics “CRISPR/Cas9 gesteuerte Mutagenese in *Caenorhabditis elegans*“
2002 - 2010	Abitur, Werner-von-Siemens Gymnasium Bad Harzburg

Publications:

Daniel Becker, Anna Greta Hirsch, Lysann Bender, Thomas Lingner, Gabriela Salinas, and Heike Krebber

Nuclear Pre-snRNA Export Is an Essential Quality Assurance Mechanism for Functional Spliceosomes

Cell reports 2019, doi: 10.1016/j.celrep.2019.05.031

Anna Greta Hirsch, Daniel Becker, Jan-Philipp Lamping and Heike Krebber

Unraveling the stepwise maturation of the yeast telomerase

bioRxiv: doi.org/10.1101/2021.04.30.442090

9. Appendix

Article

Cell Reports

Nuclear Pre-snRNA Export Is an Essential Quality Assurance Mechanism for Functional Spliceosomes

Graphical Abstract

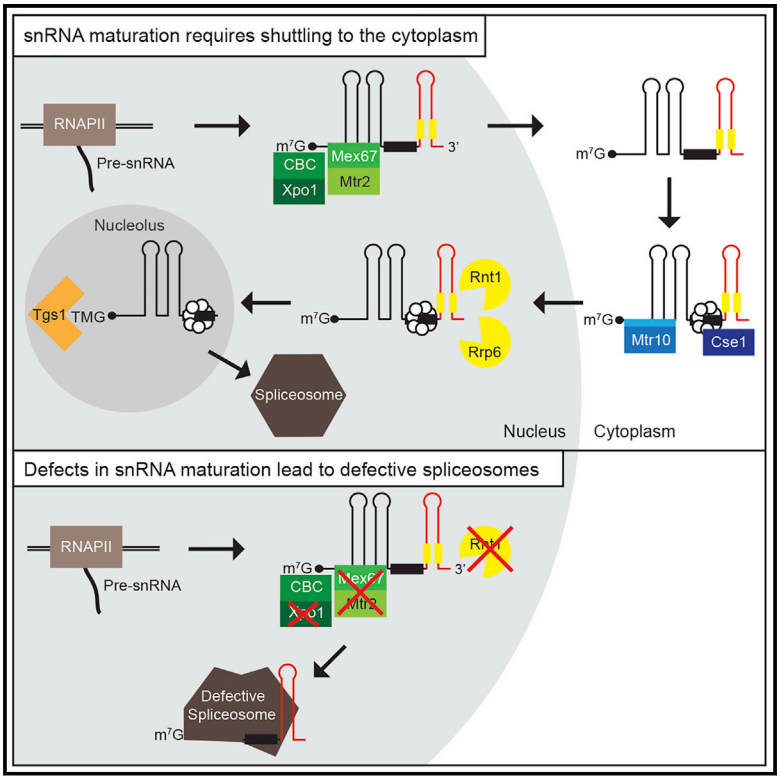

Highlights

- All yeast snRNAs, including U6, shuttle into the cytoplasm
- Export is mediated by Mex67 and Xpo1, and re-import requires Mtr10 and Cse1
- snRNA export prevents an incorporation of immature snRNAs into spliceosomes
- Spliceosomal assembly with immature snRNAs results in genome-wide splicing defects

Authors

Daniel Becker, Anna Greta Hirsch, Lysann Bender, Thomas Lingner, Gabriela Salinas, Heike Krebber

Correspondence

heike.krebber@biologie.uni-goettingen.de

In Brief

Becker et al. show snRNA maturation in yeast involves nuclear export and re-import mediated by Mex67-Mtr2 and Xpo1/Crm1 and by Mtr10 and Cse1, respectively. They propose a model for obligatory shuttling in eukaryotes by showing spliceosomes assemble with immature snRNAs when export is prevented, resulting in defective spliceosomes and genome-wide splicing defects.

Becker et al., 2019, Cell Reports 27, 3199–3214
June 11, 2019
https://doi.org/10.1016/j.celrep.2019.05.031

CellPress

Cell Reports
Article

Nuclear Pre-snRNA Export Is an Essential Quality Assurance Mechanism for Functional Spliceosomes

Daniel Becker,[1] Anna Greta Hirsch,[1] Lysann Bender,[1] Thomas Lingner,[2] Gabriela Salinas,[2] and Heike Krebber[1,3,*]
[1]Abteilung für Molekulare Genetik, Institut für Mikrobiologie und Genetik, Göttinger Zentrum für Molekulare Biowissenschaften (GZMB), Georg-August Universität Göttingen, Göttingen, Germany
[2]Transkriptomanalyselabor, Institut für Entwicklungsbiochemie, Georg-August Universität Göttingen, Göttingen, Germany
[3]Lead Contact
*Correspondence: heike.krebber@biologie.uni-goettingen.de
https://doi.org/10.1016/j.celrep.2019.05.031

SUMMARY

Removal of introns from pre-mRNAs is an essential step in eukaryotic gene expression, mediated by spliceosomes that contain snRNAs as key components. Although snRNAs are transcribed in the nucleus and function in the same compartment, all except U6 shuttle to the cytoplasm. Surprisingly, the physiological relevance for shuttling is unclear, in particular because the snRNAs in *Saccharomyces cerevisiae* were reported to remain nuclear. Here, we show that all yeast pre-snRNAs including U6 undergo a stepwise maturation process after nuclear export by Mex67 and Xpo1. Sm- and Lsm-ring attachment occurs in the cytoplasm and is important for the snRNA re-import, mediated by Cse1 and Mtr10. Finally, nuclear pre-snRNA cleavage and trimethylation of the 5′-cap finalizes shuttling. Importantly, preventing pre-snRNAs from being exported or processed results in faulty spliceosome assembly and subsequent genome-wide splicing defects. Thus, pre-snRNA export is obligatory for functional splicing and resembles an essential evolutionarily conserved quality assurance step.

INTRODUCTION

Spliceosomes contain several proteins and the small nuclear RNAs (snRNAs) U1, U2, U4, U5, and U6 (Wahl et al., 2009). All snRNAs are transcribed by RNA polymerase II (Pol II) except U6, which is synthesized by Pol III. U6 acquires a γ-monomethyl phosphate cap, while U1, U2, U4, and U5 receive m^7G-monomethyl caps that are also found on mRNAs (Matera and Wang, 2014; Didychuk et al., 2018). m^7G-caps are bound by the cap-binding complex (CBC), composed of CBP20 and CBP80 (Köhler and Hurt, 2007; Matera and Wang, 2014). In human cells, CBC binds to PHAX (phosphorylated adaptor RNA export) that in turn recruits the RanGTPase driven exportin CRM1 (chromosome maintenance 1) for nuclear export (Köhler and Hurt, 2007; Matera and Wang, 2014). In yeast, Pol II transcripts such as mRNAs and the non-coding telomerase-RNA *TLC1* use Mex67-Mtr2 (TAP-p15 in human) and Xpo1/Crm1 for their nuclear export (Tutucci and Stutz, 2011; Wu et al., 2014). Interestingly, the current literature suggests that snRNAs do not shuttle in yeast (Olson and Siliciano, 2003; Murphy et al., 2004), although they undergo similar maturation steps as in human cells (Will and Lührmann, 2001; Matera and Wang, 2014; Sloan et al., 2016; Vasianovich and Wellinger, 2017).

Small nuclear ribonucleoprotein particle (snRNP) (ribonucleoprotein complex) biogenesis includes the assembly of the Sm-ring on all snRNAs except U6. The ring is composed of the Sm B/B′, D1, D2, D3, E, F, and G proteins (encoded by *SMB1*, *SMD1*, *SMD2*, *SMD3*, *SME1*, *SMX2*, and *SMX3* in yeast) common to all spliceosomal snRNPs (Matera and Wang, 2014). The Sm-proteins are arranged into a seven-membered ring on the Sm binding site of the snRNA. In higher eukaryotes, Sm-proteins are loaded by the survival motor neuron (SMN) protein, which in low expression or upon mutation leads to the neurodegenerative disease spinal muscular atrophy (SMA) (Lefebvre et al., 1995; Lorson et al., 2010). Sm-ring binding is also critical in *S. cerevisiae*, as snRNA degradation is increased when the Sm-ring binding site is mutated (Coy et al., 2013; Shukla and Parker, 2014). However, in yeast, it was speculated that the assembly of the Sm-ring occurs in the nucleus. First, shuttling of the snRNAs had not been observed except for the shuttling of U1 and U2 snRNAs in a heterokaryon assay, in which the authors carefully discussed that their finding might be an artifact in this type of assay, because all analyzed transcripts left the nucleus and therefore a negative control was missing (Olson and Siliciano, 2003). Second, nuclear localization sequences were identified in SmB, SmD1, and SmD3, which suggested that an RNA-free pre-assembled Sm-complex would be able to enter the nucleus (Bordonné, 2000).

The Sm-ring is a prerequisite for the correct and limited trimming of the pre-snRNAs. While this step is anticipated to be cytoplasmic in human cells, as precursors accumulate in the cytoplasm (Huang and Pederson, 1999), it occurs in the nucleus of yeast through cleavage by Rnt1 and subsequent 3′ to 5′ degradation by the nuclear exosome ending at the Sm-ring (Seipelt et al., 1999; Coy et al., 2013; Shukla and Parker, 2014). The nuclear localization of Rnt1 (Catala et al., 2004) was further used as an argument that snRNAs do not need to shuttle in yeast. The Sm-ring has additionally been described to recruit the trimethylguanosine synthetase 1 (TGS1), an RNA methyltransferase that

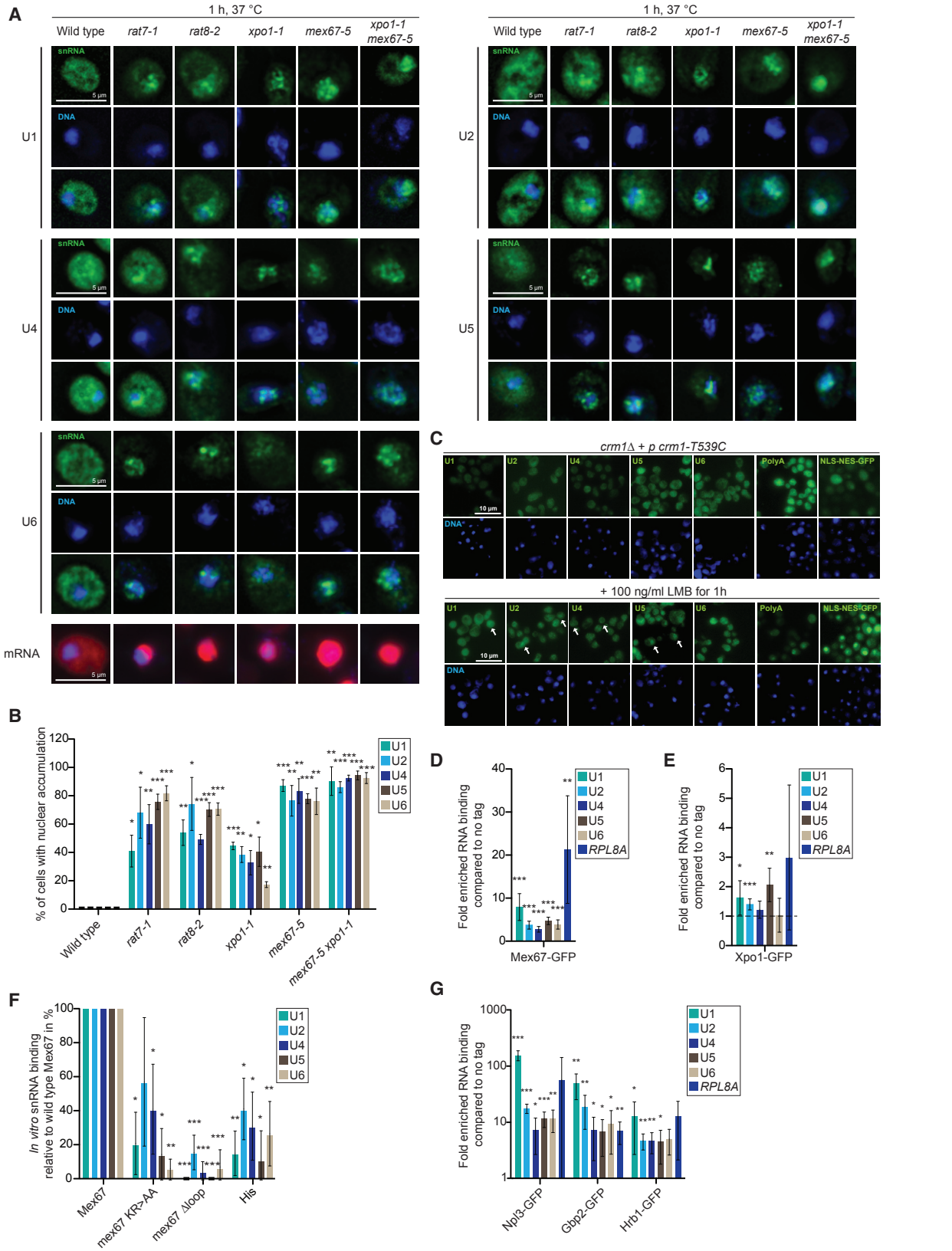

(legend on next page)

mediates a 2,2,7-trimethylguanosine (TMG) modification of the 5′ end of the snRNAs (Matera and Wang, 2014). In yeast, Tgs1, mediating this trimethylation, is localized to the nucleolus, again questioning the need for snRNA shuttling (Mouaikel et al., 2002). Contrarily, in human cells this step occurs in the cytoplasm and triggers the formation of the Ran-dependent import complex composed of the importin-adaptor Snurportin 1 (SPN) and its receptor, importin β, leading to subsequent nuclear import (Matera and Wang, 2014). Up to date, no homolog for SPN has been found in yeast.

U6 has, like other Pol III transcripts, an oligo(U) sequence at its 3′-end that is bound to an Lsm-ring, which is structurally related to the Sm-ring and composed of the Lsm proteins 2 to 8 (Matera et al., 2007). It is generally and species-wide supposed that U6 is restricted to the nucleus and does not shuttle during its biogenesis (Bertrand and Bordonné, 2004; Matera et al., 2007; Sloan et al., 2016); however, a mechanism for its nuclear retention is lacking.

This current view for snRNA shuttling of Sm-ring-containing snRNAs in humans, the nuclear retention of yeast snRNAs, and the general nuclear retention of U6 raises two important questions: First, why should shuttling only evolve for some snRNA in Mammalia, and second, what is the advantage of shuttling? It has been suggested that snRNA shuttling might provide a plausible mechanism for quality control, ensuring that partially assembled RNPs do not come into contact with their substrates (Matera and Wang, 2014). However, this has never been shown.

Here, we show that all snRNAs shuttle in yeast. They are exported via Mex67 and all except U6 additionally use the 5′-cap, bound by CBC for an Xpo1/Crm1-mediated nuclear export. All snRNAs including U6 are re-imported into the nucleus via Mtr10 and Cse1. Further maturation of the snRNAs includes the Sm-ring binding, which occurs in the cytoplasm and the subsequent 3′-end trimming and 5′-cap trimethylation in the nucleus and nucleolus, respectively. Most importantly, we show that snRNA shuttling resembles a quality assurance step, because pre-snRNAs are incorporated into the spliceosome when not exported. Similarly, the downregulation of *RNT1*, required for 3′-end trimming, leads to the incorporation of unprocessed snRNAs into the spliceosome, as does the expression of a non-cleavable mutant of pre-U1. Importantly, all three situations in which the pre-snRNAs were brought into contact with the spliceosome, this molecular machine incorporated these immature snRNPs, revealing that the spliceosome cannot distinguish between immature and mature snRNAs. Importantly, all "immature" and thus faulty spliceosomes lead to splicing defects. From these data, we suggest that snRNA shuttling is probably obligatory for all eukaryotes and for all snRNAs, including U6, because it represents a quality assurance mechanism for intact spliceosomes.

RESULTS

snRNAs Are Exported into the Cytoplasm via Xpo1 and Mex67

To challenge the current view that snRNA shuttling evolved only in higher eukaryotes, we systematically explored snRNA shuttling in *S. cerevisiae*. Due to the fact that Pol II transcripts such as mRNAs and the non-coding telomerase-RNA *TLC1* require Mex67-Mtr2 and Xpo1/Crm1 for their nuclear export (Tutucci and Stutz, 2011; Wu et al., 2014), we investigated whether the shuttling of snRNAs would also be dependent on these factors. First, we analyzed potential export defects by fluorescence *in situ* hybridization (FISH) experiments in mutant forms of Xpo1, Mex67, and its interacting partners Dbp5/Rat8 and Nup159/Rat7 (Tieg and Krebber, 2013). To visualize potential nuclear export defects, we used specific long fluorescently labeled probes (~100–250 nucleotides) that in our experience preferentially stain cytoplasmic snRNAs, because they might not penetrate the nuclear membrane. While these probes detected mainly cytoplasmic snRNAs in wild-type cells, we found strong nuclear dot-like accumulations for all snRNAs in the export mutants (Figures 1A, 1B, and S1A–S1C), indicating that snRNAs leave the nucleus. Interestingly, besides the nuclear export defects of the Sm-ring-containing snRNAs, we found a clear nuclear accumulation also for U6, suggesting that also this Pol III transcript is exported into the cytoplasm. However, in contrast to the Sm-ring-containing snRNAs, only some nuclear accumulation of U6 was detectable in *xpo1-1* mutants, which might be due to the differences in transcription-coupled loading of the export factors, or simply to the different cap structure. This phenotype was also visible in the leptomycin B (LMB)-sensitive yeast strain (Figure 1C), in which the trimeric export complex Ran-GTP-Xpo1-export protein is disrupted (Neville and Rosbash, 1999). However, the phenotype was very mild compared to *xpo1-1*, possibly because the *xpo1-1* mutation is potentially dominant as it has a slightly growth-inhibitory effect and might inhibit cell growth through misfolding when bound to the export substrate or the nuclear pore complex (NPC) upon the temperature shift (Figure S1D). In contrast, in the LMB-sensitive strain, Xpo1/Crm1 does not participate in nuclear export in the presence of LMB, because export complex formation is prevented and both mRNAs and snRNAs can still leave the nucleus via Mex67, but without Xpo1. Although the role of Xpo1/Crm1 was

Figure 1. snRNAs Are Exported to the Cytoplasm via Mex67 and Xpo1/Crm1 in Yeast

(A) Nuclear export of snRNAs is inhibited in mRNA export mutants. FISH experiments are shown with ~100- to 300-nucleotide-long specific DIG-labeled snRNA-probes, detected with FITC-labeled anti-DIG antibodies (green). Shown are deconvoluted images of single cells. n = 4.

(B) Quantification of cells with nuclear signals shown in (A). n = 3; 100–300 cells were counted.

(C) Leptomycin B slightly inhibits snRNA export in the LMB-sensitive *crm1-T539T* mutant. FISH experiments as in (A) are shown after a 1-h incubation of the cells at 30°C. n = 3.

(D and E) RIP experiments reveal a physical contact between Mex67 (D) or Xpo1 (E) and the snRNAs. The GFP-tagged export receptors were immunoprecipitated and the co-precipitated snRNAs were analyzed in qRT-PCRs. n = 5.

(F) The loop-domain of Mex67 is important for snRNA binding. qRT-PCRs of the eluates from *in vitro* RIP-experiments with Mex67 are shown. n = 3.

(G) RIP experiments reveal a physical contact between the guard proteins and the snRNAs. The GFP-tagged Mex67-adaptor proteins were immunoprecipitated and the co-precipitated snRNAs were analyzed in qRT-PCRs. n = 4.

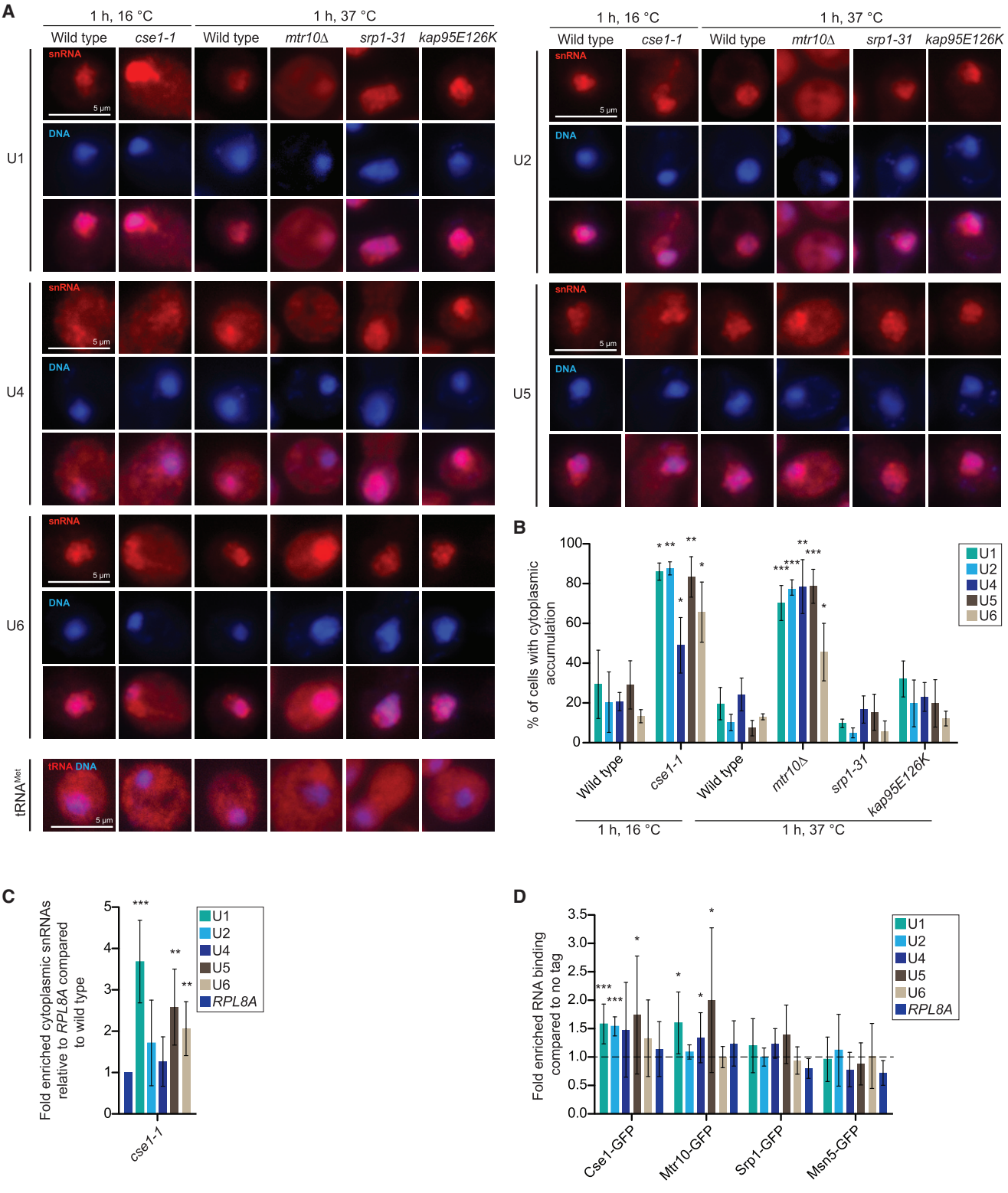

Figure 2. The Nuclear Import of snRNAs Is Mediated by Mtr10 and Cse1

(A) FISH experiments with 50-nucleotide-long Cy3-labeled probes (red) in the indicated strains that were shifted to the indicated non-permissive temperatures are shown. n = 3.

(legend continued on next page)

always controversially discussed (Stade et al., 1997; Neville and Rosbash, 1999), our data suggest that the export receptor might participate in the export of both mRNA and snRNA (Figure 1). Together, these data suggest that both Mex67 and Xpo1 participate in snRNA and mRNA export.

Second, we show that all snRNAs bind to Mex67 and Xpo1 *in vivo* by RNA-co-immunoprecipitation (RIP) experiments (Figures 1D, 1E, S1E, and S1F). The Mex67-RIP showed a more than 4-fold enriched binding of the snRNAs compared to the no-tag control, indicating that snRNAs contact this export receptor and can be purified with it. Similarly, all of the snRNAs except U6 showed an interaction with Xpo1. However, the binding was only ~1.5- and ~2-fold increased, which might be explained by the fact that upon cell lysis Xpo1-RanGTP comes into contact with the cytoplasmic GTPase-activating protein RanGAP1/Rna1, resulting in the dissociation of these export complexes. Additionally, the strong Mex67 binding of the snRNAs (between 4- and 8-fold) might reflect that Mex67 contact is less easily disrupted upon cell lysis, and it might also indicate that more molecules of Mex67 bind to the snRNAs than Xpo1. As different adaptor proteins, such as Npl3, Gbp2, and Hrb1, establish the contact between Mex67 and the RNA simply more Mex67 export receptors could bind. Indeed, RIP experiments and subsequent qRT-PCR analysis confirmed the binding of these Mex67 adapters to the snRNAs (Figures 1G and S1H). The snRNA binding to both export receptors is also less strong as for *TLC1*, which we analyzed earlier and found more than a 10-fold increased binding (Wu et al., 2014). This might simply be explained by the fact that *TLC1* is with a size of ~1.5 kb longer than the snRNAs and can potentially bind more export factors. Similarly, the *RPL8A* mRNA shows also more than 10-fold binding, which is present in the cell with many copies, as it is highly expressed (Figures 1D and 1G).

Interestingly, we did not detect binding of Xpo1 to U6. This might be due to potential differences in transcriptional loading of the export factors by the responsible Pol, or due to the different 5′-cap structures of the snRNAs. Its slight nuclear accumulation in the *xpo1-1* mutant (Figures 1A–1C and S1B) might thus rather be a secondary effect of the nuclear retention of the other snRNAs.

For Mex67 a loop-domain was shown to bind RNA directly (Figure S1G) (Yao et al., 2007, 2008; Zander et al., 2016). To investigate whether this domain is also important for the interaction with the snRNA, we carried out *in vitro* binding studies in which we used recombinantly expressed wild typical Mex67-Mtr2 heterodimer and two heterodimeric proteins with defective or absent loop-domain and incubated the proteins with isolated total yeast RNA. In a second purification step, we isolated the His-tagged heterodimeric protein complex again, this time with the attached RNA, which was subsequently analyzed in qRT-PCR experiments. These studies revealed that Mex67 also binds snRNAs directly with this domain, as mutations in this domain decreased its snRNA binding to amounts seen with the His-tag control (Figure 1F), very similar to the results seen with mRNA (Zander et al., 2016). These data suggest that yeast snRNAs leave the nucleus by contacting the same export machinery as the noncoding RNA (ncRNA) *TLC1* and mRNA. Strikingly, we detect export also for U6, indicating that it represents no exception in snRNA shuttling.

snRNAs Are Re-imported into the Nucleus via Mtr10 and Cse1

To identify the nuclear snRNP import factors, we screened mutants of all yeast karyopherins by FISH experiments (Figures S2A and S2B). We used short (50-nucleotide) snRNA probes (Figure S1A) that easily penetrate the nuclear envelope and thereby predominantly detect the bulk snRNAs that are mainly localized in the nucleus. This detection enabled us to recognize nuclear import defects by the cytoplasmic mislocalization of the snRNAs. We found that only mutations in *MTR10* and *CSE1* cause snRNA import defects, suggesting that these karyopherins are important for the nuclear import of snRNAs (Figures 2A, 2B, and S2C). These results were confirmed by cytoplasmic fractionation experiments, in which we detected an increased cytoplasmic presence of all snRNAs in *cse1-1* mutants via qRT-PCRs (Figures 2C and S2D). In support of these results, we show RIP experiments that reveal a physical interaction of Cse1 and Mtr10 with the snRNAs *in vivo* (Figures 2D, S2E, and S2F). Due to the fact that Mtr10 and Cse1 are like Xpo1, both Ran-dependent karyopherins that are dependent on an intact Ran-gradient and possibly require adaptor proteins for their binding to the RNA, we detected only a slight, ~1.5- to ~2-fold increased binding. Mtr10 was already identified to import several mRNA-binding proteins and the *TLC1* RNA (Häcker and Krebber, 2004; Gallardo and Chartrand, 2008). Therefore, its nuclear import activity for snRNAs was not surprising. However, the identification of Cse1 as an snRNA nuclear import receptor was unexpected, because up to date only one other cargo had been identified for Cse1: Importin α/Srp1, which is exported (Hood and Silver, 1998; Cook et al., 2007). It seems possible that snRNA import defects are caused by the mislocalized importin α in *cse1-1*; however, neither mutations in *SRP1* nor in *KAP95*/*RSL1* (yeast importin β) affect snRNA localization (Figures 2A, 2B, S2A, and S2C). In fact, the slow growth rate of the cold-sensitive *cse1-1* mutant is not fully suppressed by overexpression of *SRP1* (Solsbacher et al., 1998), which suggested the existence of further transport cargos, and our data suggest that these might be the snRNAs. Together, these data revealed that all snRNA in yeast shuttle into the cytoplasm, and we determined Mex67 and Xpo1 to be the responsible export factors. Mtr10 and Cse1 mediate the nuclear import of the snRNAs. Remarkably, although NLSs were identified in the proteins of the Sm-ring (Bordonné, 2000), which in higher eukaryotes is loaded in the cytoplasm, the nuclear import of U1, U2, U4, and U5 is independent of the importin α/β-pathway that recognizes the classical NLSs,

(B) Quantification of the cells with an snRNA mislocalization phenotype shown in (A). n = 3; 100–350 cells were counted.
(C) Cytoplasmic fractionation experiments reveal an increase of the cytoplasmic snRNA-pool in the import mutants, determined by qRT-PCRs. n = 6.
(D) RIP experiments reveal a physical contact between Mtr10 or Cse1 and the snRNAs. GFP-tagged transport receptors were precipitated, and the co-precipitated snRNAs were analyzed by qRT-PCRs. n = 5.

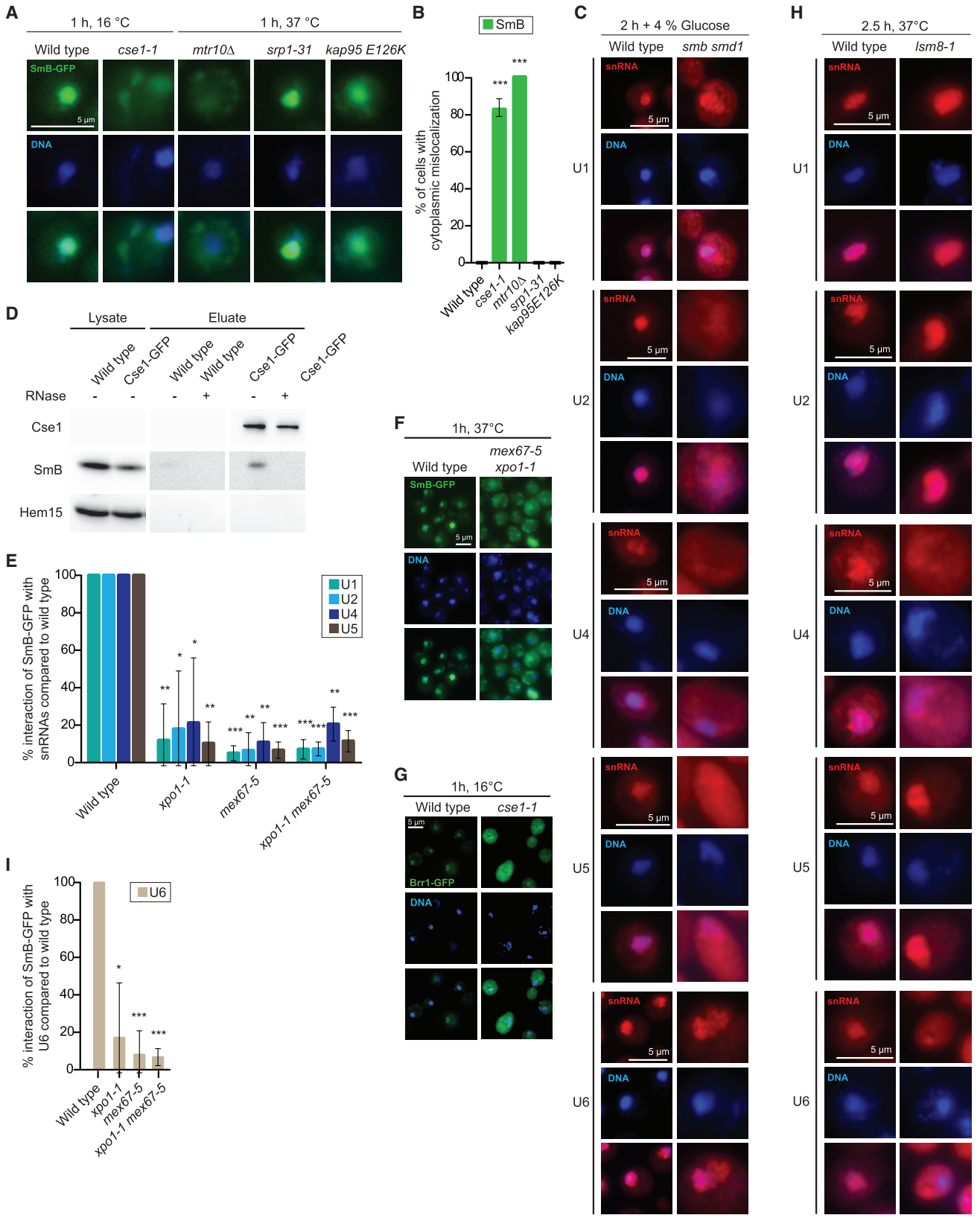

(legend on next page)

as the snRNAs are not mislocalized in *srp1-31* or *kap95E126K* (Figures 2A, 2B, S2A, and S2C).

Moreover, our results indicate that U6 also uses Mtr10 and Cse1 for its nuclear re-import. It is interesting to note that, although the Lsm-proteins can be imported without being bound to RNA via importin β (Spiller et al., 2007b), *srp1-31* and *kap95E126K* mutants cause no U6 import defect (Figures 2A, 2B, S2A, and S2C). These data might suggest that the Lsm-ring is possibly loaded onto U6 in the cytoplasm and that these proteins in association with the snRNA do not interact with importin α and β.

Sm- and Lsm-Ring Assembly Occurs in the Cytoplasm

The nucleo-cytoplasmic shuttling of the snRNAs raised the question in which compartment the Sm- and Lsm-ring assembly take place. It is currently anticipated that these proteins are imported into the nucleus, assemble there on the snRNAs, and in this way retain them in the nucleus (Bordonné, 2000; Spiller et al., 2007a, 2007b). Sm-ring assembly is critical for snRNA stability, because snRNA degradation is increased when the Sm-ring binding site is mutated (Coy et al., 2013; Shukla and Parker, 2014). Curiously, it was shown that cytoplasmic degradation factors affect the snRNA stability (Shukla and Parker, 2014). Thus, we investigated whether it might be conceivable that the Sm- and Lsm-ring association in yeast might take place in the cytoplasm. First, we localized SmB in *mtr10* and *cse1* mutants and found a strong cytoplasmic mislocalization of the protein (Figures 3A, 3B, and S3A). Second, we examined the localization of several snRNAs by FISH in the double mutant of the Sm-ring components SmB and SmD1 that mislocalize to the cytoplasm (Bordonné, 2000). We found that this localization defect results in the concomitant accumulation of the snRNAs in the cytoplasm (Figures 3C and S3B). These results suggest that Sm-ring assembly on the snRNA also in yeast occurs in the cytoplasm. Interestingly, also U6 mislocalized in the Sm-ring mutants, which suggests that its proper localization is dependent on the Sm-type snRNAs.

Moreover, we addressed how Cse1 might contact the snRNPs and show that the karyopherin does not directly interact with snRNAs by *in vitro* binding studies, in which we used recombinantly expressed GST-Cse1 that was incubated with yeast total RNA. After an RNA-co-IP the presence of the snRNAs was analyzed by subsequent qRT-PCR (Figures S3C–S3E). Instead, we identified a physical interaction between SmB and Cse1 (Figure 3D), suggesting that Cse1-mediated nuclear re-import of the snRNAs requires the Sm-ring. The sequences initially thought to be the NLS sequences, might have simply generated misfolded proteins when mutated that were not able to form a functioning Sm-ring, because these mutations lead to the cytoplasmic accumulation of the snRNP (Figure 3C). Therefore, it is conceivable that Cse1 functions as a quality control checkpoint that recognizes and imports only correctly formed Sm-ring containing snRNPs. Interestingly, the accessibility of the Sm-ring was suggested to represent the molecular basis also for the snRNP quality control in human cells, and immature, Sm-ring defective snRNPs were suggested to be sequestered to Cajal bodies (Roithová et al., 2018).

Reassuringly, the interaction of SmB with the snRNA was aborted in the nuclear snRNA-export mutants *xpo1-1*, *mex67-5* and the double mutant (Figures 3E and S3F) and led to a cytoplasmic mislocalization of SmB (Figure 3F). These data support a model in which the Sm-ring association on the snRNAs takes place in the cytoplasm.

Loading of the human Sm-ring onto the snRNAs requires SMN (Lefebvre et al., 1995; Lorson et al., 2010). Brr1 was shown to be required for snRNP biogenesis in budding yeast (Noble and Guthrie, 1996) and, as the putative Geminin2 ortholog, it is hypothesized to directly participate in Sm core assembly (reviewed in Matera and Wang, 2014). Consistent with this notion, we found that Brr1-GFP was mislocalized in *cse1-1* mutants (Figures 3G and S3G). This supports the idea that Brr1 is involved in the cytoplasmic loading of the Sm-ring onto the snRNAs.

As we found that U6 also leaves the nucleus in yeast, we addressed whether the Lsm-ring assembly also takes place in the cytoplasm. For this, we localized the snRNAs in the *lsm8-1* mutant that has defects in the U6-Lsm-ring assembly (Pannone et al., 1998). We found that U6 and interestingly also U4 were mislocalized to the cytoplasm (Figures 3H and S3H). These findings suggest that also the assembly of the Lsm-ring on the U6 snRNA takes place in the cytoplasm. The mislocalization of U4 might be a hint toward a collective nuclear re-import of U4 and U6, as they function as a di-snRNP in the spliceosome (Will and Lührmann, 2001). Such a model gets further support from the finding that also U6 binding to the Sm-ring can be also detected and this interaction is reduced in the snRNA export mutants (Figure 3I).

Figure 3. The Sm-Ring Assembles in the Cytoplasm and Contacts Cse1 for Nuclear Re-import

(A) SmB is mislocalized in *cse1* and *mtr10* mutants. SmB-GFP was localized in the indicated strains. n = 3.

(B) Quantification of cells with cytoplasmic signal shown in (A). n = 3; 50–100 cells were counted.

(C) Sm-ring assembly defects lead to the cytoplasmic mislocalization of snRNAs. The indicated strains were analyzed by FISH with the ~50-nucleotide-long snRNA-specific probes. n = 3.

(D) Cse1 interacts with the Sm-ring. Co-IP of SmB-myc with Cse1-GFP is shown on western blots. Hem15 served as a negative control. n = 3.

(E) RIP experiments reveal a decreased interaction of SmB with snRNAs in nuclear export mutants. The SmB-bound snRNA was extracted from the indicated strains and analyzed in qRT-PCR-experiments. n = 3.

(F) SmB mislocalizes to the cytoplasm in mutants of the snRNA export factors. The localization of SmB-GFP was analyzed in wild-type and the *mex67-5 xpo1-1* double mutant. n = 3.

(G) Localization of Brr1-GFP in the indicated strains. n = 3.

(H) Lsm-ring assembly defects lead to a cytoplasmic accumulation of U6 and U4. FISH experiment with Cy3-labeled 50-nucleotide-long snRNA-specific probes is shown. n = 3.

(I) Reduced formation of the U4/U6 di-snRNP occurs in export mutants. RIP experiments with the SmB-bound snRNA is shown, which was extracted from the indicated strains and analyzed in qRT-PCR experiments. n = 3.

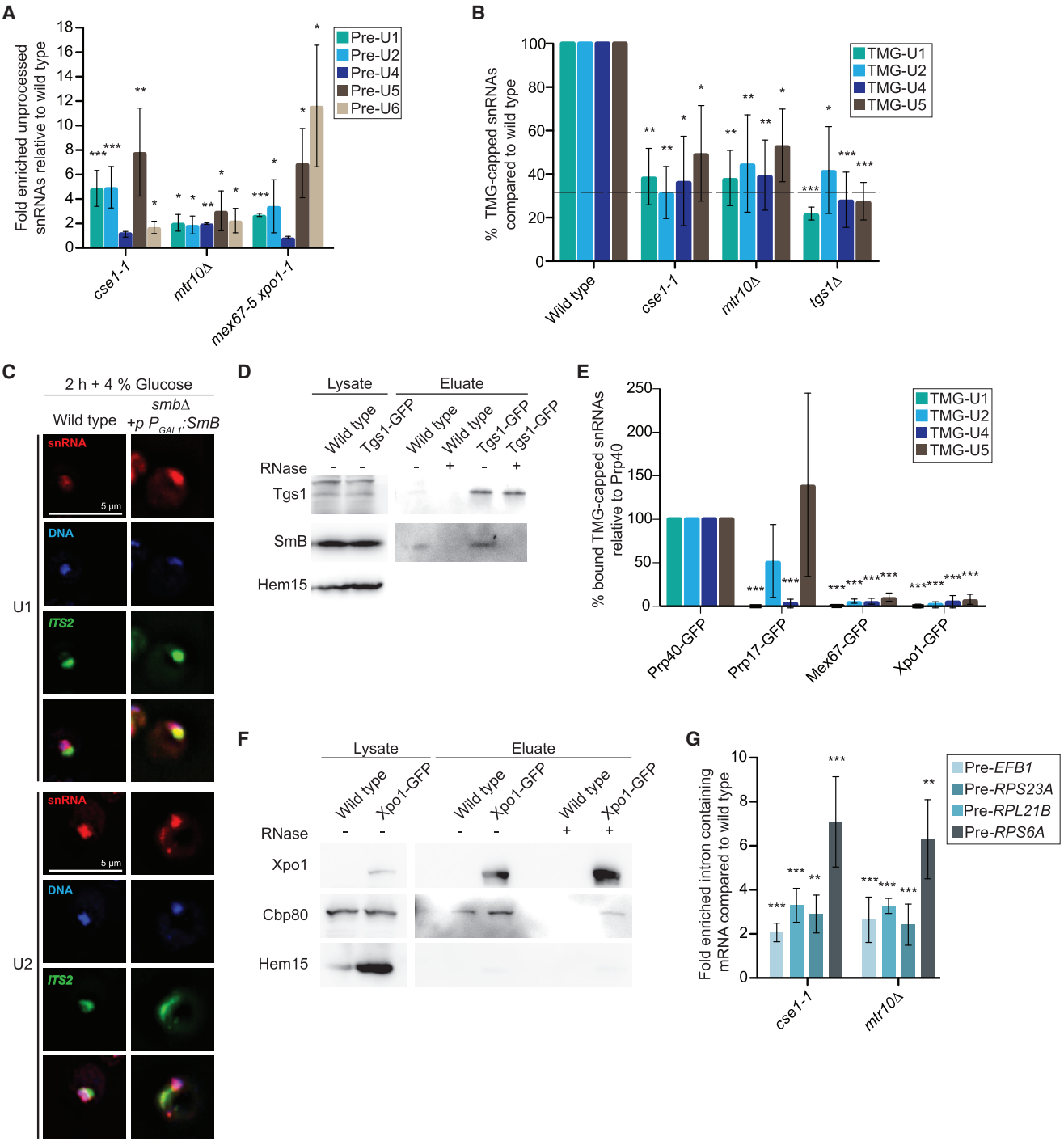

Figure 4. Processing and TMG-Capping of snRNAs Occur in the Nucleus upon snRNA Re-import

(A) Trimming of the snRNAs is carried out in the nucleus upon re-import from the cytoplasm. qRT-PCR analysis revealing the increased presence of the unprocessed snRNAs is shown in the indicated strains, shifted for 1 h to their restrictive temperatures. n = 7 for *cse1-1* strain, n = 5 for *mtr10Δ* strain, and n = 4 for *mex67-5 xpo1-1*.

(B) TMG-capping occurs after nuclear snRNA import. The amount of TMG-capped snRNAs was determined by TMG-co-IPs and subsequent qRT-PCRs from the indicated strains. *tgs1Δ* served as a positive control, and the black line indicates the amount of the precipitated non-TMG-capped RNAs resembling the baseline for TMG-capping. n = 3.

(legend continued on next page)

snRNA Cleavage and TMG-Capping Are Carried Out in the Nucleus

Sm-ring loading occurs prior to the Rnt1-mediated trimming of the snRNA precursors and is followed by the 3′-to-5′ degradation by the nuclear exosome up to the Sm-ring (Seipelt et al., 1999; Coy et al., 2013; Shukla and Parker, 2014). Thus, trimming should occur after nuclear re-import, as Rnt1 is localized to the nucleus (Catala et al., 2004). Also, the final trimming of the Pol III-generated tail from U6 by Usb1 most likely occurs in the nucleus, as this nuclease is restricted to this compartment (Mroczek et al., 2012). To investigate whether the 3′-trimming indeed occurs after snRNA shuttling, we analyzed the length of the snRNAs via qRT-PCR in the import mutants *cse1-1* and *mtr10Δ*, in which the Sm- and Lsm-rings were assembled and in the export mutant *mex67-5 xpo1-1*. An example of how the primers were chosen for U1 to distinguish the precursor from the mature form is provided in Figure S4A. Similar primer setups were chosen also for the other snRNAs. We found that the long precursors indeed accumulated in all mutants that prevent shuttling (Figure 4A). Therefore, we concluded that the pre-snRNAs are trimmed after their re-import into the nucleus and that they require the correct cytoplasmic loading of the Sm-/Lsm-ring for subsequent processing steps.

Further processing of snRNAs is accomplished by trimethylation of the 5′-cap. In humans, this step occurs in the cytoplasm and triggers the formation of the Ran-dependent import complex comprised of the importin-adaptor SPN and its receptor importin β, leading to subsequent nuclear import (Matera and Wang, 2014). In contrast, yeast Tgs1 is localized to the nucleolus (Mouaikel et al., 2002). We investigated whether TMG-capping in yeast occurs before or after shuttling by RIP experiments with a TMG-specific antibody in the snRNA re-import mutants. Because the antibody does not exclusively detect trimethylated caps, but also mentionable amounts of m^7G-capped RNAs, we used the *tgs1Δ* mutant to determine the baseline of the TMG detection. Significantly reduced amounts of TMG-capped snRNAs were detected, revealing that shuttling and Sm-ring loading occurs before the addition of the TMG-cap (Figure 4B). Our finding is in agreement with other studies that have shown that the Sm-ring is crucial for trimethylation of the cap (Mattaj, 1986). Furthermore, we show that snRNAs are retained in the nucleolus when SmB is depleted (Figures 4C and S4B), which indicates that an intact Sm-ring is required for efficient trimethylation and subsequent nucleolar release into the nucleoplasm. It is possible that SmB assists TMG-capping, as it interacts with Tgs1 *in vivo* (Figure 4D) and *in vitro* (Mouaikel et al., 2002). This interaction most likely only occurs when the proteins are bound to RNA, as it is RNase sensitive. This makes sense as it might prevent the recruitment of free SmB into the nucleolus, which could compete with the snRNP-bound SmB and subsequently lead to decreased snRNP recruitment. Reassuringly, we detected the binding of the TMG-capped snRNA and the splicing factor Prp40, but in comparison nearly no binding to the nuclear export factors, Xpo1 and Mex67 (Figures 4E, S4C, and S4D). Prp17 served in this assay as a positive and negative control, because it interacts only with U2 and U5 but not with U1 and U4 (Sapra et al., 2008). These data support a model in which the export factors only contact the monomethyl m^7G-cap-containing snRNAs.

As TMG-capping might be the final step in snRNA processing, we wondered whether this type of 5′-cap would possibly prevent re-export. A deletion of *TGS1* is cold sensitive (Schwer et al., 2011), which might result from a constant leakage of m^7G-capped snRNAs into the cytoplasm, reducing the availability of snRNAs for the spliceosome. It is conceivable that the m^7G-cap-dependent CBC-binding plays a crucial role in export; in particular, because *tgs1Δ* cells showed an increased binding of snRNAs to CBC and mutations in *CBP20* rescued the growth defect of *tgs1Δ* (Schwer et al., 2011), which could be due to a reduction of the constant export of the m^7G-capped snRNAs into the cytoplasm. Thus, we investigated whether Xpo1 might contact CBC. Indeed, co-IPs revealed a physical, RNase-insensitive interaction between Xpo1 and Cbp80 (Figures 4F and S4E). This suggests that Xpo1 participates in the export of snRNAs and also mRNAs, as both RNAs bind CBC at their 5′-caps and both RNA species are mislocalized in *xpo1-1* mutants (Figure 1A). Whether this occurs directly or via an unknown adaptor protein remains to be shown. Nevertheless, our data suggest a model in which TMG-capping finalizes nucleo-cytoplasmic shuttling in yeast. From an evolutional point of view, it is interesting to note that in higher eukaryotes the trimethylation step moved to the cytoplasm, which had the advantage of the development of a specific import factor for snRNAs, SPN (Matera and Wang, 2014), that ensures that only fully matured snRNAs can re-enter the nucleus. Therefore, SPN understandably lacks homologs in yeast.

In summary, pre-snRNAs shuttling to the cytoplasm is highly conserved and also present in yeast. Shuttling, and subsequent Sm/Lsm-ring assembly, is obligatory for the generation of mature snRNPs. Therefore, preventing the nuclear import of the snRNAs as factual in *cse1-1* and *mtr10Δ* mutants, should result in splicing defects, which were indeed detected (Figure 4G).

(C) SmB is required for proper nucleolar localization of the snRNAs. FISH experiments with Cy3-labeled specific probes against U1 and U2 were co-localized with a specific Atto488-labeled probe targeting the internal transcribed spacer region 2 (*ITS2*) of the 35S pre-rRNA in the nucleolus. Localization studies were carried out in wild-type and cells depleted for SmB and are shown after deconvolution. n = 3.

(D) Tgs1 interacts with SmB *in vivo*. Co-IP with Tgs1-GFP reveals a physical interaction with SmB-myc detected in western blots. n = 3.

(E) Xpo1/Crm1 and Mex67 interact preferentially with m^7G-capped snRNAs, while TMG-capped snRNAs are mostly bound by splicing factors. In this two-step-experiment, we first performed a RIP experiment in which the protein associated RNA of the indicated factors was purified. In a second step, a co-IP was carried out with a TMG-cap-specific antibody. Prp40 interacts with U1, U2, U4, and U5, while Prp17 as a later splicing factor only interacts with U2 and U5. n = 3.

(F) Xpo1 interacts with the cap binding complex. Western blot of co-IP of Xpo1-GFP with Cbp80-myc is shown. n = 3.

(G) Blocking nuclear import of snRNAs leads to splicing defects. The ratio of unspliced products of the indicated pre-mRNAs and total mRNAs were detected via qRT-PCR in the indicated strains. n = 6 for *cse1-1* strain; n = 5 for *mtr10Δ* strain

snRNA Shuttling Prevents the Assembly of "Immature Spliceosomes"

After showing that snRNA shuttling is common to eukaryotes and that also *S. cerevisiae* is no exception in evolution, we used this model organism to address the important unsolved question why snRNA shuttling is physiologically important.

Although it has been speculated earlier that the separation of the place of maturation in the cytoplasm from the place of function in the nucleus might prevent the incorporation of immature snRNPs into the spliceosome, which might jeopardize splicing (Matera and Wang, 2014), there is no experimental evidence available that supports such a model. Interestingly, m^7G-capped snRNAs have been found to be associated with the spliceosome in *tgs1Δ* cells (Schwer et al., 2011), suggesting that snRNPs with 5′-caps that are not trimethylated can be assembled when they come in contact with their substrate. This defect produces only a mild growth defect, because TMG-capping is just the last step of maturation that is missing, which we suggest keeps fully matured snRNAs in the nucleus and thus might result in only slight nuclear snRNA depletion. In contrast, keeping immature pre-snRNAs in the nucleus might be more destructive as defective spliceosomes could be produced. To investigate this directly, we blocked export and found that the nuclear retained immature pre-snRNAs were indeed incorporated into the spliceosomal particles. This was determined by RIP experiments in wild-type and *mex67-5* mutants with Prp40, which is part of the pre-catalytic spliceosomal complex B (Will and Lührmann, 2001). In subsequent qRT-PCR experiments with primers that either detect a total snRNA species, or the immature snRNA species, we found a ~40-fold increase of the U1 precursor for instance bound to Prp40 in *mex67-5* cells compared to wild-type (Figure 5A). But also increased amounts of the other precursors were found to interact with Prp40, when their export was blocked (Figures 5A and S5A). Importantly, these "immature spliceosomal particles" produce significant genome-wide splicing defects (Figures 5B–5D, S5B, and S5C; Data S1), suggesting that spliceosomes do not select mature snRNAs for incorporation. It is possible that the longer precursor generates structural problems and that the association with proteins to the RNA scaffold is incorrect, which might affect spliceosome function. In fact, recent work showed that structural changes indeed affect the protein binding to the snRNPs (Hardin et al., 2015).

To exclude that these effects result from other defects caused by the RNA-export block, because also mRNAs accumulate in *mex67-5* and *xpo1-1* mutants (Figures 1A and S1A), we investigated in two additional ways whether spliceosomes are able to distinguish between immature and mature snRNAs. First, we blocked snRNA maturation by inhibition of the Rnt1-mediated cleavage through downregulation of the *RNT1* transcript. The reduction of more than 50% of the *RNT1* transcript level is toxic to cells and leads to the accumulation of uncleaved snRNAs (Figures S6A–S6C), which resulted in an increased presence of the immature forms of the snRNAs in spliceosomes, which again reflects that spliceosomes cannot distinguish between mature and immature constituents (Figures 5E and S6D). Importantly, the incorporation of the longer pre-snRNAs resulted in splicing defects (Figure 5F).

As the downregulation of *RNT1* might also have side effects, we chose a third method of showing that spliceosomes only passively recruit snRNAs. We generated a mutant of U1 with mutated Rnt1 recognition sites, *snr19-rnt1*$^-$ (Figure S6E). This mutant cannot be cleaved by Rnt1 and thus cannot be further trimmed by the nuclear exosome. The resultant immature, long form led to a decreased viability at elevated temperatures and produced ~10-fold increased level of the immature U1 (Figures S6F and S6G). This mutant was also not hindered from incorporation into spliceosomal particles (Figure 5G) and produced splicing defects at 37°C (Figures 5H and S6H), which again suggested that the spliceosomes could not prevent the incorporation of immature or defective snRNAs. As expected, the splicing defects of the *snr19-rnt1*$^-$ mutant were relatively low, because in this case the trimming of only one snRNA was affected. In contrast, the defects for the downregulated *RNT1* are stronger, because it concerns more than one pre-snRNA. However, the strongest effect was obtained by trapping the pre-snRNAs in the nucleus, which might have two reasons. First, there might be higher levels of pre-snRNAs present in the nucleus and, second, the pre-snRNAs did not correctly assemble with the Sm- and Lsm-ring and potentially other proteins that might participate in spliceosome formation.

To strengthen the hypothesis that immature snRNAs can be incorporated into the active spliceosome, additional RIP experiments were carried out. However, this time, we precipitated Snu114, which is part of the later catalytic complexes B^{act} and C. In these late complexes, Snu114 RIP experiments will precipitate U5, as Snu114 is part of the U5 snRNP, but it should also be possible to detect U2, because the U2 and U5 snRNPs contact each other only in the later catalytic complexes B^{act} and C (Will and Lührmann, 2001). So if the U2 precursor was incorporated in the spliceosome, it should be detectable. Indeed, the precipitated Snu114 did not only precipitate the U5 pre-snRNA, but also that of U2 (Figure 5I), which is only possible if the spliceosome assembly took place and passed through complexes A and B and became part of the complex B^{act} (Will and Lührmann, 2001). Because immature snRNAs can in principle be incorporated into assembling spliceosomes and then jeopardize splicing, eukaryotic cells have developed a way to prevent that by immediate nuclear export of immature snRNAs, so that they are out of reach for spliceosome formation.

Taken together, we have shown that the immediate export of pre-snRNAs to the cytoplasm is essential for the generation of functional spliceosomes. The removal of immature pre-snRNAs into another cellular compartment keeps them out of reach of assembling spliceosomes that cannot distinguish between immature and mature components (Figure 6).

DISCUSSION

One characteristic of eukaryotic cells is the separation of the place of transcription and mRNA maturation in the nucleus from the place of translation in the cytoplasm. This prevents the translation of immature, intron-containing transcripts and allowed the establishment of intron sequences. The work presented here shows that the same principle evolved also for

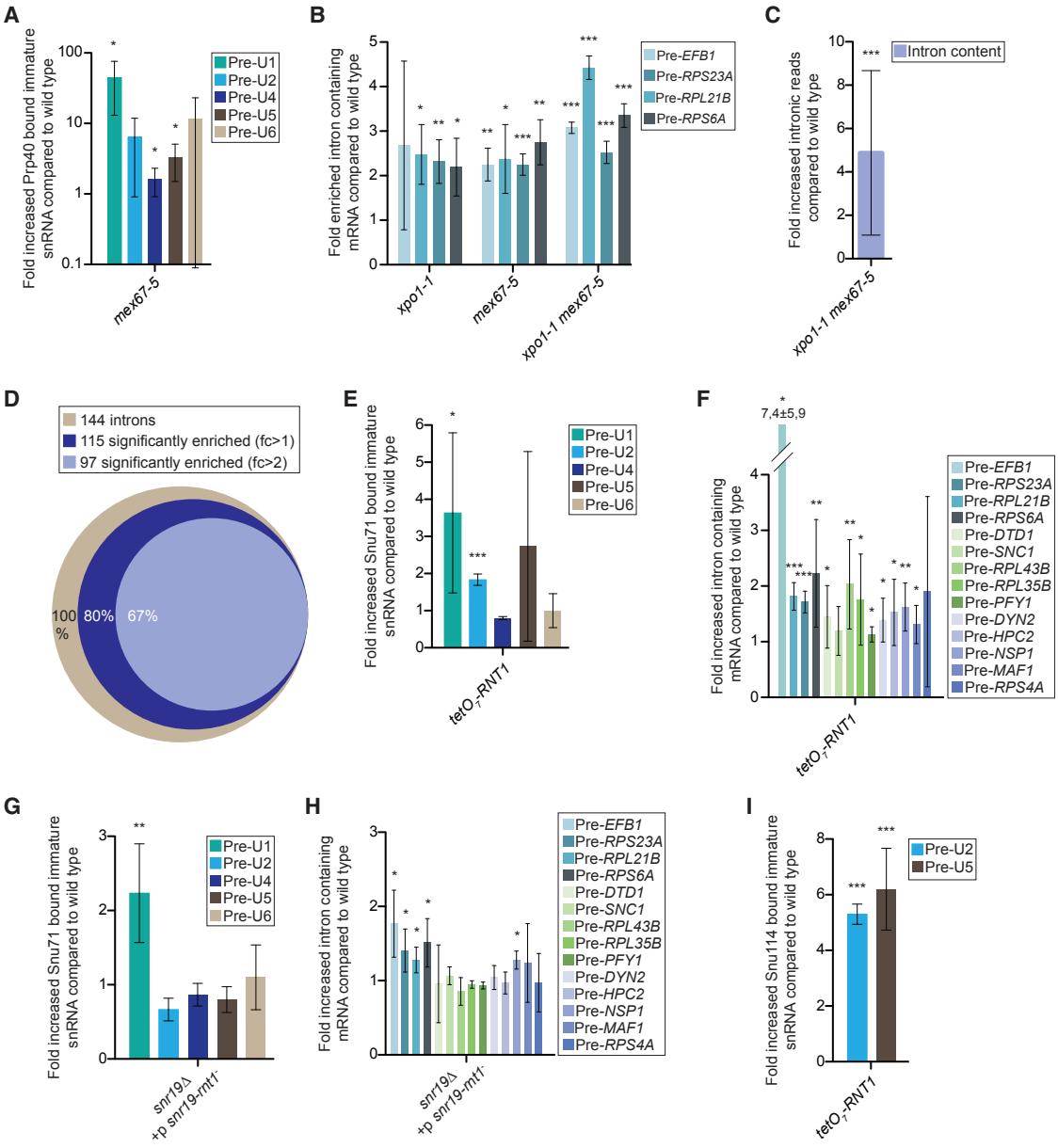

Figure 5. Shuttling of the snRNAs Is a Prerequisite for Proper Spliceosome Assembly and Splicing

(A) Blocking nuclear export of pre-snRNAs leads to the incorporation of these precursors into the spliceosome. RIP experiments with Prp40-GFP in *mex67-5* reveal the presence of immature snRNAs in the spliceosome. n = 4.

(B) Blocking nuclear export of snRNAs leads to splicing defects. Unspliced products of the indicated mRNAs were detected via qRT-PCR in the indicated strains. n = 4.

(C) Genome-wide determination of splicing defects in the snRNA-export mutant *xpo1-1 mex67-5*. RNA-sequencing (RNA-seq) analysis revealed genome-wide increased amounts of intron-containing transcripts in the double mutant compared to wild-type. n = 2.

(D) Number of introns that were increased in *xpo1-1 mex67-5* compared to wild-type detected in the RNA-seq experiment shown in (C). n = 2.

(E) Blocking Rnt1-mediated cleavage of snRNAs leads to the incorporation of immature pre-snRNAs into the spliceosome. RIP experiments with the spliceosomal protein Snu71 reveal the presence of pre-snRNAs in the spliceosome. n = 4.

(F) Blocking Rnt1-mediated cleavage of snRNAs leads to splicing defects. Unspliced products of the indicated mRNAs were detected via qRT-PCR upon *RNT1* downregulation and compared to wild-type. n = 7.

(G) Expression of an Rnt1-insensitive U1 snRNA leads to incorporation of immature pre-U1 snRNA into the spliceosome. RIP experiments with Snu71 reveal the presence of the pre-U1 snRNA in the spliceosome. n = 4.

(H) Expression of an Rnt1-insensitive U1 snRNA leads to splicing defects. Unspliced products of the indicated mRNAs were detected via qRT-PCR in the *snr19-rnt1*$^{-}$ strain shifted to 37°C for 2 h. n = 4.

(I) RIP experiments with the spliceosomal protein Snu114 reveal the presence of pre-snRNAs in the complex B^{act} or C of the late spliceosome. n = 3.

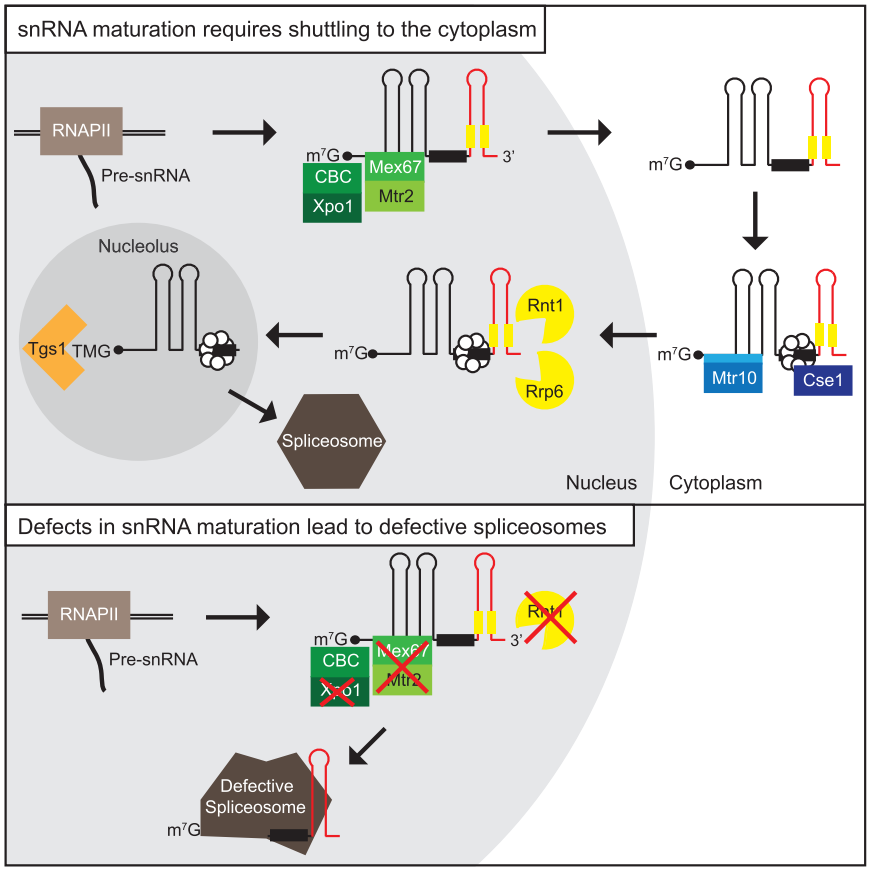

Figure 6. snRNA Maturation Requires the Immediate Pre-snRNA Nuclear Export for Quality Assurance

Top: Pre-snRNA export to the cytoplasm enables the unhindered assembly of the mature spliceosome. Yeast pre-snRNAs are transcribed in the nucleus and immediately exported into the cytoplasm upon binding of the export receptor Mex67-Mtr2 and the karyopherin Xpo1/Crm1, the latter of which interacts with CBC-bound m^7G-caps. Upon export, Mex67 and Xpo1/Crm1 are displaced and the Sm-ring assembles on the pre-snRNP in the cytoplasm. Subsequently, the snRNPs are re-imported back into the nucleus via Mtr10 and Cse1, the latter of which contacts the snRNA via its Sm-ring. In the nucleus, the import receptors dissociate and the pre-snRNA is cleaved by Rnt1 at its 3′-end and further trimmed up to the Sm-ring by the nuclear exosome. Finally, TMG-capping occurs in the nucleolus assisted by SmB, which interacts with Tgs1. This step terminates shuttling, because export receptors cannot be loaded anymore. Mature snRNAs are incorporated into the spliceosome. We have depicted a scheme of the structure of U1 as an example for the snRNAs in this model. Bottom: Pre-snRNAs can be incorporated into the spliceosome, when not exported or processed correctly. The spliceosome cannot distinguish between immature and mature snRNAs. Any reason that retains immature pre-snRNA in reach of the spliceosome increases the danger of a recruitment of faulty, immature snRNPs, which results in defective spliceosomes and severe splicing defects.

spliceosomes. snRNAs are transcribed in the nucleus and they have to be quickly exported into the cytoplasm to prevent the unwanted access of the spliceosome. Here, we show that erroneously incorporated pre-snRNAs into the spliceosome jeopardize splicing.

Current literature suggested that snRNA shuttling is not conserved, and it remained an open question why shuttling evolved for human cells (Will and Lührmann, 2001; Matera and Wang, 2014; Sloan et al., 2016; Vasianovich and Wellinger, 2017). Here, we have shown that *S. cerevisiae* is no exception in evolution. Upon transcription, snRNAs are exported into the cytoplasm by the mRNA-export receptor Mex67 and the nuclear export signal (NES)-export receptor Xpo1/Crm1 (Figures 1A–1C). Mex67 is able to directly bind RNA (Yao et al., 2007; Zander et al., 2016), including snRNA (Figure 1D), and might therefore also export snRNAs in direct association. Alternatively, it is also possible that Mex67-adaptor proteins are involved in the nuclear export and Mex67 is recruited via them. The Mex67 adaptor proteins Npl3, Gbp2, Hrb1, and Nab2 function as guard proteins for pre-mRNA maturation and in this way prevent a premature access of Mex67 and thus the export of immature mRNAs (Zander et al., 2016; Zander and Krebber, 2017). Interestingly, they bind also to the snRNAs (Figure 1G). However, their role in the quality control of the snRNA maturation needs to be determined in future experiments.

Xpo1/Crm1 supports snRNA export (Figures 1A–1C and 1E). It contacts the snRNAs through interaction with the CBC, associated with the monomethyl cap (Figure 4F), which is typically found on Pol II transcripts. This is in principle very similar to the situation in human cells; however, in addition to CRM1, a particular CBC adaptor protein, PHAX, is required to recruit CRM1 for nuclear export via the Ran GTPase system (Köhler and Hurt, 2007; Matera and Wang, 2014). Whether such an adaptor for Xpo1 is also present in yeast is currently unclear; however, the mechanism is conserved as Xpo1 contacts the CBC (Figure 4F).

The current view is that the Pol III transcribed U6 snRNA also in human cells does not shuttle (Sloan et al., 2016). Remarkably, for yeast, we show that U6 enters the cytoplasm via Mex67 (Figure 1). However, its export is not much affected in *xpo1-1*, most likely because U6 does not contain a monomethyl cap, and its nuclear export is thus independent of Xpo1/Crm1 (Figures 1A–1C). The slight effect seen for U6 in *xpo1-1* might have secondary reasons, resulting from the depletion of available Mex67, as it accumulates on the other snRNAs and mRNAs that are retained in *xpo1-1* (Figure 1).

In human cells, it was shown that the addition of the Sm-ring occurs in the cytoplasm (Matera and Wang, 2014), while this was suggested to happen in the nucleus of yeast cells, as NLSs were identified in SmD1, D3, and SmB (Bordonné, 2000). Here, we have shown that also in yeast Sm-ring assembly on

the snRNAs occurs in the cytoplasm, because Sm-proteins do not interact with the snRNAs in nuclear export mutants (Figure 3E). Most importantly, mutations of the NLSs do not only lead to the cytoplasmic mislocalization of the Sm-proteins, but also to the cytoplasmic mislocalization of the snRNAs (Figure 3C). Thus, it seemed likely that the Sm-ring contributes to the nuclear import of snRNAs. Interestingly, neither mutations in importin α (*srp1-31*) nor in importin β (*kap95E126K*) affect the nuclear localization of the snRNAs (Figures 2A and 2B). Therefore, it is evident that, after Sm-ring assembly, the identified NLSs play no role in nuclear import of the snRNPs. Instead, we show that SmB contacts Cse1 (Figure 3D).

snRNA trimming should take place on the Sm-ring-bound snRNA, because the ring restricts further degradation and thus elimination of the snRNA from the cell. While this step is anticipated to be cytoplasmic in human cells, as precursors accumulate in the cytoplasm (Huang and Pederson, 1999), it occurs in the nucleus of yeast through cleavage of Rnt1 and subsequent 3′-to-5′ degradation by the nuclear exosome up to the Sm-ring (Seipelt et al., 1999; Coy et al., 2013; Shukla and Parker, 2014). For this reason, pre-snRNAs accumulate in nuclear import mutants (Figure 4A). It remains to be shown whether the pre-snRNA shortening in human cells is indeed cytoplasmic, because the trimming enzyme is unknown (Matera et al., 2007).

An interesting difference for human and yeast cells is the place of the addition of the TMG-cap. In yeast, Tgs1 is localized to the nucleolus, and we have shown that trimethylation occurs after snRNA shuttling (Figure 4B). In human cells, this step moved to the cytoplasm, which allowed the development of a specific TMG-binding protein, SPN, that supports nuclear import via importin β (Will and Lührmann, 2001; Matera and Wang, 2014; Sloan et al., 2016). Interestingly, besides importin β, also importin 7 and the SMN complex support nuclear import in human cells (Fischer et al., 1994; Ospina et al., 2005; Natalizio and Matera, 2013), suggesting that joint effort is necessary to transport these huge ribonucleoparticles through the hydrophobic interior of the NPC. Our work identifies two import factors for snRNAs in yeast: Mtr10 and Cse1 (Figure 2). Mtr10 was already identified to import another ncRNA, *TLC1* of the telomerase (Gallardo and Chartrand, 2008). Additionally, it reimports several of the guard proteins that function as adaptor proteins for Mex67 and accompany mRNAs to the cytoplasm (Segref et al., 1997; Windgassen and Krebber, 2003; Häcker and Krebber, 2004). Whether the guard proteins function also as adaptor proteins between *TLC1* and/or the snRNAs and Mtr10 is currently unknown. Interestingly, the homolog of Mtr10 in human cells is Transportin-SR, which in analogy imports the Mex67-adaptor proteins, SRSF1 (SF1/ASF), SRSF3 (SRp20), and SRSF7 (9G8) that are homologs to the yeast guard proteins (Huang and Steitz, 2005).

The second nuclear import factor is Cse1, which contacts the snRNA at its Sm-ring (Figures 2 and 3D). This interaction may serve as a signal for the completed cytoplasmic maturation of the snRNP and induce nuclear import. With identifying the snRNAs as the first nuclear import substrates for Cse1 (Figure 2), is noteworthy that this karyopherin is one of the few transport receptors that moves cargoes in both directions, because it exports also importin α (Cook et al., 2007). It will be interesting for the future to explore potential similarities for the human homologs of Cse1 and Mtr10, CAS and Transportin-SR, respectively.

Although shuttling had not been reported for U6, even in human cells (Bertrand and Bordonné, 2004; Matera et al., 2007; Sloan et al., 2016), we found that U6 is exported in yeast via Mex67 (Figures 1A and 1B). Interestingly, in contrast to the other snRNAs, U6 does not utilize Xpo1/Crm1 as a supporting export factor, which is most likely due to its unique γ-monomethyl phosphate cap structure. In fact, Xpo1-mediated export of the Pol II-transcribed snRNAs involves the m^7G-cap binding complex CBC, with which Xpo1 interacts (Figure 4F). It remains to be shown whether U6 in higher eukaryotes also undergoes a cytoplasmic phase. However, it seems most likely as immature pre-U6 can also be captured by the spliceosome, which jeopardizes splicing (Figure 5).

Recent reviews on snRNA biogenesis speculated that their shuttling could provide a plausible mechanism for quality control, as the contact of immature snRNAs with the spliceosome would be prevented (Matera and Wang, 2014; Sloan et al., 2016). Because evidence for such a model was lacking, we used yeast as a eukaryotic model organism to address this question with three independent methods. We blocked snRNA export to retain immature snRNAs in the nucleus, we depleted the cleaving enzyme Rnt1, and we mutated the cleavage site in U1, and show with each method that pre-snRNAs are subsequently assembled into defective spliceosomes (Figure 5). Thus, this molecular machine cannot select for matured snRNAs, and because it is unable to distinguish between immature and mature forms, it builds functionally disabled spliceosomes when the pre-snRNAs come into contact with them. Consequently, these impaired spliceosomes produce general, genome-wide splicing defects (Figure 5). Therefore, the immediate nuclear export of immature pre-snRNAs is required for the production of functional spliceosomes and indeed resembles a quality control mechanism (Figure 6). Maturation and proper formation of the protein-associated snRNPs can occur without time limitations and without permanent recruitment attempts from arising spliceosomes. Thus, separation of the place of maturation and the place of function represents an elegant way of quality assurance to generate fully functional molecular machines.

The generation of correct molecular machines is in general important for cellular fitness and survival. Compartmentalization separates in several cases the places of synthesis and the places of function. Ribosomes are synthesized as ribosomal subunits in the nucleus and function as decoding machines in the cytoplasm. Their functionality is proved and defective ribosomes are eliminated by the ribosome quality control (RQC) (Sarkar et al., 2017). Similarly, aberrantly processed mRNAs are detected in the nucleus by the guard proteins that initiate faulty mRNA degradation (Zander et al., 2016; Zander and Krebber, 2017). In particular, Gbp2 and Hrb1 are important for the elimination of pre-mRNAs with splicing defects (Hackmann et al., 2014). Furthermore, mRNAs are monitored for a functional open reading frame and eliminated in the cytoplasm in case of defects by the no-stop-, no-go-, and the nonsense-mediated decay pathways (Shoemaker and Green, 2012; Brogna et al., 2016).

Because all these fail-safe systems exist, it seems on the first sight not necessary to have an additional quality assurance system that warrants the functionality of the spliceosomes. However, without the quick nuclear export of immature pre-snRNAs, cells would be overwhelmed with disabled spliceosomes and non-spliced transcripts (Figure 5). Therefore, we suggest that the instant export of immature pre-snRNAs is a quality assurance mechanism, obligatory for all eukaryotes to ensure functional spliceosomes and efficient splicing.

STAR★METHODS

Detailed methods are provided in the online version of this paper and include the following:

- KEY RESOURCES TABLE
- CONTACT FOR REAGENT AND RESOURCE SHARING
- EXPERIMENTAL MODEL AND SUBJECT DETAILS
- METHOD DETAILS
  - Fluorescent *in situ* hybridization experiments (FISH)
  - RNA co-immunoprecipitation experiments (RIP)
  - *In vitro* binding studies
  - Cytoplasmic fractionation
  - GFP-microscopy
  - Co-immunoprecipitation (IP) experiments
  - RNA-sequencing
- QUANTIFICATION AND STATISTICAL ANALYSIS
- DATA AND SOFTWARE AVAILABILITY

SUPPLEMENTAL INFORMATION

Supplemental Information can be found online at https://doi.org/10.1016/j.celrep.2019.05.031.

ACKNOWLEDGMENTS

We thank H. Bastians and G. Zander for discussion and comments on the manuscript. We are also very thankful to G. Matera for his thoughtful comments and suggestions. We are grateful to J. Beggs, R. Bordonné, P. Fabrizio, R. Ficner, R. Lill, R. Lührmann, P.A. Silver, E. Hurt, B. Seraphin, K. Weis, and S. Wente for providing plasmids, strains, or antibodies. This work was funded by grants of the GGNB to D.B. and the Deutsche Forschungsgemeinschaft (DFG) and the SFB860 awarded to H.K.

AUTHOR CONTRIBUTIONS

Experiments were designed and data interpreted by D.B., A.G.H., L.B., T.L., G.S., and H.K.; all experiments were performed by D.B. except Figure 1F, which was executed by D.B. and L.B.; Figure 2C, by D.B. and A.G.H.; Figures 1C, 1G, and 3G, by A.G.H.; and Figures 5C and 5D, which was carried out by D.B., T.L., and G.S. The manuscript was written by H.K.; all authors discussed the results and commented on the manuscript.

DECLARATION OF INTERESTS

The authors declare no competing interests.

Received: September 5, 2018
Revised: April 3, 2019
Accepted: May 9, 2019
Published: June 11, 2019

SUPPORTING CITATIONS

The following references appear in the Supplemental Information: Brune et al. (2005); Gorsch et al. (1995); Legrain and Rosbash (1989); Liu et al. (1999); Loeb et al. (1995); Pemberton et al. (1999); Ryan et al. (2007); Seedorf and Silver (1997); Senger et al. (1998); Sikorski and Hieter (1989); Snay-Hodge et al. (1998); Taura et al. (1998); Winston et al. (1995); Titov and Blobel (1999); and Xiao et al. (1993).

REFERENCES

Bertrand, E., and Bordonné, R. (2004). Assembly and traffic of small nuclear RNPs. Prog. Mol. Subcell. Biol. *35*, 79–97.

Bordonné, R. (2000). Functional characterization of nuclear localization signals in yeast Sm proteins. Mol. Cell. Biol. *20*, 7943–7954.

Brogna, S., McLeod, T., and Petric, M. (2016). The meaning of NMD: translate or perish. Trends Genet. *32*, 395–407.

Brune, C., Munchel, S.E., Fischer, N., Podtelejnikov, A.V., and Weis, K. (2005). Yeast poly(A)-binding protein Pab1 shuttles between the nucleus and the cytoplasm and functions in mRNA export. RNA *11*, 517–531.

Catala, M., Lamontagne, B., Larose, S., Ghazal, G., and Elela, S.A. (2004). Cell cycle-dependent nuclear localization of yeast RNase III is required for efficient cell division. Mol. Biol. Cell *15*, 3015–3030.

Cook, A., Bono, F., Jinek, M., and Conti, E. (2007). Structural biology of nucleocytoplasmic transport. Annu. Rev. Biochem. *76*, 647–671.

Coy, S., Volanakis, A., Shah, S., and Vasiljeva, L. (2013). The Sm complex is required for the processing of non-coding RNAs by the exosome. PLoS ONE *8*, e65606.

Didychuk, A.L., Butcher, S.E., and Brow, D.A. (2018). The life of U6 small nuclear RNA, from cradle to grave. RNA *24*, 437–460.

Dobin, A., Davis, C.A., Schlesinger, F., Drenkow, J., Zaleski, C., Jha, S., Batut, P., Chaisson, M., and Gingeras, T.R. (2013). STAR: ultrafast universal RNA-seq aligner. Bioinformatics *29*, 15–21.

Fischer, U., Heinrich, J., van Zee, K., Fanning, E., and Lührmann, R. (1994). Nuclear transport of U1 snRNP in somatic cells: differences in signal requirement compared with *Xenopus laevis* oocytes. J. Cell Biol. *125*, 971–980.

Gallardo, F., and Chartrand, P. (2008). Telomerase biogenesis: the long road before getting to the end. RNA Biol. *5*, 212–215.

Gallardo, F., Olivier, C., Dandjinou, A.T., Wellinger, R.J., and Chartrand, P. (2008). TLC1 RNA nucleo-cytoplasmic trafficking links telomerase biogenesis to its recruitment to telomeres. EMBO J. *27*, 748–757.

Gorsch, L.C., Dockendorff, T.C., and Cole, C.N. (1995). A conditional allele of the novel repeat-containing yeast nucleoporin RAT7/NUP159 causes both rapid cessation of mRNA export and reversible clustering of nuclear pore complexes. J. Cell Biol. *129*, 939–955.

Gottschalk, A., Tang, J., Puig, O., Salgado, J., Neubauer, G., Colot, H.V., Mann, M., Seraphin, B., Rosbash, M., Luhrmann, R., et al. (1998). A comprehensive biochemical and genetic analysis of the yeast U1 snRNP reveals five novel proteins. RNA *4*, 374–393.

Häcker, S., and Krebber, H. (2004). Differential export requirements for shuttling serine/arginine-type mRNA-binding proteins. J. Biol. Chem. *279*, 5049–5052.

Hackmann, A., Wu, H., Schneider, U.M., Meyer, K., Jung, K., and Krebber, H. (2014). Quality control of spliced mRNAs requires the shuttling SR proteins Gbp2 and Hrb1. Nat. Commun. *5*, 3123.

Hardin, J.W., Warnasooriya, C., Kondo, Y., Nagai, K., and Rueda, D. (2015). Assembly and dynamics of the U4/U6 di-snRNP by single-molecule FRET. Nucleic Acids Res. *43*, 10963–10974.

Hood, J.K., and Silver, P.A. (1998). Cse1p is required for export of Srp1p/importin-alpha from the nucleus in Saccharomyces cerevisiae. J. Biol. Chem. *273*, 35142–35146.

Huang, Q., and Pederson, T. (1999). A human U2 RNA mutant stalled in 3′ end processing is impaired in nuclear import. Nucleic Acids Res. *27*, 1025–1031.

Huang, Y., and Steitz, J.A. (2005). SRprises along a messenger's journey. Mol. Cell *17*, 613–615.

Köhler, A., and Hurt, E. (2007). Exporting RNA from the nucleus to the cytoplasm. Nat. Rev. Mol. Cell Biol. *8*, 761–773.

Lefebvre, S., Bürglen, L., Reboullet, S., Clermont, O., Burlet, P., Viollet, L., Benichou, B., Cruaud, C., Millasseau, P., Zeviani, M., et al. (1995). Identification and characterization of a spinal muscular atrophy-determining gene. Cell *80*, 155–165.

Legrain, P., and Rosbash, M. (1989). Some *cis*- and *trans*-acting mutants for splicing target pre-mRNA to the cytoplasm. Cell *57*, 573–583.

Liao, Y., Smyth, G.K., and Shi, W. (2014). featureCounts: an efficient general purpose program for assigning sequence reads to genomic features. Bioinformatics *30*, 923–930.

Liu, Y., Guo, W., Tartakoff, P.Y., and Tartakoff, A.M. (1999). A Crm1p-independent nuclear export path for the mRNA-associated protein, Npl3p/Mtr13p. Proc. Natl. Acad. Sci. USA *96*, 6739–6744.

Loeb, J.D., Schlenstedt, G., Pellman, D., Kornitzer, D., Silver, P.A., and Fink, G.R. (1995). The yeast nuclear import receptor is required for mitosis. Proc. Natl. Acad. Sci. USA *92*, 7647–7651.

Lorson, C.L., Rindt, H., and Shababi, M. (2010). Spinal muscular atrophy: mechanisms and therapeutic strategies. Hum. Mol. Genet. *19* (*R1*), R111–R118.

Love, M.I., Huber, W., and Anders, S. (2014). Moderated estimation of fold change and dispersion for RNA-seq data with DESeq2. Genome Biol. *15*, 550.

Matera, A.G., and Wang, Z. (2014). A day in the life of the spliceosome. Nat. Rev. Mol. Cell Biol. *15*, 108–121.

Matera, A.G., Terns, R.M., and Terns, M.P. (2007). Non-coding RNAs: lessons from the small nuclear and small nucleolar RNAs. Nat. Rev. Mol. Cell Biol. *8*, 209–220.

Mattaj, I.W. (1986). Cap trimethylation of U snRNA is cytoplasmic and dependent on U snRNP protein binding. Cell *46*, 905–911.

Mouaikel, J., Verheggen, C., Bertrand, E., Tazi, J., and Bordonné, R. (2002). Hypermethylation of the cap structure of both yeast snRNAs and snoRNAs requires a conserved methyltransferase that is localized to the nucleolus. Mol. Cell *9*, 891–901.

Mroczek, S., Krwawicz, J., Kutner, J., Lazniewski, M., Kuciński, I., Ginalski, K., and Dziembowski, A. (2012). C16orf57, a gene mutated in poikiloderma with neutropenia, encodes a putative phosphodiesterase responsible for the U6 snRNA *3′* end modification. Genes Dev. *26*, 1911–1925.

Murphy, M.W., Olson, B.L., and Siliciano, P.G. (2004). The yeast splicing factor Prp40p contains functional leucine-rich nuclear export signals that are essential for splicing. Genetics *166*, 53–65.

Natalizio, A.H., and Matera, A.G. (2013). Identification and characterization of Drosophila Snurportin reveals a role for the import receptor Moleskin/importin-7 in snRNP biogenesis. Mol. Biol. Cell *24*, 2932–2942.

Neville, M., and Rosbash, M. (1999). The NES-Crm1p export pathway is not a major mRNA export route in Saccharomyces cerevisiae. EMBO J. *18*, 3746–3756.

Noble, S.M., and Guthrie, C. (1996). Transcriptional pulse-chase analysis reveals a role for a novel snRNP-associated protein in the manufacture of spliceosomal snRNPs. EMBO J. *15*, 4368–4379.

Olson, B.L., and Siliciano, P.G. (2003). A diverse set of nuclear RNAs transfer between nuclei of yeast heterokaryons. Yeast *20*, 893–903.

Ospina, J.K., Gonsalvez, G.B., Bednenko, J., Darzynkiewicz, E., Gerace, L., and Matera, A.G. (2005). Cross-talk between snurportin1 subdomains. Mol. Biol. Cell *16*, 4660–4671.

Pannone, B.K., Xue, D., and Wolin, S.L. (1998). A role for the yeast La protein in U6 snRNP assembly: evidence that the La protein is a molecular chaperone for RNA polymerase III transcripts. EMBO J. *17*, 7442–7453.

Pemberton, L.F., Rosenblum, J.S., and Blobel, G. (1999). Nuclear import of the TATA-binding protein: mediation by the karyopherin Kap114p and a possible mechanism for intranuclear targeting. J. Cell Biol. *145*, 1407–1417.

Roithová, A., Klimešová, K., Pánek, J., Will, C.L., Lührmann, R., Stanek, D., and Girard, C. (2018). The Sm-core mediates the retention of partially-assembled spliceosomal snRNPs in Cajal bodies until their full maturation. Nucleic Acids Res. *46*, 3774–3790.

Ryan, K.J., Zhou, Y., and Wente, S.R. (2007). The karyopherin Kap95 regulates nuclear pore complex assembly into intact nuclear envelopes in vivo. Mol. Biol. Cell *18*, 886–898.

Sapra, A.K., Khandelia, P., and Vijayraghavan, U. (2008). The splicing factor Prp17 interacts with the U2, U5 and U6 snRNPs and associates with the spliceosome pre- and post-catalysis. Biochem. J. *416*, 365–374.

Sarkar, A., Thoms, M., Barrio-Garcia, C., Thomson, E., Flemming, D., Beckmann, R., and Hurt, E. (2017). Preribosomes escaping from the nucleus are caught during translation by cytoplasmic quality control. Nat. Struct. Mol. Biol. *24*, 1107–1115.

Schwer, B., Erdjument-Bromage, H., and Shuman, S. (2011). Composition of yeast snRNPs and snoRNPs in the absence of trimethylguanosine caps reveals nuclear cap binding protein as a gained U1 component implicated in the cold-sensitivity of tgs1Δ cells. Nucleic Acids Res. *39*, 6715–6728.

Seedorf, M., and Silver, P.A. (1997). Importin/karyopherin protein family members required for mRNA export from the nucleus. Proc. Natl. Acad. Sci. USA *94*, 8590–8595.

Segref, A., Sharma, K., Doye, V., Hellwig, A., Huber, J., Lührmann, R., and Hurt, E. (1997). Mex67p, a novel factor for nuclear mRNA export, binds to both poly(A)+ RNA and nuclear pores. EMBO J. *16*, 3256–3271.

Seipelt, R.L., Zheng, B., Asuru, A., and Rymond, B.C. (1999). U1 snRNA is cleaved by RNase III and processed through an Sm site-dependent pathway. Nucleic Acids Res. *27*, 587–595.

Senger, B., Simos, G., Bischoff, F.R., Podtelejnikov, A., Mann, M., and Hurt, E. (1998). Mtr10p functions as a nuclear import receptor for the mRNA-binding protein Npl3p. EMBO J. *17*, 2196–2207.

Shoemaker, C.J., and Green, R. (2012). Translation drives mRNA quality control. Nat. Struct. Mol. Biol. *19*, 594–601.

Shukla, S., and Parker, R. (2014). Quality control of assembly-defective U1 snRNAs by decapping and 5′-to-3′ exonucleolytic digestion. Proc. Natl. Acad. Sci. USA *111*, E3277–E3286.

Sikorski, R.S., and Hieter, P. (1989). A system of shuttle vectors and yeast host strains designed for efficient manipulation of DNA in *Saccharomyces cerevisiae*. Genetics *122*, 19–27.

Sloan, K.E., Gleizes, P.E., and Bohnsack, M.T. (2016). Nucleocytoplasmic transport of RNAs and RNA-protein complexes. J. Mol. Biol. *428* (*10 Pt A*), 2040–2059.

Snay-Hodge, C.A., Colot, H.V., Goldstein, A.L., and Cole, C.N. (1998). Dbp5p/Rat8p is a yeast nuclear pore-associated DEAD-box protein essential for RNA export. EMBO J. *17*, 2663–2676.

Solsbacher, J., Maurer, P., Bischoff, F.R., and Schlenstedt, G. (1998). Cse1p is involved in export of yeast importin alpha from the nucleus. Mol. Cell. Biol. *18*, 6805–6815.

Spiller, M.P., Boon, K.L., Reijns, M.A., and Beggs, J.D. (2007a). The Lsm2-8 complex determines nuclear localization of the spliceosomal U6 snRNA. Nucleic Acids Res. *35*, 923–929.

Spiller, M.P., Reijns, M.A., and Beggs, J.D. (2007b). Requirements for nuclear localization of the Lsm2-8p complex and competition between nuclear and cytoplasmic Lsm complexes. J. Cell Sci. *120*, 4310–4320.

Stade, K., Ford, C.S., Guthrie, C., and Weis, K. (1997). Exportin 1 (Crm1p) is an essential nuclear export factor. Cell *90*, 1041–1050.

Taura, T., Krebber, H., and Silver, P.A. (1998). A member of the Ran-binding protein family, Yrb2p, is involved in nuclear protein export. Proc. Natl. Acad. Sci. USA *95*, 7427–7432.

Tieg, B., and Krebber, H. (2013). Dbp5—from nuclear export to translation. Biochim. Biophys. Acta *1829*, 791–798.

Titov, A.A., and Blobel, G. (1999). The karyopherin Kap122p/Pdr6p imports both subunits of the transcription factor IIA into the nucleus. J. Cell Biol. *147*, 235–246.

Tutucci, E., and Stutz, F. (2011). Keeping mRNPs in check during assembly and nuclear export. Nat. Rev. Mol. Cell Biol. *12*, 377–384.

Vasianovich, Y., and Wellinger, R.J. (2017). Life and death of yeast telomerase RNA. J. Mol. Biol. *429*, 3242–3254.

Wahl, M.C., Will, C.L., and Lührmann, R. (2009). The spliceosome: design principles of a dynamic RNP machine. Cell *136*, 701–718.

Will, C.L., and Lührmann, R. (2001). Spliceosomal UsnRNP biogenesis, structure and function. Curr. Opin. Cell Biol. *13*, 290–301.

Windgassen, M., and Krebber, H. (2003). Identification of Gbp2 as a novel poly(A)+ RNA-binding protein involved in the cytoplasmic delivery of messenger RNAs in yeast. EMBO Rep. *4*, 278–283.

Winston, F., Dollard, C., and Ricupero-Hovasse, S.L. (1995). Construction of a set of convenient *Saccharomyces cerevisiae* strains that are isogenic to S288C. Yeast *11*, 53–55.

Wu, H., Becker, D., and Krebber, H. (2014). Telomerase RNA TLC1 shuttling to the cytoplasm requires mRNA export factors and is important for telomere maintenance. Cell Rep. *8*, 1630–1638.

Xiao, Z., McGrew, J.T., Schroeder, A.J., and Fitzgerald-Hayes, M. (1993). CSE1 and CSE2, two new genes required for accurate mitotic chromosome segregation in *Saccharomyces cerevisiae*. Mol. Cell. Biol. *13*, 4691–4702.

Yao, W., Roser, D., Köhler, A., Bradatsch, B., Bassler, J., and Hurt, E. (2007). Nuclear export of ribosomal 60S subunits by the general mRNA export receptor Mex67-Mtr2. Mol. Cell *26*, 51–62.

Yao, W., Lutzmann, M., and Hurt, E. (2008). A versatile interaction platform on the Mex67-Mtr2 receptor creates an overlap between mRNA and ribosome export. EMBO J. *27*, 6–16.

Zander, G., and Krebber, H. (2017). Quick or quality? How mRNA escapes nuclear quality control during stress. RNA Biol. *14*, 1642–1648.

Zander, G., Hackmann, A., Bender, L., Becker, D., Lingner, T., Salinas, G., and Krebber, H. (2016). mRNA quality control is bypassed for immediate export of stress-responsive transcripts. Nature *540*, 593–596.

STAR★METHODS

KEY RESOURCES TABLE

REAGENT or RESOURCE	SOURCE	IDENTIFIER
Antibodies		
α-Snu71 polyclonal antibody	Gottschalk et al., 1998	N/A
α-Snu114 polyclonal antibody	Gottschalk et al., 1998	N/A
Anti-2,2,7-trimethylguanosine-antibody (K121)	Millipore	Cat# NA02-100UG; RRID:AB_213109
Anti-Zwf1	Sigma	Cat# A9521; RRID:AB_258454
Anti-Nop1 (28F2)	Santa Cruz	Cat# Sc-57940; RRID:AB_630044
Anti-GFP (GF28R)	Pierce	N/A
c-myc (9E10)	Santa Cruz	Cat# Sc-40; RRID:AB_627268
Anti-Hem15	R. Lill	N/A
Anti-Digoxigenin Fab-FITC antibody	Roche	Cat# 11207741910; RRID:AB_514498
Chemicals, Peptides, and Recombinant Proteins		
Doxycycline	PanReac AppliChem	Cat# A2951
Formaldehyde 37%	Carl Roth	Cat# 4979.2
Leptomycin B 98%, 1mM soln. in ethanol	Thermo Fisher (Kandel)	Cas Numer 87081-35-4
mex67-Δloop409-435 and mex67–loopKR > AA proteins in complex with Mtr2	Zander et al., 2016	N/A
Trizol	Ambion by life technologies	Cat# 15596018
Critical Commercial Assays		
Digoxygenin (DIG)-UTP RNA labeling mix	Roche	Cat# 11 277 073 910
Nucleo-Spin RNA Kit	Macherey and Nagel	Cat# 740955
cDNA Synthese –Maxima reverse transcriptase	Thermo Scientific	Cat# EP0741
qRT-PCR	PCRBIOSYSTEMS	Cat# PB20.11
TruSeq RNA Sample Prep Kit v2	Illumina	Cat# RS-122
Deposited Data		
RNA-Sequencing raw data	This paper	GEO: GSE93307
Experimental Models: Organisms/Strains		
S. cerevisiae Strains, see Table S1		N/A
Oligonucleotides		
See Table S2		N/A
Recombinant DNA		
See Table S3		N/A
Software and Algorithms		
Fiji-software	W. Rasband (NIH/USA)	NA
Deconvolution (3 iterations) by the LAS AF 2.7.3.9 software	Leica	N/A
Illumina BaseCaller software *bcl2fastq* (version 2.17)	Illumina	N/A
STAR software	Dobin et al., 2013; version 2.5	N/A
featureCounts (subread version 1.5.0-p1)	Ensembl annotation version 84	N/A
R/Bioconductor environment: *DESeq2* package	Love et al., 2014	http://www.bioconductor.org
Other		
GFP-Trap®-Agarose beads	Chromotek	Cat# gta-400
Protein G Sepharose beads	Amersham Biosciences	N/A

CONTACT FOR REAGENT AND RESOURCE SHARING

Further information and requests for resources and reagents should be directed to and will be fulfilled by the Lead Contact, Heike Krebber (heike.krebber@biologie.uni-goettingen.de).

EXPERIMENTAL MODEL AND SUBJECT DETAILS

All *Saccharomyces cerevisiae* strains used in this study are listed in the Table S1, oligonucleotides in Table S2 and plasmids in Table S3. Plasmids and yeast strains were generated by conventional methods.

METHOD DETAILS

Fluorescent *in situ* hybridization experiments (FISH)

The experiments were essentially carried out as described (Gallardo et al., 2008). RNA probes were synthesized by *in vitro* transcription, using the T7-RNA polymerase (Thermo Scientific) and labeled with digoxygenin (DIG)-UTP using an RNA labeling mix (Roche) or with Cy3-labeled oligonucleotides (Sigma), which are listed in Table S2. To detect poly(A)$^+$ RNA a Cy3-labeled oligo d(T)$_{50}$ probe (Sigma) was used. Co-localization studies were performed using an Atto 488-labeled probe (Sigma) against *ITS2*. Cells were grown to mid log phase (1x10^7 cells/ml) prior to the indicated temperature shifts to 37°C, 30°C or 16°C for 1 h (Figures 1A, 2A, 3A, 3F–3H, S1A–S1C, S2B, S2C, S3A, and S3H). For Sm-ring dependent localization studies, cells were grown to log phase in YP medium containing 2% galactose. Afterward 4% glucose was added and cells were incubated at 25°C for 2 h (Figures 3C, 4C, S3B, and S4B). Samples were fixed by adding formaldehyde to a final concentration of 4% for 45 min at room temperature. Cells were spheroplasted by adding zymoylase, subsequently permeabilized in 0.1 M potassium phosphate buffer pH 6.5, 1.2 M sorbitol, 0.5% Triton® X-100, pre-hybridized with Hybmix (50% deionized formamide, 5 × SSC, 1x Denhardts, 500 μg/ml tRNA, 500 μg/ml salmon sperm DNA, 50 μg/ml heparin, 2.5 mM EDTA pH 8.0, 0.1% Tween® 20, 10% dextran sulfate) for 1 h on a polylysine coated slide at 37°C and hybridized in Hybmix with the specific probe over night at 37°C. After hybridization, cells were washed with 2x SSC and 1x SSC at room temperature, each for 1 h and 0.5x SSC at 37°C and room temperature, each for 30 min. For detection of DIG probes the cells were treated with blocking buffer containing 5% heat inactivated fetal calf serum (FCS) for 1 h and incubated with sheep anti-digoxigenin Fab-FITC antibody (Roche) over night at 4°C. Cells were washed three times with blocking buffer for 15 min at 25°C. DNA was stained with Hoechst 33342 (Sigma). Microscopy studies were performed with a Leica AF6000 microscope and pictures were obtained by using the LEICA DFC360FX camera and the LAS AF 2.7.3.9 software (Leica) and quantified by using the Fiji-software. For deconvolution (Figures 1A, 4C, S1A, and S4B) z stacks (10 stacks; 0,2 μm) were recorded and the maximal projection was deconvoluted (3 iterations) by the LAS AF 2.7.3.9 software (Leica).

RNA co-immunoprecipitation experiments (RIP)

All yeast strains were grown to mid log phase (2x10^7 cells/ml). For RIP experiments seen in Figures 3E, 4B, 5A, S3F, and S5A, cells were shifted to a non-permissive temperature for 1 h (16°C or 37°C, respectively), in Figures 5G and S6H cells were shifted to 37°C for 2.5 h and the cells shown in Figures 5E and S6D were incubated with 20 μg/ml doxycycline for 6 h prior to lysis. Afterward cells were harvested and lysed in RIP buffer (25 mM Tris HCl pH 7.5, 100 mM KCl, 0.2% (v/v) Triton X-100, 0.2 mM PMSF, 5 mM DTT, 10 U RiboLock RNase Inhibitor (Thermo Scientific) and protease inhibitor (Roche) using the FastPrep®-24 machine (MP Biomedicals) three times for 20 s at 6 m/s. After centrifugation the supernatant was incubated for 3 h at 4°C with GFP-Trap®_A beads (Chromotek) (Figures 1D, 1E, 1G, 2D, 3D, 3E, 3I, 4D–4F, 5A, and S5B) or with G-Sepharose beads with 2μl of α-Snu71 or α-Snu114 polyclonal antibodies, respectively (Gottschalk et al., 1998) (Figures 5E, 5G, and 5I). For TMG-cap-IPs total RNA was extracted from yeast lysates using trizol-chloroform (Ambion® RNA by Life technologies). 50 μg of the total RNA was incubated for 1 h at 4°C with Anti-2,2,7-trimethylguanosine-antibody (Milipore) and Protein G Sepharose beads (Amersham Biosciences) (Figure 4B).

The beads were washed five times with RIP buffer and for GFP-RIP split in two portions after the last washing step. Proteins were detected by western blot. Eluates were purified via trizol-chloroform (Ambion® RNA by Life technologies) extraction. The purified RNA was reverse transcribed with Maxima reverse transcriptase (Thermo Scientific) for subsequent qRT-PCR analyses. For Figure 4E first GFP-RIP experiments were performed as described above. Afterward 200 ng of eluted RNA was used for TMG-cap-IP followed by trizol-chloroform (Ambion® RNA by Life technologies) extraction, reverse transcription and qRT-PCR. In all cases, the RNA was measured and normalized to the total RNA before reverse transcription.

In vitro binding studies

Purification and *in vitro* binding studies with recombinant Mex67, mex67-Δloop409-435 and mex67–loopKR > AA proteins in complex with Mtr2 and subsequent RNA isolation and reverse transcription was carried out as described in Zander et al. (2016).

Cytoplasmic fractionation

For detection of snRNAs in the cytoplasm (Figures 2C and S2D) cells were grown to mid log-phase (2x10^7 cells/ml). After harvest, cells were washed once with 1ml YPD/ 1 M Sorbitol/ 2 mM DTT and resuspended in YPD/ 1 M Sorbitol/ 1 mM DTT. Cells

were spheroblasted using zymolyase and diluted in 50 mL YPD/ 1 M Sorbitol to recover for 30 min at 25°C before shift 16°C for 1 h. Cells were put on ice, centrifuged at 900 g for 5 min and resuspended in 500 µl Ficoll buffer (18% Ficoll 400, 10 mM HEPES pH 6.0). Cells were lysed by addition of 1 mL buffer A (50 mM NaCl, 1 mM $MgCl_2$, 10 mM HEPES pH 6.0). The suspension was mixed and centrifuged at 1,500 g for 15 min. The supernatant was used for cytoplasmic analyses. To verify correct fractionation of the cytoplasmic lysates, samples were analyzed in western blot for the presence of the cytoplasmic Zwf1 and nucleolar Nop1. RNA was isolated using the Nucleo-Spin RNA Kit (Macherey and Nagel). The purified RNA was reverse transcribed with Maxima reverse transcriptase (Thermo Scientific) for subsequent qRT-PCR analyses.

GFP-microscopy

Cells were grown, treated and harvested as described in FISH. Cells were fixed with 3% formaldehyde for 2 min at room temperature, before incubation on a polylysine-coated slide for 30 min at 4°C. Permeabilization, DNA staining, microscopy and quantification was performed as described above.

Co-immunoprecipitation (IP) experiments

All yeast strains were grown to log phase (2-3x10^7 cells/ml). Afterward, the cells were harvested and lysed in IP buffer (1 x PBS, 3 mM KCl, 2.5 mM $MgCl_2$, 0.5% Triton X-100 and protease inhibitors from Roche). 2,5% of this lysate was loaded onto the SDS-gels for the lanes designated as lysate. The supernatant was incubated for 3 h at 4°C with GFP-Trap®_A beads (Chromotek) (Figures 3D, 3E, 3I, 4D–4F, 5A, and S5B) or with G-Sepharose beads with 2 µl of α-Snu71 or α-Snu114 polyclonal antibody, respectively (Gottschalk et al., 1998) (Figures 5E, 5G, and 5I). The beads were washed five times with IP buffer, and finally resuspended in 25µl SDS-sample buffer. The entire sample was loaded onto the SDS-gels in the lanes designated as eluate. Subsequently, the proteins were detected by western blot analyses with the indicated antibodies (GFP (Pierce) 1:5,000; c-*myc* (9E10) (Santa Cruz) 1:1,000; Hem15 (R. Lill) 1:5,000; Zwf1 1:50,000 (Sigma); Nop1 1:5,000 (Santa Cruz)). Signals were detected with the Fusion SL system (PeqLab).

RNA-sequencing

For genome wide analysis of intron containing transcripts (Figures 5C, 5D, and S5C) strains were shifted to 37°C for 1 h. RNA was isolated using the Nucleo-Spin RNA Kit (Macherey and Nagel). The sequencing of RNA samples was conducted at the Microarray and Deep-Sequencing Facility Göttingen (Transcriptome and Genome Analysis Laboratory, TAL). Samples were prepared with the "TruSeq RNA Sample Prep Kit v2" according to the manufacturer's protocol (Illumina). Single read (50 bp) sequencing was conducted using a HiSeq 4000 (Illumina). Fluorescence images were transformed to BCL files with the Illumina BaseCaller software and samples were demultiplexed to FASTQ files with *bcl2fastq* (version 2.17). Sequences were aligned to the genome reference sequence of *Saccharomyces cerevisiae* (assembly R64-1-1, obtained from https://www.ncbi.nlm.nih.gov/geo/query/acc.cgi?acc=GSE93307) using the *STAR* software (Dobin et al., 2013; version 2.5) allowing for 2 mismatches. Subsequently, abundance measurement of reads overlapping with exons or introns was conducted with *featureCounts* (Liao et al., 2014; *subread* version 1.5.0-p1, Ensembl annotation version 84). Data was processed in the R/Bioconductor environment (http://www.bioconductor.org) using the *DESeq2* package (Love et al., 2014; version 1.8.2) to yield candidates for differential exonic/intronic expression ($|\log2\text{-fold change}| > 1$, FDR adjusted p value < 0.05). Intron retention analysis was performed by comparing fold changes of exonic expression (between wild-type and mutant) against fold changes of intronic expression. The sequencing data and abundance measurement files have been submitted to the NCBI Gene Expression Omnibus (GEO) under the accession number GSE93307.

QUANTIFICATION AND STATISTICAL ANALYSIS

All experiments shown in this work were performed biologically independent as indicated in the figure legend. Error bars represent the standard deviation. P values were calculated using a one-tailed, two-sample unequal variance t test. P values are indicated as follows: ***p < 0.001, **p < 0.01, *p < 0.05. For quantification of cells with displayed phenotypes (Figures 1B, 2B, and 3B) for each experiment between 50 and 350 cells were counted.

DATA AND SOFTWARE AVAILABILITY

RIP-Seq data have been deposited at the NCBI gene expression omnibus (GEO; https://www.ncbi.nlm.nih.gov/geo/) with the GEO accession number GSE93307.